A COMPARATIVE STUDY OF MIXED METAL OXIDE CATALYSTS FOR THE OXIDATION OF C4, C6 AND C8 LINEAR ALKANES

by

NISHLAN GOVENDER
M.Sc.

School of Chemistry
University of Kwazulu-Natal
Howard College
Durban
4041

Submitted in fulfillment of the academic
requirements for the degree of
Doctor of Philosophy in the
School of Chemistry,
University of KwaZulu-Natal,
Howard College,
Durban

July 2007

ABSTRACT

The Fischer-Tropsch process in South Africa, used for producing chemicals from synthesis gas, which is mostly derived from the gasification of coal, gives a large amount of medium chain length alkanes (C_4-C_8), which have little commercial value. Internationally, industry has recently placed more focus on the conversion of alkanes to value-added products. Two important routes to achieving this are dehydrogenation and oxidative dehydrogenation. The latter is an economically feasible route, in which there is growing interest by the international research community, and was investigated in this study.

A comparative investigation of promoted and unpromoted vanadium phosphorous oxide (VPO) and vanadium magnesium oxide (VMgO) catalysts in the selective heterogeneous oxidation of C_4, C_6 and C_8 linear alkanes was conducted in a continuous-flow solid-gas phase system, showing trends with different catalyst phases and their product profiles. There are no reports in the literature on heterogeneous oxidation of linear C_6 and C_8 alkanes over these catalysts.

Incorporating and impregnating a promoter onto a catalyst gave the catalyst different physical properties with different phase compositions. These phases could be identified and related to selective or non-selective oxidation. The VPO catalyst generally gave higher selectivities to carbon oxides than a VMgO catalyst under similar reaction conditions. The orthovanadate phase of the VMgO catalyst was found to be more selective than the pyrovanadate phase of the VPO catalyst in the oxidation of hydrocarbon chains longer than C_4. Important factors that determined selectivity were the morphology of the catalyst, crystallinity, phase composition, type of active catalytic species, the average oxidation state of the active metal and surface area of the catalyst.

For the selective oxidation of *n*-butane to MA, a platelet morphology was found in the best performing VPO catalysts. A $(VO)_2P_2O_7$ phase, which was present in the used VPO catalyst, was obtained from various synthesis methods. The ideal precursor phase for selective

oxidation was found to be $VOHPO_4 \cdot 0.5H_2O$. Higher selectivities to carbon oxides were obtained from the $(VO)_2P_2O_7$ phase formed from V_4O_9 and $VOPO_4 \cdot 2H_2O$ precursor phases.

The oxidation of *n*-hexane and *n*-octane gave benzene in the presence and absence of a catalyst. The silica in glass and the metals in stainless steel reactors (e.g. Mn, Co and Fe), the surface of the inert packing material and the voids in a reactor contributed to reactions in the absence of a catalyst. The selectivity to benzene from the oxidation of *n*-hexane could be improved by complementing catalytic and non-catalytic processes by optimizing the location of catalyst and voids in the reactor. A relationship was found to exist between the sizes of the voids in the inter-granular spaces between the carborundum particles and selectivity to desired products. A less oxidizing catalyst than VPO, like VMgO, was more selective for the oxidation of long chain linear alkanes ($>C_4$) and better suited to combining with non-catalytic reactions to improve selectivity to products obtained from combined catalytic and non-catalytic reactions.

The oxidation of linear alkanes gave alkenes in the presence and absence of a catalyst, which cyclised to give aromatic products. The oxidation of *n*-hexane gave benzene and the oxidation of *n*-octane gave styrene. A mechanism of *n*-hexane to benzene was proposed based on the reactivity of the intermediates. There was a combination of a catalytic and non-catalytic contribution to the formation of these alkenes and aromatic products and their selectivities could be optimized by varying the operating temperatures, residence times, amount of promoter incorporated in the catalyst and diluting the catalyst.

DECLARATION

I hereby declare that the work presented in this thesis is my own work and has never before been submitted for any degree at this or any other university. The research work was carried out at the University of KwaZulu-Natal, Howard College, under the supervision of Prof Holger B. Friedrich.

_____

N. Govender

As the candidate's supervisor I have approved this thesis for submission:

_____

Supervisor: Prof H.B. Friedrich

_____ day of _____ 2007

PUBLICATIONS

The following work has already been presented:

Conference contributions:

1. 'A VPO catalyst for the oxidation of *n*-butane', N. Govender and H.B. Friedrich, Sasol Technology Symposium, Rand Afrikaans University, South Africa, 2000 (ORAL)
2. 'A comparative study of VPO catalysts and promoters in the oxidation of *n*-butane', N. Govender and H.B. Friedrich, 35th Convention of the South African Chemical Institute, Potchefstroom, South Africa, 2000
3. 'A comparative study of VPO catalysts and promoters in the oxidation of *n*-butane', N. Govender and H.B. Friedrich, Fifteenth Indian National Symposium on Catalysis and Second Conference of the Indo-Pacific Catalysis Association, IPCAT-2 & CATSYMP-15, Pune, India, 2001
4. 'Oxidation of *n*-butane on a cobalt-promoted vanadyl pyrophosphate catalyst', N. Govender and H.B. Friedrich, SACI Young Chemists Colloquium, University of Natal, Pietermaritzburg, 2001 (ORAL)
5. 'Cobalt promoted VPO catalysts in the selective oxidation of *n*-butane to maleic anhydride', N. Govender and H.B. Friedrich, CATSA/SACI Conference on Catalysis and Inorganic Chemistry, Pilanesburg, South Africa, 2001 (ORAL)
6. 'Cobalt promoted VPO catalysts in the selective oxidation of *n*-butane', H.B. Friedrich and N. Govender, 4th World Congress on Oxidation Catalysis, Potsdam, Berlin, Germany, 2001
7. 'Selective alkane conversion to maleic anhydride', N. Govender and H.B. Friedrich, Catalysis Society of South Africa (CATSA) Conference, Cape Town, South Africa, 2002
8. 'A comparative study of C_4, C_6 and C_8 alkane conversion over promoted VPO catalysts', N. Govender, Science Faculty Research Day, University of Kwazulu-Natal, Howard College, Durban, 2003 (ORAL)

9. `The selective conversion of C_4, C_6 and C_8 alkanes over a mixed metal oxide catalyst', N. Govender, Catalysis Society of South Africa (CATSA), Durban, South Africa, 2003 (ORAL)
10. 'A comparative study of C_4, C_6 and C_8 alkane conversion over promoted VPO catalysts', N. Govender, The 3rd Conference of the Indo-Pacific Catalysis Association and the 21st Taiwan Symposium on Catalysis and Reaction Engineering, Taipei, Taiwan, 2003 (ORAL)
11. `The selective conversion of C_4, C_6 and C_8 alkanes over mixed metal oxide catalysts', N. Govender, Catalysis Society of South Africa (CATSA), Potchefstroom, 2004 (ORAL)

Publications

1. 'A comparative study of VPO catalysts in the oxidation of butane to maleic anhydride', N. Govender, Masters thesis, University of Natal, Durban (2002)
2. 'Controlling factors in the selective conversion of *n*-butane over promoted VPO catalysts at low temperature', N. Govender, H.B. Friedrich, M. Janse van Vuuren, Catal. Today, **97**, 315-324 (2004)
3. 'The effect of voids and dilution on *n*-hexane oxidation over a VMgO catalyst', H.B. Friedrich, N. Govender, M. R. Mathebula, Appl. Catal. A: General, **81**, 297 (2006)

DEDICATION

To my angel, my mother,

Rumba

(1954-2003)

ABBREVIATIONS

acac	=	acetylacetonate
AV	=	average oxidation state of vanadium
BET	=	Brenauer-Emmet-Teller (surface area characterization technique)
EDX	=	electron dispersive X-ray spectroscopy
FC	=	flow controller
FID	=	flame ionization detector
FT-IR	=	Fourier transform-infrared
GC	=	gas chromatograph
GC-MS	=	gas chromatography-mass spectrometry
GHSV	=	gas hourly space velocity
ICP-AES	=	inductively coupled plasma-atomic emission spectroscopy
ID	=	inner diameter
lfl	=	lower flammability limit
MA	=	maleic anhydride
OD	=	outer diameter
PA	=	phthalic anhydride
PC	=	pressure controller
ppm	=	parts per million
STP	=	standard temperature and pressure
TCD	=	thermal conductivity detector
TPR	=	temperature programmed reduction
ufl	=	upper flammability limit
VPO	=	vanadium-phosphorous-oxide
VPO-A	=	attempted synthesis of a 2.5 % Au-VPO catalyst (co-precipitation)
VPO-B	=	attempted synthesis of a 5.0 % Au-VPO catalyst (co-precipitation)
X	=	conversion
XPS	=	X-ray photoelectron spectroscopy
XRD	=	X-ray diffraction

DEFINITIONS AND CALCULATIONS

1. Gas hourly space velocity (GHSV) = $\frac{\text{flowrate (ml hr}^{-1})}{\text{volume of catalyst bed (ml)}}$ (at STP)

2. Specific yield = $\frac{\text{molar yield of species}}{\text{total surface area of catalyst}}$

3. Specific rate = $\frac{\text{rate of reaction}}{\text{total surface area of catalyst}}$

4. Average vanadium oxidation state (AV) = $5 - \frac{\text{volume } KMnO_4 \text{ solution (ml)}}{\text{volume } Fe(NH_4)_2(SO_4)_2 \text{ solution (ml)}}$

   This is a titrimetric method employed, which is outlined in Section 3.6.6 of Chapter 4

5. Carbon mass balance calculation (e.g. for *n*-butane conversion)

   n-Butane feed + $O_2 \rightarrow$ MA + CO + CO_2 + unreacted *n*-butane

   i.e. 4 carbons + 0 carbons → 4 carbons + 1 carbon + 1 carbon + 4 carbons

   % Carbon mol balance = $\frac{\text{n(products) X 100}}{\text{n(feed)}}$ (n = number of moles C)

   $= \frac{[4 \text{ x nMA} + 1 \text{ x nCO} + 1 \text{ X nCO}_2 + 4 \text{ x n(unreacted } n\text{-butane)}] \text{ x } 100}{4 \text{ x n(}n\text{-butane feed)}}$

6. Percentage conversion of *n*-butane = $\frac{\text{n(}n\text{-butane reacted) x 100}}{\text{n(}n\text{-butane feed)}}$

7. Percentage selectivity to MA = $\frac{4 \text{ x nMA x } 100}{1 \text{ x nCO} + 1 \text{ x nCO}_2 + 4 \text{ x nMA}}$

   The percent selectivity to CO and CO_2 were calculated in a similar way, with either CO or CO_2 replacing MA in the numerator (e.g. 1 x (nCO or nCO_2) x 100).

8. % Yield MA = $\frac{\text{\% selectivity to MA x \% conversion of } n\text{-butane}}{100}$

9. Upper flammability limit (ufl): (v/v) ratio of vapour or gas in air below which the gaseous mixture will propagate flame on ignition

10. Lower flammability limit (lfl): (v/v) ratio of vapour or gas in air above which the gaseous mixture will propagate flame on ignition

11. Carbenium ion: a group of atoms that contains a carbon atom only bearing six electrons

12. Carbonium ion: protonated alkanes yielding species such as CH_5^+

13. Medium chain length alkanes = C_4-C_8 alkanes

14. Alkane:O_2 feed molar ratio $= \dfrac{\text{mol \% alkane in air}}{(\text{mol \% } O_2 \text{ in air})(100 - \text{mol \% alkane in air})}$

$$= \frac{\text{mol \% alkane in air}}{(21/100)(100 - \text{mol \% alkane in air})}$$

15. Flash point: the lowest temperature at which a liquid gives off sufficient vapour to form an ignitable mixture with air near the surface of the liquid or in the vessel used

16. Autoignition temperature: the minimum temperature for a substance to initiate self-combustion in air in the absence of a spark or flame

CONTENTS

LIST OF FIGURES

CHAPTER 1

INTRODUCTION

CHAPTER 2

CATALYST AND REACTOR

CHAPTER 3

EXPERIMENTAL

CHAPTER 4

RESULTS

CHAPTER 5

DISCUSSION

LIST OF TABLES

CHAPTER 1

INTRODUCTION

CHAPTER 2

CATALYST AND REACTOR

CHAPTER 3

EXPERIMENTAL

CHAPTER 4

RESULTS

ACKNOWLEDGEMENTS

I would like to express my gratitude to my sponsoring company SASOL and THRIP for their financial support throughout this project. I extend my heartfelt appreciation to my supervisor, Prof H. B. Friedrich, for imparting his knowledge to me as well as for his encouragement, kindness and guidance throughout this project. Thank you to Dr C. Dwyer, Dr S. Sookraj, Dr T. Botha, Dr M.J. van Vuuren, Dr R. Krause, Dr R. Meyer and Mrs L. Hattingh from SASOL R&D for their advice and support.

Thank you to Sastech R&D for performing XRD, BET and GC-MS analyses, Mr B. Stole from Süd-Chemie for performing BET analyses, the School of Geology at the University of KwaZulu-Natal, Pietermaritzburg campus for performing SEM and EDX analyses and the Howard College campus for XRD analyses and Mrs R. Maharaj from the School of Chemical Engineering at the University of KwaZulu-Natal, Howard College for GC-MS analyses. Thank you to the late Dr F. Graham from the Electron Microscope Unit at the University of KwaZulu-Natal, Howard College for performing EDX and SEM analyses.

The Technical staff at the University of KwaZulu-Natal, Howard College, was invaluable in their support, assistance and efficiency. The efficient staff included Mrs M. Naidoo, Mrs J. Govender, Mr J. Couling, Mr A. Blose, Mrs T. Naidoo, Mrs B. Soko, Mrs Z. Sayed-Ally, Mr R. Suchipersad, Mr K. Singh, Mr G. Moodley, and Mr B. Parel. Thank you to my colleagues Sam, Avinash, Rivash, Jonathan, Zanele, Ruwaida, Bavani, Thirusha and Mayashree for their moral support.

A special thank you to Mr Mfanwenkosi R. Mathebula, whose eagerness as a research assistant to learn, enthusiasm for the field of catalysis and work ethic was impeccable.

The project was extensive with regard to setting up. Thank you to my spiritual guide for giving me the strength and capability to see the project through. The research and academic skills I have acquired in this project are invaluable.

To my departed mother, Rumba, in who I found sanctity and humility, an angel who showed me the grace and glory of life, who had faith in my every endeavour in life and offered

unstinted support and encouragement and continues to do so until this very day through her spirit.

To my darling sister, Preesha, for her love and support throughout this project, who lifted my spirits during the rough times.

To my father and departed grandparents for their support.

CHAPTER 1

INTRODUCTION

1.1 Scope and objectives

To investigate:

(i) the oxidation of medium chainlength linear alkanes (C_4-C_8) using promoted mixed metal oxide catalysts and identify the phases responsible for selective oxidation and overoxidation

(ii) the relationship between the method of promoter addition (incorporation and impregnation) and the types of phases present in the catalyst

(iii) the effect of voids in a reactor on catalyst activity and the product distribution

As the demand for olefins and aromatics as feedstocks increases, research into alternate sources of feedstocks is becoming more important (Sookraj, S.H. *et al.* (1999)). Alkanes are easily obtained from natural gas and petroleum. Since gas to liquid (GTL) processes also produce considerable amounts of *n*-alkanes, and world production is expected to rise enormously as more and more of these plants are built, these easily available and cheap alkanes appear to be prime substitutes for olefinic and aromatic feedstocks. Furthermore, the utilization of alkanes as feedstocks could facilitate lower environmental impact processes and lower cost processes. Alkanes are easier to store and use as feedstocks than olefins and many toxic aromatics based on the level of toxicity (Centi, G. *et al.* (1992)). The potential of alkanes in catalytic oxidation has been realized by the selective oxidation of *n*-butane to maleic anhydride. *n*-Butane oxidation is a clean oxidation, producing only traces of acetic acid and carbon oxides (Centi, G. *et al.* (1992), Centi, G. *et al.* (1993), Govender, N. *et al.* (2004)). Since the world supply of medium to long chain alkanes is expected to increase significantly with increased

utilization of GTL technology, there is growing interest in the oxidation chemistry of these alkanes.

There is a large production of linear hydrocarbons (C_4-C_{20}) in South Africa from Sasol's Fischer Tropsch process (Dry, M.E. (2002), Ji, Y. *et al.* (2001)). This abundance of medium chain length hydrocarbons (C_4-C_{20}) in South Africa, together with tfheir low cost and low environmental impact makes them ideal feedstocks for oxidation, in the presence of air (which is a cheap, readily available and a green oxidant), to more valuable chemicals.

The structure-activity relationship for mixed metal oxide catalysts (vanadium fphosphorous oxide (VPO) and vanadium magnesium oxide (VMgO)) were investigated in the oxidation of selected medium chainlength hydrocarbons (C_4-C_8) to higher value products in work carried out in this thesis. Intermediates to these value added products and the stability of the products were investigated. This was a comparative investigation used to identify the phases in the mixed metal oxide catalysts responsible for the types of products obtained (alkenes, cyclic oxygenated or overoxidation products). The configuration of a reactor with respect to material of construction and method of packing a catalyst and inert material into a reactor are investigated. Suitable reactor configurations for this type of catalysis are proposed.

From an industrial perspective, industrially valuable commodities were obtained viz. MA, benzene and styrene from the oxidation of C_4, C_6 and C_8 alkanes. There is an increasing demand to produce styrene monomers for synthetic polymers. Currently processes operate via the dehydrogenation of ethylbenzene to styrene at high temperatures (Sakurai, Y. *et al.* (2002)) and a means of converting linear C_8 alkane in a single reaction to styrene was investigated.

VPO and VMgO have been extensively reported as selective catalysts for the oxidative dehydrogenation of short chain hydrocarbons (mainly C_4); however, they have never been compared under similar reaction conditions in the literature to draw structure-activity correlation data.

The work carried out here, further investigated their performance in the oxidation of medium chainlength hydrocarbons (C_4-C_8). Magnesium-vanadium phases have been repeatedly

reported as effective catalysts for the oxidative dehydrogenation of propane to propene (Gao, X. *et al.* (1994), Kung, M.C. *et al.* (1992), Burch, R. *et al.* (1993)), butane to butadiene (Kung, M.C. *et al.* (1992)) and ethylbenzene to styrene (Chang, W.S. *et al.* (1995), Sakurai, Y. *et al.* (2002)). There is no literature on *n*-hexane or higher alkane conversion over a VMgO catalyst. The selectivity patterns in the catalytic oxidation of medium chainlength alkanes is investigated in work carried out in this thesis.

The only well established industrial linear alkane oxidation process reported in the literature involves the selective oxidation of *n*-butane to maleic anhydride over a vanadium phosphorous oxide (VPO) catalyst. There are few reports on the oxidation of longer chain length alkanes and none on an industrial scale. There is a wealth of knowledge to be gathered from the oxidation of *n*-butane to maleic anhydride and to apply this knowledge to longer chainlength hydrocarbons.

The conversion and product profiles from longer chainlength alkane oxidation were compared to the well-established *n*-butane oxidation process using similar and modified VPO catalytic systems with air as an oxidant.

Cyclohexane was commonly used as a substrate in the literature to investigate the fundamental role of oxidants and catalysts on the activation of a CH bond. Cyclohexane contains only secondary substituted carbons, making all the carbons identical in nature and hence giving a simple product profile. The product profile from a linear hydrocarbon substrate is complicated because of the different reactivities of primary and secondary substituted carbon centres, as well as different secondary substituted carbons in the chain having different reactivities. The product profiles obtained from the oxidation of different linear alkanes with different carbon numbers are reported and trends are identified. A study of this nature was not reported in the literature; however, the results obtained from fundamental studies on simple catalytic systems in the literature were used in designing a more selective catalytic system for the oxidation of longer chainlength hydrocarbons.

The physical and chemical attributes of mixed metal oxide catalysts (viz. VPO and VMgO) were identified and correlated to the activity of the catalyst and product selectivity profiles from C_4, C_6 and C_8 alkane oxidation. The structure-activity relationship of promoted VPO and VMgO was investigated.

Continuous flow fixed-bed micro-reactors are used in the investigation of catalytic activity in the literature because of their ease of operation. There is a need for more careful handling of data generated from these reactors in the literature. Blank reactor studies have been neglected in the literature. Non-catalytic reactions (i.e. reactions occurring in the absence of a catalyst) that occur on the surfaces of the "inert" packing material and the walls of the reactor have thus been mostly ignored, and yet are significant even at low operating temperatures where conversions are low. Cracking and other free radical reactions involving H abstraction become significant with the conversion of linear hydrocarbons in continuous flow gas-phase reactors at temperatures higher than 300^{o}C. Understanding the effect of temperature, residence time of the alkane in the reactor, material used in the construction of the reactor, voids in the reactor and the method of packing the reactor play a major role in determining the conditions to prevent non-catalytic reactions and especially over-oxidation products. The operating conditions for a reactor that are suitable for linear hydrocarbon oxidation are not well-defined in the literature and are outlined in this thesis.

Over the years there have been various proposals in the literature to explain the selectivities and yields of products from alkane oxidation over various heterogeneous catalysts, however, none have investigated the effect of voids and method of catalyst packing on the product selectivity profile in the oxidation of medium chainlength alkanes. Voids in the reactor and dilution of the catalyst can affect the conversion as well as selectivity to thermodynamically favoured products. The contribution of the location of voids in a reactor to cracking and whether they enhance the selectivity to products that are formed catalytically in the reactor was investigated.

A means of decreasing the amount of carbon oxides as by-products from chemical processes has been a major challenge facing the chemical industry for the past few decades. These non-selective reactions are significant with the oxidation of hydrocarbons. It is generally found in the literature that over-oxidation is limited by operating at low temperatures where conversions are low, but this is not always effective if factors responsible for over-oxidation are still present in the process. Besides identifying the ideal catalyst phases to limit overoxidation, this problem is further addressed in terms of (i) the reactor material and (ii) the method of packing a catalyst and inert material in the reactor. The latter focuses on the sizes of voids in the reactor, reactor materials and dilution of the catalyst as a means of optimizing operating conditions to decrease over-oxidation.

The stability of products is also an important consideration in catalytic investigations. Poorer stability of the product relative to the substrate can enhance over-oxidation. The stability of products from linear alkane oxidation is investigated and a mechanism to their formation is proposed.

1.2 Historical background and general scope of catalysis

In the early 19th century, it was noticed that a number of chemical reactions were affected by trace amounts of substances that were not consumed in the reaction. It was found that traces of acid could hydrolyse starch and low compositions of metal ions could effect the decomposition of hydrogen peroxide. Michael Faraday demonstrated that platinum sponge was able to sustain the oxidation of ethanol vapour thus producing heat that made it white hot (Thomas, J.M. *et al.* (1996)).

J.W. Döbereiner discovered that platinum could oxidize hydrogen. He then generated hydrogen by means of a small Kipps apparatus containing zinc and diluted sulphuric acid. The hydrogen was then passed over the platinum sponge where it catalytically combined with oxygen to yield a gentle flame. His apparatus was called a “tinderbox”. The “tinderbox” was commercialized for lighting fires and smoking pipes and over a million tinderboxes were sold in

the 1820s. He also mixed platinum sponge with clay, anticipating those methods for supporting the active metal which came into widespread use almost a century later (Lancaster, S.J., webpage). In 1831, P. Phillips patented a process involving platinum in the oxidation of sulphur dioxide, and this later became the basis of sulphuric acid manufacture.

In 1903 Ostwald showed that ammonia could be catalytically oxidized over a platinum gauze to yield oxides of nitrogen which, in turn, were converted to nitric acid (Petrucci, R.H. *et al.* (2002)). A landmark discovery in the history of applied catalysis was made in 1909, when Fritz Haber succeeded in preparing copious quantities of ammonia from nitrogen and hydrogen in the presence of a reduced magnetite (Fe_3O_4) catalyst using a high pressure apparatus (Brady, J.E. *et al.* (1993)).

In the late 1930s, catalytic cracking, which is the rupture of C-C bonds in order to convert large petroleum molecules, such as those that occur in gas oil, into small hydrocarbons of the kind found in fuel, first became known. The most popular catalysts at the time were acid treated clays to produce alkanes and alkenes from the cracking of the large petroleum molecules.

The observations made then could not be reconciled with what is known now about chemical reactivity, since this was long before methods were available for accurate measurements for rates of reactions. The first attempt at rationalizing these findings was made in 1836 by J.J. Berzelius. He called the phenomenon “catalysis”. The word catalysis comes from two Greek words, the prefix cata-, meaning down and the verb lysein, meaning to split or break. Berzelius defined the catalyst as a substance that broke down the normal forces which inhibit the reactions of molecules.

In our modern definition, a catalyst is usually referred to as a substance that increases the rate at which a chemical system approaches equilibrium, without being consumed in the process.

Great effort was expended over the past 50 years to make selective oxidation processes and their catalysts more efficient and environmentally friendlier. The fundamental

understanding of catalyst behaviour on an atomic and molecular level improved over the last 50 years. Newer technology is continuously replacing the old with a move towards "green chemistry". For example, the inefficient and expensive process of I.G. Farben which used HCN and acetylene to produce acrylonitrile was totally replaced in the 1960s by the highly efficient and environmentally more friendly SOHIO process which uses propylene, ammonia and air. Owing to these more efficient catalysts, the acrylonitrile yield has been increased over the past 40 years from 50 to over 80 % (Grasselli, R.K. *et al.* (2001)).

More than 90 % of the chemical manufacturing processes in use throughout the world utilize catalysts in one form or the other. Food, medicines, clothing, building materials and fuels are produced by heterogeneously catalysed reactions.

From a commercial perspective, catalysis is a means of obtaining high yields of desired products from chemical processes. The high yields reduce raw material cost, capital cost and operating costs which include those for separation, recycling and removal of environmentally unacceptable by-products.

Catalytic processes in industry are aimed at highly selective oxidation reactions. More than 60 % of the chemicals and intermediates synthesized via catalytic processes worldwide are products of oxidation. Rough estimates placed the worth of world products from a catalytic oxidation step at $20 to $40 billion per annum (Oyama, S.T. *et al.* (1993)).

The estimate for the worth of specialty chemicals worldwide in 1999 was $ 50 billlion (Stinson, S.C. (2001)). These chemicals are used in drugs, food and feed additives, dyes and agrochemicals (Fig. 1.1), with drug synthesis claiming the major use. Western Europe, Japan and North America account for 80 % of the international market for specialty chemicals.

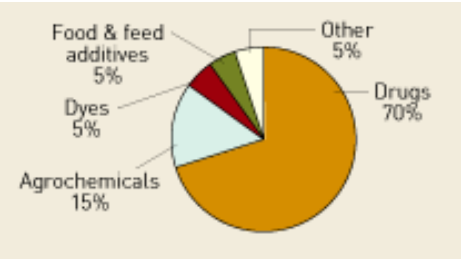

Fig. 1.1 Product distribution of fine chemicals internationally (Stinson, S.C. (2001))

Selective heterogeneous oxidation catalysis produces about 25 % of the world's most important industrial organic chemicals and intermediates used in the manufacture of industrial products and consumer goods.

One of the most important applications of selective oxidation catalysis is the functionalisation of hydrocarbons. The limitations in catalytic oxidation processes include the formation of undesired by-products such as carbon oxides. Carbon oxides are the chief by-products from alkane oxidation. Since the formation of carbon oxides is a highly exothermic reaction, non-selective reactions leading to their production may give hotspots in the reactor. Catalytically active phases are temperature sensitive and hotspots destroy these phases. None of the reactions run at maximum theoretical selectivity and few reactions attain total or close to total conversion. Processes can also generate co-products that are not always of economic interest. Total catalytic oxidation, however, is becoming increasingly important as a method for destroying trace pollutants and contaminants in gaseous streams (Catalytica (1993)).

Activation of the oxidant on the surface of the catalyst is important for selective oxidation. Some processes use stoichiometric oxidants such as permanganates and chromium salts to limit the production of carbon-oxides, however, molecular oxygen is the preferred and desirable source of oxygen in any process, because it is relatively inexpensive and environmentally friendly.

1.3 A review of alkane oxidation

This section reviews the

(i) major sources of alkanes,

(ii) types of alkane oxidation reactions found in the literature,

(iii) specific reactions for C_1-C_8 linear alkane oxidation, which is the region of the homologous series this thesis focuses on, giving details on chainlength-reactivity relationships,

(iv) homogeneous reactions associated with alkane oxidation,

(v) cracking of alkanes,

(vi) influence of feed composition on the catalysis,

(vii) factors affecting the steady state conditions in alkane oxidation,

(viii) mechanistic detail for the production of valuable products from the oxidation of alkanes (with relevance to the production of maleic anhydride and styrene),

(ix) reactor material of construction and their influence on the activation of alkanes,

(x) challenges in alkane activation and the progress made until now.

There are many sources of alkanes. By far the largest amount of saturated hydrocarbons is obtained from the natural sources natural gas and petroleum, either by separation or by suitable conversion reactions. Additional sources include various products derived from coal processing. Natural gas contains methane as the major component. Depending on the source, natural gas may contain acyclic saturated hydrocarbons up to C_5. The isolation of individual compounds from natural gas can be performed either by absorption or by partial condensation at low temperature, followed by distillation. Petroleum is the most abundant source of saturated hydrocarbons. Petroleum is separated into individual fractions by distillation. These fractions are processed for the recovery of alkanes and cycloalkanes. From the liquefied petroleum gas fraction, *n*-butane is isolated by distillation. From the higher boiling petroleum, gas-oil and wax distillate fractions and mixtures of homologous *n*-alkanes are isolated by molecular sieve separation or urea extractive crystallization. Higher boiling petroleum distillates and distillation residues can be converted into mixtures of lower molecular mass hydrocarbons by hydrocracking. Saturated $C_{3\text{-}5}$ hydrocarbons and a broad spectrum of higher *n*-alkanes can be recovered from such mixtures.

For a long time the most important sources of saturated hydrocarbons were coal and the products derived from the liquefaction, coking and gasification of coal. These sources became less important when natural gas and petroleum became essential raw materials for organic chemicals.

In South Africa, the liquefaction of coal provides the greatest variety of saturated hydrocarbons. Sasol's Fischer Tropsch synthesis can produce alkanes in the range C_1 to C_{30} or higher. The fluidized bed synthesis affords predominantly liquid hydrocarbons in the gasoline range, along with gases from C_1 to C_4. The liquid hydrocarbons contain considerable proportions of branched and alkene compounds. The fixed bed synthesis provides higher molecular mass hydrocarbons in the range of diesel oil or paraffin wax. These products are rich in *n*-alkanes.

This abundance of alkanes with poor reactivity and low market value has prompted the scientific community to investigate ways of transforming these alkanes to more valuable products. The aim was to increase the value of the linear hydrocarbons by converting them to more marketable products or intermediates that are easily activated to give valuable products. In particular, there is an industrial demand for terminally activated hydrocarbons (including alcohols and alkenes that are used in detergent synthesis and as monomers in polymers (Labinger, J.A. (2002)).

The reaction of an alkane proceeds via cleavage of C-H or C-C bonds. The scope of primary reaction steps is essentially limited to oxidative dehydrogenation, dehydrogenation, substitution and chain cleavage. Most industrial reactions involving saturated hydrocarbons are radical reactions, e.g. thermal cracking, oxidation, sulphoxidation, halogenation, sulphochlorination and nitration.

Reactions of saturated hydrocarbons are non-selective because of the lack of functional groups, with there being no preferred reaction site (poor regioselectivity), unless the molecule possesses specific structural features such as tertiary substituted carbon atoms. Such reactions frequently give mixtures of isomeric or structurally analogous compounds, where separation becomes difficult.

On the basis of enthalpy of formation, saturated hydrocarbons are thermodynamically unstable (Table 1.1).

Table 1.1 Enthalpy of formation for saturated hydrocarbons as gases at 25°C (Perry, R.H. et al. (1999)

Alkane	ΔH^o (kJ mol^{-1})
n-butane	-126.232
n-hexane	-167.305
n-octane	-208.586

They are, however, kinetically stable at ambient temperature. Thermal decomposition of saturated hydrocarbons proceeds stepwise by loss of hydrogen or hydrocarbon fragments with concomitant formation of industrially useful unsaturated cracked products such as acetylene, alkenes and aromatic hydrocarbons (Rossini, F.D. (1947)).

Methods of selectively oxidizing alkanes to dehydrogenated products and oxygenated products have gathered interest due to their expected low environmental impact and potential low cost processes, in terms of investment and operation, compared to traditional feedstocks. An example is the oxidation of *n*-butane to maleic anhydride over a vanadium phosphorous oxide (VPO) catalyst, where benzene was replaced as a feedstock. A substantial price differential developed between benzene and C_4 feedstocks. The differential continued to grow due to scarcity of benzene, caused by its increasing use in unleaded automobile fuels, coupled with generally increasing oil prices. The introduction of costly process control, particularly in the United States, prohibiting any detectable benzene emission from plants also favoured the alkane feedstock, because of benzene's potential to cause leukaemia (Centi, G. *et al.* (2001)).

There is theoretically no carbon loss during the oxidation of *n*-butane to MA, which further contributes to its advantage over benzene as a feedstock. In terms of product quality, *n*-butane oxidation is a very clean reaction with minimal formation of by-products (apart from the carbon oxides, only minimal amounts of acetic acid are produced) (Sookraj, S.H. *et al.* (1999)). The flammability limit for *n*-butane is lower than that for benzene, resulting in safer operating conditions. The catalysts involved in the *n*-butane route were also found to have a longer lifespan than catalysts used in the production of maleic anhydride from butene. Butene

reactivity is higher and there are fewer reaction steps involved in the process, yet, the abundance of butane and its relatively environmentally friendlier nature lead commercial producers to choose *n*-butane. It was as a direct result of these factors that interest intensified in the C_4 partial oxidation route during the 1970s.

The petrochemical industry now places demand on isobutene, high purity alkenes and hydrogen production. The market value of alkenes has thus increased in recent years (Centi, G. *et al.* (2001)). The high demand for alkenes has created a supply shortage due to their primary use as monomers and co-monomers in polymer synthesis. There is consequently new interest in producing them from alkanes. It is simpler and cost effective to convert alkanes directly to oxygenates rather than via intermediate production utilizing endothermic processes (such as steam reforming, steam cracking and dehydrogenation, which require a costly energy supply and also large plants with high investment costs and subsequent exothermic oxidative dehydrogenation processes to form the desired product). There is, thus, an increasing interest by industry in exothermic processes such as the oxidation of CH_4 to CO and H_2 as an alternative to methane steam reforming, and oxidative dehydrogenation of alkanes as an alternative to dehydrogenation. There is a need to develop a process that starts from natural gas components, which would avoid problems associated with variation in competitive prices of the alkenes.

The best-suited catalysts for the selective oxidation of a C_4 linear alkane were VPO and VMgO. The VPO and VMgO catalysts operate via an oxidative dehydrogenation mechanism. Oxidative dehydrogenation of alkanes overcomes the thermodynamic limitations, allows operation under relatively mild conditions and avoids the need for continuous regeneration of the catalyst, but has a major drawback in the difficulty of controlling the consecutive oxidation to carbon oxides. Other problems are the removal of the heat of reaction, the flammability of the reaction mixture and the possibility of reaction runaway.

The major challenge for oxidative dehydrogenation processes is to improve the selectivity to desired products, i.e. generally alkenes, because there is a worldwide demand for

them and the reduction of carbon oxide production. This requires a good catalyst but also reactor technology that can maximize catalyst effectiveness for alkene formation.

Oxidative dehydrogenation takes place in the presence of a hydrogen acceptor such as oxygen. This gives rise to an exothermic reaction, so avoiding the thermodynamic limitations of a reversible endothermic reaction such as dehydrogenation. The exothermicity arises from the formation of water from oxygen and hydrogen. This exothermic reaction also prevents the formation of products containing high C/H ratios, which can lead to fast catalyst deactivation.

The dehydrogenation processes have the advantage of high selectivities to desired alkene products. The oxidative process has the advantages of avoiding catalyst deactivation and not requiring high operating temperatures, thus improving process economics. There is thus interest in combining the dehydrogenation and the oxidative dehydrogenation processes. Some commercial companies have proposed catalysts that are capable of this (Imai, T. (1983), Bricker, J.C. *et al.* (1988), Herber, R.R. *et al.* (1989), Imai, T. (1989)).

Alkanes are flammable in air within a certain concentration range, better defined as a flammability range (Centi, G. *et al.* (2001)). Optimal conditions for oxidative dehydrogenation work near or in the flammability range of the alkane. This is unsafe, however, and can be achieved with the use of a fluidized bed reactor, where continuous movement of the catalyst mass efficiently inhibits radical chain propagation. It is, however, necessary that outside the catalyst bed, the feed mixture is outside the flammability range and fluidization of the catalyst is completely homogeneous to avoid gas pockets where explosions can occur. Control of these parameters is difficult, especially in the case of malfunctioning of the system. For these reasons, it is preferable to operate the process outside the flammability range.

The alkane in air mixture can be introduced to the reactor in three different ways:

(i) low alkane to oxygen ratio

(ii) near the stoichiometric ratio of alkane to oxygen

(iii) high alkane to oxygen ratio

The major disadvantage of having a low alkane-to-oxygen ratio is the high selectivity to carbon oxides because of the oxygen rich environment. A low alkane to oxygen ratio is thus usually uneconomical and unsuitable for selective alkane oxidation because the alkane conversion is high and the selectivity to desired products is low.

For a stoichiometric ratio of alkane to oxygen, the possibility is to operate directly with alkane and oxygen as the feed. The alkane is in excess when the oxygen is consumed in side reactions such as combustion. The main advantage of this mode of operation is the high alkane to oxygen ratio that favours high selectivities, however, the disadvantages are the great amount of heat released due to combustion, difficulty in obtaining high conversion of the alkane due to oxygen starvation and difficulty in controlling catalyst deactivation (due to the exothermic combustion reaction).

Considering the problems associated with working below the flammability range and under stoichiometric conditions of alkane to oxygen, it is favoured to work above the flammability range, where there is a hydrocarbon rich environment. The conversion of hydrocarbon is low and this can improve selectivity to desired products. The carbon oxide production is lower compared to the other two feed compositions due to less available oxygen (Centi, G. *et al.* (2001)).

A major challenge for oxidation catalysis is to selectively convert linear alkanes to higher value products. Terminal activation of the linear alkane is desired for use of the products in detergents and polymers. The four groups of products that can be obtained from alkane oxidation under catalytic conditions using molecular oxygen as the oxidant are shown in Fig. 1.2.

One of the major problems with medium chainlength hydrocarbon oxidation in a fixed-bed reactor is the production of carbon oxides and cracking of the substrate at operating temperatures higher than 300^{o}C. Carbon oxide generation is highly exothermic. These exotherms can increase the temperature in the catalyst bed up to 100^{o}C higher than the set operating temperature. This can destroy the catalyst when testing at 500^{o}C. A catalyst destroyed

by exotherms in this way gives a system in non-steady steady. If the system regains steady state after the catalyst is destroyed, the data becomes irreproducible.

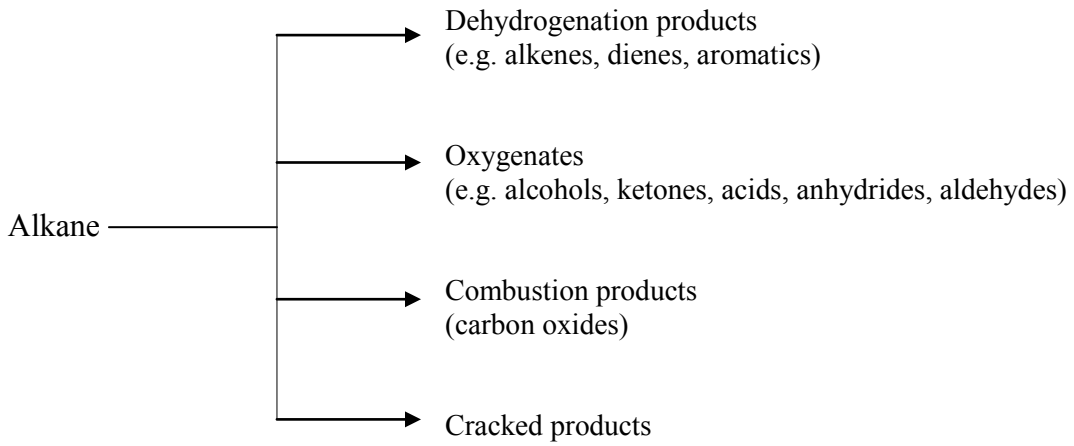

Fig. 1.2 Four groups of products from alkane oxidation

Heterogeneous reactions (solid-gas system) which display more than a single steady state are usually exothermic processes in which heat and mass transport between the fluid phase and the solid catalyst play a dominant role. Heat is generated by an exotherm at the catalyst surface and is dissipated by convection, conduction and for some conditions radiation processes. A steady state of thermal equilibrium is reached when the rate of heat generation in the catalyst particle is balanced by the rate of heat loss from its exterior surface area.

With alkane oxidation at elevated temperatures (300-500^{o}C) in solid-gas phase reactions, instabilities in the reactor may arise from thermal gradients in the catalyst bed due to combustion and the oxidative dehydrogenation process. These problems are corrected for by having a suitable reactor configuration. The reactor material needs to be highly conductive to allow for heat loss to the exterior thus preventing temperature runaways. Dilution of the catalyst particles can also limit temperature runaways if the catalyst is very active.

1.3.1 C_1-C_8 alkane oxidation

1.3.1.1 Methane, ethane and propane

Syngas may be produced from the oxidation of methane (Maitra, A.M. (1993), Lunsford, J.H. (1994), Fujimoto, K. (1994), Zhang, Z. *et al.* (1994)). Focus was placed on methane as a source of hydrogen for fuel cell applications and internal combustion engines due to its high H/C loading (Hickman, D.A. *et al.* (1993), Ashcroft, A.T. *et al.* (1990), Bharadwaj, S.S. *et al.* (1995)). Methane was converted to H_2 with a selectivity of up to 70 %, using a monolith reactor coated with a rhodium catalyst (Schmidt, L.D. *et al.* (2003)). Homogeneous combustion was used to rapidly heat the catalyst.

Ethane was converted over a VPO catalyst to ethylene with selectivities between 50 and 80 % with conversions between 2 and 30 % (Michalakos, P.M. *et al.* (1993)). Ethylene is generally the most selective product obtained from ethane oxidation to date (Roy, M. *et al.* (1996), Barthe, P. *et al.* (1990)).

Chao, Z. *et al.* (2004) investigated the oxidation of ethane under catalytic (using a VMgO catalyst) and non-catalytic conditions. The effects of reactor configuration such as empty tube, tube containing inert material or containing catalysts and inert material, reaction temperature, reactant composition, flowrate, as well as catalyst composition and structure were investigated. High conversions and selectivities were obtained at high temperatures during ethane thermolysis to ethene, accompanied, however, by high carbon depositions, especially in the presence of a catalyst. The contribution of homogeneous reactions to the oxidative dehydrogenation of ethane was less at low temperatures and when the fraction of inert material in the reactor was large. Products from non-catalytic reactions included alcohols, aldehydes, ketones and acids. Under catalytic conditions, a higher fraction of the feed was converted to oxygenates, with the selectivity to formaldehyde being higher than under non-catalytic conditions at similar conversions.

Kung, H.H. *et al*. (1993) reported on the conversion of propane and *n*-butane over VMgO catalysts. The author presented the requirements for selective dehydrogenation, whilst

classifying the VMgO catalyst as among the most selective and active catalysts for oxidative dehydrogenation of an alkane. The major product of propane conversion over the VMgO catalyst was propene. Higher selectivities to propene were obtained over the $Mg_3(VO_4)_2$ (orthovanadate) phase of the catalyst compared to the $Mg_2V_2O_7$ (pyrovanadate) phase.

Sugiyama, A. *et al.* (2003) investigated the redox behaviours of $Mg_3(VO_4)_2$ and $Mg_2V_2O_7$ phases of the VMgO catalyst in the oxidative dehydrogenation of propane. The orthovanadate phase ($Mg_3(VO_4)_2$) was more selective to propene. The author stripped the lattice oxygen from the catalyst by flushing the reactor with nitrogen. By subsequently passing oxygen over the catalyst, it was observed that the $Mg_2V_2O_7$ phase required more oxygen to regenerate itself. The larger amount of oxygen that was released from the pyrovanadate phase was reported as the reason for its poorer selectivity to propene and higher selectivity to over-oxidation products.

Kozhevnikov, I.V. *et al.* (1997), Moffat, J.B. (1996), Ai, M. (1996) and Ono, Y. (1992) investigated the oxidation of propane to acrylic acid and isobutene to methacrylic acid over Keggin type heteropolymolybdates. The molybdate catalysts are covalent and amphoteric in nature, which makes them suited to the formation of acidic products with a limited selectivity to over-oxidation products.

Large crystallites with low surface defect concentration are suggested as reasons for the decreased activity and selectivity of metal phosphorous oxide catalysts in the oxidative dehydrogenation of propane. This was established by varying the metal in the catalyst using Mg, Pb and Zn which creates different crystallite sizes and defect concentrations (Rybarczyk, P. *et al.* (2001)). This inspired work carried out in this thesis to investigate the morphology-activity relationships for the oxidation of medium-chain length alkanes over VPO and VMgO catalysts.

1.3.1.2 n-Butane

The principle products from *n*-butane oxidation include isomers of butene viz. but-1-ene, but-2-ene in cis and trans conformation, butadiene (Eon, J.G. *et al.* (1994), Michalakos, P.M. *et al.* (1993), Bhattacharya, D. *et al.* (1992)), acetic acid (Slinkadt, W.E. *et al.* (1981)), tetrahydrofuran (Zazhigalov, V.A. et al. (1994)), furan (Centi, G. et al. (1986)), methyl vinyl ketone, methyl ethyl ketone, crotonaldehyde and maleic anhydride (Cavani, F. *et al.* (1983), Centi, G. *et al.* (1988b), Centi, G. *et al.* (2001)) depending on the catalyst and reaction conditions.

The best understood process in linear alkane conversion is the oxidation of *n*-butane to MA. It is thus necessary to understand the mechanism of this reaction and identify key steps that may be employed in designing a system for the oxidation of longer chainlength hydrocarbons. There is, however, a lot of controversy over the mechanism. A mechanism that is well supported is discussed here. It is possible to have abstraction of hydrogen from the *n*-butane molecule in the 1- or 2- position, with the former being less favourable (Fig. 1.3).

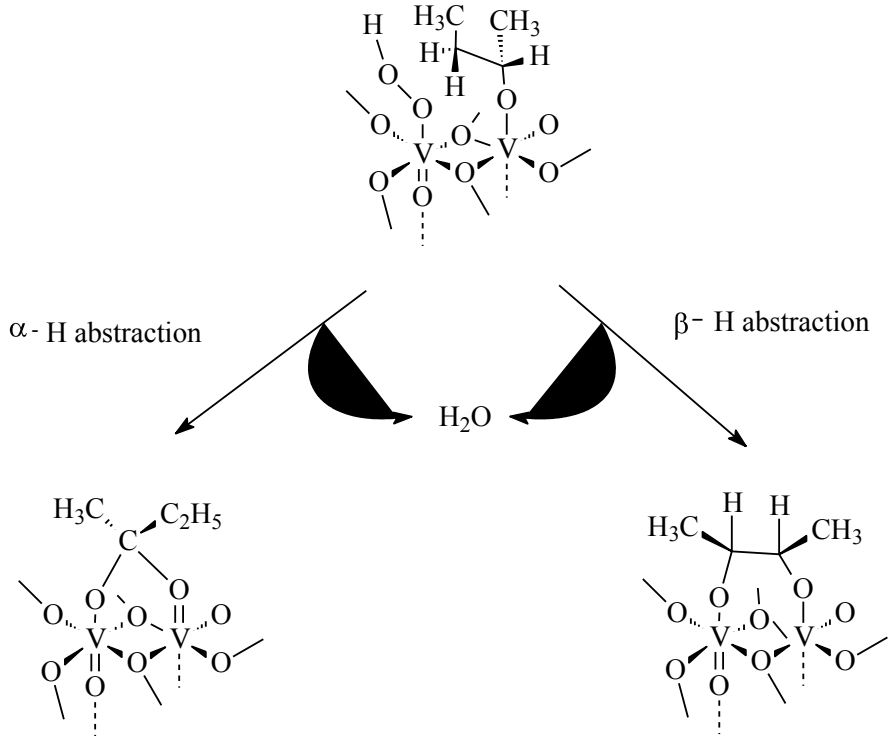

Fig. 1.3 Proton abstraction step in n-butane oxidation

The rate-determining step of this reaction is the activation of *n*-butane through abstraction of a proton (Zazhigalov, V.A. *et al.* (1993)). The methylene hydrogen is abstracted by a superoxo species to give a surface bound hydroperoxy group with the simultaneous capture of the alkyl radical by the adjacent vanadyl group to give a surface bound alkoxy group as illustrated in Fig. 1.3.

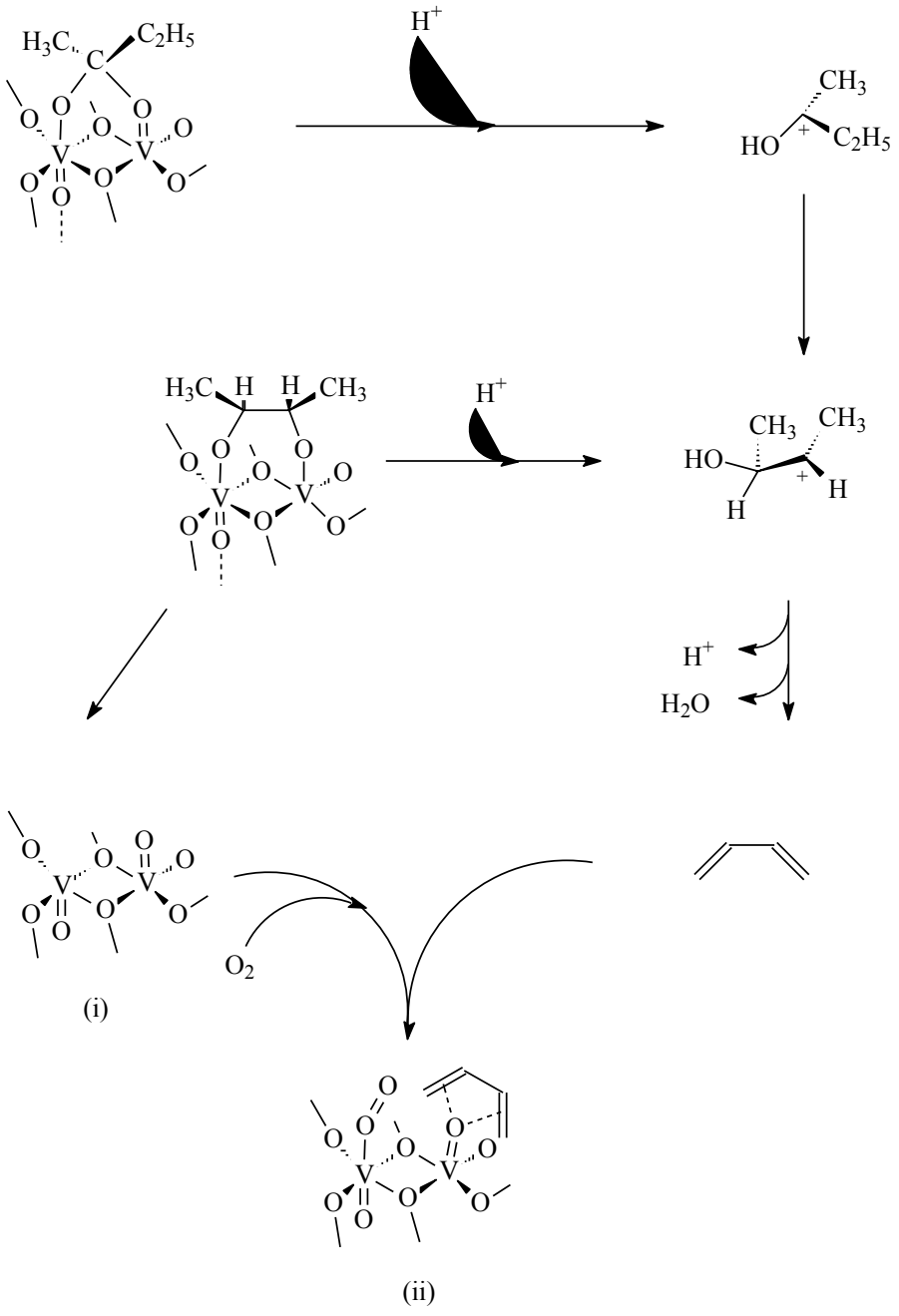

Fig. 1.4 Butadiene formation on the surface of the catalyst

The hydroperoxy group can then rapidly abstract another hydrogen, from either the same methylene group or from one of the adjacent -CH_x groups, to generate a molecule of water and a metal bound ketaloxy or glycoloxy group respectively (Agaskar, P.A. *et al.* (1994)). Hydrogen abstractions are also possible in the 1,4-positions followed by oxygen insertion to form a tetrahydrofuran-like species (Zazhigalov, V.A. *et al.* (1994)).

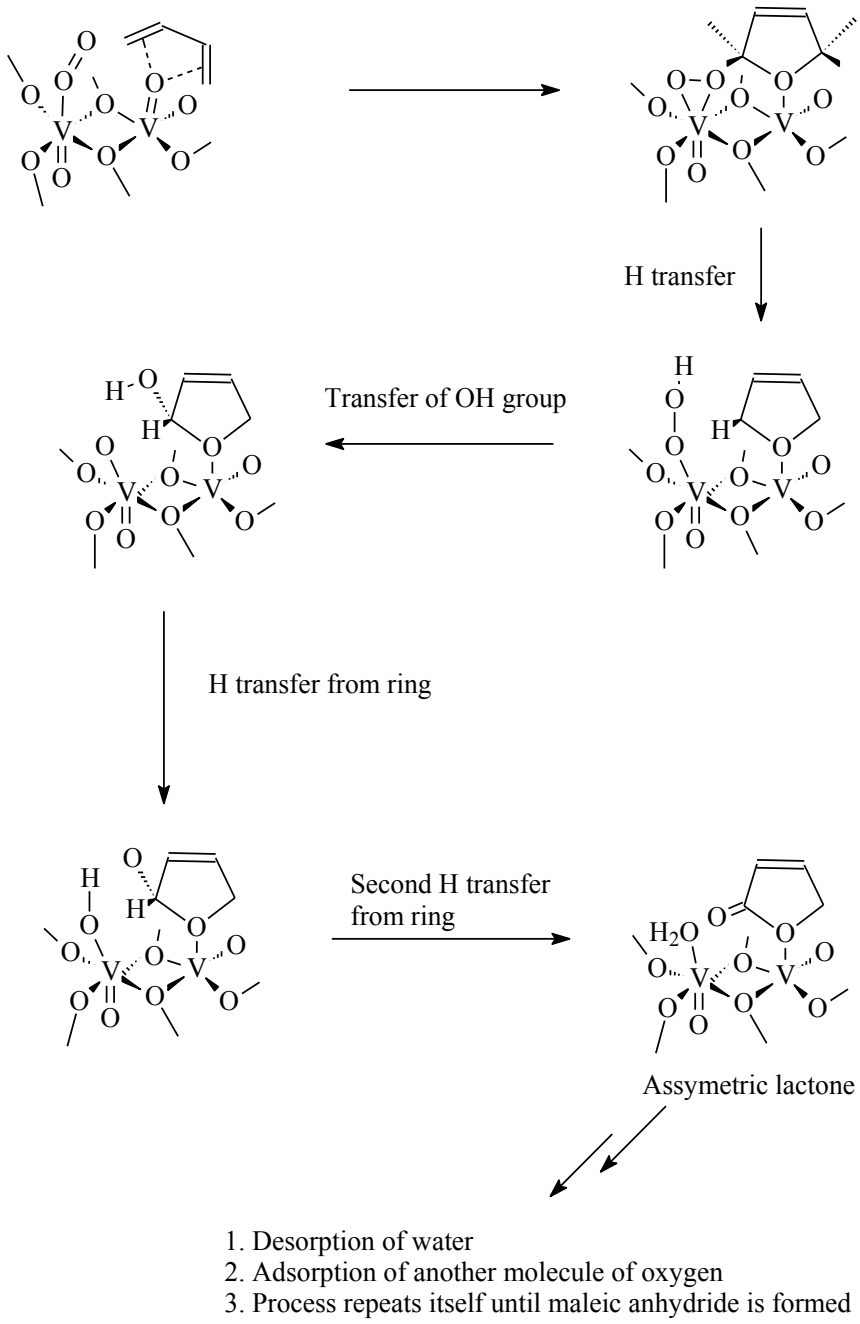

Fig. 1.5 2,5-Dihydrofuran and consequent lactone formation (Sookraj, S.H. et al. (1997))

The next step in the mechanism involves the acid catalysed conversion of partially bound surface intermediates to 1,3-butadiene. The active site is first converted to a species represented by (i) in Fig 1.4, which is capable of adsorbing a molecule of dioxygen and is therefore converted to species (ii). The vanadyl oxygen reacts with 1,3-butadiene (species (ii), Fig. 1.4) giving 2,5-dihydrofuran (Fig. 1.5). A similar mechanism may be proposed for the oxidation of *n*-hexane and *n*-octane oxidation to alkenes over a VPO catalyst.

Interaction between one of the oxygens in the adsorbed molecular oxygen species and the C-H bond in the 2-position of the 2,5-dihydrofuran leads to transfer of a hydrogen atom from 2,5-dihydrofuran to the peroxo species giving a surface bound hydroperoxide group (Fig. 1.5). There is considerable C-O interaction (bond length = 1.60 Å) with this orientation of the two adsorbed species. The OH group can therefore be transferred to the neighbouring 2,5-dihydrofuran derivative giving the corresponding 2-hydroxy derivative (Fig. 1.5).

The asymmetric lactone forms with the migration of a hydrogen atom from the 2-lactone hydroxy derivative giving a surface hydroxy group. The second hydrogen atom migrates to give the desired asymmetric lactone and one molecule of water (Fig. 1.5). This process repeats itself until maleic anhydride is formed (Agaskar, P.A. *et al.* (1994), Wenig, R.W. *et al.* (1987)).

The oxidation of *n*-butane to maleic anhydride is a multi-step polyfunctional reaction mechanism occurring entirely on the surface.

In summary the oxidation of *n*-butane over VPO to MA involves dehydrogenation and cyclisation with oxygen insertion (Fig. 1.6).

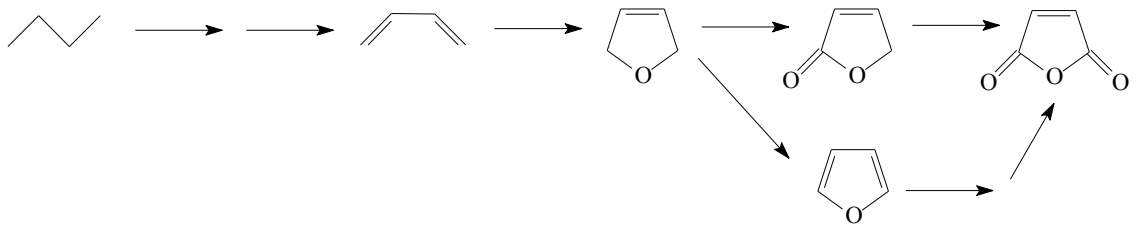

Fig. 1.6 Reaction sequence for the transformation of n-butane to maleic anhydride

Magnesium-vanadium phases have been repeatedly reported as effective catalysts for the oxidative dehydrogenation of propane to propene (Gao, X. *et al.* (1994), Kung, M.C. *et al.* (1992), Burch, R. *et al.* (1993)), butane to butadiene (Kung, M.C. *et al.* (1992)) and ethylbenzene to styrene (Chang, W.S. *et al.* (1995), Sakurai, Y. *et al.* (2002)). Conversion of *n*-butane to butenes over another mixed metal oxide catalyst (Fe-Sb-O) was reported by Ven'yaminov, S.A. (1977).

Kung, H.H. *et al.* (1993) reported higher selectivities to alkenes from C_4 oxidation over the Mg orthovanadate phase compared to the Mg pyrovanadate phase at similar conversions.

Chaar, M.A. *et al.* (1987) reported that the selectivity to dehydrogenation products over the VMgO catalyst increased with increasing vanadium content until an optimum was reached for samples containing 24 to 54 wt. % V_2O_5. The magnesium orthovanadate phase was suggested as the active phase. The absence of V=O in the VMgO catalyst was reported to limit oxidation of the catalyst surface.

Promoters may be added in the form of a metal or metal oxide to mixed metal oxide catalysts to improve their selectivity. MoO_3, Cr_2O_3 and TiO_2 promoters improved the selectivity of the VMgO catalyst in the oxidative dehydrogenation of *n*-butane to butadiene (Bhattacharya, D. *et al.* (1992)). These metal oxide promoters usually replenish lattice oxygen in the VMgO catalyst, but sometimes are also involved in the direct oxidative dehydrogenation of the alkane. The effect of Mg and Zr promoters on the activity of VO_x/Al_2O_3 catalysts was investigated in the dehydrogenation of butanes (Harlin, M. E. *et al.* (2001)). The promoters decreased the acidity of the catalyst thus limiting cracking.

1.3.1.3 n-Pentane

Maleic anhydride and phthalic anhydride were obtained from *n*-pentane oxidation over VPO (Centi, G *et al.* (1987), Buratini, M. *et al.* (1987), Busca, G. *et al.* (1989), Centi, G. *et al.* (1989), Centi, G. *et al.* (1990), Cavani, F. *et al.* (1999)). Phthalic anhydride production can be

attributed to a dimerisation of two hydrocarbon molecules at some stage in the reaction network as indicated by the template addition step in Fig. 1.7.

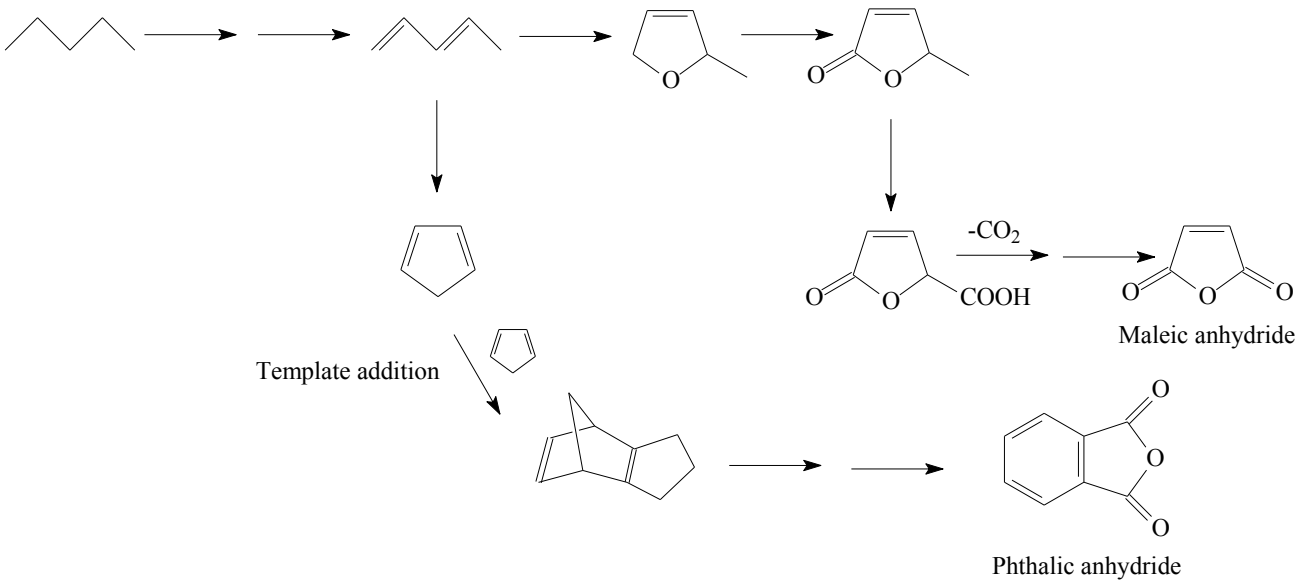

Fig. 1.7 Reaction network for the transformation of n-pentane to maleic anhydride and phthalic anhydride

In *n*-butane oxidation to MA, the alkene intermediates are butenes and butadienes, which are products of oxidative dehydrogenation. The oxygen inserted intermediates include dihydrofuran, butyrolactone and furan. In the case of *n*-pentane, a similar sequence of transformations should lead to the formation of pentadiene. However, at this stage there is a major difference between butadiene (from *n*-butane) and pentadiene (from *n*-pentane). The latter has allylic hydrogens not present in butadiene and thus further hydrogen abstraction is possible, which leads to the formation of cyclopentadiene as an intermediate (Fig. 1.7). Cyclopentadiene interacts strongly with the surface Lewis acid centres of the vanadyl pyrophosphate catalyst, which is the active catalytic phase of the VPO catalyst. These Lewis acid centres are due to coordinatively unsaturated vanadyl ions. These strongly coordinated cyclopentadiene molecules are susceptible to Diels-Alder type reactions with other adsorbed cyclopentadiene molecules. A

C_{10} intermediate that forms subsequently undergoes oxygen insertion giving phthalic anhydride. These cyclic reactions are expected to take place with longer chainlength hydrocarbons.

Pt single gauze reactors were employed by Iordanoglou, D.I. *et al.* (1999) to examine the partial oxidation of C_1-C_5 alkanes in a fuel rich environment at contact times as low as 100 μs. The authors reported that methane and ethane produced mostly CO and ethylene respectively, whilst propane, butane and pentane gave high selectivities to oxygenates and alkenes. Butane oxidation gave significant amounts of oxygenated products, mainly formaldehyde and acetaldehyde. Pentane oxidation gave up to 60 % selectivities to oxygenates, the main products being acetaldehyde and propionaldehyde. The authors report that total combustion was primarily catalysed by the Pt surface and oxygenates and alkenes formed subsequently by gas phase reactions from the exotherm generated from combustion.

Goetsch, D.A. *et al.* (1996) also reported on the oxidation of C_1-C_4 in a similar reactor setup as Iordanoglou, D.I. *et al.* (1999) but at shorter contact times of 10 μs. The authors reported that different reaction pathways operated at different residence times. Alkenes, oxygenates and carbon oxides were reported for C_2-C_4 feeds.

Pentenes (1-pentene, 2-pentenes and pentadienes) from pentane oxidation over unpromoted VMgO catalysts were reported by Armas, N. *et al.* (conference contribution, Prague, 2004) and Acevedo, A. *et al.* (conference contribution, Barquisimeto, 2002). The incorporation of antimony improved the selectivity to pentene (Korili, S.A. *et al.* (1996), Weng, L.T. *et al.* (1991)). The role of antimony in improving the selectivity to alkenes from an alkane oxidation is not fully understood.

1.3.1.4 n-Hexane

Mikovsky, R.J. *et al.* (1971) reported on the conversion of *n*-hexane to benzene over tellurium loaded NaX and KX zeolites. The authors obtained conversions of higher than 80 % with selectivities to benzene higher than 90 % via a dehydrocyclisation process. The other products obtained were $C_{1\text{-}5}$ cracked products and coke.

There is no literature on the heterogeneous oxidation of *n*-hexane or longer paraffins over a VMgO catalyst, however, there are reports on the oxidation of cyclohexane to cyclohexanol and cyclohexanone (Centi, G. *et al.* (2001)). There is ongoing research on the ammoxidation of cyclohexane to adiponitrile (Ovsitser, O. Y. *et al.* (1989)).

Kung, H.H. *et al.* (1993) and Michalakos, P.M. *et al.* (1993) reported on the oxidation of cyclohexane over magnesium orthovanadate and magnesium pyrovanadate phases of a VMgO catalyst giving benzene, cyclohexene and carbon oxides.

Centi, G. *et al.* (1988a) reported on the oxidation of *n*-hexane over a VPO catalyst giving maleic anhydride, phthalic anhydride, benzoic acid, cracked products and carbon oxides. The authors reported 23 % selectivity to maleic anhydride at a conversion of 50 %. Maleic anhydride, phthalic anhydride, and benzoic acid were not observed as products in work carried out in this thesis. The reason for this, which is attributed to different operating conditions, is discussed in Chapter 5.

Skotak, M. *et al.* (2002) reported on the conversion of *n*-hexane in excess hydrogen in air over Pd/Al_2O_3 and Pt/Al_2O_3 catalysts giving benzene and cyclohexane as minor products, whilst the main products were methylpentanes, methylcyclopentane and hydrogenolysis products. Panizza, M. *et al.* (2003) reported that benzene and cyclohexene was obtained at low conversions from cyclohexane oxidation over V-, Fe- and Ce- phosphate catalysts.

Schmidt, L.D. *et al.* (2003) reported on the partial oxidation of *n*-hexane and cyclohexane on Rh-coated alumina monoliths in an effort to determine whether higher alkanes can be successfully converted to mainly H_2 and CO in short contact time reactors. The conversions for each hydrocarbon were reported to be ~ 100 % for C/O ratios near syngas stoichiometry and decreased as the C/O ratio was increased. At C/O ratios much less than syngas stoichiometry, selectivities to H_2 and CO fell due to combustion, whilst at ratios higher than the syngas ratio, selectivities fell due to alkene production.

1.3.1.5 n-Octane and longer paraffins

Herrington, E.F.G. *et al.* (1945) reported on the cyclisation and subsequent aromatisation of *n*-octane over a Cr_2O_3 catalyst. The products included ethylbenzene, *ortho*-, *meta*- and *para*-xylene (Fig. 1.8).

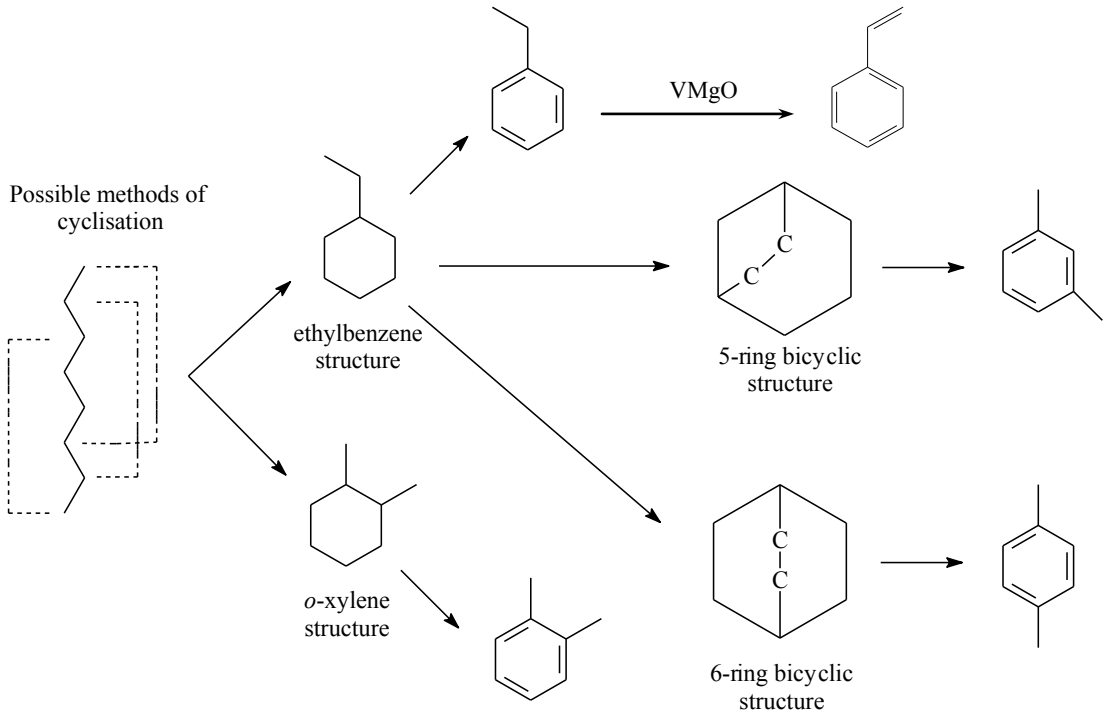

Fig. 1.8 Isomerisation in the cyclisation of n-octane (modified from Herrington, E.F.G. et al. (1945))

n-Octane can cyclise on the catalyst to form ethylbenzene and *o*-xylene, but *m*- and *p*-xylene formed as well. This could happen by simultaneous isomerisation with ring closure, which was proposed by Herrington, E.F.G. *et al.* (1945) (Fig. 1.8).

It was proposed that after cyclisation of the main ring the ethyl group can form an additional 5- or 6-membered ring (Fig. 1.8). On further dehydrogenation, the bicyclic naphthenic rings which are non-planar are transformed into the planar aromatic structures. The resulting strain breaks the 5- and 6-membered rings with simultaneous formation of *m*- and *p*-xylene.

Herrington, E.F.G. *et al.* (1945) also proposed that the alkene and alkane can compete for the same active centre on the catalyst. The alkene is usually strongly adsorbed and can displace the weakly adsorbed alkane from the catalyst surface. The rate of cyclisation of the alkene is more rapid than the dehydrogenation of the alkane to the alkene.

Another proposal for the mechanism of formation of aromatic products involves the combination of small alkene fragments on the surface of the catalyst. Hightower, J.W. *et al.* (1965) conducted C-14 tracer experiments on the cracking of *n*-hexadecane over a silica alumina catalyst and reported that more than 50 % of all aromatic compounds are formed this way.

There are a number of reports in the literature on liquid phase catalytic systems for the oxidation of *n*-octane (Thomas, J.M. *et al.* (1999) and Poladi, R.H.P.R. *et al.* (2002)). The main products were oxygenates such as C_8 ketones, aldehydes and acids. The catalysts employed were aluminophosphate molecular sieves and Ti-MMM-1. TS-1 in the presence of H_2O_2 also gives these products from the oxidation of *n*-octane (Kong, L. *et al.* (2004)).

Krummenacher, J.J. *et al.* (2004) reported on the partial oxidation of *n*-decane, which is a major component of diesel fuel, to produce H_2, ethylene and α-alkenes over rhodium and platinum in autothermal reactors at short contact times.

There is considerable interest in fuel reforming for pollution abatement with respect to internal combustion engines in the automotive industry. Reforming of gasoline or diesel into H_2 and other small molecules creates a fuel that burns very efficiently, thus reducing or eliminating exhaust emissions of hydrocarbons, CO and particulate matter (Cohn, D.R. *et al.* (1996)).

1.3.1.6 Cracking and autoxidation of alkanes

Two catalyst families were investigated in the oxidation of medium alkanes to higher value products in this thesis, viz. the vanadium phosphorous oxide (VPO) catalyst and the vanadium magnesium oxide (VMgO) catalyst. The VPO catalyst, which is acidic in nature, can crack an alkane feed. There have been over 5000 articles published in the last 10 years on

conventional cracking catalysts providing detailed mechanistic proposals in this regard (Corma, A. *et al.* (2000)).

Commercial scale plants for the selective air oxidation of paraffinic waxes are generally of metal construction. Sheldon, R.A. *et al.* (1981) reported that some metal ions such as Co, Mn, Fe and Cu in the stainless steel (which is used in the construction of the reactor) can initiate the autoxidation of hydrocarbons. The metals can act as either catalysts or inhibitors depending on the metal concentration (Betts, A.T. *et al.* (1966)). Hydroperoxides, alcohols and ketones are possible products from autoxidation processes in steel reactors (de Klerk, A. (2004)). Stainless steel is also known to improve C_2H_4 and C_2H_6 yields, where the steel is an active surface for the coupling reaction of methane (Hutchings, G.J. *et al.* (1988)). Laboratory scale experiments done in metal equipment may therefore be susceptible to rate enhancement or suppression due to the formation of corrosion products such as carboxylic, formic and acetic acids from the reaction of alkane feedstocks with the metal reactor.

Gas phase reactions can, however, take place in steel and glass (which is considered inert) reactors. Silica, as part of a catalyst, exhibits oxidising properties (Cavani, F. *et al.* (1999)). It has been found to be active in the oxidation of methane to formaldehyde (Parmaliana, A. *et al.* (1994)) and in the ammoxidation of cyclohexanone to a cyclohexanone oxime intermediate in the synthesis of caprolactam (Bendandi, A. *et al.* (1996)). The formation of O_2^- species, which are initiators for free radical reactions, may occur on the surface of the silica (Bendandi, A. *et al.* (1996)).

The cracking and autoxidation of an alkane in the investigation of catalyst performance is a matter of concern for both industrial and laboratory scale experiments and understanding the mechanisms by which they form can be a way of eliminating them, thus improving the selective oxidation of alkanes. Cavani, F. *et al.* (1999) reported that at temperatures higher than 500^{o}C in the reactor under catalytic conditions for alkane oxidation, homogeneous reactions become prevalent. The authors reported that radical species are generated at the catalyst surface and then:

(i) converted to the corresponding alkene via β-elimination or by undergoing non-selective oxidative attack by adsorbed oxygen species

(ii) react further in close proximity to the catalyst surface

(iii) are transferred into the gas phase where the reaction proceeds

Lemonidou, A.A. *et al.* (1998) reported that oxygen participates in the free radical reaction mechanism of *n*-butane dehydrogenation in an empty reactor. The author reported that oxygen was necessary for the initiation and propagation steps of the mechanism. This was previously reported by Pitz, W.J. *et al.* (1986) in an independent study, who proposed the following reactions for the formation of free radicals from *n*-butane under non-catalytic oxidation. These free radicals were postulated as precursors to C_2 and C_3 cracked products and C_4 alkenes:

$$C_4H_{10} \longrightarrow C_2H_5^{\bullet} + C_2H_5^{\bullet} \quad (1.1)$$

$$C_4H_{10} \longrightarrow C_3H_7^{\bullet} + CH_3^{\bullet} \quad (1.2)$$

$$C_4H_{10} + O_2 \longrightarrow C_4H_9^{\bullet} + HO_2^{\bullet} \quad (1.3)$$

Pitz, W.J. *et al.* (1986) reported that the activation energy (49 kcal mol^{-1}) of reaction (1.3) is lower than for reactions (1.1) and (1.2) (85 and 81 kcal mol^{-1} respectively). Similar conclusions about the participation of oxygen during the initiation steps in the non-catalytic oxidative dehydrogenation of ethane are reported by Burch, R. *et al.* (1993). Hence the absence of $C_{2\text{-}3}$ cracked products from non-catalytic oxidation of *n*-butane in work carried out in this thesis.

It was observed from work carried out in this thesis that the oxidation of *n*-hexane either catalytically or non-catalytically in glass or steel reactors gave $C_{3\text{-}4}$ cracked products. Examining the following reaction of *n*-hexane cracking to form propane and propene:

$$C_6H_{14(g)} \longrightarrow C_3H_{8(g)} + C_3H_{6(g)}$$

The enthalpy for the reaction is:

$$\Delta H = \Delta H^{o} \text{ (propane+propene)} - \Delta H^{o} \text{ (}n\text{-hexane)}$$

$$= (-104+21) \text{ kcal mol}^{-1} - (-167) \text{ kcal mol}^{-1}$$

$$= 84 \text{ kcal mol}^{-1}$$

The entropy for the reaction is:

$$\Delta S = S^{o} \text{ (propane+propene)} - S^{o} \text{ (}n\text{-hexane)}$$

$$= (+270+267) \text{ cal mol}^{-1} \text{ K}^{-1} – (389) \text{ cal mol}^{-1} \text{ K}^{-1}$$

$$=148 \text{ cal mol}^{-1} \text{ K}^{-1}$$

The free energy for the reaction at ambient temperature is:

$$\Delta G = \Delta H - T\Delta S$$

$$= 84 \text{ kcal mol}^{-1} - (298 \text{ K})(148 \text{ cal mol}^{-1} \text{ K}^{-1}) \quad (1.4)$$

$$= 44 \text{ kcal}$$

The free energy for the reaction at 400^{o}C is:

$$= 84 \text{ kcal mol}^{-1} - (673 \text{ K})(148 \text{ cal mol}^{-1} \text{ K}^{-1}) \quad (1.5)$$

$$= -16 \text{ kcal}$$

It is shown by the Gibbs free energy calculation (equation 1.4) that the reaction is not spontaneous at room temperature. The process is spontaneous, however, at 400^{o}C to give propane and propene from the oxidation of *n*-hexane (equation 1.5). Cracking is thus favoured at high temperatures. This explains the increase in selectivity to propane and propene with increasing temperature above 300^{o}C under catalytic and non-catalytic conditions.

For both thermal (non-catalytic) cracking and acid-catalysed (catalytic) cracking, it is well known that scission of the β C-C bond accounts for most of the C-C bond cracking of alkanes (Wojciechowski, B.W. *et al.* (1986), Olah, G.A. *et al.* (1995)).

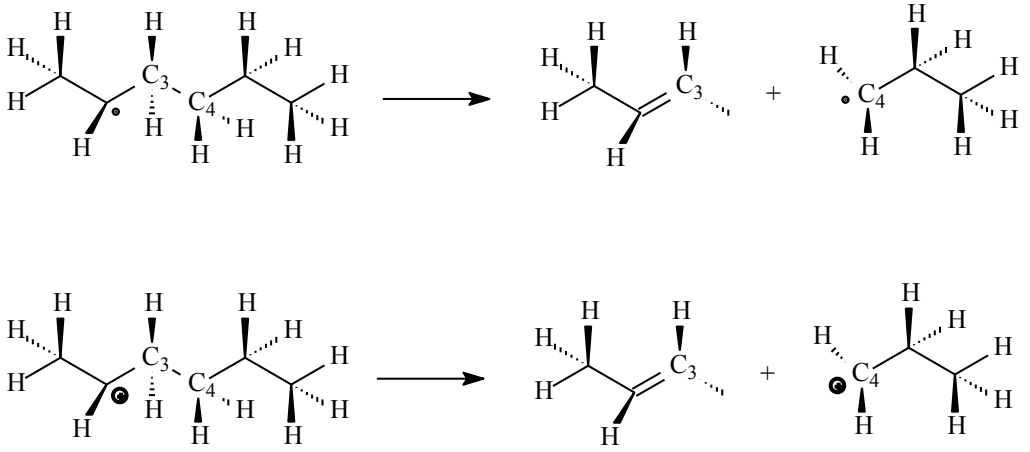

Fig. 1.9 β-scission via an alkyl radical (top) and an alkyl cation (carbenium ion) (bottom) (Hunter, K.C. et al. (2002))

Both types of cracking occur in a VPO catalyst system, due to high operating temperatures and the acidic nature of the catalyst. In thermal cracking the *β*-scission occurs with alkyl radicals, while in acid-catalysed cracking it occurs with alkyl cations (carbenium ions) to form C_3 products from *n*-hexane (Fig. 1.9).

The initiation step for thermal cracking of *n*-hexane is proposed to be C-C bond fission to form two radicals, with C-C rupturing occurring between the most highly substituted carbons viz. the secondary substituted carbons in the *n*-hexane molecule (Fig. 1.9) (Hunter, K.C. *et al.* (2002)).

The initiation steps for acid-catalysed cracking of *n*-hexane involves the generation of the active carbenium ion (Fig. 1.9). Three possible activation mechanisms for the generation of this ion are proposed:

(i) The abstraction initiation: involves a Lewis-acid catalyst, such as the orthovanadate phase of the VMgO catalyst (Védrine, J.C. (2002)), stripping a hydride (H^-) from *n*-hexane to create a carbenium ion (Brouwer, D.M. *et al.* (1972), Scherzer, J. (1989)).

(ii) The redox initiation: involves an oxidising catalyst, such as the pyrovanadate phase of the VPO catalyst (Centi, G. *et al.* (2001)), stripping an electron from *n*-

hexane, with the alkane radical cation further decomposing to create a carbenium ion (Culmann, J.C. *et al.* (1990), Fărcaşiu, D. (2001)).

(iv) The carbonium initiation: involves the protonation of *n*-hexane by the catalyst, forming unstable carbonium ions that dissociate to form carbenium ions (Olah, G.A. *et al.* (1973), Haag, W.O. *et al.* (1985)). This would most likely occur on a catalyst with Brønsted acid sites (such as the P-OH groups on the VPO catalyst surface (Centi, G. *et al.* (2001)) and not on a basic catalyst such as VMgO (Centi, G. *et al.* (2001)).

Cavani, F. *et al.* (1999) proposed a mechanism for the generation of hexene isomers from alkyl radical fragments in the gas phase. The alkyl radicals are generated on the catalyst surface and are released to the gas phase for further reaction. The alkyl radicals may also be generated in the gas phase giving alkenes. The amount of alkyl radical fragments in the gas phase is a function of temperature. The reaction of the alkyl radical and O_2 proceeds by a simple reversible addition process with the formation of a peroxide species:

$$C_nH^{\bullet}_{2n+1} + O_2 \rightleftharpoons C_nH_{2n+1}O^{\bullet}_2$$

This $C_nH_{2n+1}O^{\bullet}_2$ adduct may be subsequently converted to oxygenated products or be a precursor to carbon oxide production (Cavani, F. *et al.* (1999)). Oxygenated products and carbon oxides were obtained from non-catalytic and catalytic oxidation of alkanes. The authors proposed the following homogeneous reaction mechanism for the formation of oxygenated products from alkane oxidation:

$$2C_nH_{2n+1} + 2O^{\bullet}_2 \rightleftharpoons H_{2n+1}C_nOOOOC_nH_{2n+1}$$

$$H_{2n+1}C_nOOOOC_nH_{2n+1} \rightleftharpoons 2C_nH_{2n+1}O^{\bullet} + O_2$$

$$C_nH_{2n+1}O^{\bullet} + C_nH_{2n+2} \rightleftharpoons C_nH^{\bullet}_{2n+1} + C_nH_{2n+1}OH$$

$$H_{2n+1}C_nOOOOC_nH_{2n+1} \longrightarrow C_nH_{2n}O + O_2 + C_nH_{2n+1}OH$$

$$C_nH_{2n+1}O^{\bullet} \rightleftharpoons C_{n-x}H^{\bullet}_{2(n-x)+1} + C_xH_{2x}O$$

$$C_nH_{2n+1}OH + C_nH^{\bullet}_{2n+1} + O_2 \rightleftharpoons C_nH_{2n}O + C_nH_{2n+2} + HO^{\bullet}_2$$

Only small amounts of alkenes are formed via direct H abstraction from $C_nH_{2n+1}^{\bullet}$ by O_2 at temperatures lower than 350°C (Cavani, F. *et al.* (1999)):

$$C_nH_{2n+1}^{\bullet} + O_2 \rightleftharpoons C_nH_{2n} + HO_2^{\bullet}$$

Above 350°C, selectivity to the alkene usually increases with a decrease to carbon oxides, since at high temperatures the equilibrium:

$$C_nH_{2n+1}^{\bullet} + O_2 \rightleftharpoons C_nH_{2n+1}O_2^{\bullet}$$

is in favour of the hydrocarbon, thus consumption of the radical must be accounted for by a different mechanism.

1.4 Recent trends and the future of oxidation catalysis

There is increasing interest in alkanes replacing aromatics and alkenes as raw materials because of them being relatively environmentally friendly and inexpensive. New processes are directed towards generating fewer or no undesired co-products with a growing commitment to protecting the natural environment.

Oxidative dehydrogenation is more attractive than dehydrogenation processes from an industrial-economic perspective because of the exothermic nature of these processes and consequent operation at lower temperatures, which would be less costly due to lower energy demands. This involves process engineering rather than just designing a suitable catalyst for the selective oxidation.

Alkane activation remains a challenge due to their robust nature. Alkane activation needs to be achieved in a single step at low temperatures and high conversions so as to limit cracking and combustion associated with high temperature reactions. It is important that the conversions are high so as to avoid any recycling of the feed, which is expensive to achieve industrially.

Technological challenges include increasing product selectivity, stereoselectivity, reducing undesirable by-products, minimizing energy consumption and utilizing and controlling exothermicities. There is a need for integration between catalyst and reactor design to meet these challenges.

Terminal activation of the alkane to give alcohols and alkenes has gathered a lot of interest in recent years. The market value of these products has increased through the years due to their shortage and demand for them in the use of detergents and polymers. To synthesise them from cheap feedstocks, such as alkanes, would make economic sense.

Chemical factors that govern reaction rates under heterogeneous conditions are not as well known as those for homogeneous conditions. The compositions, properties or concentrations of reaction intermediates are rarely known. Physical characteristics of the catalyst system, however, and their effects on catalyst performance are better known today. The physical phenomena can guide the choice of catalyst porosity and porous structure, catalyst size and shape and reactor type and size, which are some of the aspects discussed in this thesis.

References

Acevedo, A., Armas, N., Papa, J., Acta Cientifica Venezolana, 53 (Sup. 1), 341 (2002)

Acevedo, A., Armas, N., Papa, J., Conference contribution, Deshidrogenación oxidativa de *n*-pentano sobre catalizadores de VMgO soportados y promovidos galio y antimonio, 52 Convención Anual de AsoVAC, Barquisimeto (2002)

Acevedo, A., Armas, N., Papa, J., López Nieto, J.M., Solsona, B., Conference contribution, Deshidrogenación oxidativa de *n*-pentano sobre catalizadores de VMgO soportados y VMgO promovidos con galio y atimonio, Jornados de Investigación Facultad de Ingeniera, UCV (Jifi2002), Caracas (2002)

Agaskar, P.A., DeCaul, L., Graselli, R.K., Catal. Lett., **23**, 339 (1994)

Ai, M., J. Mol. Catal. A, **114**, 3 (1996)

Albonetti, S., Cavani, F., Trifiro, F., Catal. Rev. Sci. Eng., **38**, 413 (1996a)

Armas, N., Papa, J., López Nieto, J.M., Solsona, B., De Risi, L., Rosillo, C., Conference contribution, Deshidrogenación Oxidativa de *n*-Pentano sobre catalizadores de VMgO soportados y MgVO promovidos, VI Congreso Venezolano de Quimica, Margarita (2003)

Armas, N., Papa, J., López Nieto, J.M., Solsona, B., Acevedo, A., Conference contribution, Oxidative dehydrogenation of *n*-pentane over unsupported or promoted VMgO catalysts, XVIII North American Catalysis Society Meeting, Cancún, Mexico (2003)

Armas, N., Papa, J., Lopez Nieto, J.M., Solsona, B., De Risi, L., Rosillo, C., Conference contribution, *n*-Pentane oxidative dehydrogenation on some VMgO supported or promoted catalysts, 16th International Conference of Chemical and Process Engineering, Prague (2004)

Ashcroft, A.T., Cheetham, A.K., Foord, J.S., Green, M.L.H., Grey, C.P., Murrel, A.J., Vernon, P.D.F., Nature, **344**, 319-321 (1990)

Barthe, P., Blanchard, G., France Pat. 90 12 519 (1990)

Bendandi, A., Fornasari, G., Guidoreni, M., Kubelkova, L., Lucarini, M., Trifirò, F., Top. Catal., **3**, 337 (1996)

Betts, A.T., Uri, N., Makromol. Chem., **95**, 22 (1966)

Bharadwaj, S.S., Schmidt, L.D., Fuel Processing Technology, **42**, 109-127 (1995)

Bhattacharya, D., Bej, S.K., Rao, M.S., Appl. Catal. A: General, **87**, 29 (1992)

Bocuzzi, F., Chiorino, A., Tsubota, S., Haruta, M., Catal. Lett., **56**, 195 (1998)

Bondzie, V.A., Parker, S.C., Campbell, C.T., Catal. Lett., **63**, 143 (1999)

Brady, J.E., Holum, J.R., Chemistry: The study of matter and its changes, John Wiley and Sons Inc., p 626 (1993)

Bricker, J.C., Imai, T., Mackowiak, D., US Patent 4,717,779 (1988)

Brouwer, D.M., Hogeveen, H., Prog. Phys. Org. Chem., **9**, 179 (1972)

Brutovsky, M., Gerej, S., Czechslovak Chem. Commun., **47**, 403 (1982)

Burattini, M., Centi, G., Trifirò, F., Appl. Catal., **32**, 353 (1987)

Burch, R., Crabb, E.M., Appl. Catal. A, **100**, 111 (1993).

Busca, G., Cavani, F., Centi, G., Trifirò, F., J. Catal., **99**, 400 (1986)

Busca, G., Centi, G., J. Am. Chem. Soc., **111**, 46 (1989)

Catalytica, Catalysts for the Elimination of Volatile Organic Compounds: Nanohalogenated Compounds, Environmental Report E4, Catalytica Studies Division, Mountain View, CA, (1993)

Cavani, F., Centi, G., Manenti, I., Riva, A., Trifirò, F., Ind. Eng. Chem. Prod. Res. Dev., **22**, 565 (1983)

Cavani, F., Trifirò, F., Catal. Today, **51**, 565 (1999)

Centi, G., Trifirò, F., J. Mol. Catal., **35**, 255 (1986)

Centi, G., Trifirò, F., Catal. Today, **3**, 155 (1988a)

Centi, G., Trifirò, F., Ebner, J.R., Franchetti, V.M., Chem. Rev., **88**, 55 (1988b)

Centi, G., Lopez Nieto, J., Pinelli, D., Trifirò, F., Ind. Eng. Chem. Res., **28**, 400 (1989)

Centi, G., Golinelli, G., Busca, G., J. Phys. Chem., **94**, 6813 (1990)

Centi, G., Gleaves, J.T., Golinelli, G., Trifirò, F., New Developments in Selective Oxidation by Heterogeneous Catalysis, Studies in Surface Science and Catalysis, Vol. 72, Elsevier Science: Amsterdam, p 231 (1992)

Centi, G., Cavani, F., Trifirò, F., Selective Oxidation by Heterogeneous Catalysis, Kluwer Academic/ Plenum Publishers, p 26 (2001)

Chaar, M.A., Patel, D., Kung, M.C., Kung, H.H., J. Catal., **105**, 485 (1987)

Chang, W.S., Chen, Y.Z., Yang, B.L., Appl. Catal. A., **124**, 221 (1995)

Chao, Z., Ruckenstein, E., J. Catal., **222**, 17 (2004)

ChemDAT® software, MerckKGaA, Darmstadt, Germany (2005)

Choudary, T.V., Goodman, D.W., Top. Catal., **21**, 25 (2002)

Cohn, D.R., Rabinovich, A., Titus, C.H., Int. J. Vehicle Design, **17**, 550 (1996)

Corma, A., Orchillés, A.V., Microporous and Mesoporous Materials, **35-36**, 21 (2000)

Culmann, J.C., Sommer, J., J. Amer. Chem. Soc., **112**, 4057 (1990)

Dadyburjor, D.B., Jewur, S.S., Ruckenstein, E. Catal. Rev.-Sci Eng., **19**, 293 (1979)

de Kerk, A., Ind. Eng. Chem. Res., **43**, 6898 (2004)

de Oliviera, A.L., Wolf, A., Schuth, F., Catal. Lett., **73**, 157 (2001)

Dry, M.E., J. Chem. Tech. and Biotech, **77**, 43 (2002)

Eon, J.G., Olier, T., Volta, J.C., J. Catal., **145**, 318 (1994)

Fărcaşiu, D., Catal. Lett., **71**, 95 (2001)

Fujimoto, K. in: Curry-Hyde, H.E., Howe, R.F. (Eds.), Natural Gas Conversion II, Elsevier, Amsterdam, p 73 (1994)

Galli, A., Lopez Nieto, J.M., Dejoz, A., Vazquez, M.I., Catal. Lett., **34**, 51 (1995)

Gao, X., Ruiz, P. Xin, Q., Guo, X, Delmon, B., J. Catal., **148**, 56 (1994)

Goetsch, D.A., Schmidt, L.D., Science, **271**, 1560 (1996)

Govender, N., Masters thesis, University of Natal, Durban, p 27 (2002)

Govender, N., Friedrich, H.B., Janse van Vuuren, M., Catal. Today, **97**, 315 (2004)

Grasselli, R.K., Proceedings of DGMK Conference, Hamburg, Germany, p 147; La Chimica e l' Industria, **83**, 25 (2001)

Haag, W.O., Dessau, R.M., Proc. 8th Int. Congr. Catal., **2**, 305 (1985)

Harlin, M.E., Niemi, V.M., Krause. A.O.I., Weckhuysen, B.M., J. Catal., **203**, 242 (2001)

Haruta, M., Tsubota, S., Kobayashi, T., Kageyama, H., Genet, M.J., Delmon, B., J. Catal., **144**, 175 (1993)

Haruta, M., J. Catal., **36**, 153 (1997)

Herber, R.R., Thompson, G.J., US Patent 4,806,624 (1989)

Herrington, E.F.G., Rideal, E.K., Proc. Roy. Soc. A., **184**, 431 (1945)

Hickman, D.A., Schmidt, L.D., Science, **259**, 343-346 (1993)

Higgins, R., Hutchings, G.J., U.S. Patent 4 317 777 (1982), assigned to Imperial Chemical Industries

Hodnett, B.K., Catal. Rev-Sci. Eng., **27**, 373-424 (1985)

Hunter, K.C., East, A.L.L., J. Phys. Chem. A, **106**, 1346 (2002)

Hutchings, G.J., Higgins, R., GB Patent 1 601 121 (1981)

Hutchings, G.J., Scurrell, M.S., Woodhouse, J.R., J. Chem. Soc., Chem. Commun., 254 (1988)

Hutchings, G.J., Gold Bulletin, **29**, 124 (1996)

Hutchings, G.J., Scurrel, M.S., Cattech, **7**, 94 (2003)

Imai, T., US Patent 4,418,237 (1983)

Imai, T., Smidt, R.J., US Patent 4,886,928 (1989)

Iordanoglou, D.I., Bodke, A.S., Schmidt, L.D., J. Catal., **187**, 400 (1999)

Ji, Y., Xiang, H.,Yang, J., Xu, Y., Li, Y., Zhong, B., **214**, 77 (2001)

Korili, S.A., Ruiz, P., Delmon, B., Symposium on Heterogeneous Hydrocarbon Oxidation Presented before the Division of Petroleum Chemistry, Inc. 211th National Meeting, American Chemical Society, New Orleans, L.A., p 179 (1996)

Kozhevnikov, I.V., J. Mol. Catal A, **117**, 151 (1997)

Krishnamachari, N., Calvo, C., Can. J. Chem., **49**, 1630 (1971)

Krummenacher, J.J., West, K.N., Schmidt, L.D., J. Catal., **215**, 332 (2003)

Krummenacher, J.J., Schmidt, L.D., J. Catal., **222**, 429 (2004)

Kung, M.C., Kung, H.H., J. Catal., **134**, 668 (1992)

Kung, H.H., Michalakos, P., Owens, L., Kung, M., Anderson, P., Owen, O., Jahan, I., J. Amer. Chem. Soc., 389 (1993)

Kung, H.H., Kung, M.C., Appl. Catal. A, **157**, 105 (1997)

Labinger, J.A., Nature, **417**, 507 (2002)

Lancaster, S.J., http://www.chemsoc.org/timeline/pages/1823.html

Lee, E.H., Catal. Rev. Eng. Sci., **8**, 285 (1973)

Lemonidou, A.A., Stambouli, A.E., Appl. Catal. A: General, **171**, 325 (1998)

Lozana-Calero, D., Bruque, S., Aranda, M.A.G., Martinez-Lara, M., Moreno, L., J. Solid State Chem., **103**, 481 (1993)

Lunsford, J.H. in: Curry-Hyde, H.E., Howe, R.F. (Eds.), Natural Gas Conversion II, Elsevier, Amsterdam, p 1 (1994)

Maitra, A.M., Appl. Catal. A, **104**, 11 (1993)

Mavrikakis, M., Stoltze, P., Nørskov, J.K., Catal. Lett., **64**, 101 (2001)

Michalakos, P.M., Kung, M.C., Jahan, I., Kung, H.H., J. Catal., **140**, 226 (1993)

Mikovsky, R.J., Silvestri, A.J., Dempsey, E., Olson, D.H., J. Catal., **22**, 374 (1971)

Moffat, J.B., Appl. Catal. A, **146**, 65 (1996)

Olah, G.A., Molnar, A., Hydrocarbon Chemistry, Wiley, New York (1995)

Ono, Y. in: Thomas, J.M., Zamaraev, K.I. (Eds.), Perspectives in Catalysis, Blackwell Scientific, Oxford, p 431 (1992)

Olah, G.A., Halpern, Y., Stein, J., Mo, Y.K., J. Amer. Chem. Soc., **95**, 4960 (1973)

Olah, G.A., Molnar, A., Hydrocarbon Chemistry, Wiley, New York (1995)

Ovsitser, O. Y., Davydov, A., Osipova, Z.G., Sokolovskii, V.D., React. Kinet. & Catal. Lett., **38**, 125 (1989)

Owens, L., Kung, H.H., J. Catal., **144**, 202 (1993)

Oyama, S.T., Somorjai, G.A., J. Phys. Chem., **94**, 5922 (1990)

Oyama, S.T., Desikan, A.N., Hightower, J.W., Catalytic Selective Oxidation (Oyama, S.T. & Hightower, J.W., eds.), ACS Symposium Series 523, American Chemical Society, Washington DC, Chapter 1, p 1, (1993)

Panizza, M., Resini, C., Busca, G., Lopez., E. F., Escribano, V.S., Catal. Letters, **89,** 199 (2003)

Parmaliana, A., Sokolovskii, V., Miceli, D., Arena, F., Giordano, N., J. Catal., **148**, 514 (1994)

Patel, D., Kung, M.C., Kung, H.H., Proceedings 9th International Congress on Catalysis, Chemical Institute of Canada, Toronto, p 1554 (1988)

Pepera, M.A., Callahan, J.L., Desmond, M.J., Millberger, E.C., Blum, P.R., Bremer, N.J., J. Amer. Chem. Soc., **107**, 4883 (1985)

Perry, R.H., Green, D.W., Perry's Chemical Engineers' Handbook, The McGraw Hill Companies, Section 26, p 54 (1999)

Petrucci, R.H., Harwood, W.S., Herring, F.G., General Chemistry: Principles and Modern Applications, 8th edition, Prentice-Hall Inc., p 273 (2002)

Pitkethly, R.C., Steiner, H., Trans. Faraday Soc., **35**, 979 (1939)

Pitz, W.A., Westbrook, C.K., Combus. Flame, **63**, 113 (1986)

Poladi, R.H.P.R., Landry, C.C., Microporous and Mesoporous Materials, **52**, 11 (2002)

Roy, M., Gubelmann-Bonneau, M., Ponceblanc, H., Volta, J.C., Catal. Lett., **42**, 93 (1996)

Rybarczyk, P., Berndt, H., Radnik, J., Pohl, M. M., Buyevskaya, O., Baerns, M., Brückner, A., J. Catal., **202**, 45 (2001)

Sakurai, Y., Suzaki, T., Nakagawa, K., Ikenaga, Na-oki, Aota, H., Suzuki, T., J. Catal, 209, **16** (2002)

Sananés-Schulz, M.T., Tuel, A., Hutchings, G.J., Volta, J.C., J. Catal., **166**, 388-392 (1997)

Scherzer, J., Catal. Rev.-Sci. Eng., **31**, 215 (1989)

Schmidt, L.D., Klein, E.J., Leclerc, C.A., Krummenacher, J.J., West, K.N., Chem. Eng. Sci., **58**, 1037 (2003)

Sheldon, R.A., Kochi, J.K., Metal-Catalysed Oxidations of Organic Compounds, Academic Press, New York (1981)

Skotak, M., Karpiński, Z., J. Chem. Eng., **90**, 89 (2002)

Slinkadt, W.E., Degroot, P.B., J. Catal., **68**, 423 (1981)

Sookraj, S.H., Engelbrecht, D., Confidential Report Number 290/97, Sastech R&D Applied Catalysis Research, p 24 (1997)

Sookraj, S.H., Engelbrecht, D., Catal. Today, **49**, 161 (1999)

Steiner, H., J. Amer. Chem. Soc., **67**, 2052 (1945)

Stinson, S.C., Chem. Eng. News, **79**, 77 (2001)

Sugiyama, S., Hashimoto, T., Shigemoto, N., Hayashi, H., Catal. Lett., **89**, 229 (2003)

Thomas, J.M., Raja, R., Sankar, G., Bell, R.G., Nature, **398**, 227 (1999)

Thomas, J.M., Thomas, W.J., Principles and Practice of Heterogeneous Catalysis, VCH Publishers Inc., p 4 (1996)

Thompson, M.R., Hess, A.C., Nicholas, J.B., White, J.C., Anchell, J., Ebner, J.R., New Developments in Selective Oxidation II, p 167 (1994)

Valden, M., Pak, S., Lai, X., Goodman, D.W., Catal. Lett., **56**, 7 (1998)

Védrine, J.C., Top. Catal., **21**, 100 (2002)

Ven'yaminov, S.A., in Mechanism and Kinetics of Catalytic Processes, Institute of Catalysis, Novosibirsk, p 107 (1977)

Weng, L.T., Ruiz, P., Delmon, B., New Developments in Selective Oxidation by Heterogeneous Catalysis, Elsevier, Amsterdam, p 399 (1991)

Wenig, R.W., Schrader, G.L., J. Phys. Chem., **91**, 5674-5680 (1987)

Wojciechowski, B.W., Corma, A., Catalytic Cracking: Catalysts, Chemistry and Kinetics, Dekker, New York (1986)

Wolf, A., Schüth, F., Appl. Catal. A: General, **226**, 1 (2002)

Zazhigalov, V.A., Konovalova, N.D., Zaytzev, Yu. P., Belousov, V.M., Stoch, J., Krupa, R., Haber, J., Ukr. Khim. Zhurn., **53**, 1145 (1987)

Zazhigalov, V.A., Haber, J., Stoch, J., Komashko, G.A., Pyatniskaya, A.I., Bacherikova, I.V., New developments in selective oxidation II, Studies in surface science and catalysis, vol. 82, Elsevier science, Amsterdam, p 265 (1992)

Zazhigalov, V.A., Haber, J., Stoch, J., Pyatnitzkaya, A.I., Komashko, G.A., Belousov, V.M., Appl. Catal. A: General, **96**, 135 (1993)

Zemal, R.Z., Vekemans, J.A., GB Patent 1 475 309 (1977)

Zhang, Z., Verykios, X.E., Baerns, M., Catal. Rev. Sci. Eng., **36**, 507 (1994)

CHAPTER 2

CATALYST AND REACTOR

2.1 Introduction

This Chapter is a review of fundamental aspects of a catalyst in terms of active site distribution, oxygen activation, interaction of phases in a catalyst, catalyst promotion and acid/base properties. How do these factors influence the oxidation of alkanes? These fundamental aspects are considered with respect to the activity of the VPO and VMgO catalysts, looking into selective vs. over-oxidation and the effect of catalyst promotion on selective alkane conversion. The design of fixed-bed continuous flow micro-reactors for heterogeneous catalysis is reviewed. The effects of heat and mass transfer, flow patterns, particle size of the catalyst and inert packing material on the catalysis are discussed.

Catalytic technologies continue to advance rapidly, driven by strong economic pressures to improve the selectivity, activity, lifetime and cost of catalysts. More selective, active and durable catalysts have a large impact, not only on feedstock utilization, but also on overall plant capital and operating economics. Catalyst research activities are divided between those aimed at new catalyst-process combinations and those aimed at new or improved catalysts for existing processes.

A catalyst designed and tested in the laboratory is somewhat different when used commercially. A complexity arises from the inclusion of dopants, selectivity enhancers, structure stabilizers, dispersion stabilizers etc. for industrial application.

Besides high activity and selectivity, a good catalyst possesses long-term stability. Classification of the catalyst according to structural type is somewhat arbitrary; however, emphasis is placed on the atomic structure of the most active constituent. The catalysts may also be classified according to bond types or electronic properties. Catalysts are even separated into metals or semiconductors or insulators, which is a valuable classification for photo-catalytic

processes. Division of catalysts according to their acid-base or redox properties is another basis of classification.

Poor selectivity in alkane oxidation can be the result of secondary oxidation. The likelihood of further reactions is enhanced if the products of the primary catalytic reactions are more reactive than the reactants. When the conversion of reactants to products is over 20 %, the product distribution usually includes the products of secondary reactions (Dwyer, D. J. *et al.* (1978)). Thus it is ideal to carry out catalytic investigations at low temperatures to give conversions of 10 % and lower to gain a better understanding of the catalysis that gives primary products.

Metals have many binding sites, where simultaneous bonding of substrates to many metal atoms is possible, which make them good catalysts. Bonding can occur on both the topmost atomic layer and the layer beneath. Thus metals can catalyse a sequence of complex reactions that begin with dissociative adsorption, followed by complex rearrangements through the formation and breaking of multiple bonds, and finally desorption of the products. The high density of reaction sites on the surface of the metal makes it active and versatile in catalyzing many reactions. The disadvantage of this is that a diverse number of competing reactions can occur with little selectivity to a desired reaction pathway.

Catalytic reactions may be grouped into three categories viz. (i) those that occur directly on the metal surface, (ii) reactions that occur on top of a strongly bound layer of adsorbates in the second layer and (iii) reactions that occur on coadsorbate-modified surfaces. A brief discussion of each follows:

Catalytic reactions on metal surfaces usually involve strongly adsorbed intermediates and are surface structure sensitive. Atomically rough surfaces usually exhibit the highest turnover rates (Spencer, N.D. *et al.* (1982)). Atomic steps and kinks give rise to rough surfaces. Smaller particles usually have a higher concentration of kinks and steps. Kinked sites in platinum single-crystal studies proved to be centres of strong hydrogenolysis (C-C bond breaking) activity (Davis, S. M. (1984)).

Catalytic reactions on top of a strongly adsorbed overlayer are usually structure insensitive because they do not occur directly on the metal surface. Strongly adsorbed overlayers usually cover the metal and thus the incoming reactants cannot form strong metal-adsorbate bonds. An organic overlayer may form and serve as a template to orient and align the reactants. Reactions of this type usually occur at temperatures below 400 K and can be likened to hydrogenation processes (Davis, S. M. (1984)).

The location and bonding of an adsorbed molecule is altered when another molecule or atom co-adsorbs with it. The relatively weak interactions of benzene and carbon monoxide when co-adsorbed on platinum or rhodium demonstrate this (Somorjai, G.A. *et al.* (1985)). Benzene forms a disordered monolayer over Pt in the absence of CO. When CO is introduced, several ordered structures form. These structures change depending on the CO:benzene ratio on the Pt surface. The ordering of benzene is facilitated by the weak attractive interaction with CO that also blocks certain alternative adsorption sites. The coadsorbed molecules may be viewed as surface modifiers and they have profound influence on the structure and distribution of the bonding sites and also on the nature of the chemical bond that the reactants form with the catalyst surface. Coking of catalysts is common in oxidative dehydrogenation reactions of alkanes due to the formation of alkenes and cyclic compounds, which can polymerize on the surface of the catalyst and this layer of material may catalyse the reaction (Bhasin, M.M. *et al.* (2001)).

2.2 Mixed metal oxide catalysts

2.2.1 Fundamental aspects of a selective oxidation catalyst

A number of fundamental aspects need to be considered in order to link a catalyst structure to its activity. Some of these aspects are reviewed here and associated with the VPO and VMgO catalysts in the latter part of this Chapter.

One of the key components to selective hydrocarbon oxidation was identified as lattice oxygen. The importance of lattice oxygen was recognized by a team at BP America in the early

1950s (Callahan, J.L. *et al.* (1963)). They postulated that lattice oxygen of a reducible metal oxide might serve as a more versatile and more selective oxidizing agent than gaseous dioxygen. When lattice oxygen, O^{2-}, on the surface of a reducible catalyst is exposed to a reductant e.g. but-1-ene, one lattice oxygen removes two hydrogens from the butene molecule, producing one molecule of butadiene and one molecule of water, and thereby creating one anion vacancy on the surface of the catalyst. This anion vacancy is filled by migration of the surrounding lattice oxygens. The catalyst is then re-oxidised by dioxygen from the gaseous phase, to reconstitute the original fully oxidized state of the catalyst.

The host structure must be able to accommodate anion vacancies, that form from reduction, without structural collapse, and be capable of rapid electron transfer and lattice oxygen diffusion. The redox cycle is well illustrated in the oxidation of propylene to acrolein (Grasselli, R.K. (1986)).

The reduction of the metal oxide proceeds as follows:

$$M^{n+}O^{2-}{}_{1/2(n)} + CH_2{=}CHCH_3 \longrightarrow M^{(n-x)}{+}O^{2-}{}_{1/2(n-x)} + CH_2{=}CHCHO + H_2O \qquad (2.1)$$

where n=valence of the metal and x=number of lattice oxygens $[O^{2-}]_L$ removed from the metal oxide by the oxidation of the hydrocarbon.

Reoxidation of the metal oxide then occurs:

$$M^{(n-x)+}O^{2-}{}_{1/2(n-x)} + O_{2(g)} \longrightarrow M^{n+}O^{2-}{}_{1/2(n)} \qquad (2.2)$$

The overall catalytic reaction being:

$$CH_2{=}CHCH_3 + O_{2(g)}\text{-catalyst} \longrightarrow CH_2\text{-}CHCHO + H_2O \qquad (2.3)$$

Propylene is oxidized to acrolein by the metal oxide in reaction 2.1, whereby lattice oxygen of the metal oxide is the oxidizing agent and the metal oxide was reduced in the process. The anion vacancies thus created in reaction 2.1 of the reduced metal oxide can concurrently be replenished by the lattice oxygen of adjacent fully oxidized sites on the catalyst.

Lattice oxygen is involved in the catalytic process (Keulks, G.W. (1970)). This was verified by $^{18}O_2$ experiments. When $^{18}O_2$ and propylene are co-fed over Bi-molybdate catalysts, ^{16}O-acrolein and ^{18}O-acrolein forms. The relative concentration of ^{18}O-acrolein to ^{16}O-acrolein increases with time on stream. The author also showed that the dioxygen generally dissociates at a site different to that of the catalytically active one. There is a tendancy for the dissociated dioxygen to get incorporated into the lattice of the catalyst and move in the direction of the reduced active site and the anion vacancies concurrently move towards the oxygen dissocation site. Chang, W.S. *et al.* (1995) and Lopez-Nieto, J.M. *et al.* (1999) confirmed that in the absence of oxygen, the catalytic activity sharply decreases with a decrease in the amount of available lattice oxygen.

The active sites of catalysts usually perform various functions in the catalytic cycle such as chemisorption of the substrate, abstraction of hydrogen from the substrate, insertion of oxygen into the activated substrate and desorption of the product.

The above is synonymous with the Mars and van Krevelen mechanism (Fig. 2.1).

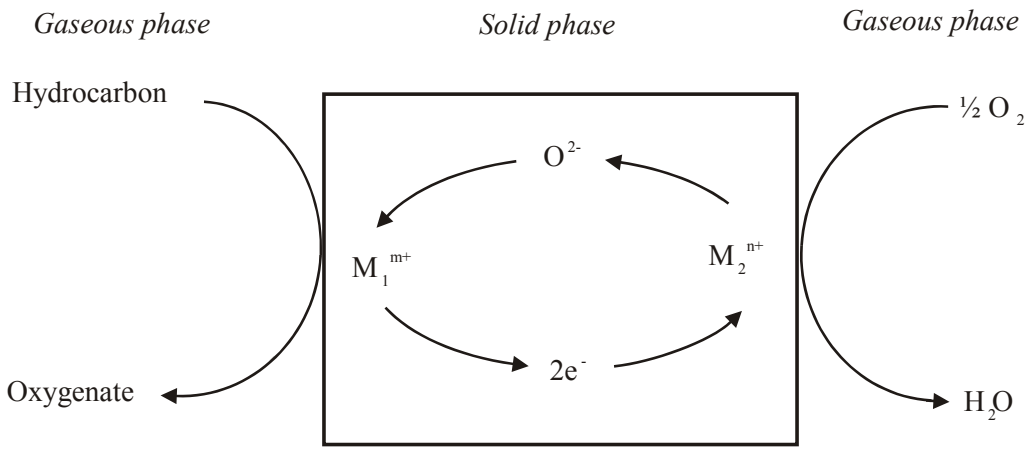

Fig. 2.1 Mars and van Krevelen mechanism (adapted from Mars, P. et al. (1954))

There are three essential properties a catalyst should possess in order to obey a Mars and van Krevelen mechanism: (i) contain a feasible redox couple at the operating temperature, which is possible with transition metal ions, (ii) exhibit high electrical conductivity to favour electron transfer and (iii) have a high lattice oxygen anion mobility within the material to ensure the re-oxidation of the reduced catalyst.

According to this mechanism, the substrate is oxidized by the solid and not directly by molecular oxygen of the gaseous phase. The role of dioxygen is to regenerate or maintain the oxidized state of the catalyst. The oxygen species introduced in the substrate from the lattice is in an oxidation state of -2.

The regeneration of the reduced metal oxide catalyst must be faster than its reduction for the catalyst to perform efficiently.

The metal oxygen bond needs to be of intermediate strength under reaction conditions for effective oxidation of the hydrocarbon, since lattice oxygen is responsible for oxidation of the substrate (Callahan, J.L. *et al.* (1963)). If the metal-oxygen bond is too strong, no reaction will occur, if it is too weak, over-oxidation will occur, leading to undesired waste products. Intermediate metal oxide bonds are usually covalent and amphoteric in nature, e.g. molybdates, antimonates and vanadates.

The selectivity of a product can be categorized by two factors, viz. how many oxygen atoms are incorporated into the reactant and where in the molecule they are incorporated. The number of oxygen atoms that are incorporated into a substrate is determined by (i) the residence time of the molecule on the surface, (ii) the number of oxygen atoms available at the active site during the residence of the molecule on the surface and (iii) the reactivity of the oxygen at the active site. The number of oxygen atoms at the active site may be affected by the diffusivity of the lattice oxygen as well as the atomic arrangement of the active site and the size of the surface species with respect to the size of the site (Morooka, Y. *et al.* (1967)).

Callahan, J.L. *et al.* (1963) claimed that good selectivity from a catalyst is determined by spatial isolation of the reactive surface lattice oxygens in defined groups. A defined group or

domain is a group of adjacent surface lattice oxygens. The number of oxygen atoms in the domain determines the selectivity to valuable products or over-oxidation products. For example, for the partial oxidation of propylene, 2-5 surface oxygens in the domain are required to obtain the desired acrolein product. If there are more than 5 oxygens in the domain, then over-oxidation products are obtained. Completely isolated single oxygens would either be inactive or could produce allyl radicals that could couple in the vapour phase to give hexadiene and ultimately benzene. Recently there have been numerous reports of selective oxidation catalyst examples conforming to the site isolation principle (Thomas, J.M. (2001); Volta, J.C. (2001)).

A single host structure may not be best suited to carry out key catalytic functions sometimes and hence a concert of phases may be employed to obtain the desired catalytic reaction. These phases need to be brought into intimate proximity to each other so they can interact with each other (Grasselli, R.K. (1997)).

With the advances in characterization techniques, it is possible to identify less than one-hundredth of a monolayer of adsorbed material on a solid surface area of a catalyst of less than 1 cm^2. Oxidation states of surface atoms, their steady state concentrations, as well as their spatial distributions can be determined for model catalysts, but not usually for their real life analogues. However, it is difficult to probe the transition states directly, in view of their exceptionally short lifetimes. The lifetime of an intermediate species in heterogeneous catalysis exceeds 10 μs, however, the electronic and atomic rearrangement generally involve a much more rapid timescale, of the order of pico- or femto-seconds.

Preferential adsorption on a catalyst surface usually takes place at those atoms situated at peaks, fissures and other topographical discontinuities. It was also implied that such atoms would have higher catalytic activity than those on flat surfaces. The active site could be described as the locus of catalytic conversion or the site at which adsorption is strongest. The former is more befitting because the active site for chemisorption is by no means the most favourable site for facile chemical conversion (Bowker, M. (1998)).

The effect of acido-base catalyst properties on the activation of hydrocarbons depends on both the nature of the oxide and the nature of the hydrocarbon, even within the same class of hydrocarbons (Chaar, M.A. *et al.* (1988), Eon, J.G. *et al.* (1994)). For different hydrocarbons, the chemistry of the transformation is the same, but the pathway of transformation may be different owing to the activation of different carbons on the alkane chain and the different stabilities of intermediate species formed. There is general agreement in the literature that the rate-determining step in alkane conversion is the breaking of the first C-H bond of the alkane leading to the formation of an alkyl species (Michalakos, P.M. *et al.* (1993)). There are various possibilities for the generation of this species. Breakage of the C-H bond can be homolytic with the formation of a propyl radical (Burch, R. *et al.* (1991)). This radical species transforms into an alkene either after desorbing in the gas phase and reacting with other gas phase molecules or via a surface reaction (Chang, Y. *et al.* (1993)). The relative rates of the two competitive routes depend on both the nature of the catalyst, especially the reducibility, and the reaction temperature (Burch, R. *et al.* (1993)). Low temperatures and reducible catalysts promote the surface reaction route, in which the second proton abstraction occurs by the OH^- species created in the first H abstraction step, with the generation of a water molecule. A more likely mechanism is where a neighbouring basic oxygen on the catalyst surface abstracts a second proton from the alkane and there is subsequent shift of hydrogen from this OH^- species created to the one created in the initial proton abstraction from the alkane. A water molecule is thus generated. The basic character of the lattice oxygen and associated OH^- species determines the rates of reaction. Busca, G. *et al.* (1986) suggested the heterolytic splitting of the C-H bond, with the formation of a carbocation by hydride abstraction, which takes place with strong basic catalysts. The activity trend may be correlated to the stability of carbocations, with the methyl group being the least reactive:

Benzyl ≈ allyl > *tert*-butyl > isopropyl > ethyl > methyl

This sequence suggests a relationship between the rate of the first C-H breaking and Lewis acidity of the catalyst. This relationship was demonstrated for butane oxidation over vanadia-based catalysts (Busca, G. *et al.* (1994)). Sokolovskii, V.D. (1990) suggested that nucleophilic oxygen on the catalyst surface abstracts a proton from the hydrocarbon substrate and a carbanion is formed which is stabilized on the catalyst surface.

Redox equilibria occur on the surface of a catalyst irrespective of whether the activation is homolytic or heterolytic. The position of the equilibrium depends on the acid-base properties of the catalyst and the reaction conditions such as temperature and reaction atmosphere.

To obtain a selective oxidation product, it is necessary for the product to desorb relatively easily from the catalyst surface to reduce the possibility of any further transformation. Mixed metal oxide catalysts, which have an acidic catalytic surface, are good for the synthesis of acid products from an alkane (Busca, G. *et al.* (1996)). In some cases where both the reactant and the final product are strong acids (e.g. isobutyric acid to methacrylic acid) very strong acidic catalysts such as heteropolyacids are required (Okuhara, N. *et al.* (1996)).

Alkenes are more basic than alkanes. Catalysts for alkene synthesis from alkanes need a basic surface to assist in alkene desorption as well as prevent their oxidative degradation by Brønsted acid sites. Selective alkene production from alkanes is usually promoted by the incorporation of alkaline metals in the catalyst.

All catalytic reactions occur on the exterior and interior surfaces of porous solid catalysts. The larger the amount of surface area accessible to the reactants, the higher the conversion of the reactant. Metal catalysts can be dispersed on the surface of a suitable porous support. This enhances exposure of the catalytic surface, which can promote activity of the catalyst, however, metal oxide catalysts often have a sufficiently high surface area and open pore structure for them to be employed directly.

If the pores of the catalyst material or support are sufficiently wide not to impede the passage of reactants or products and the internal surface evenly distributed with active sites, then the rate of conversion of reactants to products is directly proportional to the specific

surface area. Some sites on the catalyst, however, are more active than others in the conversion of the reactant. This can be attributed to the heterogeneity in the distribution of the active sites on the catalyst surface. This results in deviation from direct proportionality of conversion of reactants and specific surface area.

A support or promoter may either increase the surface area available for adsorption and subsequent reaction or it may increase the catalyst activity per unit surface area. The surface area of a catalyst is important in predicting the performance of the catalyst. The pore structure of the catalyst is another major contributing factor to its performance. The distribution of pore sizes in a given catalyst preparation may be such that some of the internal surface area is completely inaccessible to large reactant molecules and may restrict the rate of conversion to products by impeding the diffusion of reactants and products through the porous medium. The actual mode of transport within the porous structure will depend largely on the average pore radius and the conditions of pressure within the reactor.

The reaction of a reactant and an oxidant are proposed in the literature to take place on the surface of a catalyst via two general mechanisms viz. the Langmuir-Hinshelwood and Eley-Rideal mechanisms (Bowker, M. (1998)). There are two distinct mechanisms by which gas phase reactants A and B can be transformed on the surface of a catalyst to product C: either both species are attached to the surface and atomic rearrangement takes place in the resulting adsorbed layer (according to the Langmuir-Hinshelwood mechanism) or only one of them is bound and is converted to product when the other impinges upon it from the gas phase (according to the Eley-Rideal mechanism) (Fig. 2.2).

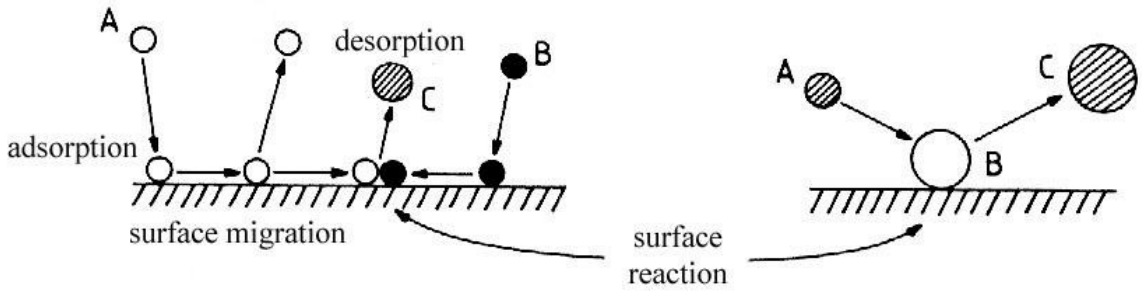

Fig. 2.2 The Langmuir-Hinshelwood mechanism (left) and the Eley-Rideal mechanism (right) (modified from Thomas, J.M. et al. (1996))

The catalyst surface can be reconstructed due to rearrangement of the outermost layers upon adsorption of the reactant molecules. The ideal surface structures of the high symmetry planes of face-centred cubic and body-centred cubic metals would hence not be seen anymore from crystallographic studies. At elevated temperatures there is motion of exposed atoms of the catalyst about their time-averaged positions. Catalysts are thus not rigid entities during a reaction.

Equilibrium distribution of the adsorbate between the surface of the adsorbent and the gas phase is dependant on pressure, temperature, the nature and area of the adsorbent and the nature of the adsorbate. An adsorption isobar shows how the amount adsorbed varies with temperature at constant pressure (Fig. 2.3). There is a general decrease in adsorption with increasing temperature. The fluctuation in the adsorption vs. temperature curve is attributed to equilibration during adsorption and desorption of the adsorbate. The desorbed species may then react homogeneously.

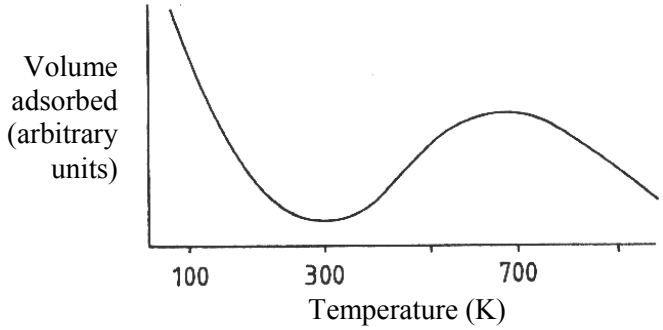

Fig. 2.3 Schematic illustration of an adsorption isobar on the surface of a catalyst (Thomas, J.M. et al. (1996))

2.3 The VMgO and VPO catalyst systems

The selective oxidation of *n*-butane to maleic anhydride (MA) on a VPO catalyst is a well studied reaction in heterogeneous catalysis (Centi, G. *et al.* (1984), Birkeland, K.E. *et al.* (1997), Sookraj, S.H. *et al.* (1999), Centi, G. *et al.* (2001)). Monsanto operated the first commercial process in 1974 using a VPO catalyst for the selective oxidation of *n*-butane to MA (MA) (Ebner, J.R. *et al.* (1988)). There are two main synthetic routes in the literature to obtain

the VPO catalyst viz. the aqueous route where aqueous HCl is used as a reductant and the organic route where an organic solvent is used as the reductant (Overbeek, R.A. *et al.* (1994), Hutchings, G.J. *et al.* (1994)). The organic route to synthesising the catalyst was chosen in work carried out in this thesis, since the catalyst prepared by this route is more active and stable under catalytic conditions (Hutchings, G.J. *et al.* (1994)).

The VPO catalytic system for the conversion of *n*-butane to MA is a catalytically efficient system, and the alkane feedstock is environmentally friendly relative to most feedstocks in the market where the product is a C_4 compound obtained from a C_4 feed. The catalyst not only makes the process environmentally friendly but also highly selective. A proposed mechanism for this highly selective oxidation of *n*-butane over the VPO catalyst appears in Chapter 1.

The VMgO catalytic system was also investigated in work carried out in this thesis. Kung, H.H. *et al.* (1993) reported on the conversion of *n*-butane and cyclohexane to alkenes over a VMgO catalyst. It was reported in the literature that the catalyst gives mainly dehydrogenation products (Michalakos, P.M. *et al.* (1993), Patel, D. *et al.* (1988), Bhattacharya, D. *et al.* (1992)).

The VPO and VMgO catalysts are composed of a reducible transition metal oxide, which activates the alkane at much lower temperatures than catalysts composed of alkali and alkaline earth ions and metal oxides. The phosphorous and magnesium coordinate differently to the vanadium and oxygen in the different catalysts. This difference gives different phases, which are responsible for different kinds of oxidative dehydrogenation reactions (very oxidizing in the case of the VPO catalyst and mildly oxidizing in the case of the VMgO catalyst). These phases determine how selective the catalysts are in oxidation reactions. This section deals with these phases and their role in catalysing reactions with alkanes, focusing on structure-activity relationships.

2.2.2 Catalyst phase and interaction with an alkane

The rate limiting step in alkane oxidation is the breaking of the first C-H bond (Centi, G. *et al.* (1984)). As the chain length of the alkane increases, the rates of reaction on the catalyst increase because the strength of the C-H bonds decrease. Thus *n*-octane is more reactive on the catalyst surface than alkanes that precede it in the homologous series (Centi, G. *et al*. (2001)). There is also a higher statistical chance of multiple activation due to the number of bonds when C>6.

The selectivity to a desired product over an oxidation catalyst can be categorized by two factors viz. how many oxygen atoms are incorporated into the reactant and where in the molecule they are incorporated (Graselli, R. *et al.* (1980)). These two factors are controlled by the number of oxygen atoms available at the active site, the size of the site and the surface intermediate and the reactivity of the oxygen.

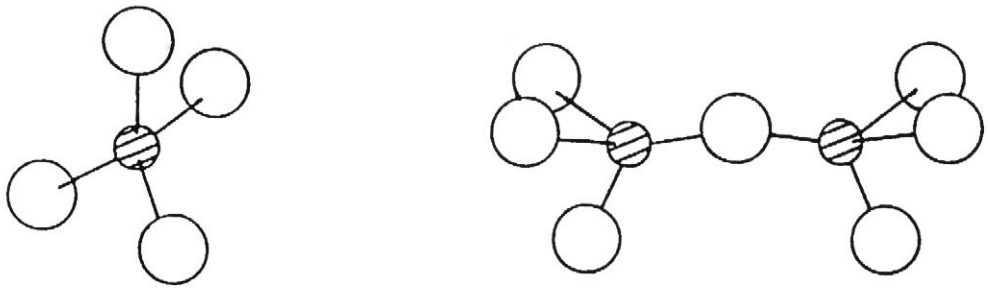

Fig. 2.4 Left: VO_4 unit in $Mg_3(VO_4)_2$ (orthovanadate phase). Right: V_2O_7 unit in $Mg_2V_2O_7$ (pyrovanadate phase). The open circles are oxygen ions and the filled circles are vanadium ions (Graselli, R. et al. (1980))

The active site in the $Mg_3(VO_4)_2$ catalyst consists of a MO_4 tetrahedron, whilst the $Mg_2V_2O_7$ catalyst contains the M_2O_7 unit, which consists of two corner-sharing MO_4 tetrahedra (Fig. 2.4). The reactivity of the lattice oxygen in these sites can be represented by the heat of removal of the lattice oxygen. This heat increases with the increasing number of oxygen atoms removed from the site. If each of these two catalysts adsorbs one surface intermediate species, the intermediate will be able to take up a larger number of oxygen atoms from the M_2O_7 site

than from the MO_4 site. Thus the oxide with the M_2O_7 site will be less selective than the one with the MO_4 sites.

Looking at the available oxygen in the V_2O_8 unit of the $(VO)_2P_2O_7$ catalyst (Fig. 2.5), it can be suggested that this species will offer more oxygen to the surface intermediate than the M_2O_7 unit of $Mg_2V_2O_7$, thus rendering the catalyst less selective. This was seen by comparing the VMgO catalyst (with an orthovanadate active phase) (Chaar, M.A. *et al.* (1987)) and the VPO catalyst (with a pyrovanadate active phase) ((Busca, G. *et al.* (1986), Igarashi, H. *et al.* (1993), Okuhara, T. *et al.* (1993), Ebner, J.R. *et al.* (1993)). The VMgO catalyst gave predominantly dehydrogenation products and very little oxygenates, whilst oxygenates were favoured over the VPO catalyst with very few dehydrogenation products from C_{2-4} alkane oxidation (Michalakos, P.M. *et al.* (1993)).

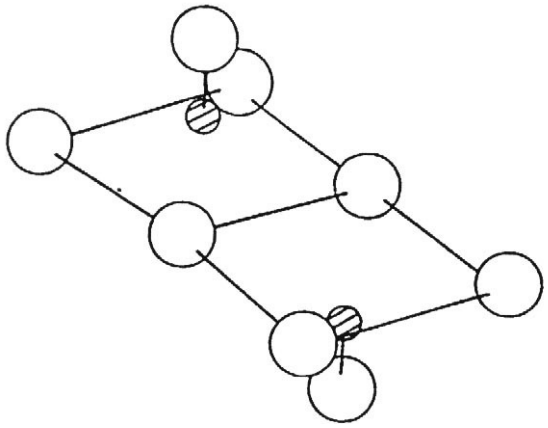

Fig. 2.5 V_2O_8 unit in $(VO)_2P_2O_7$ (pyrovanadate phase). The open circles are oxygen ions and the filled circles are vanadium ions (Graselli, R. et al. (1980))

Bielanski, A. (1991) reported that the position at which the oxygen on the catalyst surface reacts with the surface intermediate is determined by electron density of the oxygen. A nucleophilic oxygen species will attack the carbon atom to form C-O bonds, whereas an electrophilic oxygen species will attack the region of high electron density of the molecule such as the C=C bonds, leading to breaking of the carbon skeleton and eventually to degradation products.

Catalyst reducibility is an important factor in oxidative dehydrogenation. Oxygen anion vacancies are generated on the surface of the catalyst during the oxidation process. These vacancies can be replenished by migration of oxygen ions from nearby positions in the lattice, where the rate of this process is dependant on the surface residence time of the hydrocarbon species (Kung, H.H. *et al.* (1997)). The catalyst surface can be modified by extraction of a second or more lattice oxygens. The local creation of more than one oxygen vacancy is energetically unfavourable unless surface reconstruction occurs rapidly. When two or more lattice oxygens get incorporated into a hydrocarbon, carbon oxide production is usually favoured.

Vanadyl pyrophosphate ($(VO)_2P_2O_7$) is an acidic catalyst. Alkenes, which are basic in nature, will not be easily released from the surface of the VPO catalyst because of the acid base interaction and thus further transformation of this product takes place (giving secondary products). The addition of magnesium oxide (MgO), which contains an alkaline metal, to V_2O_5 generally gives more selective alkene production, related to a decrease in activity of the V_2O_5 species (Siew Hew Sam, D. *et al.* (1990), Patel, D. *et al.* (1990), Corma, A. *et al.* (1993), Bhattacharya, D. *et al.* (1992)). This modification of the V_2O_5 is not simply a change from acidic properties to basic properties, but there is also a change in the reducibility of vanadium and the coordination in the catalyst.

The nature of the alkane together with the nature and reactivity of the catalyst influences the selectivity to alkenes. The selectivity to corresponding alkenes from ethane, propane and butane oxidation on unsupported V_2O_5 is dependant on the chainlength of the hydrocarbon (Fig. 2.6).

The nature of the alkane not only has significant effect on the selectivity at equal conversion, but also influences the rate of decrease in selectivity with increasing conversion for oxidation catalysts (Owens, L. *et al* (1993), Oyama, S.T. *et al.* (1990)).

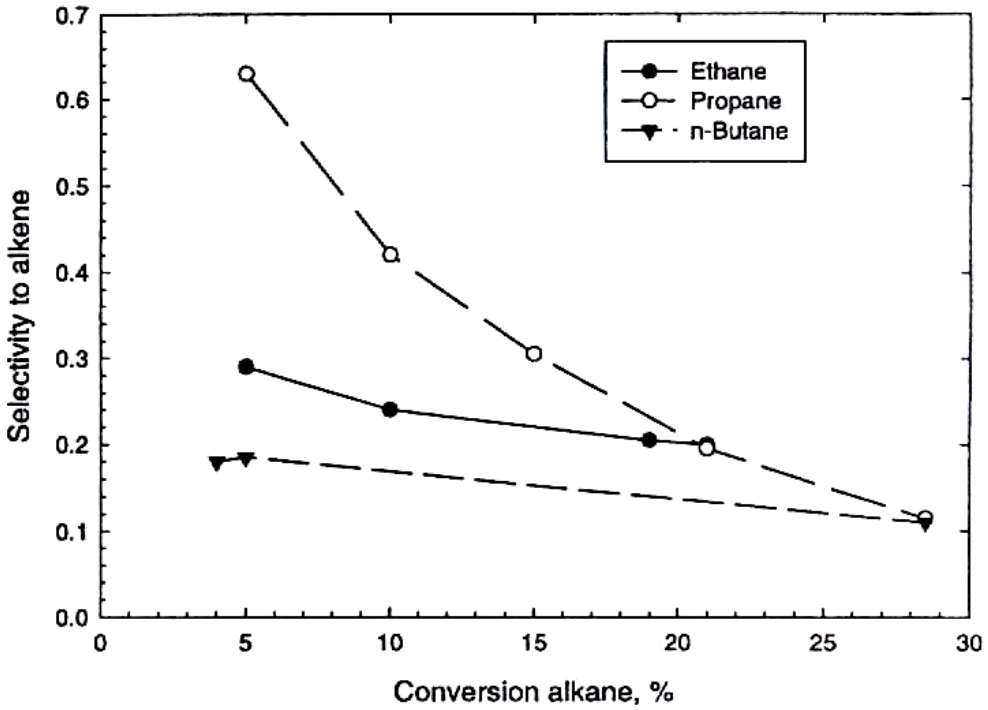

Fig. 2.6 Selectivity to the corresponding alkenes from ethane, propane and butane on unsupported V_2O_5 vs. conversion of the alkanes (Owens, L. et al. (1993))

Kung *et al.* (1997) investigated the selectivity-determining step for alkane oxidation over VPO catalysts, which is different from the rate-determining step. They explained that an adsorbed alkyl is the first intermediate. Depending on the surface VO_x units interacting with the adsorbed alkyl, size of the adsorbed hydrocarbon, rate of re-oxidation of the vanadium active centre and the type of catalyst, the reaction can be selective or proceed to carbon oxides.

The three types of vanadium magnesium oxide phases present in a VMgO catalyst are magnesium orthovanadates, magnesium pyrovanadates and magnesium metavanadates. In magnesium orthovanadate, where the VO_4 units are isolated from each other, adsorbed ethyl, propyl or butyl species can only interact with one surface VO_4 unit. With each VO_4 unit supplying a certain number of oxygen atoms to react with an adsorbed hydrocarbon molecule, the reaction of these alkanes should show the same average number of oxygen molecules that react with each hydrocarbon molecule. Kung *et al.* (1997) indicated that this average oxygen stoichiometry is 2 on magnesium orthovanadate.

In magnesium pyrovanadate this value is around 2 only for ethane and propane and doubles for *n*- and *i*-butane, because it contains V_2O_7 units, which comprise of pairs of corner sharing VO_4 units. These units can provide twice the number of oxygen atoms for the larger hydrocarbon molecules (Patel, D. *et al.* (1988)).

The pyrovanadate catalyst permits interaction of larger molecules, such as butane, with more than one VO_4 unit, which results in poor selectivity. The oxidation of the substrate at multiple points due to the close proximity of theVO_4 units gives poor selectivity to alkenes, but high selectivities to carbon oxides. For small molecules such as propane, lower selectivities to the alkene are obtained over magnesium pyrovanadate than magnesium orthovanadate. This contrast in selectivity to alkenes is more pronounced with larger molecules (Gao, X *et al.* (1994)) as seen in Table 2.1. The orthovanadate catalyst, with its isolated VO_4 units generally gives higher selectivities to alkenes.

Table 2.1 Comparison of the selectivity to alkenes over magnesium-vanadate catalysts (Kung, H. H. et al. (1997))

Alkane	Mg orthovanadate			Mg pyrovanadate		
	Temperature, °C	Alkane conversion, %	Selectivity, %	Temperature, °C	Alkane conversion, %	Selectivity, %
Ethane	540	5.2	24	540	3.2	30
Propane	541	6.7	64	505	7.9	61
n -Butane	540	8.5	65.9	500	6.8	31.8
i -Butane	500	8	64	502	6.8	25

The catalyst surface is not uniform and thus a top-on adsorption of the substrate is not energetically favourable and interactions usually occur between the adsorbed hydrocarbon and neighbouring units of the catalyst surface. The configuration of the adsorbed intermediate may change considerably as a function of (i) the local structure of the neighbouring active sites, (ii) the nature of the adsorbed molecule and (iii) the nature of the surface-hydrocarbon bond.

Abstraction of a hydrogen atom from an alkane is the first step in an oxidative dehydrogenation process. There is subsequent generation of a hydroxyl group on the catalyst

surface. The nature of the repulsive interaction between the active site and the hydrocarbon changes. The interaction between the hydrocarbon as well as the products from transformation and the catalyst depend on the nature of the hydrocarbon, the presence of reactive hydrogens and the possibility of multiple attack. The longer the hydrocarbon chain, the higher the probability of multiple attack.

The acid-base properties of a catalyst influence the selectivity in oxidative dehydrogenation of an alkane (Galli, A. *et al.* (1995)). This is also dependant on the alkane chain length and degree of saturation. The acid character of a hydrocarbon decreases as the number of carbon atoms and/or its degree of saturation decrease (Dadyburjor *et al.* (1979)). Thus an alkene intermediate on the catalyst surface formed from a short-chain alkane, such as ethane, and having a higher acidic character than alkenes from e.g. butane will be weakly adsorbed on acid sites. Lewis acid sites have been attributed to anionic vacancies during the catalytic reaction, whilst lattice oxygen is responsible for the mild basic behaviour. A balance between the number and strength of acid and base sites is responsible for selective activation of the alkane.

Zazhigalov, V.A. *et al.* (1987) reported that the surface of the VPO catalyst is acidic. This high acidity of the catalyst surface favoured desorption of the acidic MA product.

Besides interaction between the substrate and the catalyst, there is also interaction between the products and the catalyst to consider. Alkenes are products from the oxidation of alkanes with a VPO and VMgO catalyst. An equilibrium exists between the alkane and the alkene (Hoog, H. *et al.* (1939)). Intermediate alkenes in catalytic processes can adsorb onto the catalyst surface thereby suppressing dehydrogenation of alkanes (Pithkethly, R.C. *et al.* (1939), Steiner, H. (1945)). This can result in poisoning of the catalyst, thus reducing the conversion.

2.2.3 Selective oxidation versus over-oxidation products on the VPO and VMgO

The high selectivity to carbon oxides is a problem that needs to be addressed in the partial oxidation of C_4, C_6 and C_8 alkanes over VPO and VMgO catalysts. Understanding the

mechanisms of selective and over-oxidation reactions is the key to developing catalyst and reactor systems that are selective in the oxidation of alkanes. Some of the generally proposed mechanisms found in the literature for over-oxidation are discussed here and correlated to VPO and VMgO.

In a catalytic system, over-oxidation is related to the ease of removal of lattice oxygen from the catalyst for insertion into the activated alkane on the catalyst surface.

A surface alkyl species which is adsorbed on the surface of the catalyst is formed after the first C–H bond, which is usually the *β*-hydrogen of the alkane substrate, is broken. Dehydrogenation products are formed if another C-H bond on the adjacent carbon is broken (equation (15)).

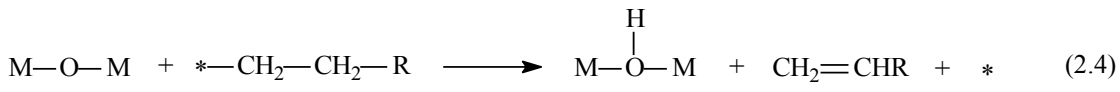

(2.4)

In equation 2.4, ∗ represents the vanadium ion (active surface ion) in the VMgO and VPO catalysts. The metal M represents vanadium for the VMgO and VPO catalysts. The oxygen between the vanadium metal ions represents lattice oxygen for the VMgO and VPO catalysts.

An oxygen-containing organic product can be formed if the alkyl species undergoes hydrogen abstraction and subsequent oxygen insertion by lattice oxygen to form a C-O bond (equation 2.5):

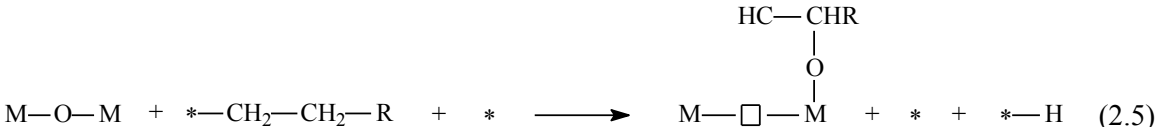

(2.5)

M—□—M represents an oxygen vacancy in the lattice of the catalyst.

An oxygen-containing product may also be formed by insertion of the lattice oxygen into a C-C bond to form C-O-C bonds (Pepera, M.A. *et al.* (1985)). This C-O-C containing product in reaction 2.6 usually combusts giving carbon oxides.

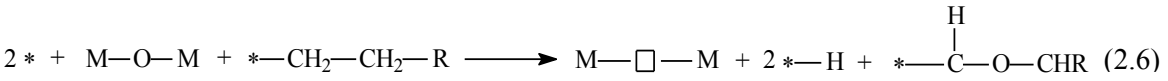

(2.6)

The selectivity of the reaction can thus be determined by the ease of removal of oxygen from the lattice to form C-O-C bonds with the surface intermediate. Oxygen is supplied more readily and in larger amounts by the VPO catalyst, where the pyrovanadate is the active phase, than the VMgO catalyst where the orthovanadate is the active phase (Michalakos, P.M. *et al.* (1993)). This results in the VPO catalysts being less selective to partial oxidation products by giving more carbon oxides than the VMgO catalysts under similar catalytic conditions for *n*-butane, *n*-hexane and *n*-octane oxidation.

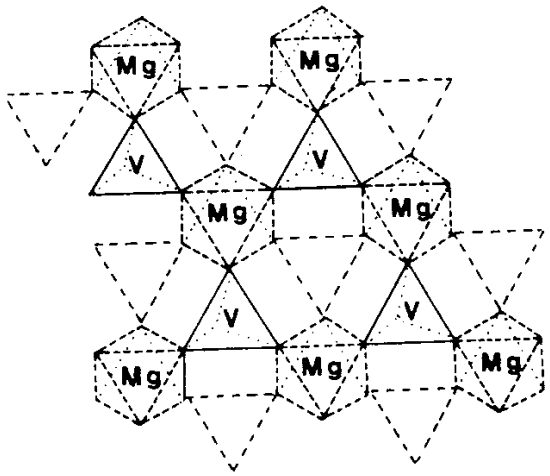

Fig. 2.7 Structure of the orthovanadate phase of the VMgO catalyst (Krishnamachari, N. et al. (1971))

Another proposal for the selectivities to carbon oxides being generally higher over the VPO catalysts compared to the VMgO catalysts for *n*-butane, *n*-hexane and *n*-octane feedstocks is based on the proximity of the V-O species on the catalyst surface. V-O is the active species for oxidation in the VMgO (Albonetti, S. *et al.* (1996a)) and VPO (Busca, G. *et al.* (1986)) catalysts. The orthovanadate phase ($Mg_3(VO_4)_2$) of the VMgO catalyst is characterized by chains of edge-sharing MgO_6 units linked by isolated VO_4 tetrahedra (Fig. 2.7), whilst the

$(VO)_2P_2O_7$ (pyrophosphate) catalyst is characterized chains of vanadia octahedra linked by chains of phosphorous tetrahedra (Figs. 2.8 and 2.9).

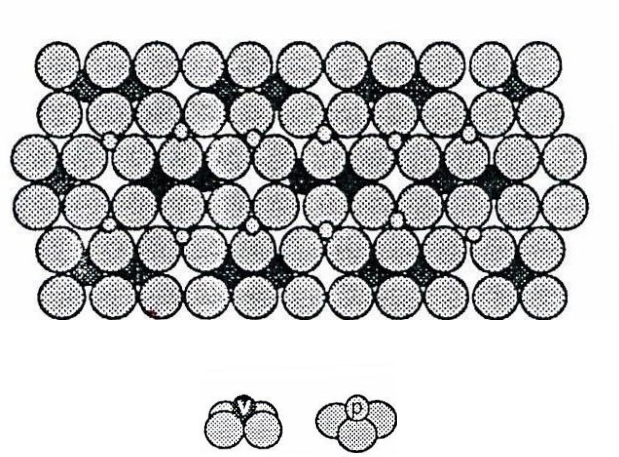

Fig. 2.8 Structure of the vanadyl pyrophosphate phase of the VPO catalyst (Thompson, M.R. et al. (1994))

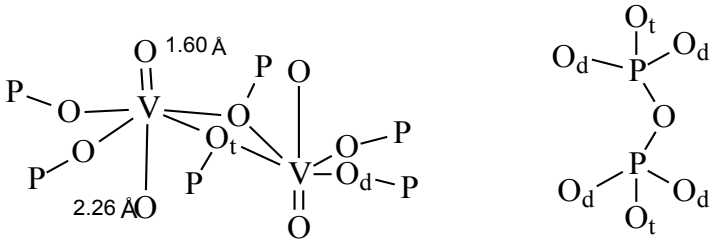

Fig. 2.9 The vanadium octahedral coordination (left) and the phosphorous tetrahedral coordination (right) in the idealized model of vanadyl pyrophosphate. Subscripted oxygen atoms represent double-bridged positions (O_d) and triple-bridged positions (O_t) (Thompson, M.R. et al. (1994))

The lattice oxygen lies between two vanadium ions on the catalyst surface (illustrated in equations 15, 16 and 17). The formation of oxygen-containing products are enhanced when the hydrocarbon intermediate on the surface of the catalyst can be bonded to the two vanadium ions such that the hydrocarbon species is held close to the reactive surface lattice oxygen. This

occurs more readily over a pyrovanadate catalyst than an orthovanadate catalyst since the active vanadium species are closer together on the pyrovanadate catalyst thus contributing to higher oxygen insertion giving C-O-C bonds and subsequently higher carbon oxide selectivities.

2.2.4 Promotion of the VPO and VMgO catalysts

Cobalt, gold and rhodium were chosen as promoters for catalysts presented in this thesis and their role as promoters and factors that control their performance is reviewed.

Promoters can be classed as substances which, when added to a catalyst as a minor component, improve one or more of the properties of the material with respect to product formation. These properties include activity, selectivity, catalyst lifetime (due to a decrease in the sintering rate or decrease in the build-up of an irreversible poison on the catalyst surface) and neutralization of acid sites. The catalysis occurs at the surface of a catalyst and thus there is a need for the promoter to be present at the surface of the catalyst. Alkali metals such as potassium usually segregate to the surface of the catalyst and are thus favoured promoters (Bowker, M. (1998)).

The promoter may be present in a VPO catalyst in four types of phases viz. (i) metallic, (ii) metal oxide, (iii) metal phosphate and (iv) bimetal phosphate (Lozana-Calero, D. *et al.* (1993)).

Busca, G. *et al.* (1986) reported that the promoter induces disorder in the VPO catalysts, which creates local modifications and forms new active centers for the oxidation of *n*-butane. Despite the extensive use of promoters in the patent literature, fundamental studies on the effect of promoters have been very limited.

Metal dopants can greatly affect the performance of a catalyst by inducing both structural as well as electronic changes to the bulk of the catalyst (Brutovsky, M. *et al.* (1982)). There is evidence to confirm that a promoter can aid in controlling the optimum oxidation state in the catalyst for the selective oxidation of the alkane to a desired product (Higgins, R. *et al.* (1982)).

The promoter may be incorporated by various methods, but these are generally classified into two groups: (i) where the promoter is incorporated into the bulk of the catalyst or (ii) where the promoter is added in such a way to favour its location on the surface of the catalyst. The way in which the promoter is added is important and affects the catalysis. Another important factor is the amount of promoter incorporated. There is an optimum loading of promoter on the catalyst surface for maximum activity, beyond which there is blocking of too many active sites that causes a decrease in activity (Bowker, M. (1998)).

The promoters used in work carried out in this thesis were Co, Rh and Au. Of these promoters, only cobalt was reported as a promoter for VPO in the literature in the selective oxidation of alkanes. The following discussion involves Co as a promoter and Rh and Au as supported catalytic materials.

Govender, N. *et al.* (2004) investigated the effect of cobalt as a promoter in the VPO catalyst for the oxidation of *n*-butane to maleic anhydride. The catalyst's selectivity improved with increasing promoter loading up to a maximum of 2.3 %, beyond which the promoter inhibited the performance of the catalyst. A cobalt promoter has the ability to stabilise the loss of oxygen anions during reduction, hence making the catalyst less active but more selective (Hodnett, B.K. (1985)). Brutovsky, M. *et al.* (1982) reported that the selectivity of *n*-butane oxidation to MA was improved by including cobalt into the VPO lattice, which gave defect sites. Cobalt is responsible for the generation of significantly crystalline $(VO)_2P_2O_7$ structures together with poorly crystalline $(VO)_2P_2O_7$ structures, a combination that gives enhanced catalytic performance (Sananés-Schulz, M.T. *et al.* (1997)).

An unpromoted VPO catalyst is already promoted when the P:V ratio exceeds unity and it usually does for industrially employed catalysts. The catalyst thus cannot be claimed to be a simple single phase system. The promotional effect of cobalt was reported to decrease with a decreasing P:V ratio (Zazhigalov, V.A. *et al.* (1993)).

Bhattacharyya, D. *et al.* (1992) investigated the effect of promoters on the activity of the VMgO catalyst for the selective conversion of *n*-butane to butadiene. These promoters (K,

Cr, Sm and Nb) changed the acidity of the catalyst, and the promoter which enhanced the basic nature of the catalyst, performed the best. Antimony has been a metal of great interest for achieving this (Grabowski, R. (2006)). The reason being that butadiene is basic and reacts strongly with the acidic surface of the VMgO catalyst, which results in secondary products (including over-oxidation) and decreased selectivity to butadiene.

Goetsch, D.A. *et al.* (1996) and Iordanoglou, D.I. *et al.* (1999) reported the conversion of C_2, C_3 and C_4 alkanes to alkenes, oxygenates and carbon oxides over a 10 % rhodium on platinum gauze catalyst at microsecond contact times and an operating temperature of 800^{o}C. The highest oxygenated product selectivities were to formaldehyde and acetaldehyde. The authors reported that the selectivity to alkenes and oxygenates were 4 times that of the selectivity to carbon oxides.

Rhodium supported on Al_2O_3 monolith catalysts for the oxidation of butane, cyclohexane, *n*-hexane and *iso*-octane, *n*-decane and *n*-hexadecane (with nearly total conversion at catalyst temperatures of ~ 800^{o}C and millisecond contact times was reported. The selectivities to synthesis gas (H_2 and CO) exceeded 80 %. The other products included CO_2, ethylene, propylene and α-alkenes. It was reported that the selectivity to alkenes increased with the increasing carbon chain-length of the alkane feedstock (Krummenacher, J.J. *et al.* (2003), Krummenacher, J.J. *et al.* (2004), Schmidt, L.D. *et al.* (2003)). This increasing selectivity to dehydrogenation products made rhodium an attractive metal to incorporate into the VPO catalyst. If not as a promoter, rhodium may enhance the selectivity to alkenes, which are intermediates in the oxidation of *n*-butane to maleic anhydride.

A large amount of literature on gold catalysis focuses on the oxidation of carbon monoxide to carbon dioxide over gold supported on TiO_2 catalysts (Bondzie, V.A. *et al.* (1999), Choudary, T.V. *et al.* (2002), Mavrikakis, M. *et al.* (2000)), gold supported on ZnO and Fe_2O_3 catalysts (Hutchings, G.J. *et al.* (2003)), gold supported on Co_3O_4, Al_2O_3, ZrO_2 and SiO_2 (Wolf, A. *et al.* (2002)), propylene epoxidation over the same catalysts (de Oliviera, A.L. *et al.* (2001))

and hydrochlorination of ethyne using impregnated $HAuCl_4$ solutions onto activated carbon (Hutchings, G. J. (1996)).

Haruta, M. (1997) showed that precipitation/deposition techniques of incorporating gold into metal oxide catalysts resulted in highly dispersed and fine gold particles, which give active gold catalysts. The activity and selectivity of the catalyst is controlled by the size of the gold particles. This suggests that there is an optimum particle size for a certain reaction to be selective. Gold is relatively inert, but this behaviour changes when gold is highly dispersed as nano-sized particles on certain metal oxides (Bocuzzi, F. *et al.* (1998), Valden, M. *et al.* (1998)). The authors suggest that the reaction takes place on the Au/metal oxide interface and that the metal oxide can act as a source of oxygen. Wolf, A. *et al.* (2002) reported 100 % yield of CO_2 at temperatures less than 300^{o}C from CO oxidation over gold supported on TiO_2, Co_3O_4 Al_2O_3 and ZrO_2 at less than 3 wt. %.

Since supported gold catalysts show high activity in reactions like the reduction of nitrogen oxides (Salama, T. *et al.* (1996)), the epoxidation of propene (Hayashi, T. *et al*. (1998)) and the low temperature oxidation of CO to CO_2 (Haruta, M. (1997), Haruta, M. *et al.* (1993)), gold can thus act as a reducing or oxidising catalyst.

2.3 Continuous flow fixed-bed reactors

Two of the major factors that concern the design of continuous flow reactors include the flow pattern of the feed and heat and mass transfer limitations. This discussion highlights the need for integration between catalyst and reactor design to control activity and selectivity.

2.3.1 The flow pattern in the reactor

Continuous flow reactors should maintain a plug flow pattern, which makes for reliable and straightforward treatment of data. Analysing data from systems with a deviation from an ideal flow pattern requires complicated mathematical treatment. Some of the conditions that ensure plug flow and other important factors for continuous flow reactions are outlined here. A

reactor diameter of at least 10 times the catalyst particle diameter eliminates the influence of the reactor walls on the flow pattern. The gas reactant stream flows between the catalyst particles. The rate of flow, relative to the catalyst particle, is an important factor, together with temperature and catalyst properties, in determining conversion. The velocity and turbulence of the flow determine how rapidly molecules are carried from the fluid phase to the exterior surface of the catalyst. Rapid transfer from fluid to solid outer surface is obtained with highly turbulent flow, which means a highly irregular flow pattern with momentary velocities strongly deviating from the main flow direction. High turbulence is obtained with large catalyst particles, high flow velocities and low viscosities of the reactant stream. Increasing turbulence decreases the rate of heat transfer between the catalyst and the fluid, and also to the wall of the reactor (Westerp, K.R. *et al.* (1992)). Ideally, rapid heat transfer to the wall of the reactor and surrounding atmosphere is required to limit any temperature runaways.

Uneven flow conditions cause a broad distribution of residence times for individual fluid packets or molecules. Residence time distribution can have an unfavorable effect on consistent selectivity and conversion.

2.3.2 Heat and mass transfer effects

Due to appreciable heat effects that accompany heterogeneous oxidative dehydrogenation reactions (Madeira, L.M. *et al.* (2002)), heat has to be removed from the catalyst particle or supplied to it to keep it in the appropriate temperature range for the production of desired products and limit secondary products and overoxidation. The combustion and oxidative dehydrogenation reactions can still generate heat that needs to be removed to maintain the reaction at steady-state. The design of the reactor plays a major role in maintaining a steady-state. The width of the reactor needs to be narrow enough to allow a rapid radial dispersion of heat. Hotspots caused by poor dispersion of heat destroy the catalyst giving poor activity and selectivity.

In a plug flow reactor, small changes in temperature can affect reaction rates significantly. Large gradients in the reactor temperature may cause deviations from isothermal conditions (Mears, D.E. (1971)). In addition to temperature gradients at the reactor level, temperature gradients can also occur at the boundary between the catalyst and the reactor fluid called inter-phase gradients. Interparticle gradients may also occur between catalyst particles. In fixed-bed reactors, axial temperature gradients always exist due to conversion. Radial temperature gradients cause unreliable data in plug flow reactors, which are attributable to the low effective thermal conductivity of the catalyst bed (Kulkarni, B.D. *et al.* (1980)). These intra-reactor temperature gradients are nearly always more severe than inter-phase temperature gradients, which are generally more severe than intraparticle temperature gradients. These temperature gradients can be minimized or eliminated by increasing the ratio of the catalyst bed diameter to the catalyst particle diameter or diluting the catalyst bed with inert particles. A smaller diameter of the tubular reactor, however, reduces the distance over which the heat must be conducted up to the wall for its efficient removal. The intraparticle temperature gradients are inconsequential because the effective thermal conductivity of the catalyst, where heat transfer occurs mostly by conduction through the solid phase, is usually faster than in the surrounding environment.

Hot spots are caused by poor heat-transfer properties of catalytic particles and from rapid reaction rates. The temperature in these zones can be 50^{o}C higher than that of the inlet and outlet fluid. All these phenomena that typically lead to the deactivation of the active component, such as sublimation of the active phase, phenomena of sintering and recrystallisation (with a reduction in the surface area and conversion of the active phases) and coking are kinetically favoured when hot spots are present in the reactor.

Temperature gradients also lead to concentration gradients, since the reaction rate is higher in a certain region of the catalyst bed. Concentration gradients may lead to different product distribution in the axial zone and in proximity of the reactor wall, especially when the reaction rates have different orders of reaction with respect to the reactants.

In a reactor design, heat and mass are generally considered to be transported by plug flow only. It is thereby assumed that there are no gradients in concentration in a cross-section. In a flow system, the flow rate can be varied while the space velocity is kept constant. If the conversion remains constant, the influence of inter-phase and intra-reactor effects may be assumed to be negligible. In gas-solid systems, inter-phase temperature gradients are avoided by using the smallest feasible particles and/or high linear flow velocities. High flowrates are usually favourable in preventing secondary reactions, however, there is a maximum flowrate taking into consideration the constraints of reactor diameter and catalyst particle size so as to avoid turbulence in the reactor and backpressure. Backpressure can significantly affect the kinetics of the reaction and is important to eliminate this when operating a fixed-bed reactor.

Changing the catalyst particle sizes can be used to test intraparticle effects. If there is no change of catalyst activity with change in particle size (assuming that the surface area of the active catalyst is constant), the catalyst is considered to be free of intraparticle gradients. Small catalyst particles are effective in avoiding intraparticle concentration gradients.

References

Bettahar, M.M., Constentin, G., Savary, L., Lavalley, J.C., Appl. Catal. A: General, **145**, 1 (1996)

Bielanski, A., Haber, J., Oxygen in Catalysis, Marcel Dekker, Inc., NY (1991)

Bhasin, M.M., McCain, J.H., Vora, B.V., Imai, T., Pujado, P.R., Appl. Catal., **221**, 397 (2001)

Bhattacharya, D., Bej, S.K., Rao, M.S., Appl. Catal. A: General, **87**, 29 (1992)

Birkeland, K.E., Babitz, S.M., Bethke, G.K., Kung, H.H., J. Phys. Chem. B, **101**, 6895 (1997)

Bond, G.C., Heterogeneous Catalysis: Principles and Applications, 2nd edition, Oxford University Press, p 9 (1987)

Bowker, M., The Basis and Applications of Heterogeneous Catalysis, Oxford University Press, p 46 (1998)

Burch, R., Swarnakar, S., Appl. Catal., **70**, 129 (1991)

Burch, R., Crabb, E.M., Appl. Catal. A: General, **100**, 111 (1993)

Busca, G., Cavani, F., Centi, G., Trifiró, F., J. Catal., **99**, 400 (1986)

Busca, G., Centi, G., Trifirò, F., Appl. Catal., **25**, 265 (1986)

Busca, G., Lorenzelli, V., Olivieri, G., Ramis, G., New Developments in selective oxidation II, Studies in Surface Science and Catalysis, vol. 82, Elsevier science: Amsterdam, p 253 (1994)

Busca, G., Finocchio, E., Ramis, G., Ricchiardi, G., Catal. Today, **32**, 133 (1996)

Callahan, J.L., Grasselli, R.K., AIChE J., **9**, 755 (1963)

Campbell, C.T., Appl. Surf. Sci., **19**, 32 (1984)

Centi, G., Trifirò, F., Appl. Catal., **12**, 1 (1984)

Centi, G., Cavani, F., Trifirò, F., Selective Oxidation by Heterogeneous Catalysis, Kluwer Academic/ Plenum Publishers, p 205 (2001)

Chaar, M.A., Patel, D., Kung, M.C., Kung, H.H., J. Catal., **105**, 485 (1987)

Chaar, M.A., Patel, D. Kung, M.C., J. Catal., **109**, 463 (1988)

Chang, Y., Somorjai, G.A., Heinemann, H., Appl. Catal. A: General, **96**, 305 (1993)

Corma, A., Lopez-Nieto, J.M., Paredos, N., Appl. Catal. A: General, **144**, 425 (1993)

Davis, S.M., Zaera, F., Somorjai, G.A., J. Catal., **85**, 206 (1984)

Dwyer, D. J., Somorjai, G.A., J. Catal., **52**, 291 (1978)

Ebner, J.R., Thompson, M.R., Catal. Today, **16**, 51 (1993)

Eischens, R.P., Pliskin, W.A., Francis, S.A., J. Chem. Phys., **22**, 1986 (1954)

Eon, J.G., Olier, T., Volta, J.C., J. Catal., **145**, 318 (1994)

Govender, N., Friedrich, H.B., Janse van Vuuren, M., Catal. Today, **97**, 321 (2004)

Grabowksi, R., Catal. Rev., **48**, 199 (2006)

Graselli, R., Burrington, J., J. Adv. Catal., **30**, 133 (1980)

Grasselli, R.K., J. Chem. Ed., **63**, 216 (1986)

Grasselli, R.K., Handbook of Heterogenous Catalysis, vol. 5, p 2303 (1997)

Hutchings, G.J., Appl. Catal., **72,** 1-32 (1991)

Hutchings G.J., Olier, R., Sananés, M.T., Volta, J.C., New Developments in Selective Oxidation II, p 213 (1994)

Igarashi, H., Tsuji, K., Okuhara, T., Misono, M., J. Phys. Chem., **97**, 7065 (1993)

Keulks, G.W., J. Catal., **19**, 232 (1970)

Kong, L., Li, G., Catal. Lett., **92**, 163 (2004)

Kulkarni, B.D., Doraiswamy, L.K., Catal. Rev.-Sci. Eng., **22**, 431 (1980)

Kung, H.H., Michalakos, P., Owens, L., Kung, M., Anderson, P., Owen, O., Jahan, I., J. Amer. Chem. Soc., 389 (1993)

Madeira, L.M., Portela, M.F., Catal. Rev., **44**, 251 (2002)

Mars, P., van Krevelen, D.W., Chem. Eng. Sci. Special Suppl., **3**, 41 (1954)

Matyshak, A., Krylov, O.V., Catal. Today, **25**, 455 (1995)

Mears, D.E., J. Catal., **20**, 127 (1971)

Michalakos, P.M., Kung, M.C., Jahan, J., Kung, N.H., J. Catal., **140**, 226 (1993)

Morooka, Y., Morikawa, Y., Ozaki, A. J. Catal., **7**, 23 (1967)

Okuhara, T., Misono, M., Catal. Today, **16**, 61 (1993)

Okuhara, T., Mizuno, N., Misono, M., Adv. Catal., **41**, 113 (1996)

Overbeek, R.A., Versluijs-Helder, M., Warringa, P.A., Bosma, E.J., Geus, J.W., New Developments in Selective Oxidation II, p 183 (1994)

Patel, D., Kung, M.C., Kung, H.H., Proc. 9th Int. Congr. Catalysis, Calgary, p 1555 (1988)

Patel, D., Anderson, P.J., Kung, H.H., J. Catal., **125**, 132 (1990)

Sananés-Schulz, M.T., Tuel, A., Hutchings, G.J., Volta, J.C., J. Catal., **166**, 388-392 (1997)

Sookraj, S.H., Engelbrecht, D., Confidential Report Number 290/97, Sastech R&D Applied Catalysis Research, p 24 (1997)

Spencer, N.D., Schoonmaker, R.C., Somorjai, G.A., J. Catal., **74**, 129 (1982)

Siew Hew Sam, D., Soenen, V., Volta, J.C., J. Catal., **123**, 417 (1990)

Sokolovskii, V.D., Catal. Rev.-Sci. Eng, **32**, 29 (1990)

Somorjai, G. A, Mate, C.M., Surf. Sci., **160**, 542 (1985)

Thomas, J.M., Top. Catal., **15**, 85 (2001)

Volta, J.C., Top. Catal., **15**, 121 (2001)

Westerp. K.R., Wijngaarden, R.J., Principles of Chemical Reaction Engineering and Plant Design, Ullman's Encylopaedia of Industrial Chemistry, **B4**, 5th edition, Weinheim: VCH (1992)

CHAPTER 3

EXPERIMENTAL

3.1 Micro-reactor setup

For heterogeneous reactions in a lab-scale heterogeneous continuous flow reactor, a micro-reactor system with a suitable temperature control device and product sampling and analytical system was set up. The three different variations of reactor systems designed for the purpose of this study were determined by the alkanes used (*n*-butane, *n*-hexane and *n*-octane): whether they were introduced as a liquid or premixture with air into the reactor system. There is a relatively low cost of construction and installation of equipment associated with the use of continuous flow fixed-bed micro-reactors for lab-scale experiments and thus this option was chosen.

3.1.1 Micro-reactor setup for butane oxidation

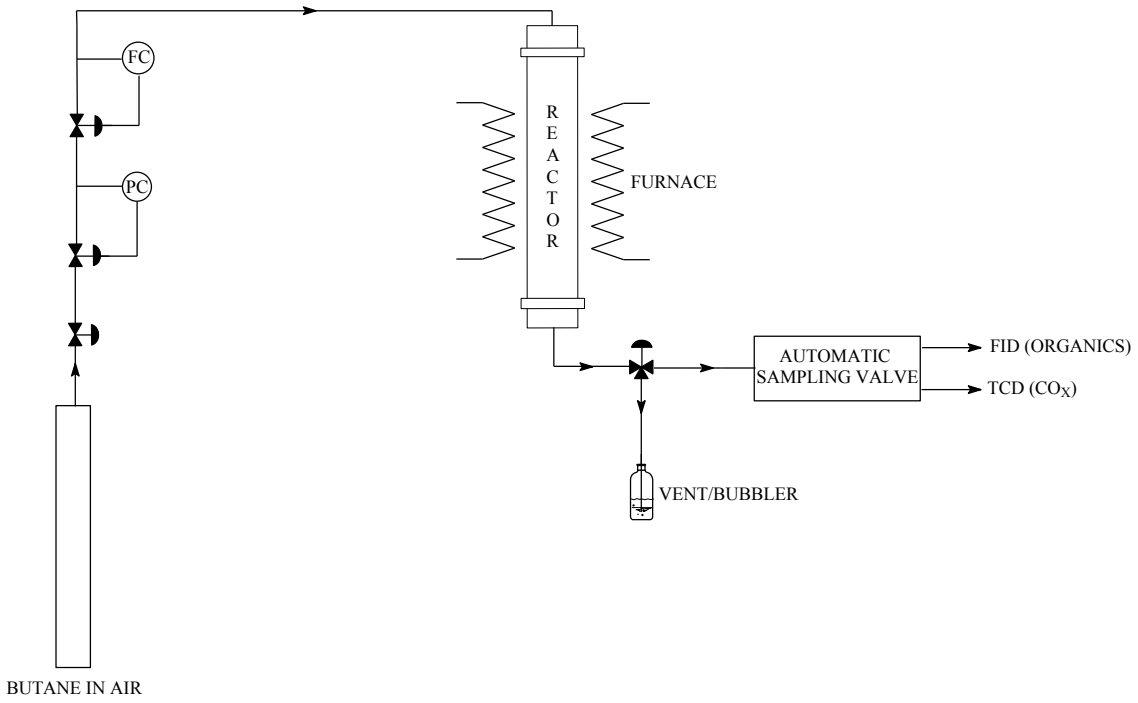

Fig. 3.1 Reactor setup for an n-butane feed

n-Butane was fed from a premix cylinder containing 1 % *n*-butane in air (Fig. 3.1). The pressure and flowrate of this gaseous mixture was regulated by a pressure controller (PC) to 100 kPa (gauge pressure) and a flow controller (FC) in the form of a rotameter before entering the reactor. The flow controller was calibrated at 100 kPa and thus this pressure was maintained. The gas hourly space velocity (GHSV) of 3000 hr^{-1} in the reactor was maintained by using 1 ml of catalyst and 50 ml min^{-1} flowrate of feed mixture. The 316 stainless steel reactor (inner diameter = 9 mm) was encased in a furnace. The outlet lines from the reactor were heated to 160^{o}C to prevent condensation of the products in the lines. The temperatures of the heating elements in the construction of all three reactors were maintained by temperature probes (thermocouples) linked to temperature controllers. All product lines in all reactor systems were stainless steel to prevent corrosion of the reactor walls by any acidic products from the reactor. A valve located immediately after the reactor directed flow to either a bubbler or the on-line gas chromatography (GC) system. When the product stream was directed to the online GC system, an automatic sampling valve equipped with two 500 μL sampling loops accurately sampled the stream by directing one sample to a GC equipped with a flame ionisation detector (FID) and the other to a GC equipped with a thermal conductivity detector (TCD). The FID detected organic products, whilst the TCD detected all other products including carbon oxides (a discussion of these detectors and the operation of the GC appears in the Appendix, p. 283).

3.1.2 Micro-reactor setup for hexane oxidation

For the reactor setup designed for an *n*-hexane feed (Fig. 3.2), air from a gas cylinder was regulated by a pressure controller to 100 kPa (gauge pressure) and a flow controller before being bubbled into *n*-hexane in a flask immersed in a chiller set at 5^{o}C. The cooled alkane has a vapour pressure of 0.079 bar at this temperature, which gave a 7.8 % alkane vapour in air (v/v) mixture in the flask. This mixture of *n*-hexane in air was flushed into the reactor by the pressure of the air supplied by the cylinder. The GHSV in the reactor was controlled by varying the flowrate of the air and the volume of the catalyst (details of which appear in the Appendix, p.

254). The steel reactor (inner diameter = 7 mm) was encased in a furnace. The outlet lines from the reactor were heated to 160°C to prevent condensation of products in the lines. The post-reactor setup for the *n*-hexane and *n*-butane reactor systems was the same. A fig. of the setup appears on p. 266 in the Appendix.

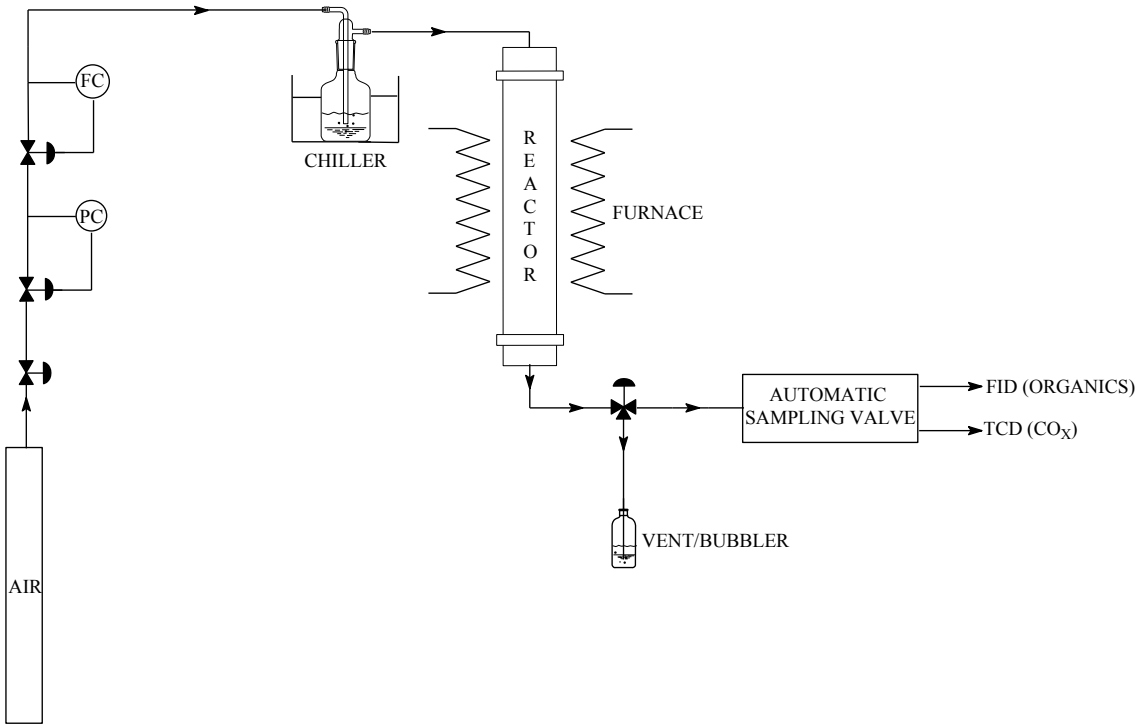

Fig. 3.2 Reactor setup for an n-hexane feed

3.1.3 Micro-reactor setup for octane oxidation

The feed system for the *n*-octane reactor was similar to that of the *n*-hexane reactor, except a high performance liquid chromatography (HPLC) pump was employed to introduce the liquid alkane into the reactor (Fig. 3.3). The pump drew *n*-octane from a reagent bottle placed on a balance. The amount of *n*-octane fed into the reactor could thus be recorded for a catalytic run. The pump fed the *n*-octane at a certain flowrate into a line continuously flushed with air at a certain flowrate (the details of which appear in the Appendix, p. 266). A mixture of 7.2 % of *n*-octane in air (v/v) was thus maintained. The feed lines to the reactor were heated to 150°C which ensured that the mixture of *n*-octane in air was vapourised before it entered the reactor.

The outlet line from the reactor was connected to a catchpot which was cooled to 4°C. Organic and aqueous products from the reaction were trapped in the catchpot. The aqueous and organic phases in the catchpot were separated and weighed. A sample of each layer was injected into the GC to separate and identify the components. The gaseous components leaving the reactor continuously flowed through the catchpot and into a wetgas flowmeter, which recorded the total volume of gas leaving the reactor. The gaseous products were intermittently analysed online by directing the flow of the product stream away from the wetgas flowmeter and towards the on-line GC with the use of a valve preceding the automatic sampling valve. Photographs of the setup appear on p. 266 in the Appendix.

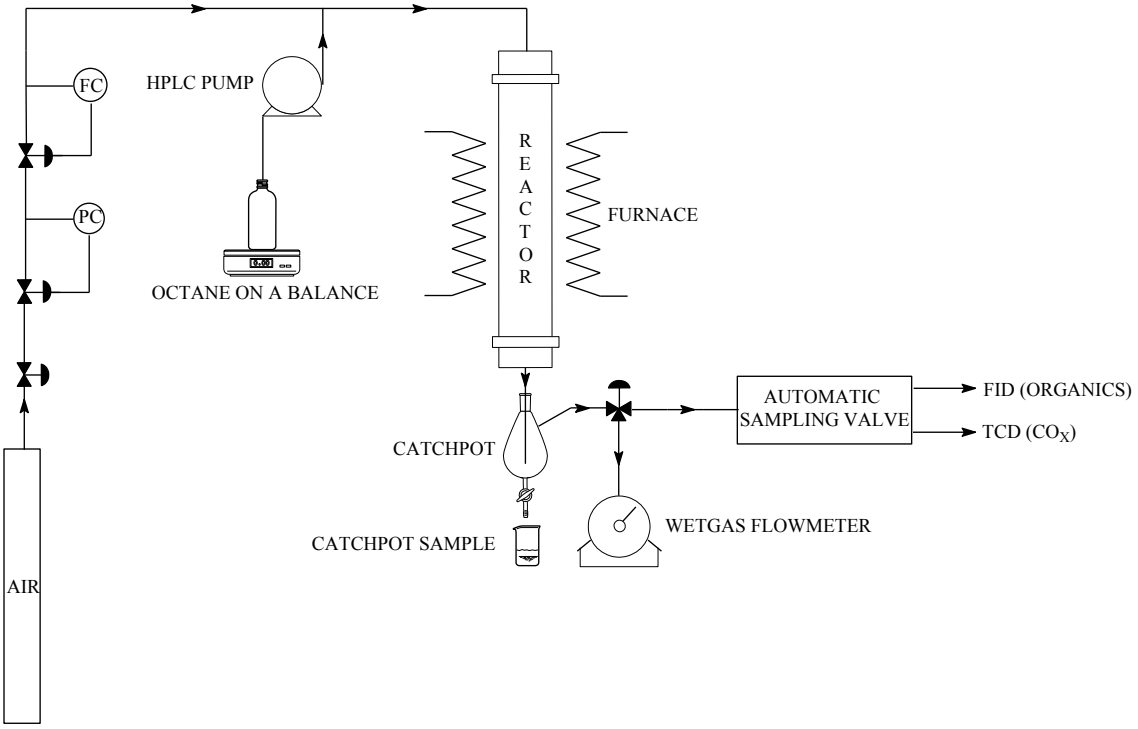

Fig. 3.3 Reactor setup for an n-octane feed

3.2 The feed

The source of the alkanes are provided in Table 3.1.

Table 3.1 Purity and source of alkane feedstocks

Alkane	M/ g mol^{-1}	Purity	Supplier
n-Butane	58.12	1 % *n*-butane in air premix	Air Liquide
n-Hexane	86.65	> 95 %	Acros Organics
n-Octane	114.23	99 + %	Fluka

Table 3.2 % Alkane in air used in relation to lower and upper flammability limits at room temperature

Feed	Lower flammability limit	Upper flammability limit	% Used
n-Butane	1.8	8.4	1.0
n-Hexane	1.7	7.7	7.8
n-Octane	1.0	6.5	7.3

With the exception of the *n*-butane mixture the alkane in air mixtures were maintained just above the flammability range (Table 3.2). The reason for maintaining *n*-butane below the flammability range was gas mixture in air restrictions imposed by the suppliers of the premixed gas.

A table of % (v/v) of alkenes in air employed for the mechanistic investigation into the oxidation of *n*-hexane to benzene appears on p. 254 in the Appendix.

3.3 Analytical system setup

3.3.1 Automatic sampling valves

Two GCs were employed in the analysis, viz. an isothermal Varian 3700 GC equipped with a thermal conductivity detector (TCD) (discussed on p. 286 in the Appendix), which was used to separate and quantify carbon oxides and a Perkin Elmer XL autosystem GC equipped with a flame ionization detector (FID) (discussed in the Appendix, p. 286) which was used to separate and quantify all other products. The automatic sampling valves consisted of two Valco rotary valves connected to electronic switches and air actuators that controlled them. The Perkin

Elmer XL autosystem GC was connected to a 10 port Valco rotary valve (Fig. 3.4) and the Varian 3700 GC was connected to a 6 port Valco rotary valve. The product stream from the reactor ran through a 500 μL sample loop contained in both valves.

A pre-column was employed in the Varian 3700 GC to trap any liquid or solid products that may be detrimental to the proper functioning of the TCD (specifications of this column are supplied in the Appendix, p. 248). Thus the sample from the reactor initially entered the pre-column, which was maintained at room temperature, and only the gaseous components passed through and subsequently entered the analytical column. This column was flushed after every week of operation by increasing the temperature of the column to 180^{o}C and applying a flow of helium gas through the column in opposite direction to the TCD and out to waste.

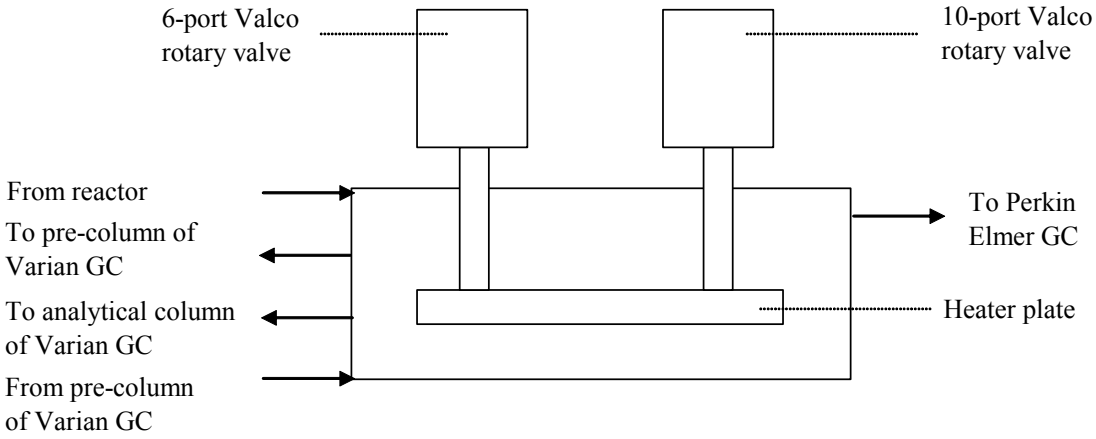

Fig. 3.4 Housing for the 6-port and 10-port Valco rotary valves mounted on a heater plate

The lines entering the gas-sampling valves were the outlet line from the reactor and the return line from the pre-column of the Varian 3700 GC (Fig. 3.4). The line returning from the pre-column of the Varian 3700 GC contained only gaseous components. The lines exiting the gas-sampling valves were the sample feed to the pre-column of the Varian 3700 GC, feed line to the analytical column of the Varian 3700 GC (after subsequent passage through the pre-column) and the feed line to the Perkin Elmer GC. The rotary valves were attached to a heater plate that maintained the sample loops at a temperature of 160^{o}C to prevent condensation of products in the lines.

3.3.2 Operation of the automatic sampling valves

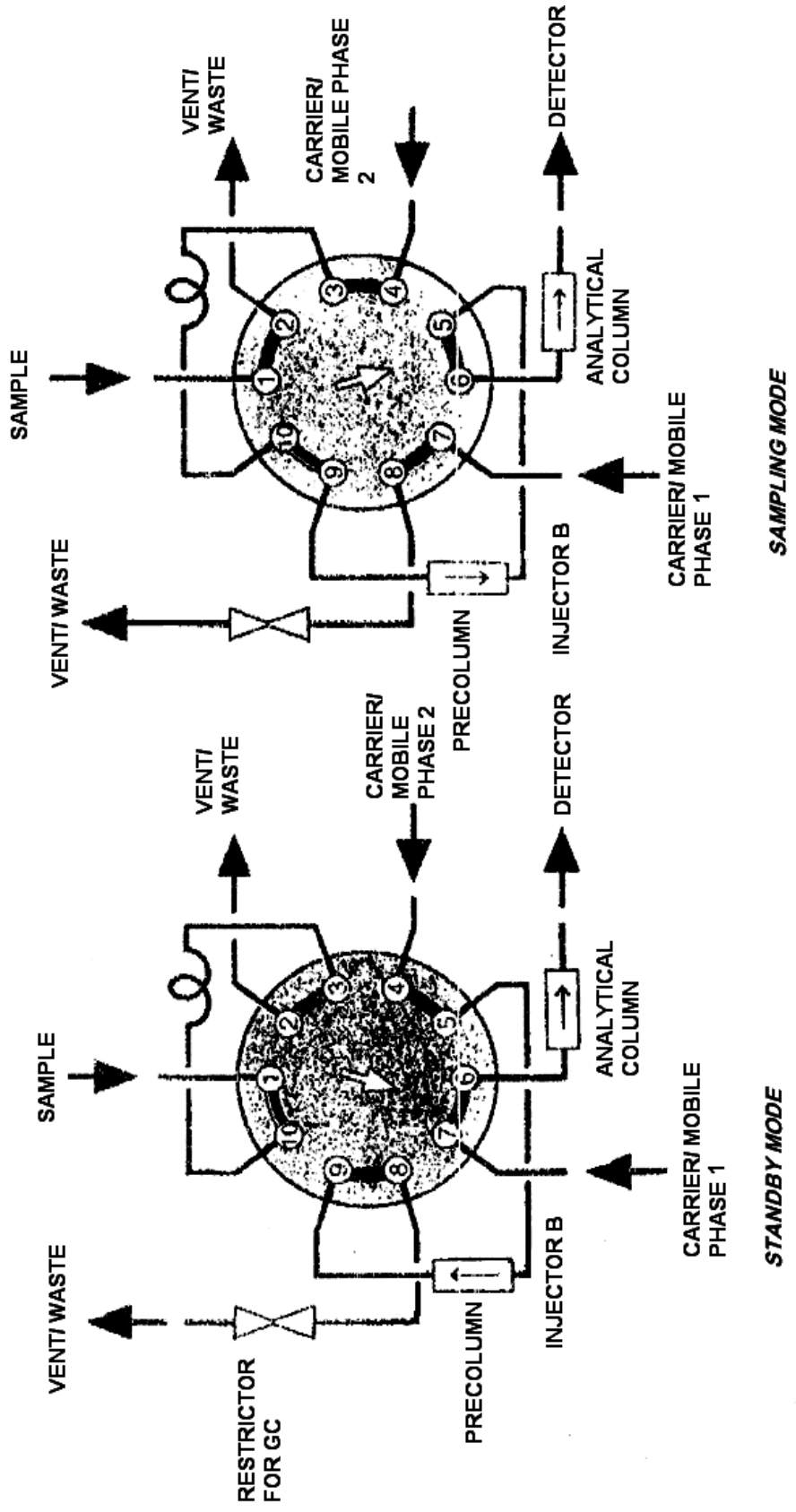

Fig. 3.5 10 port Valco rotary valve that samples to the isothermal Varian 3700 GC

A schematic of the 10-port Valco rotary valve which sampled to the Varian 3700 GC is illustrated in Fig. 3.5. The valves were electronically controlled by the Perkin Elmer GC. Pressurised air was used to turn the valves. Helium, which was the carrier gas, flowed into port 7 and out through port 6 and then through the analytical column and the detector in the standby position of the valve. The carrier gas also flowed in through port 4 and then out port 5, through the injector and through the pre-column, into port 9 and out through port 8, through a restrictor and then vented. The restrictor regulated the pressure in the system. Sample from the reactor flowed in through port 1, through the sample loop and was vented. When the valve was turned to the sampling mode, carrier gas flowed through port 7 and out through port 8 to waste.

Carrier gas also flowed into port 4 through the sample loop, containing sample from the reactor and then followed a sequence through the pre-column, the analytical column and the detector. When the valve was turned back to the standby mode, flow through the pre-column was in the opposite direction to the TCD and towards the waste line, which prevented any solid or liquid components traveling towards the TCD.

The 6-port Valco rotary valve that sampled to the Perkin Elmer GC operated in the same manner, with the exception of the sample passing through a pre-column. When the 6-port valve turned from a standby to sampling mode, the sample in the sample loop was flushed directly into the analytical column in the Perkin Elmer GC.

3.4 Product analysis

A CP-Sil 24CB column in the Perkin Elmer GC, specifications of which appear in the Appendix (p. 248) was used to separate alkanes, alkenes, aromatics and oxygenates. A Carboxen^{TM} 1000 analytical column (specifications of which appear in the Appendix, p. 248) was installed in the Varian 3700 GC separated CO and CO_2. A chromosorb WHPSP pre-column was installed in the Varian 3700 GC and was used to separate gaseous products from non-gaseous products at room temperature.

3.5 Catalyst synthesis

3.5.1 The VPO catalyst

3.5.1.1 Synthesis of the VPO catalyst (promoter inclusion via a co-precipitation technique)

Table 3.3 Reagents for the preparation of a VPO catalyst

Reagent	Molar mass/ g mol^{-1}	Supplier	Purity
V_2O_5	181.88	Aldrich	98+ %
ortho-H_3PO_4	98.00	Fluka	98+ %
Benzyl alcohol	104.14	Aldrich	99 %
Iso-butanol	74.12	Rochelle chemicals	98.5 %
$Co(acac)_3$	356.26	Acros	99 %
$RhCl_3$	209.26	Anglo-Platinum	99 %
$AuCl_3$	303.33	Aldrich	99 %

A promoted VPO catalyst was synthesised via an organic synthetic route, where organic solvents were used as reducing agents in the absence of water. The V_2O_5 (10 g, 0.055 mol) was added to a 3:2 volumetric ratio of *iso*-butanol:benzyl alcohol mixture (100 ml) which reduced the V_2O_5. The mixture, containing different masses of promoters (Table 3.4) for various promoter loadings, was refluxed for seven hours.

Table 3.4 Masses of promoters used for bulk promoter/vanadium molar % loadings

Catalyst	Promoter	Theoretical promoter/vanadium (molar %)		
		1.25	2.50	5.00
		Mass of promoter/ g		
Co-VPO	$Co(acac)_3$	0.49	0.97	1.94
Au-VPO	$AuCl_3$	-	0.83	1.67
Rh-VPO	$RhCl_3$	0.28	0.56	-

$Co(acac)_3$ was used as the source of the cobalt promoter since the acac was easily reduced during calcination of the catalyst.

The reflux mixture was cooled overnight. *ortho*-H_3PO_4 (11.7 g, 0.12 mol) was added to the cooled mixture and refluxed for a further 3 hours. The mixture was cooled and the precipitate obtained was filtered through hardened (541) ashless filter paper to give the catalyst precursor. The precipitate was washed with 20 ml *iso*-butanol. The precipitate was initially dried overnight in an oven set at 100^{o}C under an air atmosphere and then "calcined" under a nitrogen atmosphere at 450^{o}C for 5 hours to yield a black catalyst regarded as the calcined catalyst (Sookraj, S.H. *et al.* (1999)). An unpromoted catalyst was similarly synthesized with the exclusion of the promoter salt addition during the reflux stage.

3.5.1.2 Synthesis of the VPO catalyst (promoter inclusion via a precipitation/deposition technique)

The precipitation/deposition method was employed for impregnating the promoter onto the VPO catalyst surface. Gold, cobalt and rhodium promoters were investigated. The method employed for the synthesis of a gold promoted VPO catalyst was a modification of a method reported in the literature (Wolf, A. *et al.* (1992)).

Since the dominant phase of the VPO precursor catalyst was $VOHPO_4 \cdot 0.5H_2O$, 2.5 molar % of Au:V was based on this phase.

$AuCl_3$ (0.08 g) was dissolved in water (40 ml) and the pH adjusted to 8 with the dropwise addition of NH_4OH, whilst maintaining a temperature of 50^{o}C. A suspension of an unpromoted VPO catalyst precursor (1.0 g) was made in 50 ml of water. The pH of the mixture was adjusted to 8 with the dropwise addition of NH_4OH whilst maintaining the temperature of the mixture at 50^{o}C. The gold solution was added dropwise to the mixture whilst maintaining the mixture at a pH of 8. The mixture was kept at 50^{o}C for a further 15 minutes and then left to age for 72 hours at room temperature. The precipitate was filtered and dried overnight at 108^{o}C.

The cobalt and rhodium promoters were incorporated in the same way using 10 g of the unpromoted VPO catalyst precursor and 3.1 g of $Co(acac)_3$ and 0.6 g of $RhCl_3$ for a 2.5 molar % of promoter/vanadium. $Co(acac)_3$ was dissolved in acetic anhydride instead of H_2O.

3.5.2 The VMgO catalyst

Table 3.5 Reagents for the preparation of a VMgO catalyst

Reagent	Molar mass/ g mol^{-1}	Supplier	Purity
MgO	40.29	Acros Organics	98 %
NH_4VO_3	116.98	Aldrich	99 + %
NH_4OH	35.05	Rochelle Chemicals	25 % (in solution)
$Co(acac)_3$	356.26	Acros	99 %

Pure MgO was calcined at 350^{o}C for 12 hours to remove any carbonates. 850 ml of deionised water was added to 4.3 g of NH_4VO_3 and 10 ml of 25 % (v/v) NH_4OH solution to give a 0.5 weight % NH_4VO_3 and 1 weight % NH_4OH solution. The solution was heated to 70^{o}C until all the NH_4VO_3 dissolved. The MgO (6.7 g) was added to the solution while stirring and the suspension that was obtained was evaporated until it formed a slurry. The slurry was placed in an oven at 110^{o}C for 2 hours. The resulting solid was crushed and calcined for 6 hours at 550^{o}C. The powdered catalyst was pressed, ground and sieved to between 300 and 600 μm.

The promoter was incorporated via a co-precipitation method by introducing 0.33 g of $Co(acac)_3$ to the mixture of deionised water, NH_4VO_3 and NH_4OH to give a 2.5 bulk molar % (theoretical) of Co:V in the catalyst.

3.6 Catalyst characterization

The catalysts were characterized via Fourier transform-infrared (FT-IR) spectroscopy, X-ray diffraction (XRD), Brunauer-Emmet-Teller (BET) surface area determination, energy dispersive X-ray (EDX) spectroscopy, scanning electron microscopy (SEM), inductively coupled plasma-atomic emission spectroscopy (ICP-AES) and average vanadium oxidation state

(AV) analyses. The theoretical aspects of these techniques are discussed in more detail in the Appendix.

3.6.1 X-ray diffraction measurements

The XRD spectra were recorded on a Philips PW1130 instrument. Specifications of the instrument and a discussion of the principles of this technique appear in the Appendix. The spectra were recorded at Sasol Technology (Pty) Ltd and the School of Geology, University of KwaZulu-Natal, Howard College campus.

3.6.2 Scanning electron microscopy (SEM)/Energy dispersive X-ray (EDX) analyses

The catalyst samples were viewed and analysed on a Hitachi S520 scanning electron microscope (SEM) fitted with a Link ISIS energy dispersive X-ray (EDX) analytical system. Approximately 0.05 g of catalyst sample was mounted onto adhesive tape for SEM and EDX analyses. The catalyst was coated with gold to prevent movement of the catalyst particles induced by X-ray bombardment during examination under 10 000 X magnification. A discussion of the principles of these techniques appears in the Appendix. SEM and EDX analyses were conducted in the Electron Microscopy Unit at the University of KwaZulu-Natal, Howard College and Pietermaritzburg campuses.

3.6.3 Fourier-transform-infrared (FT-IR) spectroscopy measurements

Fourier transform-infrared (FT-IR) spectra were recorded on a Nicolet 400D infrared spectrometer. The IR spectra were recorded using the KBr pellet sample preparation technique. A 1:20 mass ratio of catalyst to dried KBr powder was ground and mixed in a mortar and pestle. The mixture was compressed into a pellet. All the equipment that was used in the preparation of the KBr pellet was heated to prevent moisture absorption by the sample. The background for analysis was obtained from the IR spectrum of a neat KBr pellet. A discussion of the principles of this technique appears in the Appendix.

3.6.4 Brunauer-Emmet-Teller (BET) surface area measurements

The catalyst sample was out-gassed at 200^{o}C overnight under a nitrogen atmosphere. The sample was placed into position in a Tristar sample cell where it was evacuated prior to being immersed in liquid nitrogen for the analysis. A measured portion of nitrogen was placed in the evacuated sample cell. The sample absorbed a certain amount related to its own intrinsic capacity. This measured volume of gas was then used in calculations to determine the volume adsorbed at monolayer coverage for BET, i.e. in the range 0.05 to 0.3 P/P_o, which was the ratio of the pressure in the sample cell to atmospheric pressure. The BET total surface area was calculated via the standard calculation developed by Brunauer, Emmet and Teller (Thomas, J.M. *et al.* (1996)). Samples were analysed by Sasol Technology (Pty) Ltd and Süd-Chemie, South Africa.

3.6.5 Inductively coupled plasma-atomic emission spectroscopy (ICP-AES) measurements

The bulk elemental compositions of the catalysts were determined using inductively coupled plasma-atomic emission spectroscopy (ICP-AES). A Jobin-Yvon (JY 24) instrument was used. Multi-element standards were prepared (Table 3.6). A 1000 ppm stock solution of phosphorous was prepared by calcining KH_2PO_4, cooling the sample and accurately weighing out and dissolving 0.5 g in deionised water made up to volume in a 500 ml volumetric flask.

The microwave digestion temperature, pressure profile and method employed to digest the catalyst samples appear on p. 272 in the Appendix. Approximately 0.1 g of catalyst was accurately weighed out and digested in aqua regia (3.5 ml HCl and 1.5 ml HNO_3) and then made up to volume in a 100 ml volumetric flask. A blank consisted of the same volume of aqua regia as in the sample solution made up to volume in a 100 ml volumetric flask. A blank correction was employed by subtracting the signal obtained from the blank solution from the sample solution.

Table 3.6 Multi-element standard (STD) concentrations and wavelengths used for analysis via ICP-AES

Element	Supplier	Wavelength/ nm	Concentration/ppm			
			STD 1	STD 2	STD 3	STD 4
1st set of multi-element standards						
Mg	Fluka	279.079	10	20	40	100
P	Prepared	213.618	5	10	20	50
V	Polychem	309.311	5	10	20	50
2nd set of multi-element standards						
Co	Fluka	236.379	0.08	0.4	0.8	
Rh	Prepared	249.077	0.5	2.5	5.0	

P and Rh stock solutions were prepared by digesting appropriate amounts of KH_2PO_4 and $RhCl_3$ salts, respectively, in 3 mL of a 3:2 volumetric ratio of HNO_3:HCl and diluting to 1 L giving a concentration of 1000 ppm.

The wavelength used for the analysis of each element was dictated by the detection limit based on the concentration range required. The instrument was set to automatically search for the wavelength specific to the emitting element that was being pumped into the flame. Corrections were employed for variation in wavelengths detected by the instrument. The zero emission point on the calibration curve was set using the signal obtained from deionised water. A discussion of the principles of this technique appears in the Appendix.

3.6.6 Average vanadium oxidation state (AV)

The average vanadium oxidation state (AV) was determined by a redox titration procedure, largely the same as that employed by Nakamura *et al.* (1974). About 0.1 g of catalyst was accurately weighed and dissolved in 17 ml of 12 M *ortho*-H_3PO_4 (98+ %) and boiled till a clear solution was obtained. This solution was added to a mixture of 10 ml concentrated H_2SO_4 in 250 ml water. Graphite was removed by filtration. All vanadium ions were oxidized to V^{5+} by titration with 0.01 M $KMnO_4$ solution i.e. until the analyte solution turned purple. The

pentavalent ions were reduced to V^{4+} using a 0.05 M $Fe(NH_4)_2(SO_4)_2$ solution, with 1 % diphenylamine in concentrated H_2SO_4 as an indicator. The end-point was reached when the analyte solution turned colourless. The average vanadium oxidation state was calculated as follows:

$$AV = 5 - \frac{(volume\ KMnO_4\ solution)}{(volume\ Fe(NH_4)_2(SO_4)_2\ solution)}$$

3.6.7 Gas chromatography-mass spectrometry (GC-MS) analysis

The aqueous and organic catchpot samples were analysed via gas chromatography-mass spectrometry (GC-MS) to identify the compounds present. GC-MS analyses were performed at the Chemical Engineering Department of the University of KwaZulu-Natal, Howard College campus on a Perkin Elmer Autosystem XL GC fitted with an ELITE 5 ms column and Sasol Technology (Pty) Ltd on a HP 6890 model GC-MS fitted with a PONA column (Details of these columns appear on p. 249 in the Appendix). Certain available components that were identified via GC-MS were injected into the on-line GC linked to the reactor to verify the retention times with that of the components from the reactor.

3.6.8 Transition electron microscopy-energy dispersive X-ray (TEM-EDX) analysis

The elemental composition of catalysts was determined by EDX analyses of TEM sections on a Phillips 120 Biotwin TEM and EDX instrument. The analyses were performed at a sampling voltage of 80 kV using a berylium detector. 0.05 g of catalyst sample was mixed with water in a sample vial. The fine catalyst particles that floated on the water surface were drawn into a dropper and coated onto a copper grid for analysis in the instrument. Analyses were performed at the Electron Microscopy unit at the University of KwaZulu-Natal, Pietermaritzburg campus.

3.7 Experimental procedure for catalyst testing

A neat calcined catalyst was packed tightly towards the exit end of a reactor tube. Inert carborundum (SiC having a particle size range between 300 and 600 μm) was used to fill any volume that was not occupied by the catalyst and glass wool in the reactor (Fig. 3.6). A blank reactor was fully packed with SiC having a particle size range between 300 and 600 μm.

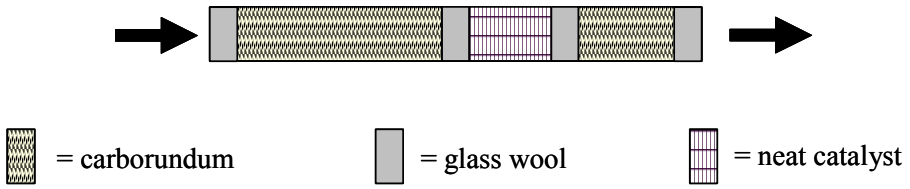

Fig. 3.6 A conventionally packed steel reactor indicating the location of catalyst, glass wool, carborundum and direction of flow

The catalyst was sandwiched between carborundum and glass wool. The glass wool prevented any particulate matter from entering the on-line sampling valves and, subsequently, the gas chromatographs.

Factors that were controlled during the testing of catalysts were the amount of promoter loaded on the catalyst, method of promoter inclusion, method of catalyst synthesis, GHSV and temperature.

The catalysts required time to reach steady-state, which was specific to the catalyst under investigation (usually longer than 5 h in work carried out in this thesis). The catalyst under steady-state conditions gave constant conversions and selectivities over time. 1 ml of catalyst was used in reactions and the GHSV was controlled by the flowrate.

The glass reactor was not subjected to temperatures higher than 520^{o}C to prevent deformation of the reactor.

3.7.1 Reactor startup and stopping procedure

Table 3.7 % Alkane in air fed into the reactor for catalytic and non-catalytic experiments showing the lower flammability limits (lfl) and upper flammability limits (ufl) for the respective alkanes

Feed	lfl	ufl	% Feed in air used
n-butane	1.8	8.4	1.0
n-hexane	1.7	7.7	7.8
n-octane	1.0	6.5	7.3

The alkane mixtures above are quoted at room temperature and atmospheric pressure. At elevated temperatures in the reactor, 1 % *n*-butane falls within the flammability range at temperatures higher than 550^{o}C, *n*-hexane and *n*-octane fall within the flammability range at temperatures higher than 300^{o}C (A table showing the variation of the flammability range at elevated temperature appears on p. 255 in the Appendix). If the temperature or pressure is increased, the lfl will decrease whilst the ufl will increase, giving a wider range of compositions over which the feed may explode. The lfl decreases by about 8 % of its value at room temperature and atmospheric pressure for every 100^{o}C increase in temperature, whilst the ufl increases by about 8 % of its value at room temperature and atmospheric pressure for every 100^{o}C increase in temperature (Perry, R.H. *et al.* (1999)).

When the upper and lower flammability limits are reached, the mixture can propagate a flame when ignited, however, there is a temperature at which this occurs. The temperature corresponding to the lfl is the flash point of the organic vapour, whilst the temperature corresponding to the ufl is considerably below the autoignition temperature. The autoignition temperatures for *n*-butane, *n*-hexane and *n*-octane are 372, 240 and 220^{o}C, respectively (ChemDAT® software (2005)) and the flammability ranges for the alkanes are 1.5-8.5, 1.1-7.5 and 0.8-6.5 (v/v) % in air, respectively (Perry, R.H. *et al.* (1999)). Since the temperatures

investigated were higher than the autoignition temperatures for the oxidation of *n*-butane, *n*-hexane and *n*-octane a flame may form which results in combustion of the alkane.

The alkane:O_2 molar ratios were maintained below the stoichiometric value (viz. 0.05 for *n*-butane, 0.4 for *n*-hexane and 0.4 for *n*-octane which were determined using the equation on p. (x)). It is usual for processes to be operated on pure oxygen when working above a stoichiometric ratio of alkane to air (Centi, G. *et al.* (2001)). Air was maintained as a source of the oxidant since it is cheaper than pure oxygen for both laboratory scale and industrial scale processes.

With the exception of the *n*-butane mixture (i.e. 1.0 % *n*-butane in air), the alkane in air mixtures were maintained just above the flammability range (i.e. 7.8 % *n*-hexane in air and 7.3 % *n*-octane in air).

It is preferable to work above the flammability range. There is an oxygen-deficient environment above the flammability range which lessens over-oxidation of the alkanes in the reactor. The concentrations of *n*-hexane and *n*-octane in air were maintained above the flammability range in catalytic and non-catalytic experiments, whilst the concentration of *n*-butane in air was maintained below the flammability range due to safety regulations. It was found experimentally that the catalyst was most active for feeds whose concentration was close to the flammability range; hence values close to the flammability range were employed.

It is essential during reactor startup and stopping procedures that the feed into the reactor does not reach an explosive mixture, which can destroy the catalyst.

For a premixture of *n*-butane in air and *n*-hexane in air, the reactor startup is relatively simple. The reactor temperature is increased from room temperature to 200^{o}C with the premixture flowing through the reactor. Conditioning of the catalyst is done at 200^{o}C, whereby the catalyst is maintained at this temperature for 5 hours before further testing.

For an *n*-octane in air mixture, *n*-octane is introduced separately as a liquid into the feed line containing a stream of air. During startup, *n*-octane is initially introduced into the feed line, thereafter air is introduced so as to maintain the mixture above the flammability range. The

reactor temperature is set at 200^{o}C to condition the catalyst for 5 hours. The mixture shall equilibrate to the desired ratio of *n*-octane to air during time on stream. The reactor is stopped by stopping the *n*-octane in air mixture through the reactor and flushing the reactor with nitrogen. This dilutes the mixture and reduces the risk of falling within the flammability range.

3.8 The effect of voids and dilution on n-hexane conversion over a VMgO catalyst

This study illustrated some of the problems associated with alkane activation and subsequent conversion to valuable products with respect to location of voids and the catalyst in the reactor. The effects of differently packed reactors and dilution factors on the product profile were investigated.

Reaction studies were performed in stainless steel and glass micro-reactors. A 7.8 % *n*-hexane in air mixture was maintained throughout the study. A fixed volume of 0.2 ml of catalyst was maintained in all catalyst testing. The gas hourly space velocity was 3000 hr^{-1}. The carborundum (SiC) particles were between 300 and 600 μm in size.

An empty reactor (referred to as setup 1) and a reactor fully packed with carborundum (setup 2) were investigated in the oxidation of *n*-hexane, thus determining the contribution made by the carborundum and voids in the oxidation of *n*-hexane in a conventionally packed reactor under catalytic conditions. A conventionally packed reactor (Fig. 3.6) was referred to as setup 3.

Fig. 3.7 illustrates the various locations of the catalyst in the reactor and the catalyst dilution setups. The neat catalyst was packed at the entrance of the reactor in setup 4 and a void followed the catalyst. A void preceded the catalyst in setup 6, with the catalyst packed at the end of the reactor. The voids in setups 4 and 6 were filled with carborundum (in setups 5 and 7 respectively). In setup 8, the catalyst was diluted 1:1 with carborundum. In setup 9, the catalyst was further diluted with the same quantity of carborundum used to pack the reactor in setup 8.

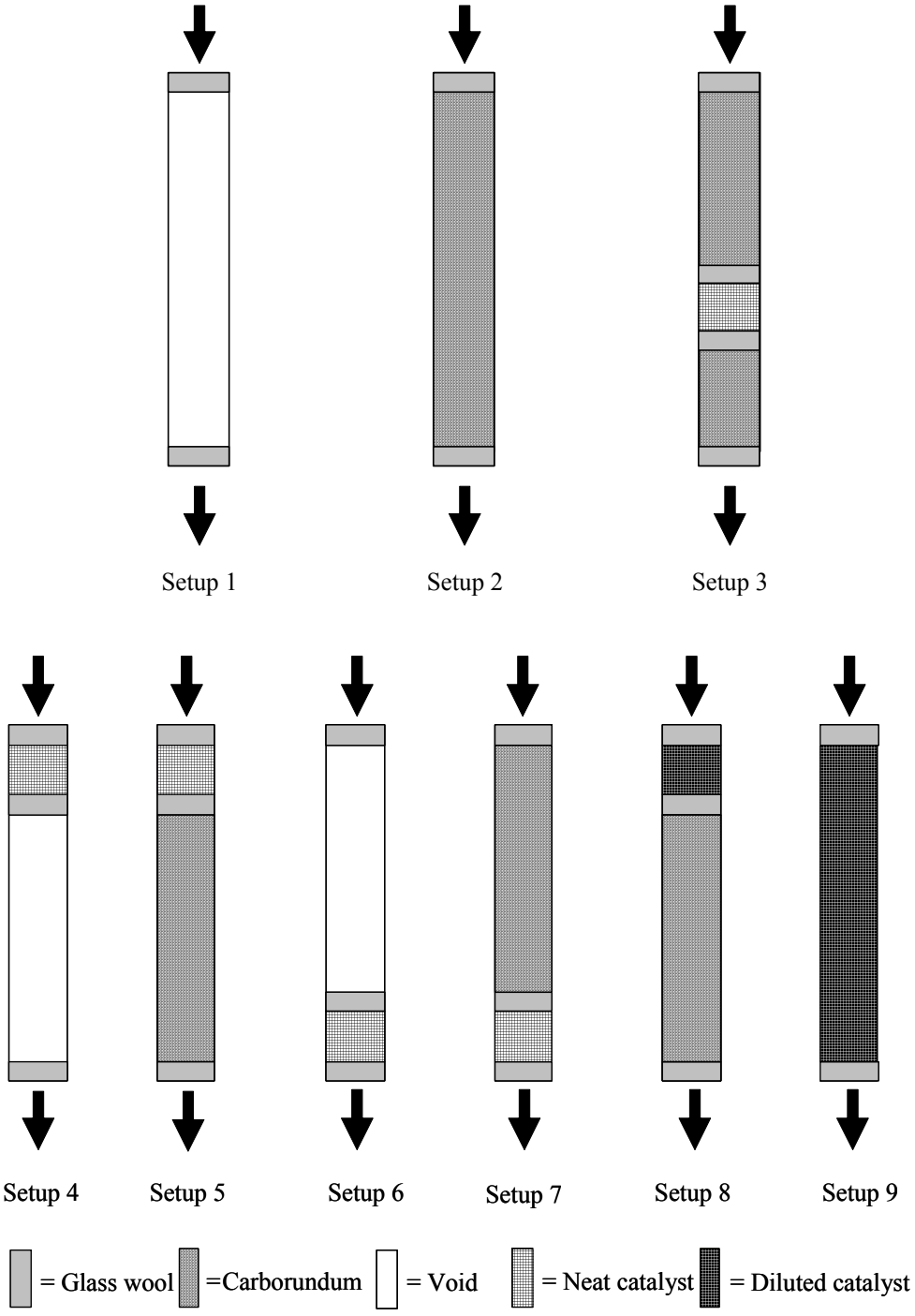

Fig. 3.7 The location of neat and diluted catalysts and voids in the reactor. The arrows indicate the flow of feed

The reactor was initially heated to 200^{o}C before the reactant was introduced into the reactor.

References

Nakamura, K., Kawai, K., Fujiwara, Y., J. Catal., **34**, 345 (1974)

Sakurai, Y., Suzaki, T., Nakagawa, K., Ikenaga, Na-oki, Aota, H., Suzuki, T., J. Catal, 209, **16** (2002)

Sookraj, S.H., Engelbrecht, D., Catal. Today, **49**, 162 (1999)

Thomas, J.M., Thomas, W.J., Principles and Practice of Heterogeneous Catalysis, VCH Publishers, New York, p 259 (1996)

Wolf, A., Schuth, F., Appl. Catal. A: General, **226**, 2 (2002)

CHAPTER 4

RESULTS

The activities of promoted and unpromoted mixed metal oxide catalysts in the oxidation of C_4, C_6 and C_8 alkanes were compared. The product selectivity profiles were examined from vanadium phosphorous oxide (VPO) and vanadium magnesium oxide (VMgO) catalysts. The effects of different promoters, different promoter loadings, different methods of incorporation, the concentration of alkane in air, operating temperature, gas hourly space velocity (GHSV), and catalyst particle and inert packing particle sizes were investigated on the activity of the catalyst and selectivity to chosen products to obtain optimum operating conditions; moreover to correlate structure and operating conditions to the activity and selectivity of the catalysts. Various promoted VPO catalysts (including Co, Rh and Au promoters) were investigated in the oxidation of *n*-butane. The cobalt promoter that best improved the selectivity to maleic anhydride (MA) in the oxidation of *n*-butane compared to the unpromoted catalyst was further investigated on *n*-hexane and *n*-octane oxidation.

The catalysts were characterized at different stages of their synthesis (precursor, calcination of the precursor, and used catalysts). The transformation of phases through the different stages of their synthesis was correlated to their activity and selectivity. The types of products obtained were attributed to the phases present in the catalyst and the catalyst was categorized based on its oxidizing nature.

With any catalytic investigation, it is important to determine any contributions the reactor material and inert packing material has on the catalysis. For this blank reaction investigations were undertaken. This was investigated further by looking at the catalytic and non-catalytic contribution to obtaining a desired product.

Results obtained from the oxidation of proposed intermediates to benzene were used to propose a mechanism for its formation, starting with hexane.

Since this work is was comparative study of different alkanes, different catalysts with different oxidizing abilities and reactor materials, the results highlight similarities and contrasts between the different systems. A description of all catalysts tested appears in the foldout section of the Appendix (p. 293).

4.1 Catalyst characterisation

4.1.1 X-ray diffraction (XRD) study

4.1.1.1 Unpromoted VPO catalyst

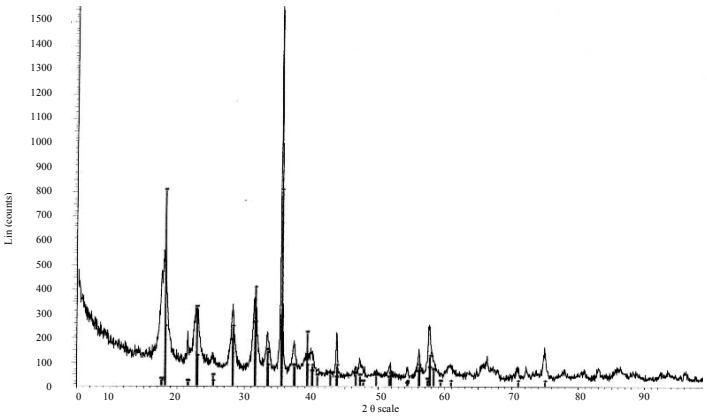

Fig. 4.1 XRD pattern of an unpromoted VPO catalyst precursor

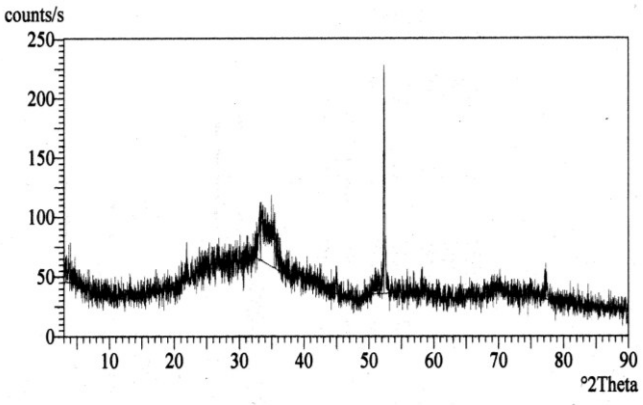

Fig. 4.2 XRD pattern of a calcined unpromoted VPO catalyst

The VPO catalyst precursor (Fig. 4.1) refers to a catalyst before calcination. The XRD pattern indicated a crystalline vanadyl hydrogen phosphate, $VOHPO_4 \cdot 0.5H_2O$, catalyst precursor phase when compared to the literature (Horowitz, H.S. *et al.* (1988)). A table of the relative intensities of the diffraction bands and 2θ values appears on p. 241 in the Appendix.

The calcined catalyst appeared rather amorphous, indicated by broad diffraction bands in the XRD pattern (Fig. 4.2), except for distinct bands at 52 and 78 2θ values. These bands were attributed to a $(VO)_2P_2O_7$ phase (Coulston, G.W. *et al.* (1997) and Albonetti, S. *et al.* (1996)). The broad bands were attributed to a mixture of phases. A table of these phases and their structural characteristics appear in the Appendix (p. 268).

The XRD pattern of the used catalyst (Fig. 4.3) showed multiple sharp bands. This indicated that the catalyst changed into a crystalline material after reaction. A table of the relative intensities of the diffraction bands and 2θ values appears on p. 241 in the Appendix.

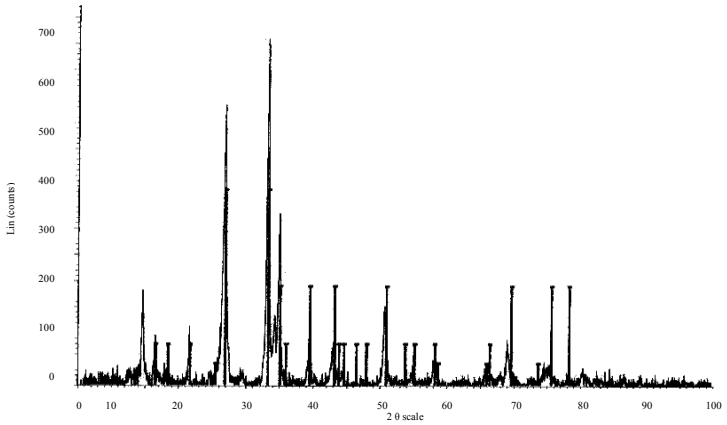

Fig. 4.3 XRD pattern of a used unpromoted VPO catalyst

The XRD pattern of the used catalyst (i.e. a catalyst after a reaction) (Fig. 4.3) was indicative of the vanadyl pyrophosphate phase, $(VO)_2P_2O_7$, which is the proposed active catalytic phase of the VPO catalyst. This indicated that the bulk of the vanadium was in the +4 oxidation state. The XRD patterns of the used catalysts appeared similar after the oxidation of alkanes of different chainlengths, indicating the presence of the same $(VO)_2P_2O_7$ phase. This single phase appeared after reaction at 300^{o}C. Hutchings, G.J. (1991) showed that the catalyst was more selective to MA formation with most of the vanadium in the +4 oxidation state as opposed to a +5 oxidation state.

4.1.1.2 Cobalt promoted catalysts (Co-VPO): co-precipitation method

XRD patterns of the three cobalt promoted catalyst precursors (Table 3.4) viz. 1.25 % Co-VPO (Fig. 4.4), 2.5 % Co-VPO (Fig. 4.5) and 5.0 % Co-VPO (Fig. 4.6) showed the presence of the $VOHPO_4 \cdot 0.5H_2O$ phase when compared to an XRD pattern in the literature (Horowitz, H.S. *et al.* (1988)). There was no indication of cobalt phases in the XRD patterns of the cobalt

promoted catalysts. This is attributed to the poor detection limit of the technique for the small quantities of promoter used.

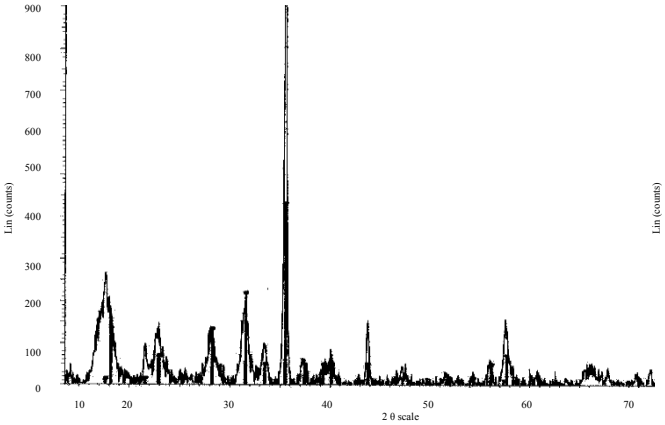

Fig. 4.4 XRD pattern of a 1.25 % Co-VPO catalyst precursor

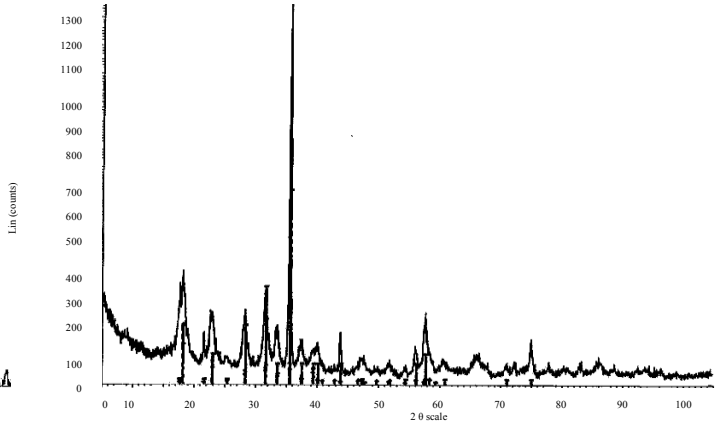

Fig. 4.5 XRD pattern of a 2.5 % Co-VPO catalyst precursor

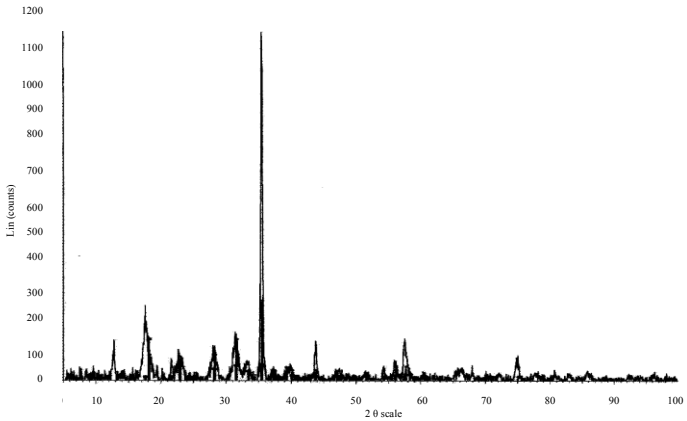

Fig. 4.6 XRD pattern of a 5.0 % Co-VPO catalyst precursor

The XRD patterns obtained from the precursor, calcined and used promoted VPO catalysts (co-precipitation) appeared similar to the precursor, calcined and used unpromoted catalysts, respectively, except that increasing the promoter loading resulted in the catalyst becoming less crystalline, which was noted from decreasing band intensities in the XRD patterns.

The (020) plane of $(VO)_2P_2O_7$ is characterized by the presence of paired vanadium pseudo-octahedra oriented *trans* to one another, and is claimed to be the catalytically selective

plane (Horowitz, H.S. *et al.* (1988)). All three cobalt promoted VPO catalysts and unpromoted catalysts were found to contain this plane (Table 4.1).

Other planes assigned to the 2θ values obtained from the XRD patterns of the VPO catalysts appear in Table 4.1. A table of all 2θ values and the relative intensities of their diffraction bands appears on p. 241 in the Appendix.

Table 4.1 2θ Values for unpromoted and cobalt promoted catalysts with their respective plane assignments

2θ				
0 % Co-VPO	1.25 % Co-VPO	2.5 % Co-VPO	5.0 % Co-VPO	Assignment
17.858	17.527	18.038	17.571	(020)[1]
21.412	21.433		21.542	(111)[1]
22.763	22.746	22.681	22.676	(200)[2]
28.150	28.113	28.119	28.093	(201)[1]
31.499	31.560	31.438	31.369	(031)[1]
33.325	33.365	33.424	33.132	(102)[1]
35.497	35.424	35.414	35.526	(112)[1]
37.354	37.224	37.271	37.164	(040)[1]
		39.923	39.935	(202)[1]
43.724	43.725	43.746	43.714	(400)[3]
		47.216	47.494	(241)[1]

[1] Johnson, J.W., Johnston, D.C., Jacobson, A.J., Brody, J.F., J. Am. Chem. Soc., **106**, 8125 (1984)
[2] Sananés-Schulz, M.T., Tuel, A., Hutchings, G.J., Volta, J.C., J. Catal., **166**, 390 (1997)
[3] Brutovsky, M., Gerej, S., Vasilco, F., Gerejova, J., Collection Czech. Chem. Commun., **47,** 1294 (1982)

4.1.1.3 Cobalt promoted catalysts (Co-VPO): precipitation/deposition method

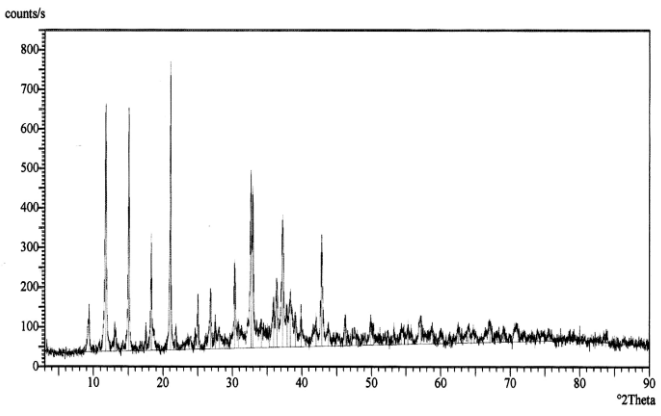

Fig. 4.7 XRD pattern of a 2.5 % Co-VPO catalyst precursor (precipitation/deposition)

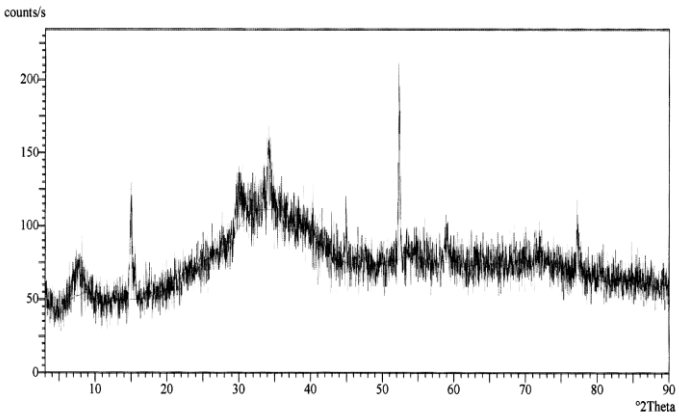

Fig. 4.8 XRD pattern of a calcined 2.5 % Co-VPO catalyst (precipitation/deposition)

The XRD pattern of the 2.5 % Co-VPO catalyst precursor obtained by the precipitation/deposition method (Fig. 4.7) is different from the 2.5 % Co-VPO catalyst precursor obtained by the co-precipitation method (Fig. 4.5). Diffraction bands at $2\theta < 43$ were sharper in the Co-VPO catalyst (precipitation/deposition) XRD pattern than the Co-VPO catalyst (co-precipitation) XRD pattern. The 100 % intensity band appeared at $2\theta \sim 35$ in the XRD pattern of the Co-VPO catalyst (co-precipitation) and at $2\theta \sim 21$ in the XRD pattern of the Co-VPO catalyst (precipitation/deposition). There was an indication of mixed phases of $VOHPO_4 \cdot 0.5H_2O$ and $VOPO_4 \cdot 2H_2O$ when comparing the 2θ values and band intensities obtained to data in the literature (Bordes, E. (1987)). The XRD pattern of the calcined 2.5 % Co-VPO catalyst (precipitation/deposition) (Fig. 4.8) appeared similar to the XRD pattern of the calcined 2.5 % Co-VPO catalyst (co-precipitation) with a broad band in the 20-60 2θ range. A table of 2θ values and their relative intensities of the diffraction bands appears on p. 241 in the Appendix.

4.1.1.4 Rhodium promoted catalyst (Rh-VPO): co-precipitation method

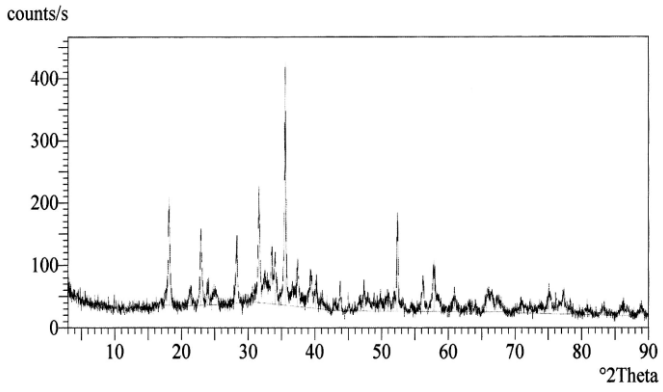

Fig. 4.9 XRD pattern of a 2.5 % Rh-VPO catalyst precursor

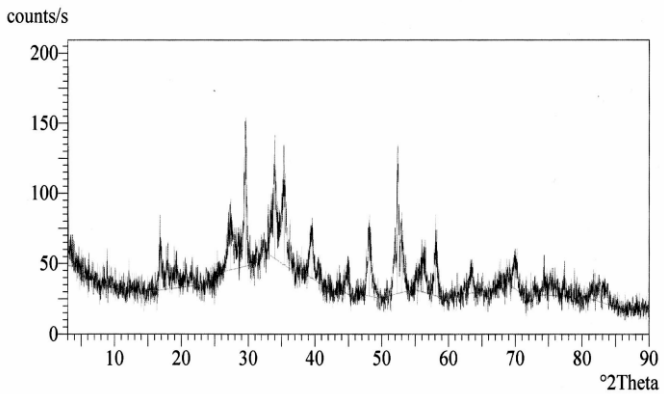

Fig. 4.10 XRD pattern of a calcined 2.5 % Rh-VPO catalyst

The XRD pattern of the 2.5 % Rh-VPO catalyst precursor (co-precipitation) (Fig. 4.9) indicated the presence of a $VOHPO_4 \cdot 0.5H_2O$ phase. It was evident from the XRD pattern of the calcined 2.5 % Rh-VPO catalyst (Fig. 4.10) that there was a higher retention of crystallinity

after calcining the Rh-VPO catalyst precursor, compared to calcination of the unpromoted VPO catalyst precursor (Fig. 4.2). The rhodium is assumed responsible for the retention of crystallinity.

4.1.1.5 Rhodium promoted catalyst (Rh-VPO): precipitation/deposition method

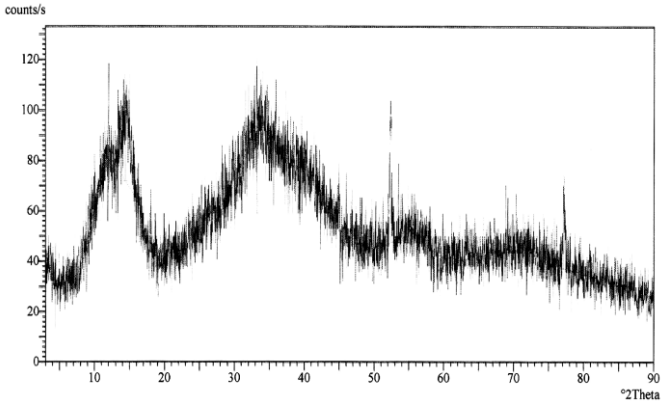

Fig. 4.11 XRD pattern of a 2.5 % Rh-VPO catalyst precursor (precipitation/deposition)

The XRD pattern of the 2.5 % Rh-VPO catalyst precursor (precipitation/deposition) (Fig. 4.11) resembled the XRD pattern of a calcined unpromoted catalyst (Fig. 4.2) with the broad band in the 20-60 2θ range. This XRD pattern indicated a lack of crystallinity or that there were multiple phases present.

The XRD pattern of the 2.5 % Rh-VPO catalyst (co-precipitation) (Fig. 4.9) and the 2.5 % Co-VPO catalyst precursors (co-precipitation and precipitation/deposition) (Figs. 4.5 and 4.7, respectively), however, showed crystallinity.

4.1.1.6 Modification of a VPO catalyst by gold using a co-precipitation synthesis method (VPO A and VPO-B)

Attempts to prepare 2.5 % and 5.0 % gold promoted VPO catalysts (referred to as VPO-A and VPO-B respectively) via the co-precipitation method were unsuccessful. Elemental

analysis of the catalyst via inductively coupled plasma-atomic emission spectroscopy (ICP-AES) (Table 4.2) and energy dispersive X-ray (EDX) (Table 4.3) showed that gold was not present in the catalyst.

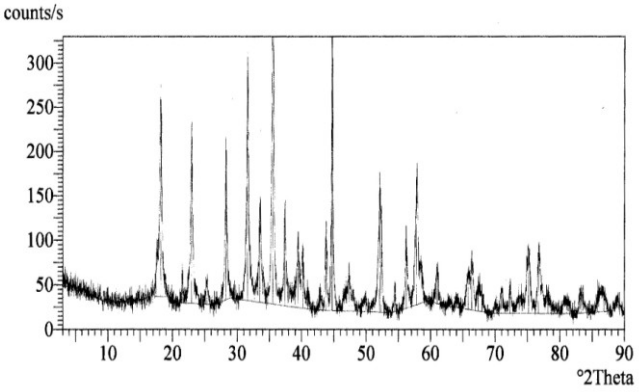

Fig. 4.12 XRD pattern of the VPO-A catalyst precursor

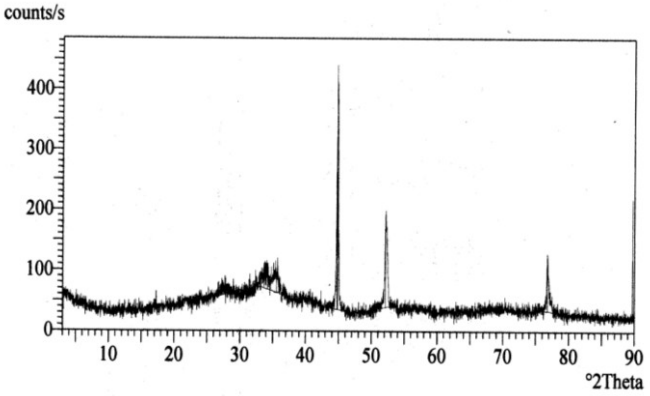

Fig. 4.13 XRD pattern of the calcined VPO-A catalyst

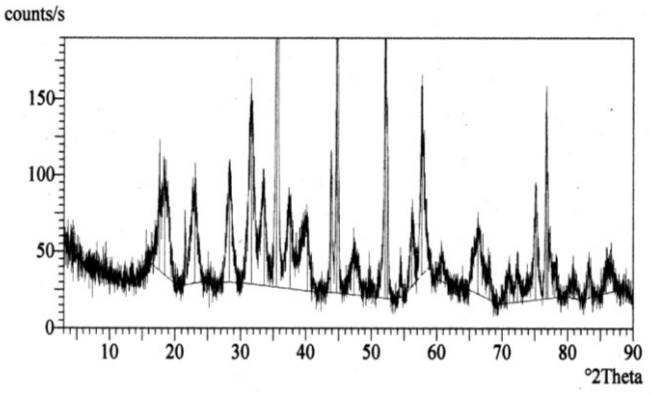

Fig. 4.14 XRD pattern of the VPO-B catalyst precursor

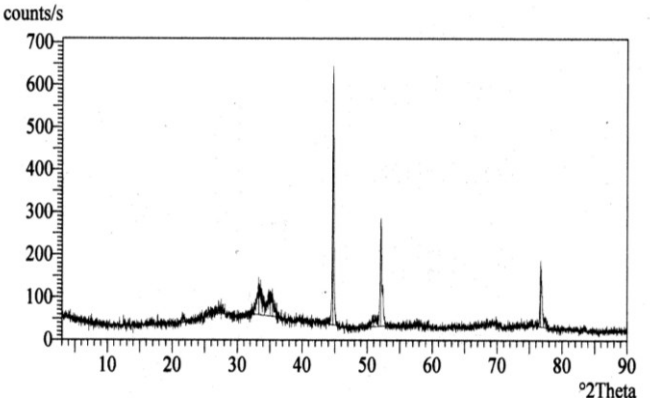

Fig. 4.15 XRD pattern of the calcined VPO-B catalyst

The XRD patterns of VPO-A and VPO-B catalyst precursors (Figs. 4.12 and 4.14) showed the presence of the $VOHPO_4 \cdot 0.5H_2O$ phase. The calcined catalysts (Figs. 4.13 and 4.15 respectively) showed a change in structure of the catalyst precursor. The bands in the XRD pattern of the VPO-B catalyst precursor (Fig. 4.14) were broader and some of lower intensity than the bands in the XRD pattern of the VPO-A catalyst precursor (Fig. 4.12), which indicated a further loss in crystallinity with a larger amount of promoter in the synthesis.

The calcined VPO-A and VPO-B catalysts showed a stronger band at 2θ=45° compared to the other calcined promoted catalysts or the calcined unpromoted VPO catalyst. From the various XRD patterns of VPO phases reported in the literature, the quasi-stable V_4O_9 phase shows a distinct band at 2θ=45°, which was reported by Miyake, T. *et al.* (1995). The used catalysts, however, still showed the $(VO)_2P_2O_7$ active catalytic phase. A table of 2θ values and their relative intensities of the diffraction bands appears on p. 244 in the Appendix.

4.1.1.7 Gold promoted catalyst (Au-VPO): precipitation/deposition method

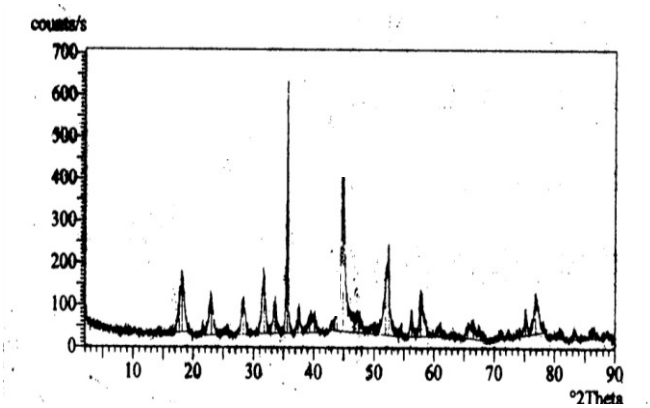

Fig. 4.16 XRD pattern of a Au-VPO catalyst precursor (precipitation/deposition)

The XRD pattern of the Au-VPO catalyst (precipitation/deposition) showed the presence of the $VOHPO_4 \cdot 0.5H_2O$ precursor phase of the VPO catalyst (Fig. 4.16). A table of 2θ values and their relative intensities of the diffraction bands appears on p. 242 in the Appendix. The broader bands in the XRD pattern compared to an unpromoted catalyst, suggested microcrystalline phases or amorphous characteristics. A V_4O_9 phase was identified in the calcined catalyst.

4.1.1.8 Unpromoted VMgO catalyst (VMgO)

The XRD pattern of the VMgO catalyst precursor indicated the presence of MgO and, clearly, the orthovanadate ($Mg_3V_2O_8$) phase of the three possible VMgO phases that can form viz. magnesium orthovanadate ($Mg_3V_2O_8$), magnesium pyrovanadate ($Mg_2V_2O_7$) and

magnesium metavanadate (MgV_2O_6) (Kung, H.H. *et al.* (1997)) (Fig. 4.17). Diffraction bands at 2θ = 42, 50 and 70 were assigned to MgO by Chaar, M.A. *et al.* (1987). The bands at 2θ = 40, 41, 52, 60, 74 and 78 are assigned to $Mg_3V_2O_8$ (JCPDS file 19-0778). Diffraction bands for a poorly crystalline magnesium orthovanadate phase were observed at 2θ ~ 41 (Chang, W.S. *et al.* (1995)). Fewer and sharper bands appeared in the XRD pattern of the calcined VMgO catalyst, which showed the presence of the magnesium orthovanadate ($Mg_3V_2O_8$) phase with the bands attributed to MgO appearing weaker (Fig. 4.18).

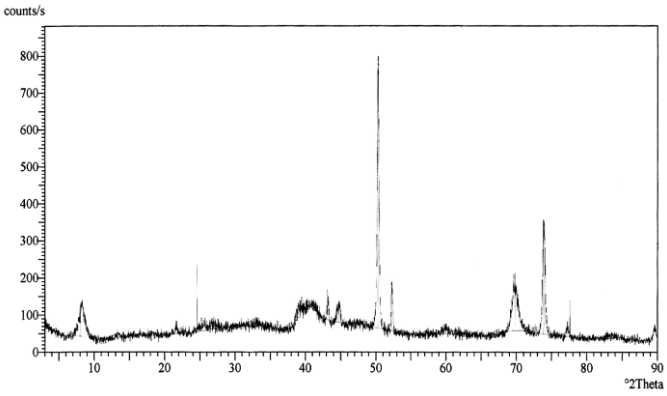

Fig. 4.17 XRD pattern of a VMgO catalyst precursor

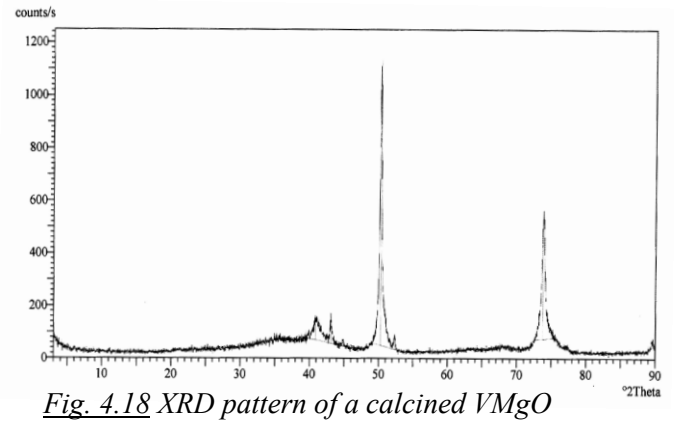

Fig. 4.18 XRD pattern of a calcined VMgO catalyst

The XRD pattern of the used VMgO catalyst appeared complex with sharper and more bands than the precursor (Fig. 4.17) and calcined catalyst (Fig. 4.18) and resembled the XRD pattern of a used Co-VMgO (Section 4.1.1.9). Under reducing conditions it has been shown that the orthovanadate phase can be converted into the pyrovanadate phase (Burrows, A. *et al.* (1999)). The alkane can serve as a reducing environment during a reaction for the reduction of the orthovanadate to the pyrovanadate phase. The complex XRD pattern of the used catalyst was attributed to the presence of both the ortho- and metavanadate phases.

4.1.1.9 Cobalt promoted VMgO catalyst (Co-VMgO): co-precipitation method

The presence of any cobalt phases in the XRD pattern of the promoted VMgO catalyst was not seen (Figs. 5.19-5.21), possibly due to the low sensitivity of the technique and/or the

amorphous nature of any possible cobalt phases that formed. The XRD patterns of the 2.5 % Co-VMgO precursor and calcined catalysts (co-precipitation) (Figs. 4.19 and 4.20, respectively) appeared similar to the unpromoted precursor and calcined catalysts (Figs. 4.17 and 4.18, respectively).

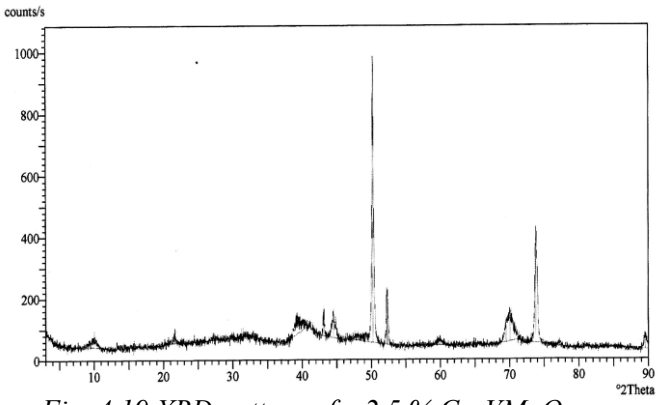

Fig. 4.19 XRD pattern of a 2.5 % Co-VMgO catalyst precursor

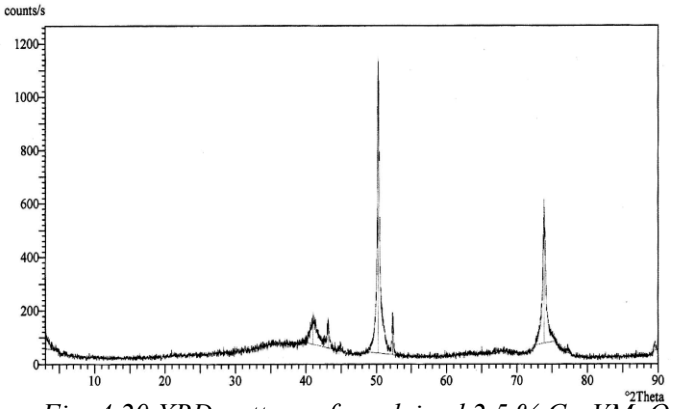

Fig. 4.20 XRD pattern of a calcined 2.5 % Co-VMgO catalyst

The XRD pattern of the used Co-VMgO catalyst (Fig. 4.21) (which resembled the XRD pattern of the used VMgO catalyst) revealed more diffraction bands than seen in the XRD pattern of the precursor (Fig. 4.19) and calcined catalyst (Fig. 4.20), thus indicating the formation of more phases during catalyst testing. The diffraction bands obtained for the used catalyst were also sharper and more intense than those obtained for the precursor and calcined catalysts. This indicated that the used catalyst was more crystalline in nature. A table of 2θ values and the relative intensities of the diffraction bands for both VMgO and Co-VMgO catalysts appears on p. 243 in the Appendix.

There appears to be an increase in the crystallinity of the VMgO and Co-VMgO catalysts (co-precipitation) after testing. More than one phase in the XRD pattern of the used Co-VMgO catalyst compared to the catalyst precursor and calcined catalysts was seen (Fig. 4.21). The new bands present at 2θ = 18, 23, 32 and 34 were attributed to the magnesium metavanadate (MgV_2O_6) phase according to Said, A.A. *et al.* (1995). The dominant orthovanadate phase, however, is the proposed catalytically active phase of the VMgO catalyst

in the literature (Gao, X. *et al.* (1994), Chang, W.S. *et al.* (1995)). The XRD patterns of the used Co-VMgO and VMgO catalysts appeared similar from the investigation of *n*-butane, *n*-hexane and *n*-octane oxidation.

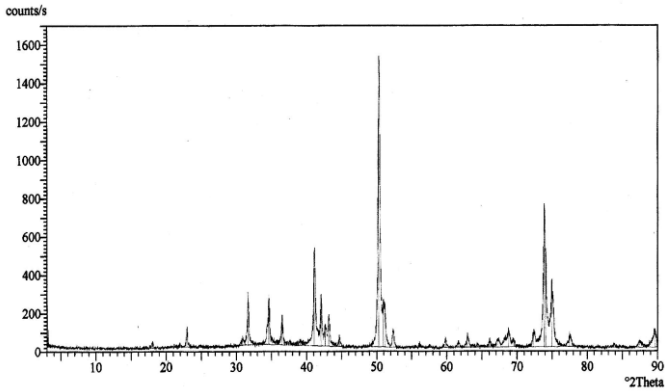

Fig. 4.21 Typical XRD pattern of a used 2.5 % Co-VMgO catalyst

The absence of cobalt phases in the XRD patterns can be attributed to the low concentration and high dispersion of the cobalt in the framework of the catalysts, which does not allow detection by X-ray phase analysis. This was also observed by Zazhigalov, V.A. *et al.* (1996) for other promoters at similar concentrations.

4.1.2 Fourier Transform-infrared study (FT-IR)

4.1.2.1 Unpromoted VPO catalyst

FT-IR spectra of the precursor, calcined and used unpromoted VPO catalysts (Figs. 4.22, 4.23 and 4.24 respectively) showed bands in the 900-1300 cm^{-1} region attributable to phosphate condensation. The bands were sharp which indicated a crystalline material that confirmed the result obtained from the XRD data.

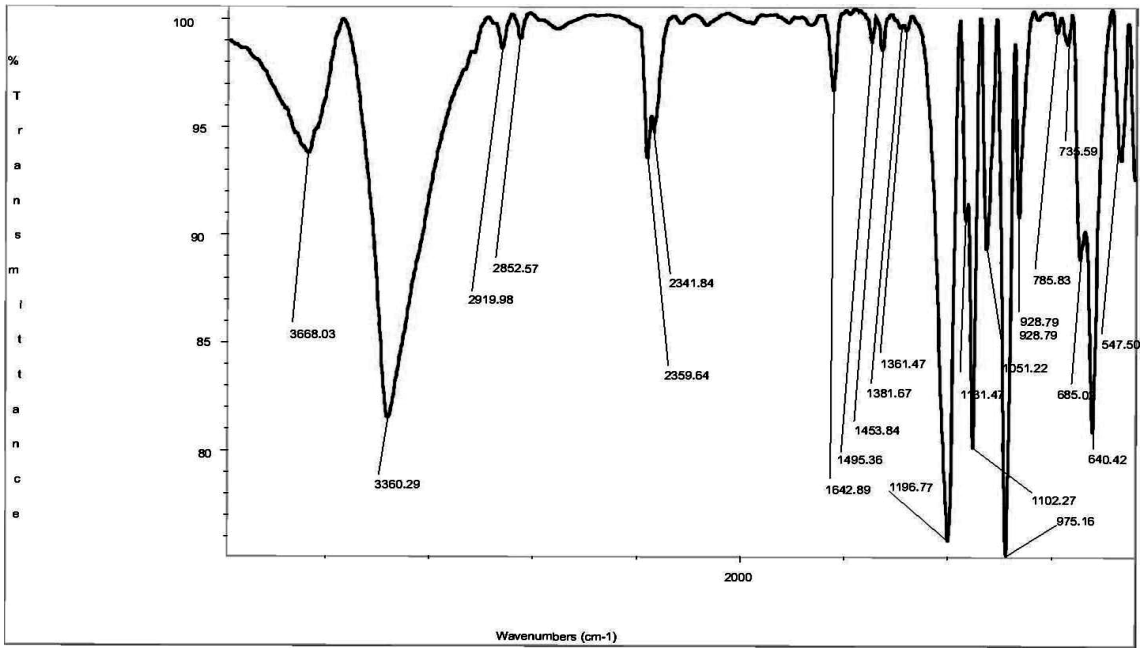

Fig. 4.22 FT-IR spectrum of an unpromoted VPO catalyst precursor

The catalyst appeared largely amorphous after calcination, which was indicated by the distinct IR bands in the 900-1300 cm^{-1} region of the FT-IR spectrum of the catalyst precursor (Fig. 4.22) being replaced by a broad absorption band in the calcined catalyst (Fig. 4.23), alluding to a variety of degrees of phosphate condensation (a table of the various phosphate species and their wavenumber assignments appears on p. 245 in the Appendix).

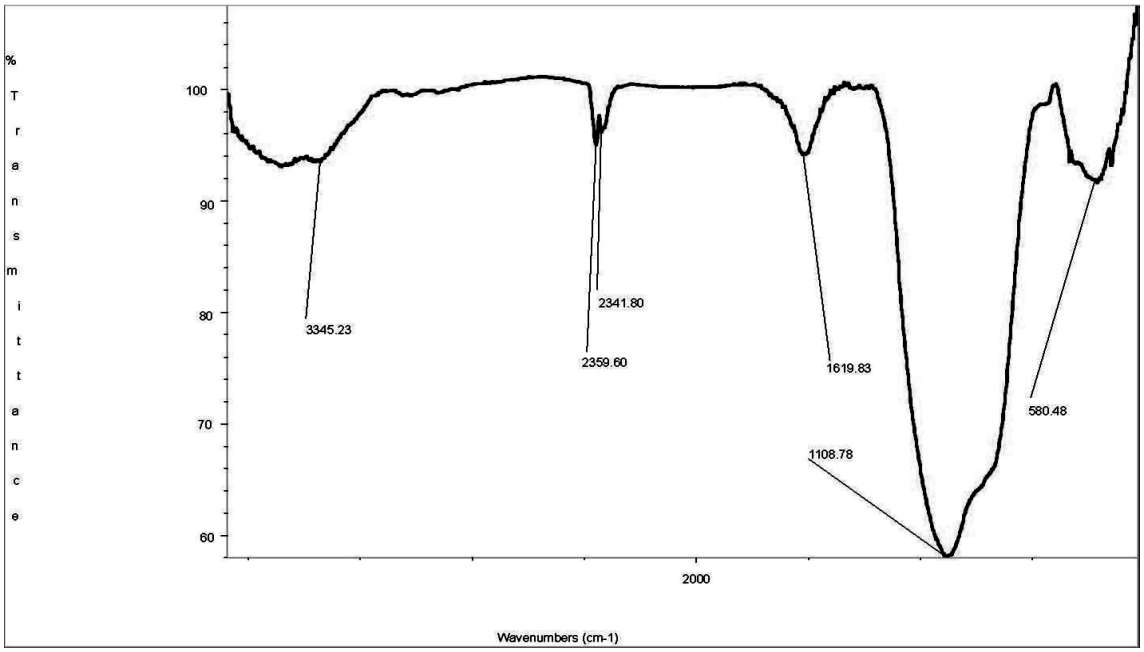

Fig. 4.23 FT-IR spectrum of a calcined unpromoted VPO catalyst

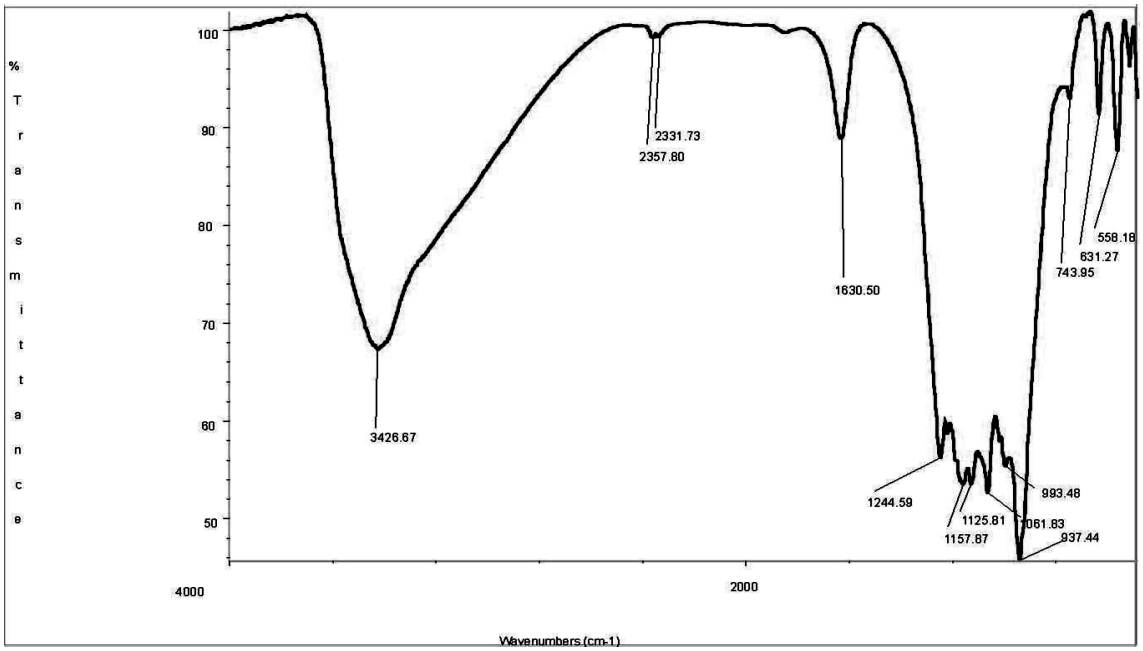

Fig. 4.24 FT-IR spectrum of a used unpromoted VPO catalyst

The FT-IR spectrum of the catalyst precursor showed the following adsorption bands in the 1200-420 cm^{-1} wavenumber region: 1196, 1131, 1102, 1051, 975, 928, 685, 640, 547, 475, 422 cm^{-1}. The bands with wavenumbers higher than 700 cm^{-1} were attributed to valence vibrations of P-O bonds in various anions of phosphorous with O, and the bands in the region below a wavenumber of 700 cm^{-1} were assigned to deformation vibrations of these anions (Brutovsky, M. *et al.* (1982)). Bordes, E. *et al.* (1979) considered the bands in the region 1050-1200 cm^{-1} to belong to the corresponding vibrations of ortho-, pyro-, tri- and higher linear phosphate ions.

The catalyst reverted to a more crystalline material (alluding to a single phosphate phase) after testing in the reactor (Fig. 4.24). The essential phosphate phase being $(VO)_2P_2O_7$, which is the proposed active catalytic phase reported in the literature (Zazhigalov, V.A. *et al.* (1993)). The presence of this phase was confirmed by the XRD pattern of the used catalyst (Fig. 4.3) and showed stretching vibrations in the FT-IR spectrum at wavenumbers of 743, 937 and 1061 cm^{-1}, which were assigned to ν_s(POP), ν_{as}(POP) and $\nu_s(PO_3)$ vibrations respectively by Bordes, E. *et al.* (1979).

The absorption band at about 975 cm^{-1} was attributed to the valence vibration of the V=O bond in the VPO catalysts based on the literature (Bordes, E. *et al.* (1979), Khodakov, A. *et al.* (1999)).

The intense bands present around wavenumbers of 970, 1100 and 1200 cm^{-1}, which were assigned to ν_{as}(POP) [$P_2O_7^{4-}$ anion], ν_s(O-PO^-) [cyclic $P_4O_{12}^{4-}$ anion] and ν_{as}(O-PO^-) [cyclic $P_4O_{12}^{4-}$ anion] vibrations respectively by Bordes, E. *et al.* (1979), appeared in the doped (co-precipitation) and undoped precursor and used catalysts (Figs. 5.22, 5.24 and 5.25, Chapter 5).

The XRD pattern of the used catalyst showed only the diffraction bands due to $(VO)_2P_2O_7$, whereas the FT-IR spectrum exhibited bands that could be assigned to vibrations of two anions ($P_2O_7^{4-}$ and cyclic $P_4O_{12}^{4-}$). This indicated that the $P_4O_{12}^{4-}$ anion was present in the X-ray amorphous state.

The IR bands at 2330 and 2360 cm^{-1} were attributed to carbon dioxide present in air during recording of the spectra and were present in all the FT-IR spectra.

The band at around 3400 cm^{-1}, which appeared in the IR spectra of the precursor, calcined and used catalysts, did not match a "standard" water peak. It was attributed to the hydroxy groups in the alcohol mixture (benzyl alcohol and *iso*-butanol) used in the synthesis of these catalysts, which was possibly trapped in the lattice of the catalyst. This band was seen in the FT-IR spectra of all VPO catalysts.

4.1.2.2 Cobalt promoted catalysts (Co-VPO): co-precipitation method

The bands in the FT-IR spectra of the cobalt promoted catalysts viz. 1.3 % Co-VPO, 2.5 % Co-VPO (Fig. 4.25) and 5.0 % Co-VPO appeared at similar wavenumbers compared to the unpromoted catalyst (Fig. 4.25). The absorption band at a wavenumber of ~ 975 cm^{-1} was assigned to the V=O bond vibration by comparison to data reported in the literature (Nakamura, M. *et al.* (1974)).

Nakamura, M. *et al.* (1974) reported that in the FT-IR spectra of VPO catalysts containing promoters, the absorption band of the V=O bond was shifted to lower wavenumbers

compared to the unpromoted catalyst. In work carried out in this thesis, the V=O vibration band did not shift, which was probably due to a lower promoter loading than those reported in the literature or the lack of coordination between the cobalt promoter and the V=O species on the catalyst surface.

The FT-IR spectra of the Co-VPO precursor, calcined and used catalysts synthesised via the co-precipitation method were similar to the unpromoted VPO precursor, calcined and used catalysts respectively.

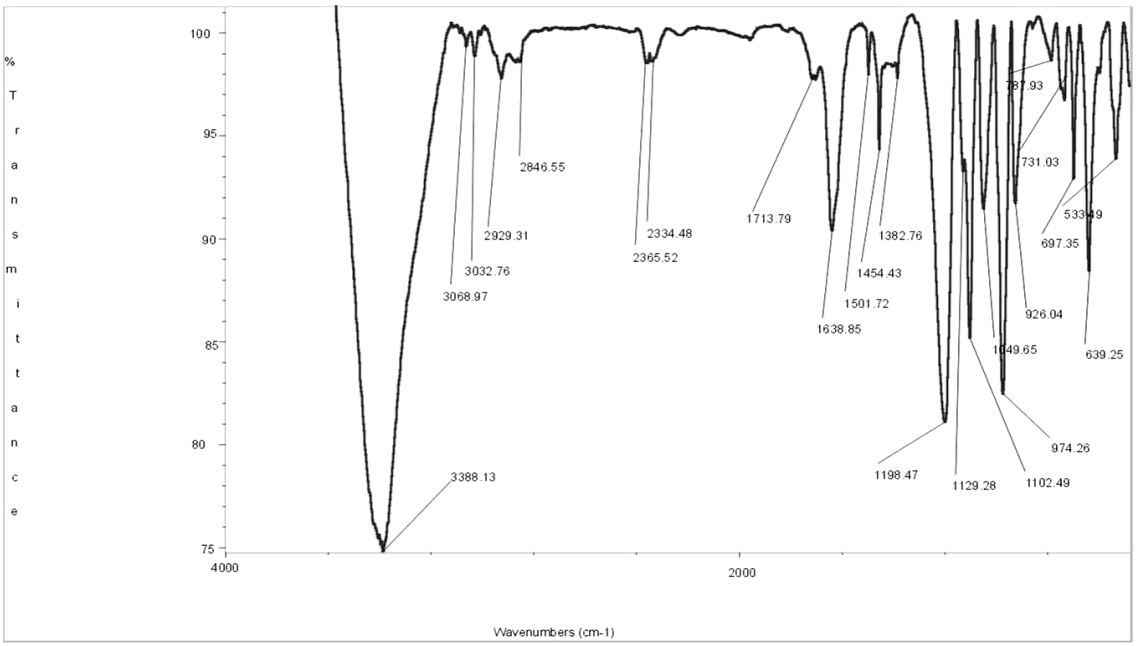

Fig. 4.25 FT-IR spectrum of a 2.5 % Co-VPO catalyst precursor (co-precipitation)

4.1.2.3 Cobalt promoted catalysts (Co-VPO): precipitation/deposition method

The absorption bands in the FT-IR spectrum of the Co-VPO catalyst (precipitation/deposition) (Fig. 4.26) appeared broader than the bands in the FT-IR spectrum of the Co-VPO (co-precipitation) (Fig. 4.25). Some bands also appeared weaker and some bands were absent in the FT-IR spectrum of the Co-VPO catalyst (precipitation/deposition) when compared to the Co-VPO catalyst (co-precipitation). The precipitation/deposition method of impregnating the promoter made the catalyst precursor amorphous or gave microcrystalline phases compared to the co-precipitation method of incorporation. The XRD pattern indicated the presence of mixed $VOHPO_4 \cdot 0.5H_2O$ and $VOPO_4 \cdot 2H_2O$ phases.

The strong IR absorption band at 1413 cm^{-1} was attributed to the ν_{as} O-PO^- vibration in the catalyst due to the presence of the PO_3^- group (Bordes, E. *et al.* (1979)), which was unique to all promoted catalysts prepared by the precipitation/deposition method (Fig. 4.26). The other phosphate condensation bands at lower wavenumbers were broader and indicated an amorphous precursor, which were common for all VPO catalysts promoted via the precipitation/deposition method and not the co-precipitation method.

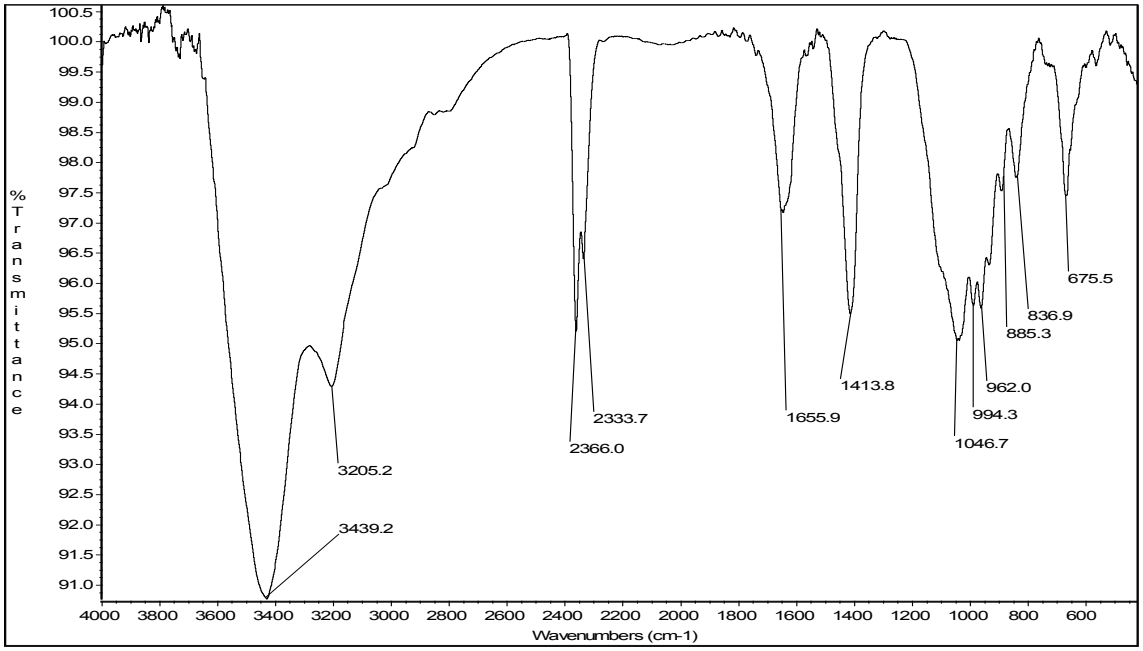

Fig. 4.26 FT-IR spectrum of a 2.5 % Co-VPO catalyst precursor (precipitation/deposition)

The FT-IR spectrum of the Co-VPO catalyst (precipitation/deposition) precursor showed a broad band in the 900-1300 cm^{-1} wavenumber region, which indicated an amorphous phase or multiple phases (Fig. 4.26). There was a shift of the V=O bond from 975 cm^{-1} in the unpromoted catalyst to 962 cm^{-1} here, which suggested coordination of the cobalt species to vanadium.

4.1.2.4 Rhodium promoted catalyst (Rh-VPO): co-precipitation method

The phosphate condensation absorption bands (900-1300 cm^{-1}) in the FT-IR spectrum of the 2.5 % Rh-VPO (co-precipitation) catalyst (Fig. 4.27) appeared broader than those obtained for the 2.5 % Co-VPO catalyst synthesized via the same method (Fig. 4.25).

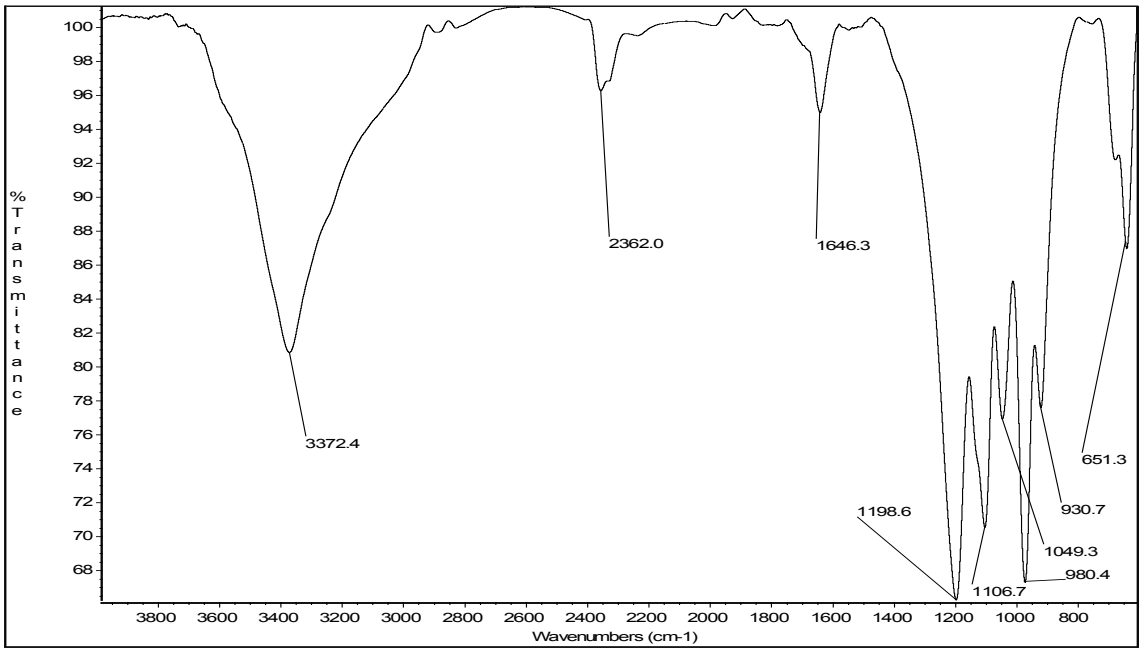

Fig. 4.27 FT-IR spectrum of a 2.5 % Rh-VPO catalyst precursor (co-precipitation)

4.1.2.5 Rhodium promoted catalysts (Rh-VPO): precipitation/deposition method

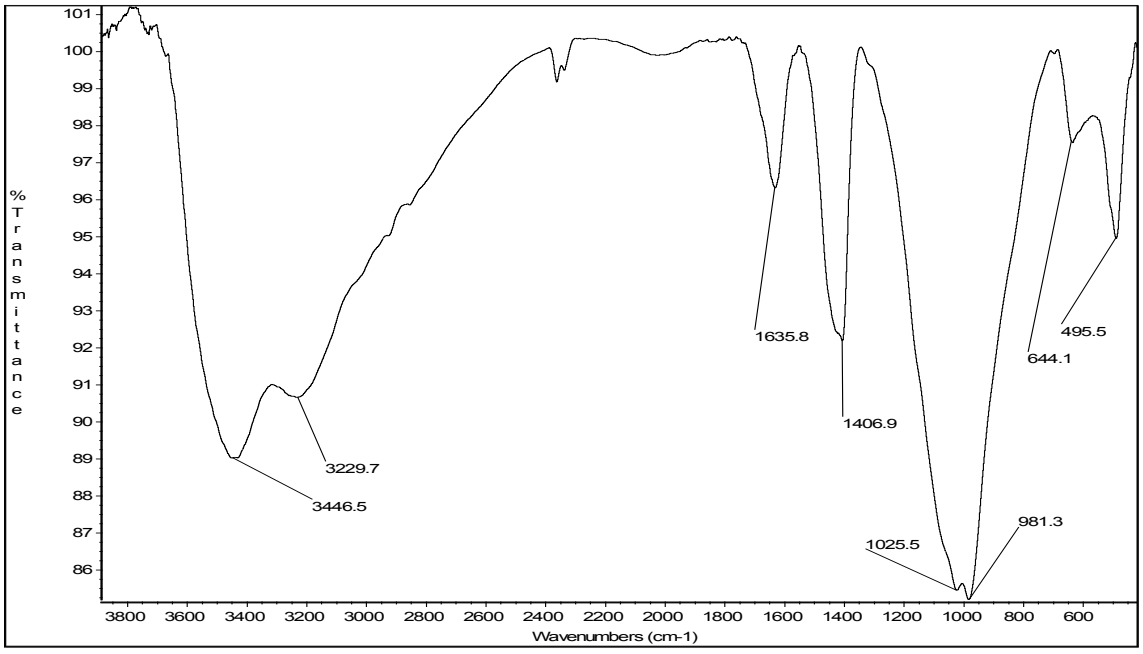

Fig. 4.28 FT-IR spectrum of a 2.5 % Rh-VPO catalyst precursor (precipitation/deposition)

The precipitation/deposition method of incorporating the rhodium promoter gave a more amorphous catalyst (Fig. 4.28) compared to the co-precipitation method (Fig. 4.27). This was shown by the broad absorption band in the 900-1300 cm^{-1} region of the FT-IR spectrum

(Fig. 4.28). The same result was obtained for the 2.5 % Co-VPO catalyst synthesized via this method.

4.1.2.6 Modification of a VPO catalyst by gold using a co-precipitation synthesis method (VPO A and VPO-B)

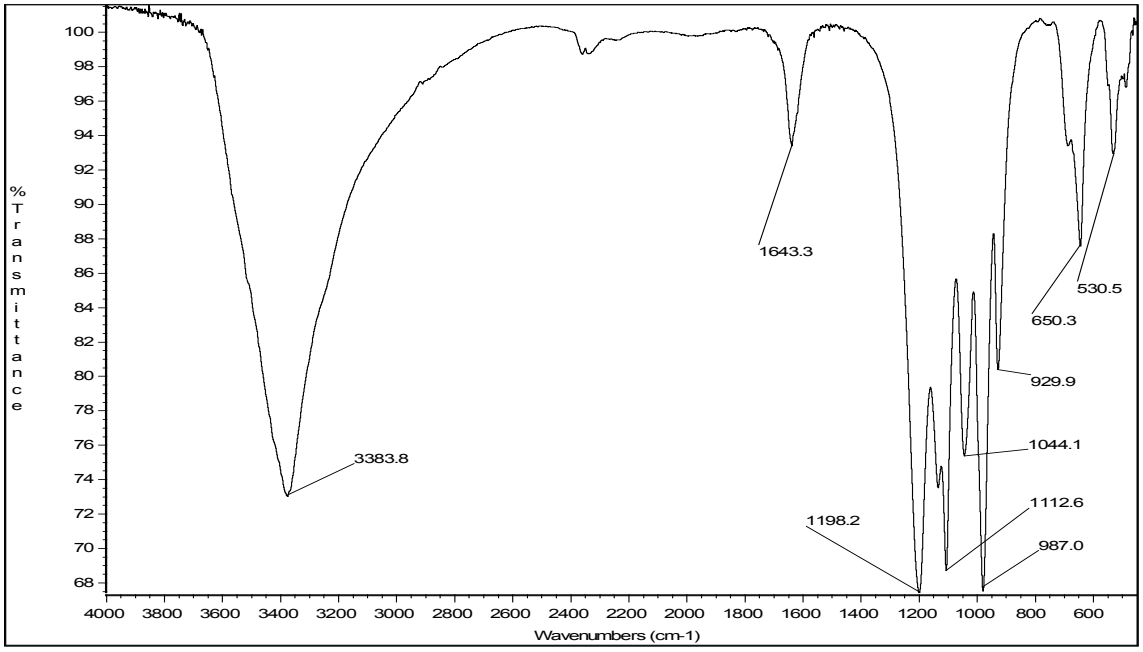

Fig. 4.29 FT-IR spectrum of the VPO-A catalyst precursor

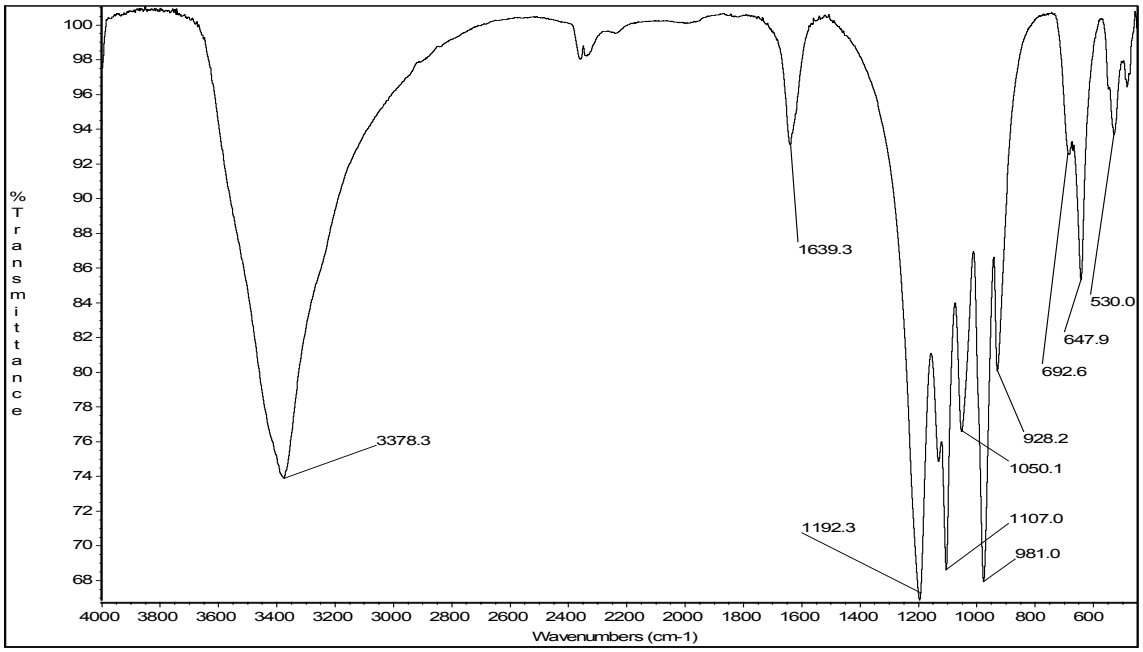

Fig. 4.30 FT-IR spectrum of the VPO-B catalyst precursor

The FT-IR spectra of VPO-A and VPO-B precursors were similar (Figs. 4.29 and 4.30 respectively). The FT-IR spectra and XRD patterns indicated an amorphous nature or microcrystalline phases in the calcined catalysts.

4.1.2.7 Gold promoted catalyst (Au-VPO): precipitation/deposition method

The band at ~ 1400 cm^{-1}, which was unique to catalysts prepared by the precipitation/deposition method, was strongest in the Au-VPO catalyst precursor (precipitation/deposition) compared to any of the other VPO catalysts synthesized (Fig. 4.31).

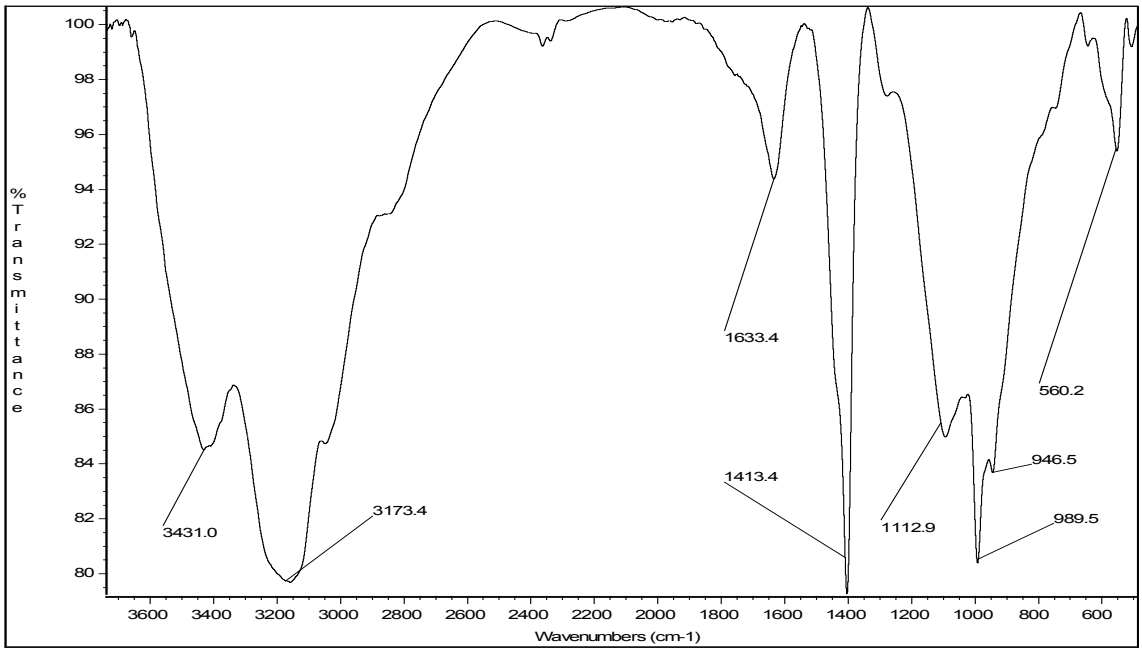

Fig. 4.31 FT-IR spectrum of a 2.5 % Au-VPO catalyst precursor (precipitation/deposition)

This band was attributed to the ν_{as} O-PO^- vibration in the catalyst due to the presence of the PO_3^- group.

There was a shift of the V=O bond from 975 cm^{-1} in the unpromoted catalyst to 946 cm^{-1} here, which suggested coordination of the gold promoter species to vanadium.

4.1.2.8 Unpromoted vanadium magnesium oxide (VMgO) catalyst

The FT-IR spectrum of the VMgO catalyst precursor appeared similar to the used VMgO catalyst (Figs. 4.32 and 4.33, respectively). XRD patterns, however, indicated the presence of multiple phases (ortho- and metavanadate) in the used catalyst.

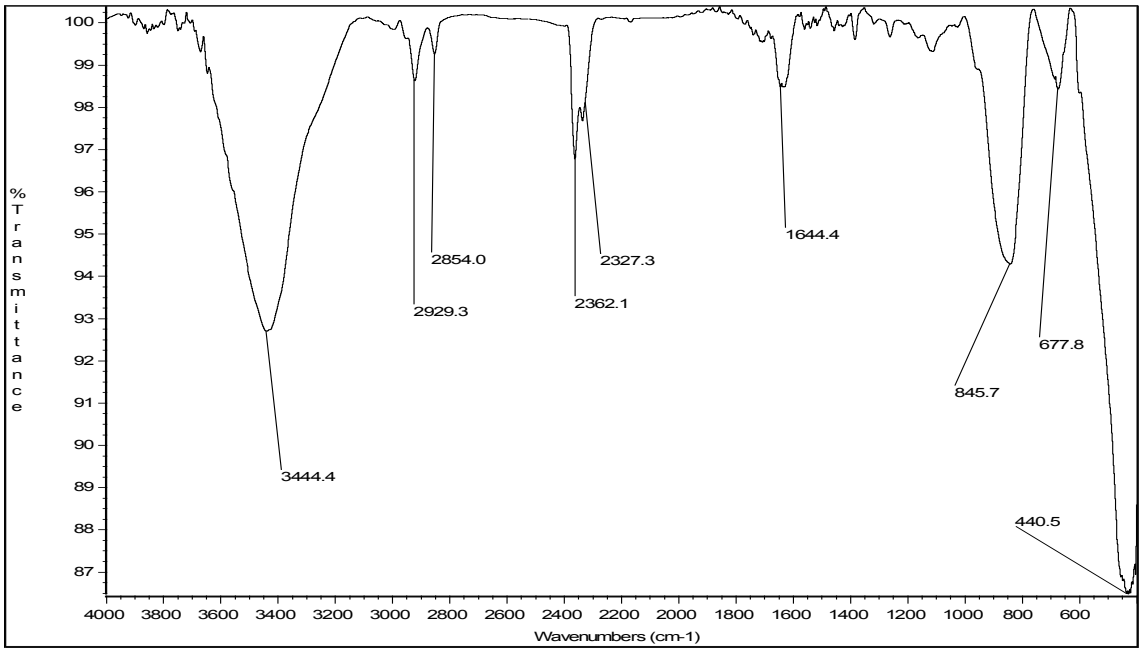

Fig. 4.32 FT-IR spectrum of a VMgO catalyst precursor

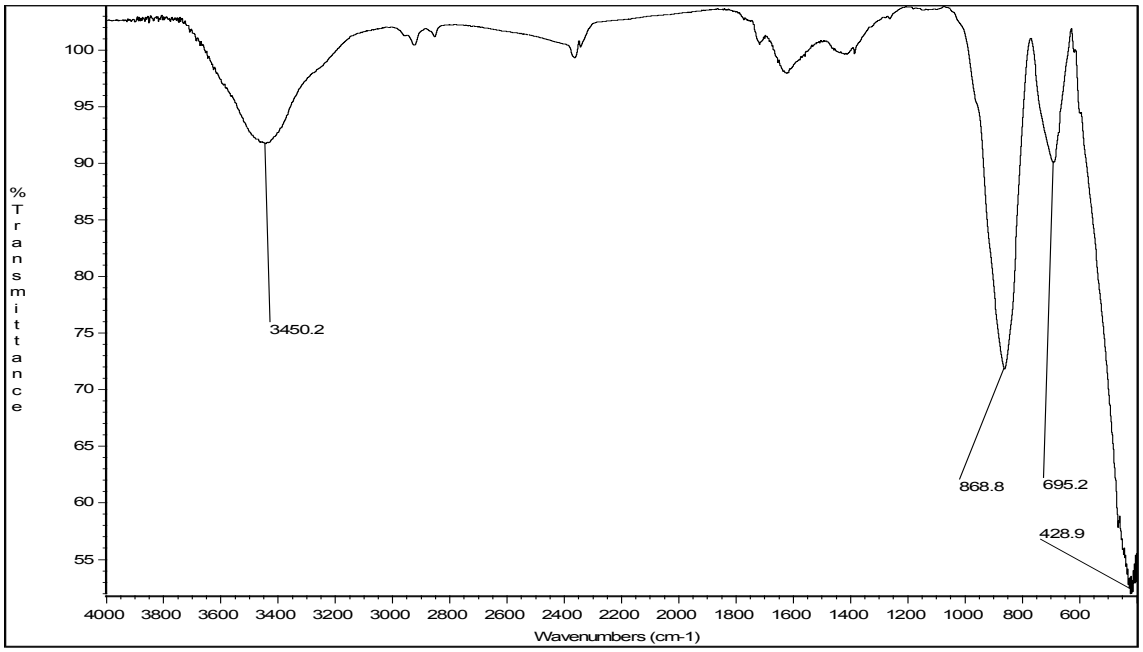

Fig. 4.33 FT-IR spectrum of a used VMgO catalyst

4.1.2.9 Cobalt promoted vanadium magnesium oxide catalyst (Co-VMgO): co-precipitation method

The FT-IR spectrum of the cobalt promoted catalyst precursor (co-precipitation) (Fig. 4.34) appeared similar to the unpromoted catalyst precursor (Fig. 4.32). This indicated that cobalt phases could not be distinguished by FT-IR methods because of poor sensitivity of the method.

The FT-IR spectra of the precursor, calcined and used promoted and unpromoted VMgO catalysts appeared similar, however, there was a difference in the XRD patterns of the precursor, calcined and used catalysts (showing different phases). This was attributed to the poor sensitivity of the FT-IR spectroscopic method.

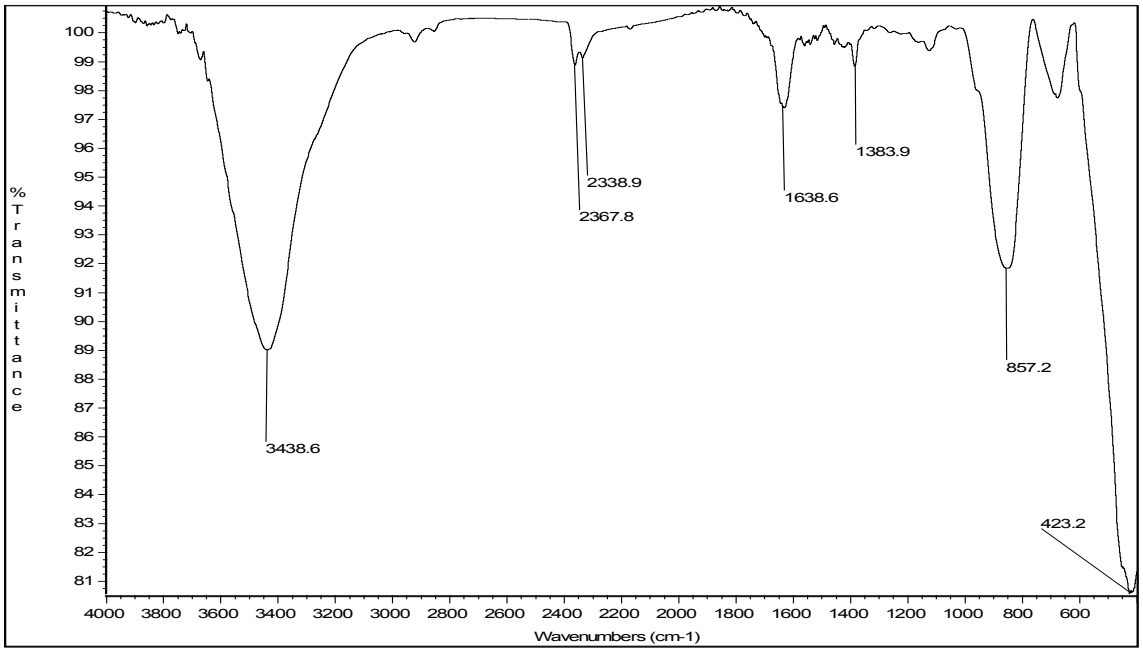

Fig. 4.34 FT-IR spectrum of a 2.5 % Co-VMgO catalyst precursor (co-precipitation)

The FT-IR spectra of the Co-VMgO and unpromoted VMgO catalyst precursors appeared similar with broad IR bands (Fig. 4.34). Absorption bands in the ~ 975 cm^{-1} wavenumber region for the VMgO and Co-VMgO precursors and used catalysts were absent, indicating the absence of V=O or isolated tetrahedral vanadyl groups with terminal V=O bonds,

which were found in the VPO catalyst. Busca, G. *et al.* (1994) reported IR bands at 3510, 3615 and 3750 cm^{-1} for the orthovanadate phase of the VMgO catalyst, where all three bands were attributed to OH stretching of surface hydroxyl-groups, with the latter due to MgOH on MgO particles. These bands were most likely superimposed on the band at ~ 3400 cm^{-1}, which is attributed to H-bonded OH's. The bands in the region 1000-1800 cm^{-1} are harmonics of the fundamental V-O stretchings and deformations observed in the 500-1000 cm^{-1} region.

The absorption bands in the 1000-1700 cm^{-1} wavenumber region appeared broader in the used VMgO catalyst than the catalyst precursor. This indicated multiple phases in the used catalyst with the presence of orthovanadate and metavanadate phases of the VMgO catalyst, which was confirmed by XRD data. Absorption bands appeared at 440, 677 and 645 cm^{-1} for promoted and unpromoted catalysts (Figs. 4.32-4.34). The absorption band at 1644 cm^{-1} was sharper in the FT-IR spectrum of the catalyst precursor (Fig. 4.32) than the used catalyst (Fig. 4.33). Burrows, A. *et al.* (1999) and Pantazidis, A. *et al.* (1998) attributed this band to V-O stretching in an overlayer of VO_4^{3-} units scattered over MgO and reported that the layer had a weakly ordered structure under catalytic conditions. Burrows, A. *et al.* (1999) used extended X-ray absorption fine structure (EXAFS) and high-resolution electron microscopy (HREM) characterisation techniques for the identification of these surface layers, because the surface layers were poorly detected using traditional methods such as XRD.

The reducing conditions (with the introduction of an alkane), however, generally induced ordering, which was observed from sharper bands present in the XRD pattern of the used Co-VMgO catalyst (Fig. 4.21) compared to the Co-VMgO catalyst precursor (Fig. 4.19)

4.1.3 Scanning electron microscopy (SEM)

4.1.3.1 Unpromoted VPO catalyst

The SEM images of the catalyst precursors and calcined catalysts revealed a platelet morphology (Figs. 4.35 and 4.36). The used catalyst (Fig. 4.37) showed signs of disintegration of this morphology.

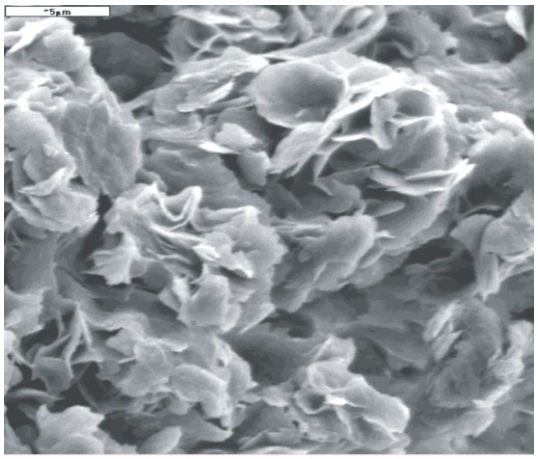

Fig. 4.35 SEM of an unpromoted VPO catalyst precursor (10 000 X mag.)

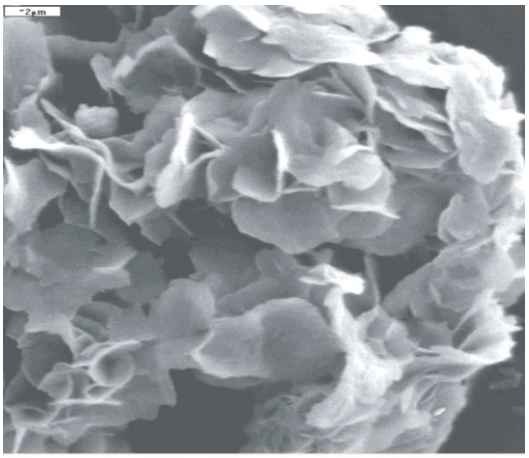

Fig. 4.36 SEM of an unpromoted VPO calcined catalyst (10 000 X mag.)

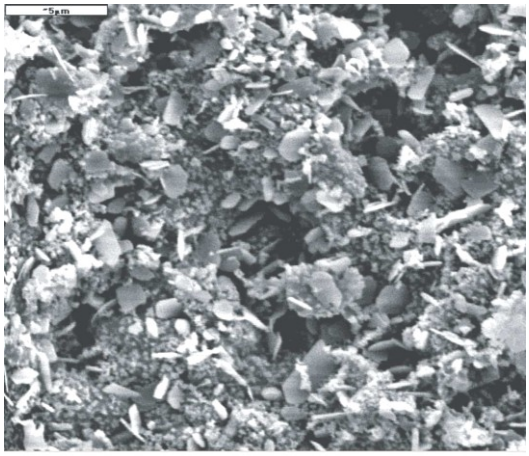

Fig. 4.37 SEM of an unpromoted VPO used catalyst (10 000 X mag.)

4.1.3.2 Cobalt promoted VPO catalyst (Co-VPO): co-precipitation method

The SEM images of the cobalt promoted catalysts synthesised via the co-precipitation method (1.3 %, 2.5 % and 5.0 % Co-VPO) were similar to those of the unpromoted catalyst in that a platelet morphology was obtained for the precursor and calcined catalysts and the used catalyst showed disintegration of these plates. A typical SEM image of a Co-VPO catalyst synthesized via the co-precipitation method appears in Fig. 4.38. The promoter, however, induced the formation of smaller platelets than those obtained for an unpromoted catalyst.

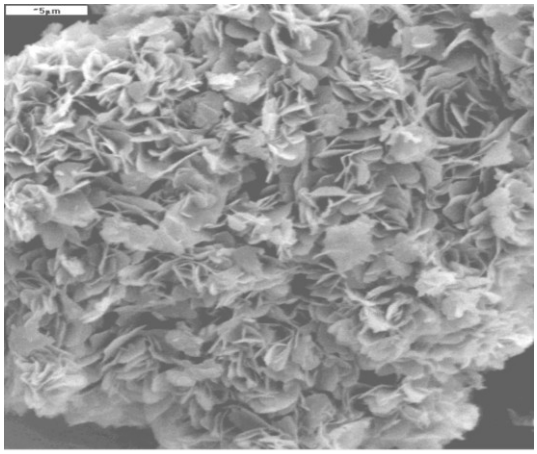

Fig. 4.38 SEM of a 2.5 % Co-VPO precursor (co-precipitation) (10 000 X mag.)

4.1.3.3 Cobalt promoted VPO catalyst (Co-VPO): precipitation/deposition method

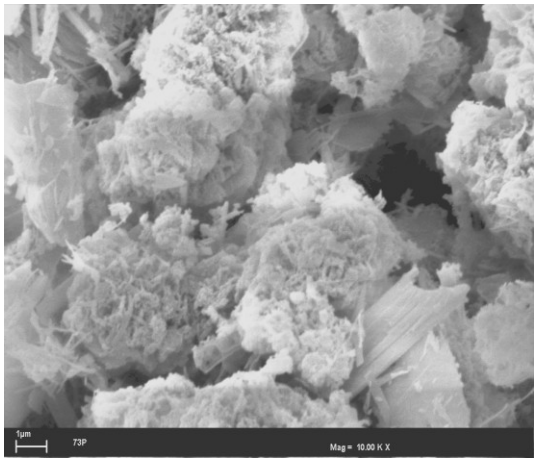

Fig. 4.39 SEM of a 2.5 % Co-VPO precursor (precipitation/deposition) (10 000 X mag.)

The SEM image of a 2.5 % Co-VPO (precipitation/deposition) precursor (Fig. 4.39), showed that the catalyst did not have the platelet morphology which was observed for the catalyst synthesized via the co-precipitation technique (Fig. 4.38), but rather showed coral-shaped crystallites.

4.1.3.4 Rhodium promoted VPO catalyst (Rh-VPO): co-precipitation method

The SEM images of the 1.25 % Rh-VPO and 2.50 % Rh-VPO catalyst precursors (Figs. 4.40 and 4.41 respectively) showed tightly packed rosettes.

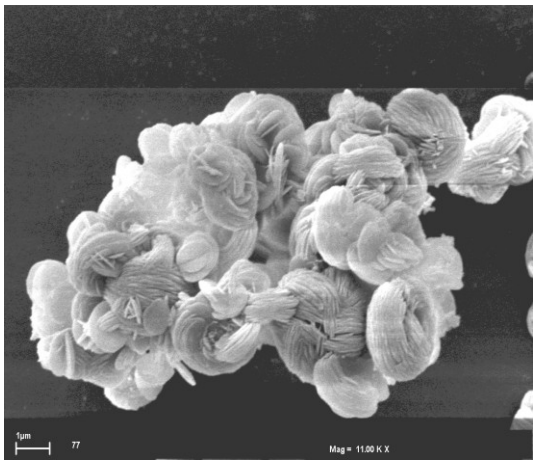

Fig. 4.40 SEM of a 1.25 % Rh-VPO precursor (co-precipitation) (10 000 X mag.)

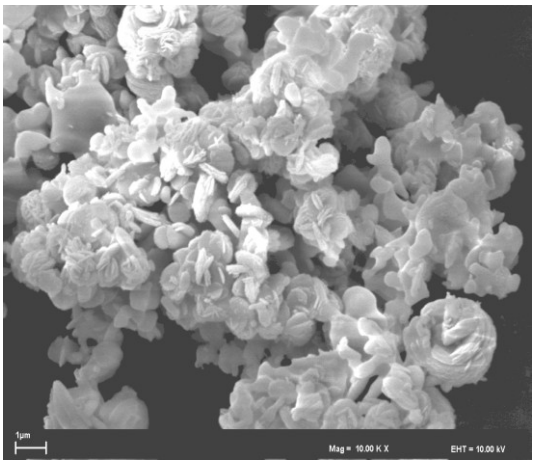

Fig. 4.41 SEM of a 2.50 % Rh-VPO precursor (co-precipitation) (10 000 X mag.)

4.1.3.5 Rhodium promoted VPO catalyst (Rh-VPO): precipitation/deposition method

The SEM images of the 1.25 % Rh-VPO and 2.50 % Rh-VPO (Figs. 4.42 and 4.43 respectively) synthesized via the precipitation/deposition method showed fragmentation of the platelets seen in the SEM images of the 1.25 % Rh-VPO and 2.50 % Rh-VPO catalysts synthesized via the co-precipitation method (Figs. 4.40 and 4.41 respectively).

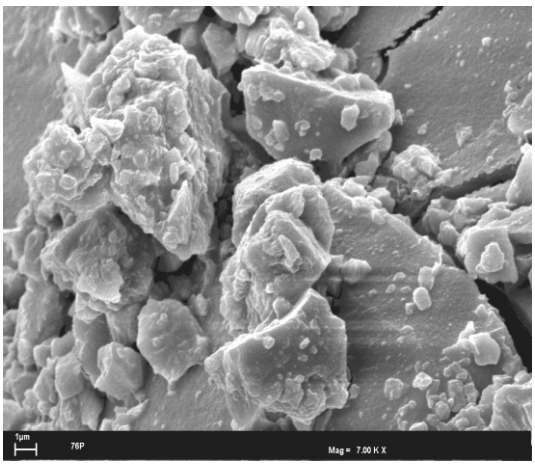

Fig. 4.42 SEM of a 1.25 % Rh-VPO precursor (precipitation/deposition) (7 000 X mag.)

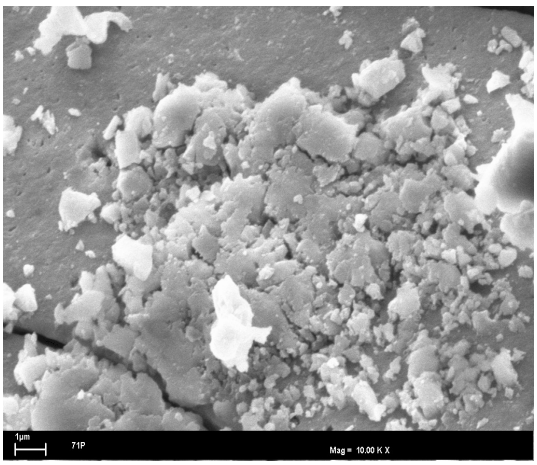

Fig. 4.43 SEM of a 2.50 % Rh-VPO precursor (precipitation/deposition) (10 000 X mag.)

The plates were scattered and layed on top of each other.

4.1.3.6 Modification of a VPO catalyst by gold using a co-precipitation synthesis method (VPO A and VPO-B)

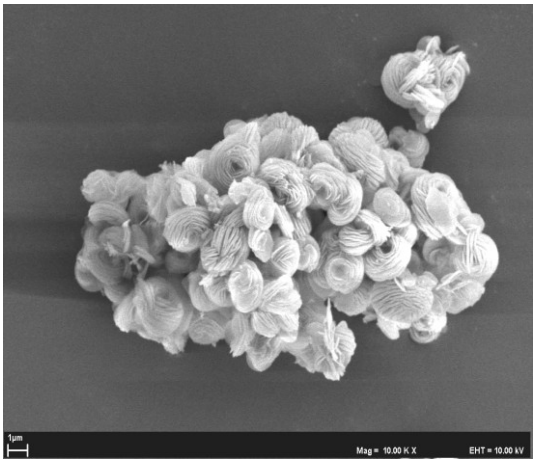

Fig. 4.44 SEM of VPO-A precursor (10 000 X mag.)

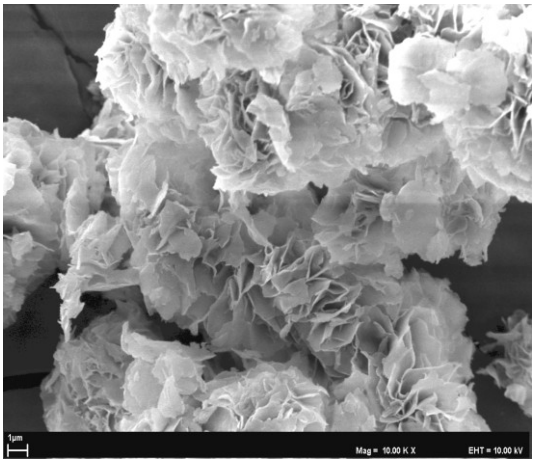

Fig. 4.45 SEM of VPO-B precursor (10 000 X mag.)

The SEM image of VPO-A showed rosettes (Fig. 4.44) and the SEM image of VPO-B showed opened rosettes (Fig. 4.45), when compared at the same magnification (10 000 X). The SEM images of the calcined VPO-A and VPO-B appeared similar to their precursors and are not shown here.

The gold promoter, although not successfully incorporated into the catalyst via the co-precipitation technique, appeared to change the morphological features of the crystallite by being present in the reaction mixture.

4.1.3.7 Gold promoted VPO catalyst (Au-VPO): precipitation/deposition method

The SEM image of the 2.5 % Au-VPO (precipitation/deposition) showed plates with disintegration along the edges (Fig. 4.46).

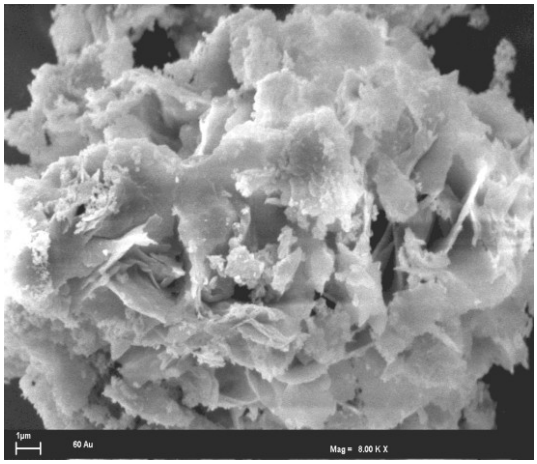

Fig. 4.46 SEM of a 2.5 % Au-VPO precursor (precipitation/deposition) (8 000 X mag.)

4.1.3.8 Unpromoted vanadium magnesium oxide catalyst (VMgO)

The SEM image of the unpromoted VMgO catalyst (Fig. 4.47) showed a rugged surface.

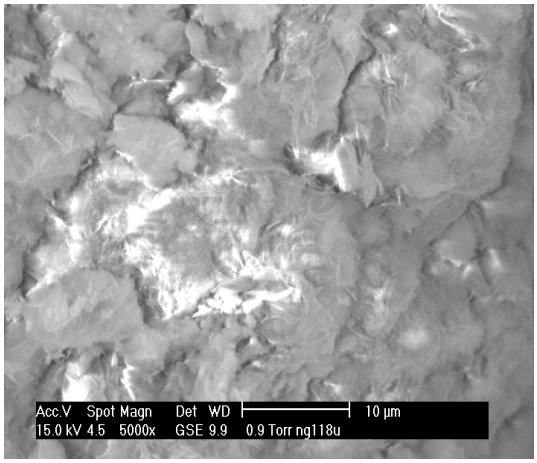

Fig. 4.47 SEM of an unpromoted VMgO catalyst precursor (5 000 X mag.)

4.1.3.9 Cobalt promoted vanadium magnesium oxide catalyst (Co-VMgO): co-precipitation method

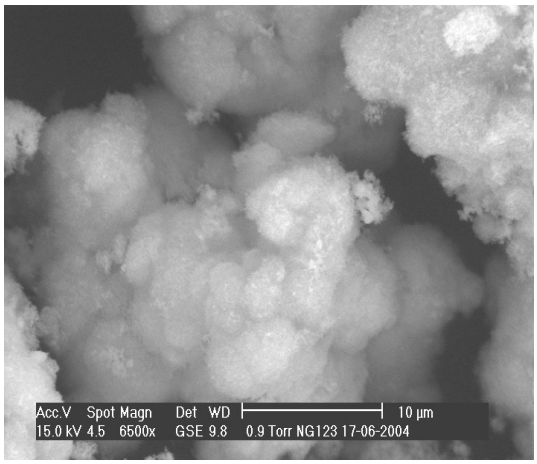

Fig. 4.48 SEM of a 2.5 % Co-VMgO catalyst precursor (co-precipitation) (6 500 X mag.)

The inclusion of cobalt in VMgO changed the morphology of the catalyst by giving a sponge-like material (Fig. 4.48).

4.1.4 Inductively coupled plasma-atomic emission spectroscopy (ICP-AES)

Table 4.2 Bulk elemental composition of catalysts from ICP-AES analysis

Catalyst	Promoter	Incorporation technique	Molar % promoter loaded/V (Theoretical)	Molar % promoter loaded/V (Experimental)	Molar P:V	Molar V:Mg	Wt. % V_2O_5/MgO
VPO	-	-	0	0	1.1		
VPO	Co	Co-precipitation	1.25	1.2	1.0		
VPO	Co	Co-precipitation	2.50	2.3	1.0		
VPO	Co	Co-precipitation	5.00	4.3	1.0		
VPO	Co	Precipitation/ deposition	2.50	15.6	0.6		
VPO	Rh	Co-precipitation	1.25	0.2	0.9		
VPO	Rh	Co-precipitation	2.50	0.1*	0.8		
VPO	Rh	Precipitation/ deposition	2.50	3.1	0.8		
VPO	Au	Co-precipitation (VPO-A)	2.50	0	1.0		
VPO	Au	Co-precipitation (VPO-B)	5.00	0	1.1		
VPO	Au	Precipitation/ deposition	2.50	6.7*	0.6		
VMgO	-	-	0	0	-	0.2	34*
VMgO	Co	Co-precipitation	2.50	1.9	-	0.2	34*

* confirmed by inductively coupled plasma-mass spectrometry (ICP-MS)

4.1.5 Energy dispersive X-ray analysis (EDX)

Table 4.3 Elemental composition of catalysts from EDX analysis

Catalyst	Promoter	Incorporation technique	Molar % promoter loaded/V (Theoretical)	Molar % promoter loaded/V (Experimental)	Molar P:V	Molar V:Mg	Wt. % V_2O_5/MgO
VPO	-	-	0	0	0.9		
VPO	Co	Co-precipitation	1.25	1.2	0.9		
VPO	Co	Co-precipitation	2.50	2.4	0.8		
VPO	Co	Co-precipitation	5.0	4.2	0.9		
VPO	Co	Precipitation/ deposition	2.50	13.2	0.5		
VPO	Rh	Co-precipitation	1.25	0.4	0.6		
VPO	Rh	Co-precipitation	2.50	1.6	0.6		
VPO	Rh	Precipitation/ deposition	2.50	3.6	0.6		
VPO	Au	Co-precipitation (VPO-A)	2.50	0	0.7		
VPO	Au	Co-precipitation (VPO-B)	5.00	0	0.7		
VPO	Au	Precipitation/ deposition	2.50	6.4	0.7		
VMgO	-	-	0	0	-	0.3	40
VMgO	Co	Co-precipitation	2.50	4.0	-	0.5	53

The promoter/vanadium molar percentage in the Co-VPO catalyst (precipitation/deposition) was ~ 6 times higher than the theoretical promoter/vanadium molar percentage (seen from ICP-AES and EDX analyses).

The molar promoter/vanadium percentage obtained for the 1.25 and 2.50 % Rh-VPO catalysts (co-precipitation) were 34 and 64 % of the theoretical amounts respectively (seen from EDX analysis), whilst an impregnation method gave a molar promoter/vanadium percentage ~ 1.5 times larger than the theoretical amount.

ICP-AES analysis indicated that the unpromoted VMgO and 2.5 % Co-VMgO catalysts had a 34 wt. % of V_2O_5 in MgO.

Point analyses of the VMgO and Co-VMgO catalysts via EDX showed a higher wt. % of V_2O_5 on MgO (40.6 and 53.0 wt. %, respectively) than results obtained from bulk analyses via ICP-AES (34 wt. %).

Transition electron microscopy-energy dispersive X-ray (TEM-EDX) point analyses of the promoted VPO and VMgO catalysts confirmed the inclusion of the promoter (TEM images of the promoted catalysts and results obtained from TEM-EDX analyses appears in p. 246 in the Appendix).

Point analyses are sensitive to the region of the catalyst surface being analysed thus elemental mapping of the catalyst was carried out. Elemental mapping of the 2.5 % Co-VPO catalyst (co-precipitation) and 2.5 % Co-VMgO catalyst (co-precipitation) surfaces showed that there was an even distribution of the elements in the catalyst (Fig. 4.49).

Although the elemental maps of the VPO and VMgO catalysts showed an even distribution of the individual elements, different average results were obtained from ICP-AES and EDX analyses.

The higher molar percentage of promoter/V when the promoter was impregnated rather than incorporated indicated agglomeration of the promoter species.

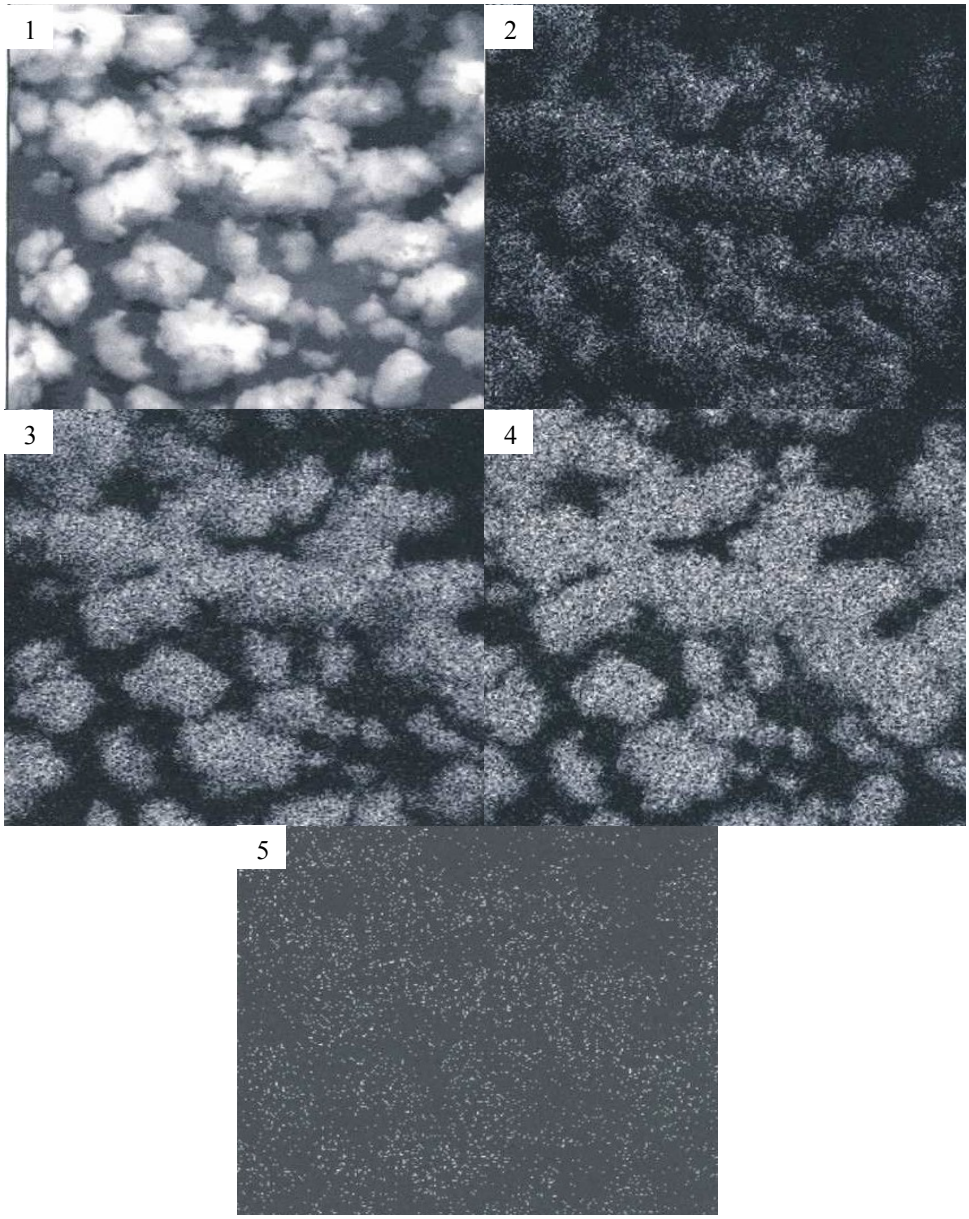

Fig. 4.49 Elemental map of a 2.5 % Co-VPO catalyst (co-precipitation) indicating (1) SEM image of a 2.5 % Co-VPO catalyst, (2) oxygen distribution, (3) phosphorous distribution, (4) vanadium distribution and (5) cobalt distribution

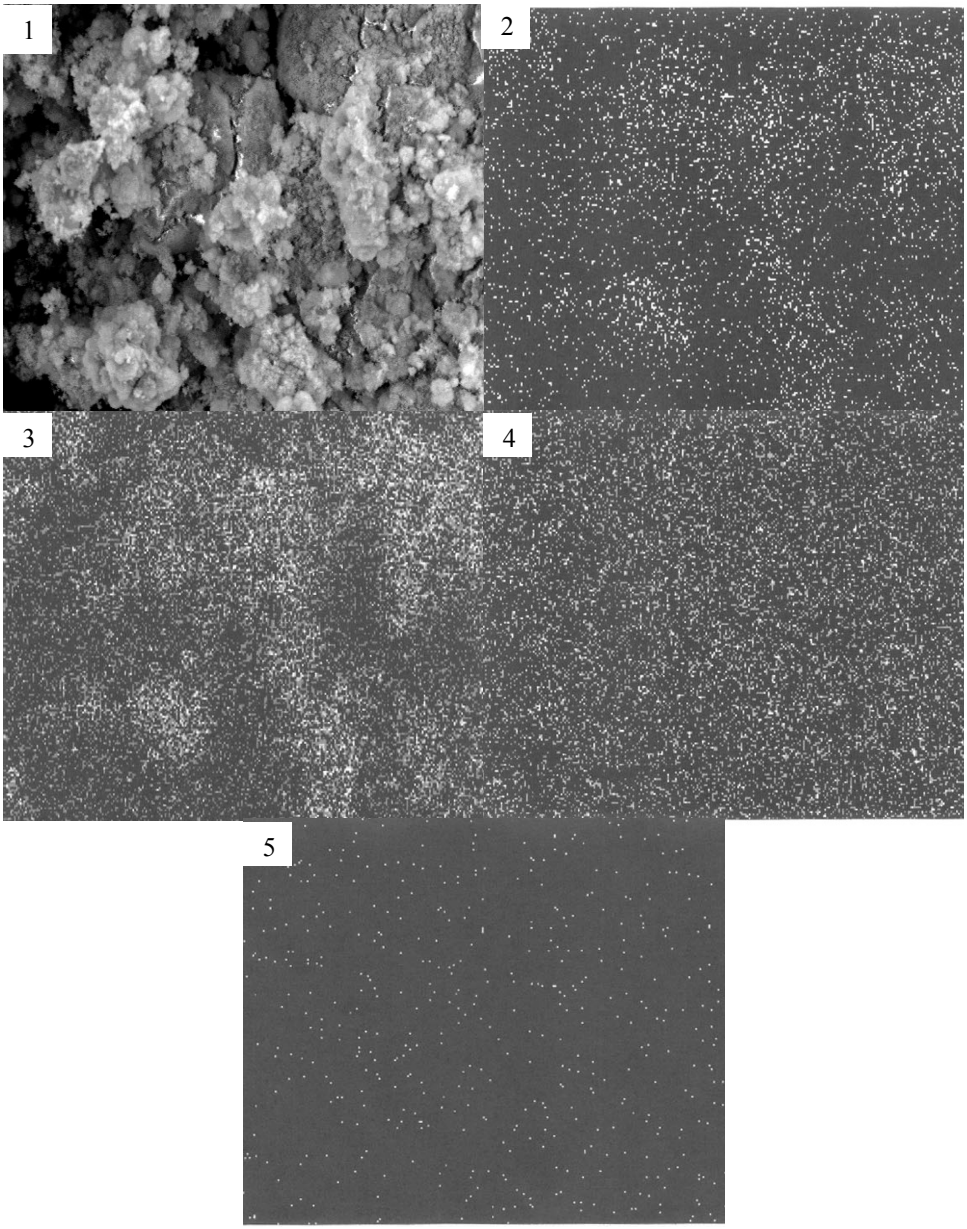

Fig. 4.50 Elemental map of 2.5 % Co-VMgO catalyst (co-precipitation) indicating (1) SEM image of a 2.5 % Co-VMgO catalyst, (2) oxygen distribution, (3) magnesium distribution, (4) vanadium distribution and (5) cobalt distribution

4.1.6 Brenauer-Emmet-Teller (BET) surface area

Table 4.4 BET surface areas of the calcined catalysts

Catalyst	Promoter	Incorporation technique	Molar % promoter loaded/V (Theoretical)	Molar % promoter loaded/V (Experimental)	BET surface area (m^2 g^{-1})
VPO	-	-	0	0	14.8
VPO	Co	Co-precipitation	1.25	1.2	16.9
VPO	Co	Co-precipitation	2.50	2.3	22.9
VPO	Co	Co-precipitation	5.00	4.3	13.2
VPO	Co	Precipitation/ deposition	2.50	15.6	16.7
VPO	Rh	Co-precipitation	1.25	0.2	3.6
VPO	Rh	Co-precipitation	2.50	0.1	21.4
VPO	Rh	Precipitation/ deposition	2.50	3.1	11.4
VPO	Au	Co-precipitation (VPO-A)	2.50	0	9.2
VPO	Au	Co-precipitation (VPO-B)	5.00	0	20.1
VPO	Au	Precipitation/ deposition	2.50	6.7	5.5
VMgO	-	-	0	0	56.9
VMgO	Co	Co-precipitation	2.50	1.9	58.0

Brenauer-Emmet-Teller (BET) surface areas were recorded on calcined catalysts. From the three Co-VPO catalysts (co-precipitation) synthesised, the highest surface area was obtained

for the 2.5 % Co-VPO catalyst (23 m^2 g^{-1}). An increase in promoter loading increased the surface area of the Co-VPO catalysts (co-precipitation) to a maximum and thereafter the surface area decreased. The 2.5 % Co-VPO catalyst (precipitation/deposition) had a surface area of 17 m^2 g^{-1}. Impregnation of a promoter generally gave catalysts with lower surface areas compared to incorporation. The surface areas obtained for the VMgO catalysts were higher than those obtained for the VPO catalysts.

4.1.7 Average vanadium oxidation state (AV)

Incorporation of a promoter generally gave average vanadium oxidation states (AV) between 4.0 and 4.3, however, impregnation of the promoter gave catalysts with a higher AV (between 4.5 and 4.7) (Table 4.5). XRD patterns of the precipitation/deposition catalysts showed mixed phases. The $VOPO_4 \cdot 2H_2O$ phase, together with $VOHPO_4 \cdot 0.5H_2O$ and other possible phases were determined from the XRD patterns. The presence of the $VOPO_4 \cdot 2H_2O$ phase in the catalyst, with its vanadium species in the +5 oxidation state, increased the AV of the catalysts synthesised via the precipitation/deposition method compared to the co-precipitation method.

The VMgO catalysts had an AV of ~ 5.00 and the presence of a magnesium orthovanadate phase, which has vanadium in the +5 oxidation state.

Table 4.5 Average vanadium oxidation states of the catalysts

Catalyst	Promoter	Incorporation technique	Molar % promoter loaded/V (Theoretical)	AV
VPO	-	-	0	4.3
VPO	Co	Co-precipitation	1.25	4.17
VPO	Co	Co-precipitation	2.50	4.22
VPO	Co	Co-precipitation	5.00	4.24
VPO	Co	Precipitation/ deposition	2.50	4.66
VPO	Rh	Co-precipitation	1.25	4.23
VPO	Rh	Co-precipitation	2.50	4.02
VPO	Rh	Precipitation/ deposition	2.50	4.66
VPO	Au	Co-precipitation (VPO-A)	2.50	4.35
VPO	Au	Co-precipitation (VPO-B)	5.00	4.29
VPO	Au	Precipitation/ deposition	2.50	4.45
VMgO	-	-	0	4.92
VMgO	Co	Co-precipitation	2.50	4.94

4.2 Blank reactor studies

Two types of blank reactor investigations were carried out. In one case, the alkane in air mixture was introduced into a reactor fully packed with carborundum. The conversion and product selectivities were then investigated over a temperature range of 300 to 550°C, which was the operating temperature range of the reactor under catalytic conditions. This study investigated any gas phase reactions in the inter-granular space of the carborundum packing. The size of the intergranular space was changed by changing the size of the carborundum particles. A correlation was obtained between intergranular space to the product selectivity profiles from homogeneous reactions. In a second case, the feed was introduced into an empty reactor under the same operating conditions. These setups are illustrated in setups 1 and 2 in the foldout section of the Appendix (p. 292). The product profiles from different hydrocarbon chainlengths (C_4, C_6 and C_8) were observed. These homogeneous reactions were investigated further on their contribution to catalytic systems by combining catalytic and non-catalytic systems.

4.2.1 n-Butane oxidation

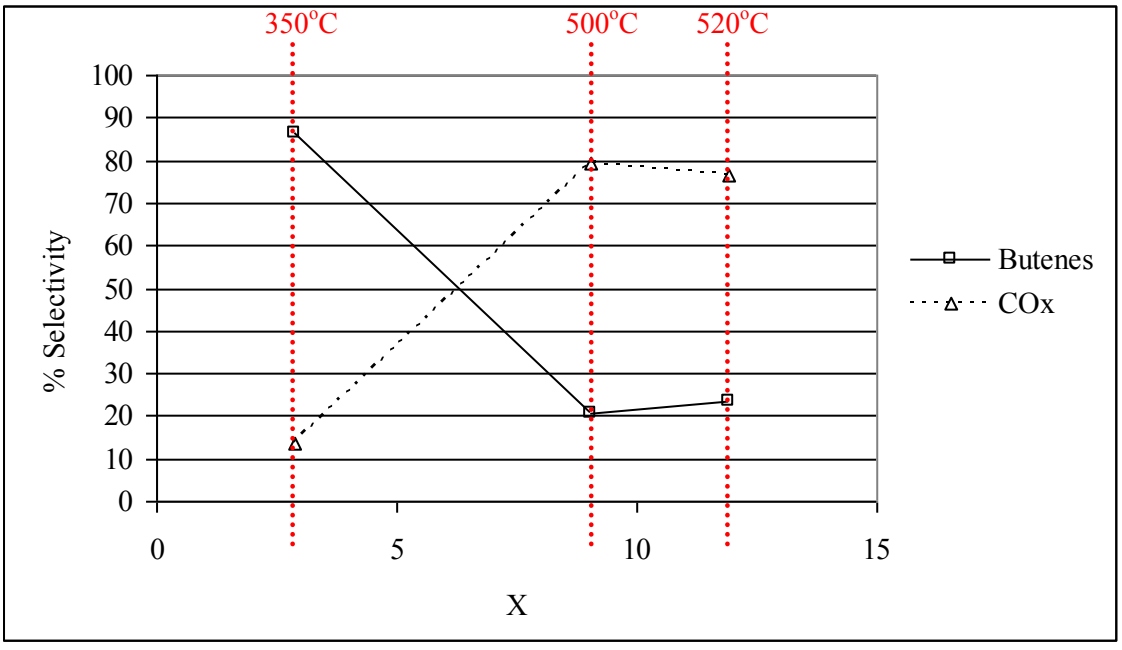

Fig. 4.51 Selectivity vs. n-butane conversion in a carborundum-packed reactor

1 % *n*-butane in air was passed through a reactor fully packed with carborundum (setup 2 in the foldout section of the Appendix (p. 292)) at 50 ml min^{-1} (Fig. 4.51) over a 350-520^{o}C temperature range. .

The selectivity to isomers of butene generally decreased with increasing temperature. There was a subsequent increase in selectivity to carbon oxides. The isomers of butene included 1-butene and 2-butene.

The products with the highest yield in a carborundum-packed reactor were isomers of butene, thus indicating that these were thermal products.

Water was produced in all reactor systems under catalytic and non-catalytic conditions, which is expected from oxidative dehydrogenation and combustion.

4.2.2 n-Hexane oxidation

n-Hexane in air (7.8 %) was fed into a stainless steel reactor fully packed with carborundum at flowrates of 10, 50 and 100 ml min^{-1}. The conversion (X) decreased with increasing flowrates when compared at the same operating temperature (Fig. 4.52).

The non-oxygenated product in highest selectivity from the gas phase reaction was benzene. Propane, propene and isomers of hexene were the other products obtained (Tables 4.6-4.8). The highest selectivity to benzene was obtained at 500^{o}C at a flowrate of 100 ml min^{-1}, which was the highest flowrate employed.

The conversions obtained in an empty reactor over a 300-500^{o}C temperature range were higher than those obtained through a carborundum-packed reactor at the same flowrate of 50 ml min^{-1} (Fig. 4.52).

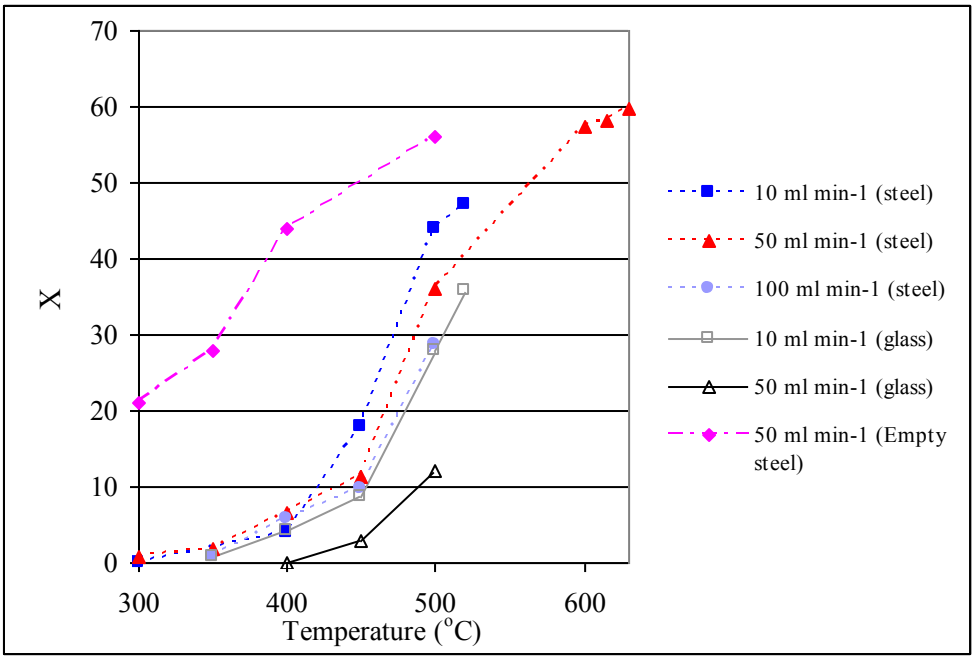

Fig. 4.52 Conversion (X) of n-hexane at varying flowrates through carborundum-packed stainless steel and glass reactors and an empty steel reactor

The carborundum particle size affected the rate of free radical generation. It was established experimentally that carborundum particles larger than a range of 300-600 µm in size gave higher conversions in a reactor fully packed with carborundum (i.e. under non-catalytic conditions). The conversions obtained at 400 and 500°C with a 100 ml min^{-1} flowrate were 15 and 40 %, respectively, in a reactor packed with carborundum particles ~ 1000 µm in size, whilst the conversions obtained at the same temperatures and flowrate through a reactor packed with carborundum particles, having a particle size range between 300 and 600 µm, were 6 and 29 %, respectively. A 300-600 µm particle size range of carborundum was employed to limit the non-catalytic contribution to conversion, and at the same time limit back-pressure in the reactor system which occurred when using carborundum particles less than 300 µm in size.

Table 4.6 Conversion of n-hexane at 10 ml min^{-1} flowrate in a carborundum-packed stainless steel reactor (X=conversion)

Reaction T(°C)	% X	Selectivity (mol %)					
		Propane/propene	2-Hexene (cis)	2-Hexene (trans)	Benzene	CO	CO_2
450	18	0	6	0	5	3	86
500	44	0	4	2	15	11	67
520	47	2	5	3	21	12	58
530	50	2	4	2	21	11	60

Table 4.7 Conversion of n-hexane at 50 ml min^{-1} flowrate in a carborundum-packed stainless steel reactor

Reaction T(°C)	% X	Selectivity (mol %)					
		Propane/propene	2-Hexene (cis)	2-Hexene (trans)	Benzene	CO	CO_2
400	7	0	0	0	0	8	92
450	11	0	11	0	0	14	75
500	36	0	4	2	10	18	65

Table 4.8 Conversion of n-hexane at 100 ml min^{-1} flowrate in a carborundum-packed stainless steel reactor

Reaction T(°C)	% X	Selectivity (mol %)					
		Propane/propene	2-Hexene (cis)	2-Hexene (trans)	Benzene	CO	CO_2
400	6	0	0	0	0	10	90
450	10	0	0	0	15	11	74
500	29	0	3	0	23	19	55

The oxidation of *n*-hexane at different flowrates was carried out in a steel and glass reactor. The conversions over the same temperature profile at the same flowrates of feed were higher in the stainless steel reactors (Tables 4.6-4.8) than in the glass reactors (Tables 4.9-4.11).

The conversion in the glass reactor decreased with increasing flowrate when compared at the same operating temperature, which was also observed in the steel reactor.

At the same flowrate of 50 ml min^{-1} and temperature of 400°C (Fig. 4.52) the conversion of *n*-hexane in a steel reactor was ~ 6 %, whilst there was no conversion in a glass reactor.

Table 4.9 Conversion of n-hexane at 10 ml min^{-1} flowrate in a carborundum-packed glass reactor

Reaction T(°C)	% X	Selectivity (mol %)					
		Propane/Propene	2-Hexene (cis)	2-Hexene (trans)	Benzene	CO	CO_2
450	9	0	27	15	0	13	46
500	28	0	13	8	23	6	45
520	36	0	9	6	32	12	35

Table 4.10 Conversion of n-hexane at 50 ml min^{-1} flowrate in a carborundum-packed glass reactor

Reaction T(°C)	% X	Selectivity (mol %)					
		Propane/Propene	2-Hexene (cis)	2-Hexene (trans)	Benzene	CO	CO_2
500	12	0	19	11	10	8	52
520	11	0	27	16	18	9	30

The conversions obtained in an empty reactor were higher than those obtained in the carborundum-packed glass and stainless steel reactors at similar operating temperatures (Table 4.12).

Table 4.11 Conversion of n-hexane at 100 ml min^{-1} flowrate in a carborundum-packed glass reactor

Reaction T(°C)	% X	Selectivity (mol %)					
		Propane/Propene	2-Hexene (cis)	2-Hexene (trans)	Benzene	CO	CO_2
500	2	0	100	0	0	0	0
520	5	0	46	26	0	21	7

Table 4.12 Conversion of n-hexane at 50 ml min^{-1} flowrate in an empty stainless steel reactor

Reaction T(°C)	% X	Selectivity (mol %)						
		Propane/Propene	Butane/Butene	2-Hexene (cis)	2-Hexene (trans)	Benzene	CO	CO_2
300	21	20	6	0	10	8	34	20
350	28	18	5	10	9	8	28	20
400	44	11	6	8	8	6	34	26
500	56	22	7	4	5	3	20	38

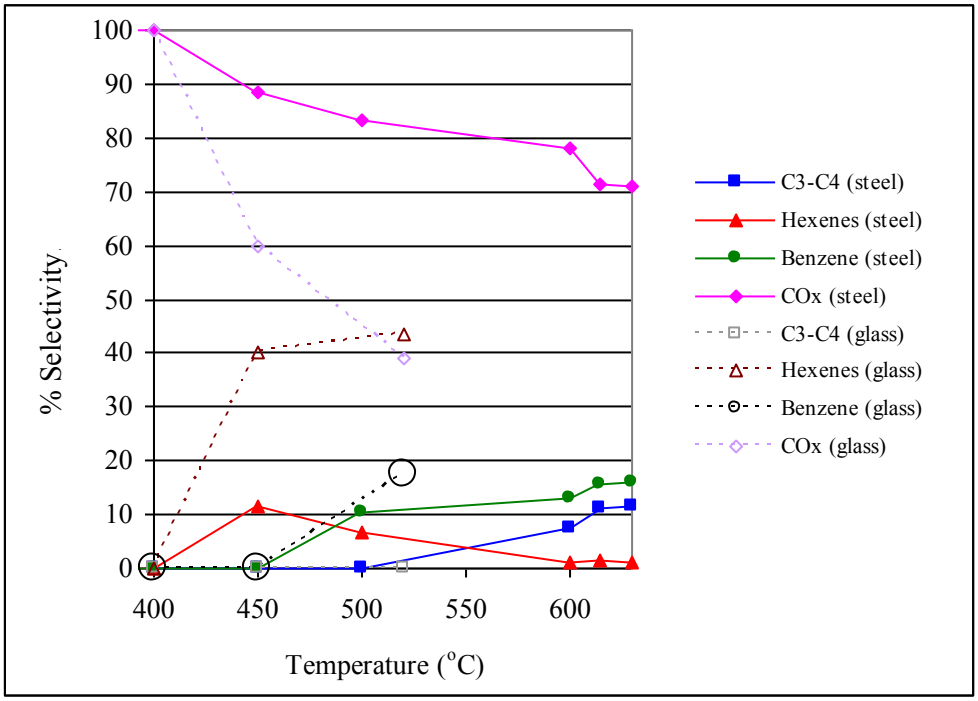

Fig. 4.53 Selectivities to C_{3-4} cracked products, hexenes, benzene and CO_x from n-hexane oxidation in carborundum-packed glass and steel reactors (at a flowrate of 50 ml min^{-1})

The selectivity to benzene increased with increasing operating temperature in a carborundum-packed stainless steel reactor. There was a decrease in selectivity to carbon oxides with increasing flowrates (Fig. 4.53). The highest selectivities to benzene and the lowest selectivities to carbon oxides were obtained at the highest flowrate employed (i.e. 100 ml min^{-1}). The selectivities to carbon oxides and benzene were similar within 3 % experimental error at 10 and 50 ml min^{-1}.

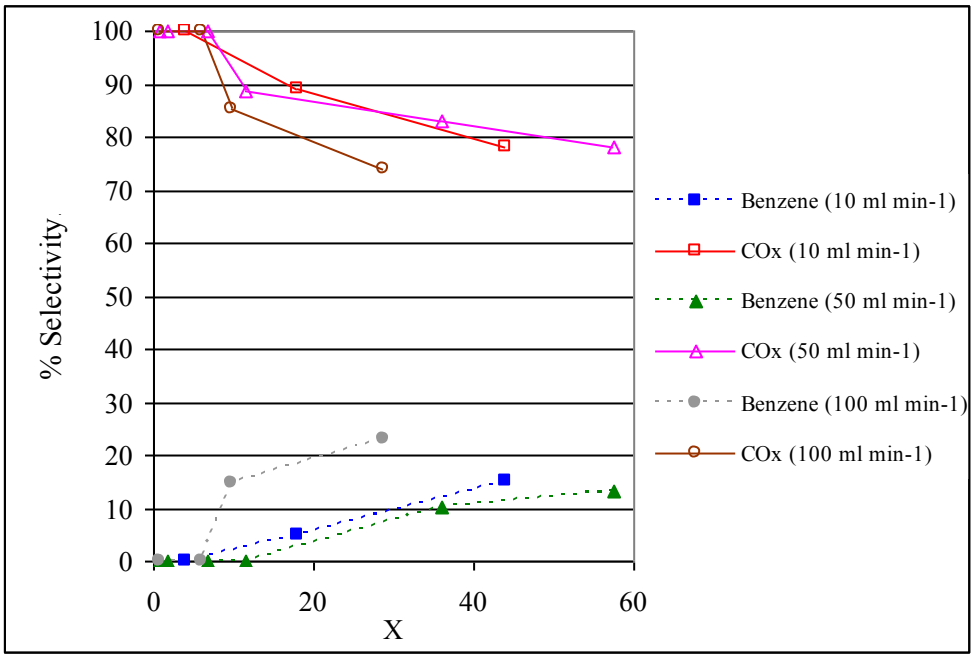

Fig. 4.54 Selectivities to benzene and carbon oxides in a carborundum-packed stainless steel reactor from the conversion of n-hexane at varying flowrates

The trend of decreasing selectivities to carbon oxides and increasing selectivities to benzene with increasing operating temperatures from *n*-hexane oxidation was obtained also in a carborundum-packed glass reactor. The selectivities to carbon oxides, however, were lower and the selectivities to benzene were higher compared to the steel reactor at the same flowrates and conversions (Figs. 4.53 and 4.54).

The selectivity to carbon oxides over a 400-500^{o}C temperature range in an empty stainless steel reactor at a flowrate of 50 ml min^{-1} was ~ 60 % (Table 4.12). The selectivity to

carbon oxides was similar in a carborundum-packed glass reactor over the same temperature range and flowrate (Table 4.10), but ~ 30 % higher in a carborundum-packed steel reactor (Table 4.7).

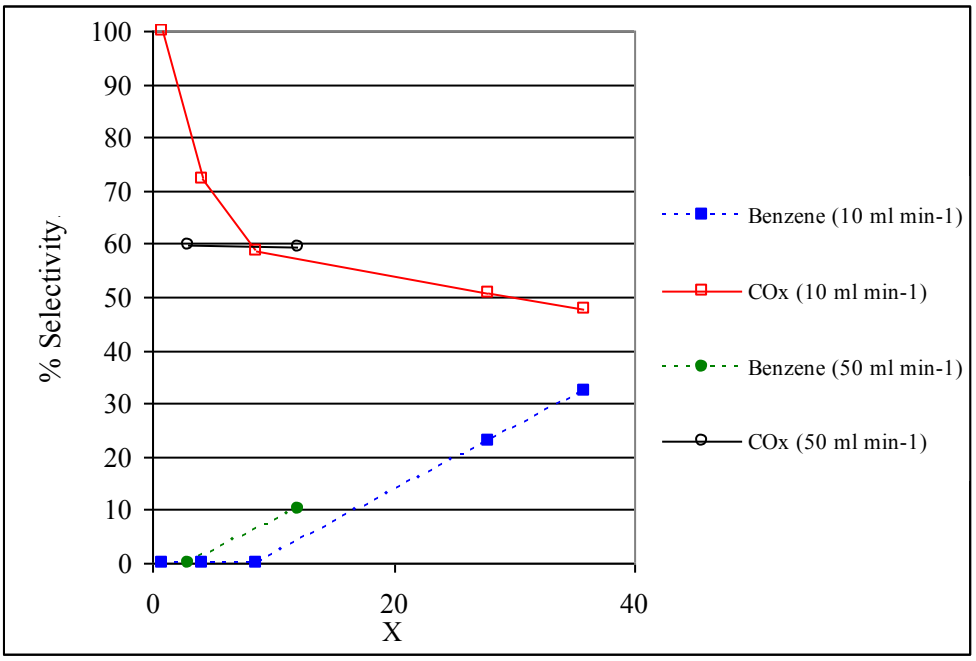

Fig. 4.55 Selectivities to benzene and carbon oxides in a carborundum-packed glass reactor from the conversion of n-hexane at varying flowrates

There was no conversion of *n*-hexane when the alkane was co-fed with nitrogen in the absence of oxygen in a carborundum-packed steel reactor over a temperature range of 300-540^{o}C. This indicated that oxygen was necessary for homogeneous reactions in the absence of a catalyst.

The organic product with the highest yield obtained from the carborundum-packed reactor, was benzene (Fig. 4.55), whilst the products with the highest yields in an empty reactor were C_3 cracked products. This showed that homogeneous reactions in small voids in a reactor propagated the formation of an aromatic compound from linear alkane oxidation, however, increasing the size of these voids favoured cracking (Table 4.12).

The selectivities to isomers of hexene were generally higher in the carborundum-packed glass reactor than in the carborundum-packed steel reactor over a 10-100 ml min^{-1} flowrate

range (Fig. 4.53) or an empty reactor. There was a decrease in selectivity to alkenes and increasing selectivity to benzene in the steel reactor. This points to secondary deep-oxidation reactions, where alkenes that formed were oxidised to carbon oxides, or alkenes oxidised to benzene.

The selectivities to C_3 cracked products from *n*-hexane oxidation at 50 ml min^{-1} in an empty reactor were generally around 20 % at temperatures between 300 and 500°C. The C_{3-4} products had a combined selectivity of ~ 30 % at a temperature of 500°C in an empty reactor, but there was no cracking in the carborundum-packed glass and steel reactors at the same flowrate.

4.2.3 n-Octane oxidation

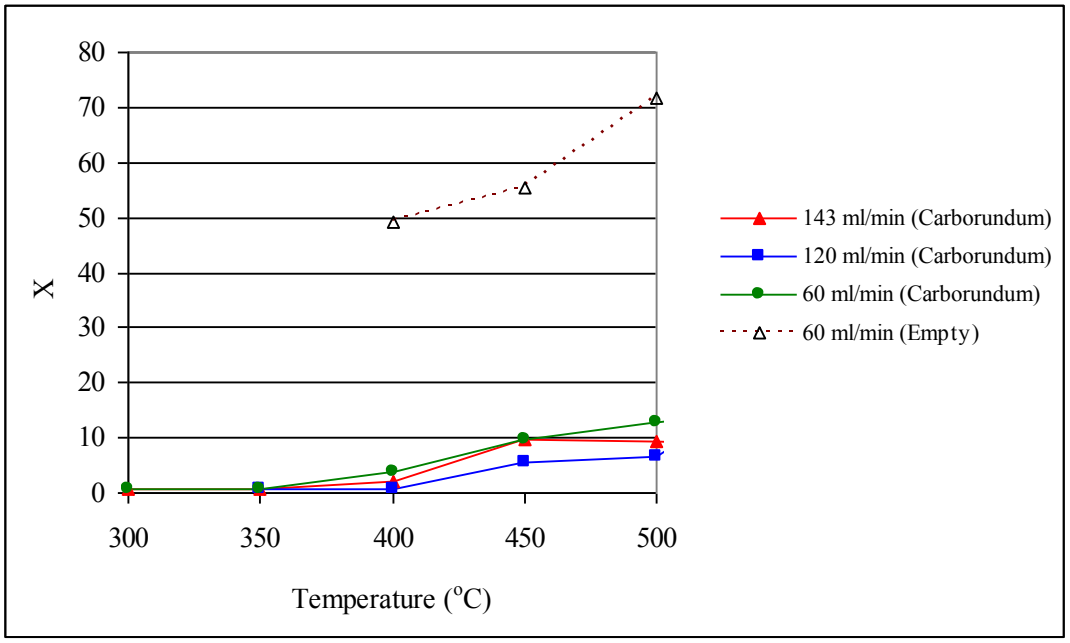

Fig. 4.56 Conversion of n-octane in a carborundum-packed and an empty stainless steel reactor at 60 ml min^{-1}, 120 ml min^{-1} and 143 ml min^{-1}

The conversions were below 15 % in a carborundum-packed steel reactor over a 300-500°C temperature range at varying flowrates of 60, 120, and 143 ml min^{-1} (Fig. 4.56). The flowrates selected for this blank study, viz. 60, 120 and 143 ml min^{-1} were the same flowrates employed in catalytic investigations. The conversion was 12 % at 500°C and a flowrate of 60 ml

min^{-1} in a carborundum-packed stainless steel reactor, but 70 % at the same operating temperature and flowrate in an empty stainless steel reactor (Fig. 4.56). The conversions obtained in an empty stainless steel reactor were between 5 and 10 times larger than those obtained in carborundum-packed reactors between 400 and 500°C (Fig. 4.56).

The oxidation of *n*-octane in a carborundum-packed reactor gave almost 95 % selectivity to carbon oxides (Figs. 4.57-4.58) and ~ 30-50 % selectivity to carbon oxides in the empty reactor over a 400-500°C temperature range. The selectivity to oxygenates (besides carbon oxides) was higher in the empty reactor than in a carborundum-packed reactor.

The selectivity to CO generally decreased and the selectivity to CO_2 increased with increasing temperature (Figs. 4.57 and 4.58, respectively).

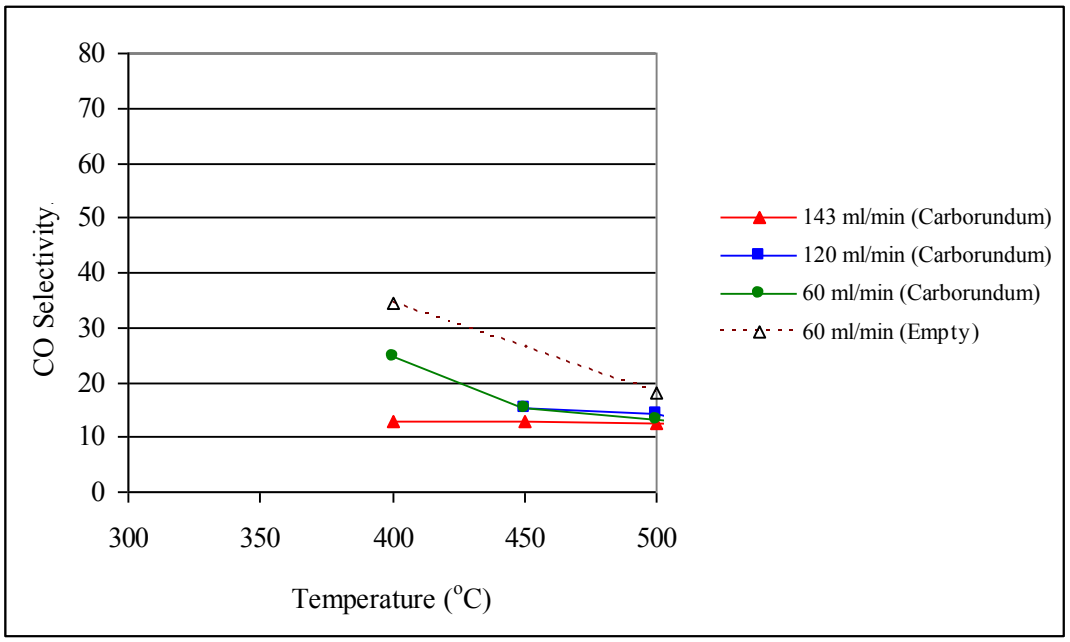

Fig. 4.57 Selectivity to CO in a carborundum-packed and an empty stainless steel reactor at 60 ml min^{-1}, 120 ml min^{-1} and 143 ml min^{-1}

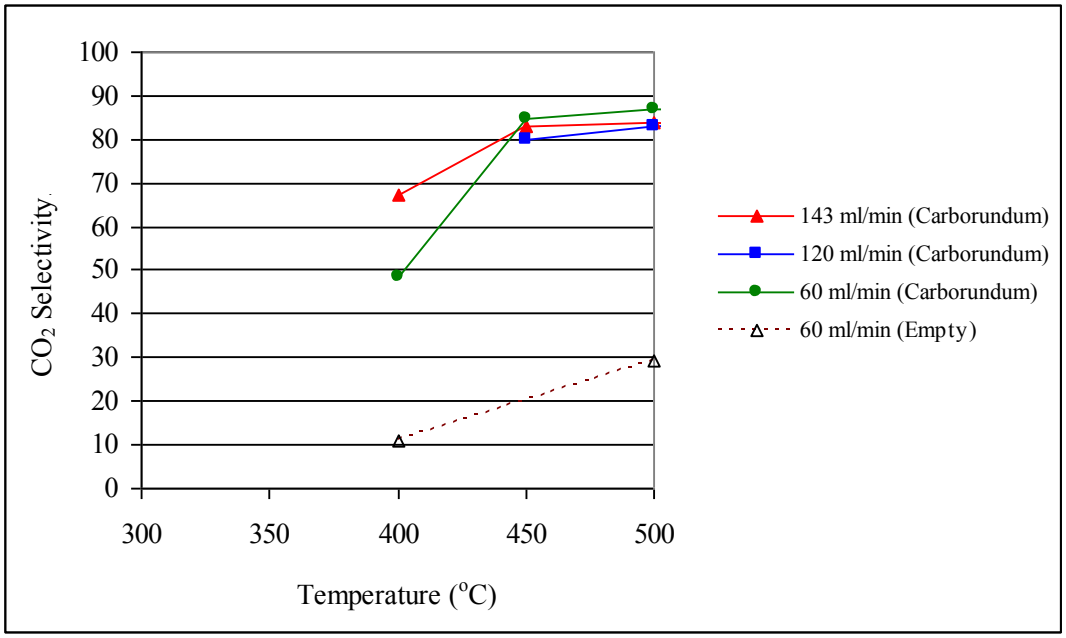

Fig. 4.58 Selectivity to CO_2 in a carborundum-packed and an empty stainless steel reactor at 60 ml min^{-1}, 120 ml min^{-1} and 143 ml min^{-1}

The product profile from *n*-octane oxidation through a carborundum-packed reactor included propane, propene, isomers of butane and butene, isomers of heptane and heptene, isomers of octane and octene, acetaldehyde, benzene, toluene and isomers of xylene at conversions lower than 5 %, which were obtained at temperatures less than 400°C (Fig. 4.59).

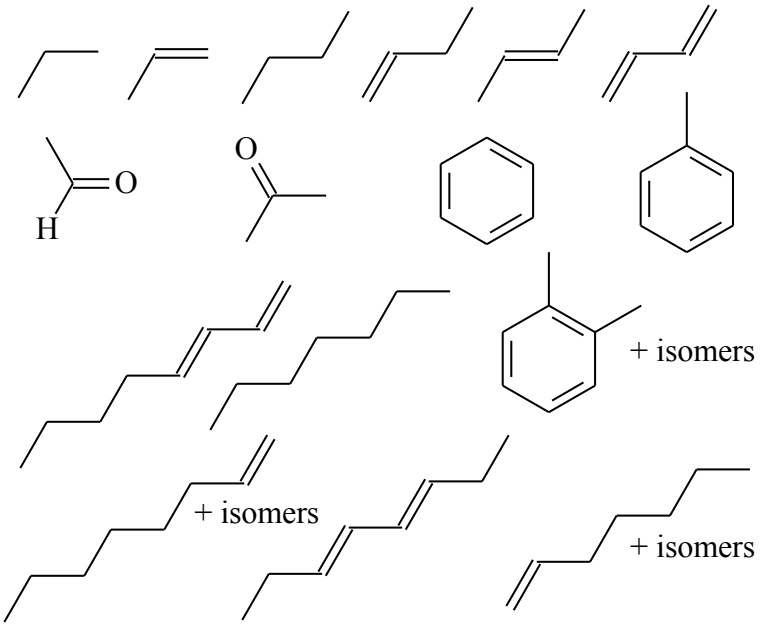

Fig. 4.59 Some of the products obtained from n-octane oxidation in a fully carborundum-packed reactor

There were more sites at which the longer chain hydrocarbon could crack and each cracked product could be converted to an oxygenate or alkene. The oxidation of both *n*-hexane and *n*-octane gave benzene, however, the product profile from the long hydrocarbon oxidation was complicated by cyclic products with an alkyl moiety.

The selectivity to benzene was less than 5 % at 10 % conversion. At similar conversions in an empty reactor, the selectivity to benzene was lower, with cyclic products being mainly oxygenates. Above 450^{o}C, the selectivities to carbon oxides approached 100 %.

Products from an empty reactor, apart from carbon oxides, included propane, propene, isomers of butene, isomers of octane and octene, isomers of heptane and heptene, acetaldehyde, toluene, benzene, 2-methyl-5-propyl-tetrahydrofuran, 2,5-diethyl-tetrahydrofuran, 1-butyl-tetrahydrofuran, 1-propyl-pentahydropyran, 1-ethyl-5-methyl-pentahydropyran and isomers of C_8 ketones (Fig. 4.60).

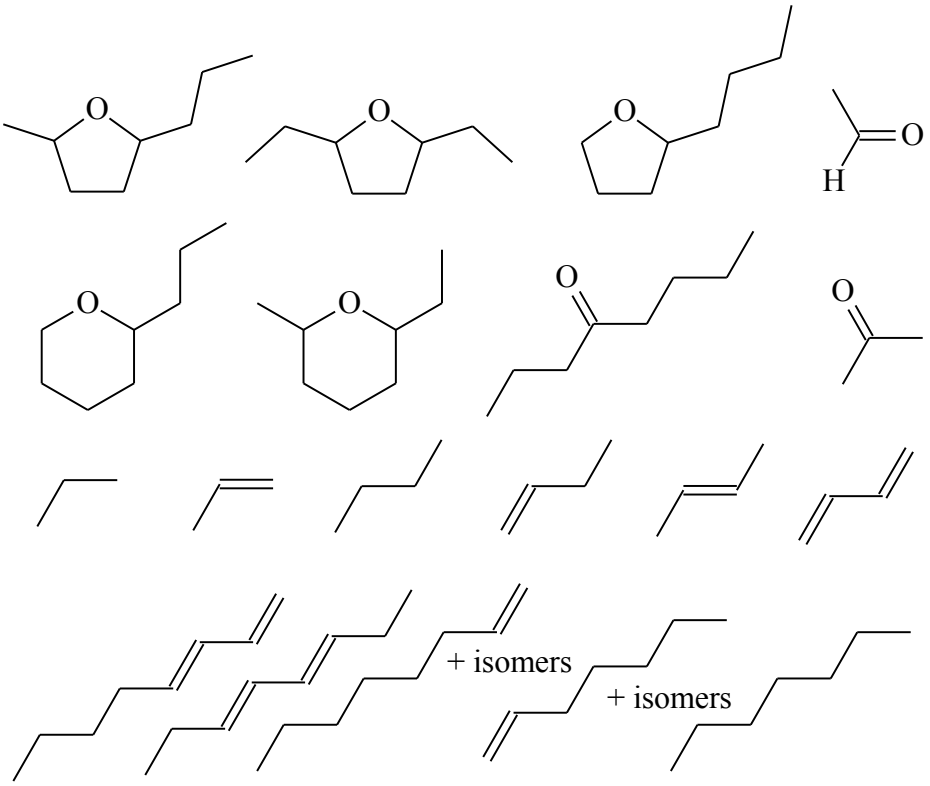

Fig. 4.60 Some of the products obtained from n-octane oxidation in an empty reactor

Total selectivities to these products over the 400-500°C temperature range were higher than 50 % with 25-40 % selectivity to C_{3-4} cracked products (conversions higher than 50 %) (Table 4.13). The products obtained from C_8 oxidation in an empty reactor were identified via gas chromatography-mass spectrometry.

The maximum selectivity to C_{3-4} products from *n*-octane oxidation in a carborundum-packed reactor was less than 3 %. The same result, where selectivity to C_{3-4} cracked products was higher in an empty reactor compared to a carborundum-packed reactor, was obtained for *n*-hexane oxidation under similar conditions.

Table 4.13 Selectivities to products obtained from n-octane oxidation in an empty reactor

Reaction T(°C)	% X	%					
		Propane/ene	Butane/ene	Acetaldehyde	Acetone	2-Methyl-1-hexene	Hexenes
400	49	34	7	2	3	3	0
450	55	19	5	1	2	1	12
500	72	20	5	1	1	1	13

Table 4.13 (continued)

Reaction T(°C)	% X
400	49
450	55
500	72

The C_7 products were obtained at selectivities below 2 % from C_8 oxidation and are not included in the above table.

More oxygenated products were obtained from *n*-octane oxidation in an empty reactor than a carborundum-packed reactor, however, there was poor selectivity to any one product. *n*-Hexane and *n*-octane oxidation did not give alcohols in an empty reactor. The product profile was more complex from *n*-octane oxidation in the empty reactor than in a carborundum-packed

reactor. Oxygen insertion into the alkane occurred more readily in the absence of an inert packing (carborundum).

4.2.4 Conversion of medium chain hydrocarbons

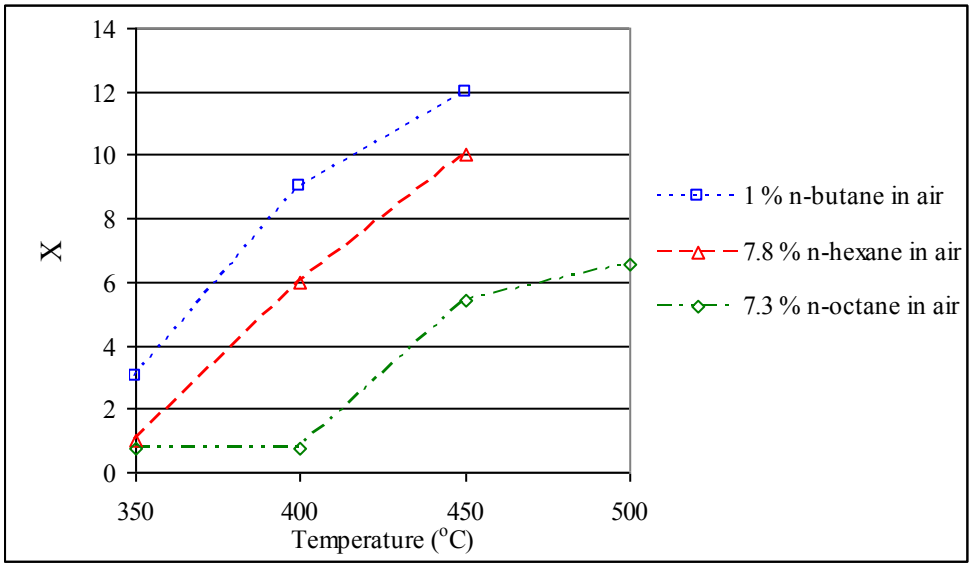

Fig. 4.61 Conversions (X) of n-butane, n-hexane and n-octane vs. temperature in a carborundum packed steel reactor at 100 ml min^{-1}

In the absence of an oxidant, the alkane remains unconverted in the reactor at temperatures lower than 600°C. However, in the presence of an oxidant, carbon oxides were the major products from alkane oxidation in blank reactions. The oxidation of *n*-octane to carbon oxides is more oxygen demanding than *n*-hexane, due to more secondary substituted carbons in the hydrocarbon. This gave an *n*-octane conversion vs. temperature curve lying below the *n*-hexane curve (Fig. 4.61). *n*-Butane was in an oxygen richer environment than *n*-hexane and *n*-octane and thus higher conversions were obtained under the same operating conditions.

The oxidation of *n*-octane in voids in a reactor gave linear and cyclic oxygenated products. The oxidation of *n*-butane and *n*-hexane in voids gave non-oxygenated products.

4.3 Catalyst testing

The GHSV was maintained at ~ 3000 hr^{-1} for all catalyst testing. The carbon mass balances were between 97 and 102 %. Above 300°C, homogeneous reactions became significant and contributed to results obtained from catalyst testing. Their contributions are discussed in terms of conversions and selectivities. The selectivity data from catalyst testing was complicated by subsequent conversion of products via homogeneous reactions, such as the cyclisation of alkenes. A foldout section in the Appendix (p. 293) lists all the catalysts tested with a short description of each.

4.3.1 Oxidation of n-butane over VPO and VMgO catalysts

4.3.1.1 Unpromoted and Co-VPO catalysts synthesized via a co-precipitation method

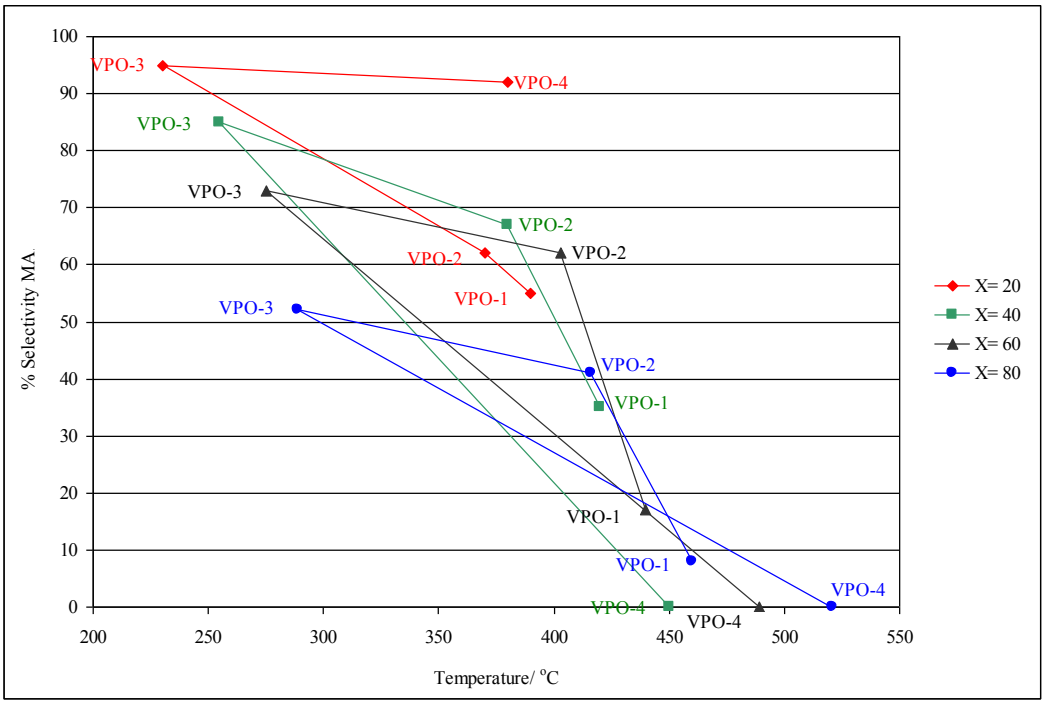

Fig. 4.62 Selectivity to MA at fixed conversions for the different loaded Co-VPO catalysts (VPO-1 = unpromoted, VPO-2 = 1.25 % Co-VPO, VPO-3 = 2.50 % Co-VPO and VPO-4 = 5.0 % Co-VPO)

An unpromoted VPO catalyst and three cobalt promoted VPO catalysts were investigated in the oxidation of *n*-butane. The promoted catalysts were synthesized via the co-

precipitation method. An expected trend of decreasing selectivity to MA with increasing temperature for the four catalysts, which was concurrent with increasing *n*-butane conversion (Fig. 4.62) was observed. The other products from this reaction were carbon oxides. In a separate investigation it was shown that the selectivity to MA decreased with increasing GHSVs at constant conversions, whilst there was an increase in selectivity to carbon oxides. This suggested over-oxidation of MA.

Comparison of the selectivities to MA obtained at constant conversions of 20, 40, 60 and 80 % for the unpromoted and the three Co-VPO catalysts (co-precipitation) indicated that the 2.5 % Co-VPO catalyst (co-precipitation) gave the highest selectivities at the lowest operating temperatures (Fig. 4.62).

The 2.5 % Co-VPO catalyst was more selective to MA compared to the unpromoted and other cobalt promoted VPO catalysts. The highest yield of MA was obtained over the Co-VPO catalyst (co-precipitation) with the highest surface area (i.e. 2.5 % Co-VPO). Addition of a dopant beyond this optimum amount gave a decrease in surface area of the catalyst.

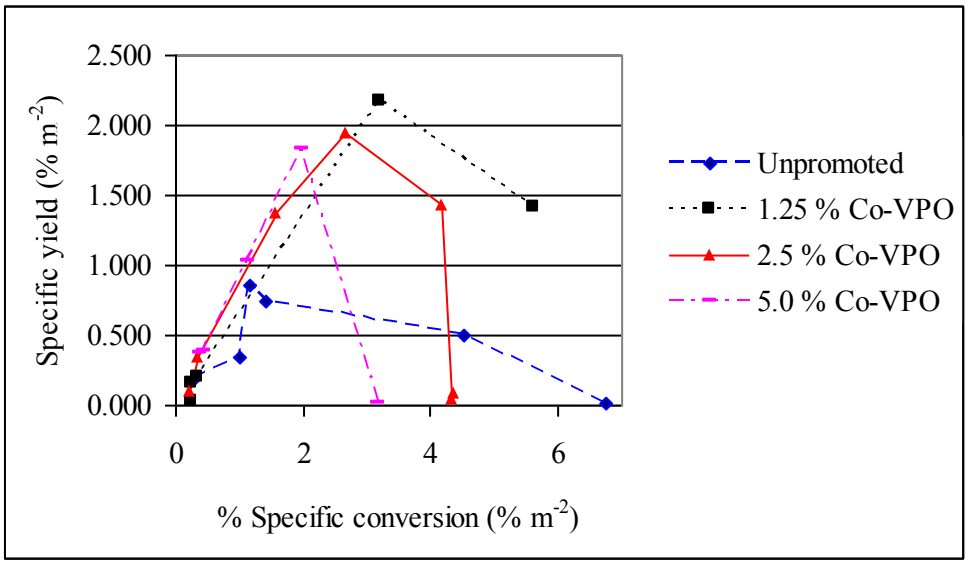

Fig. 4.63 Specific yield of MA vs. specific conversion of n-butane over an unpromoted and three cobalt promoted VPO catalysts

A plot of specific yields and conversions eliminated the effect of different catalyst surface areas on the yields when comparing different catalysts (Fig. 4.63). Specific yields and specific conversions were calculated as follows:

$$\text{Specific yield} = \frac{\%\ \text{Yield}}{\text{Surface area } (m^2\ g^{-1})}$$

$$\text{Specific conversion} = \frac{\%\ \text{Conversion}}{\text{Surface area } (m^2\ g^{-1})}$$

By keeping the temperature constant and increasing the GSHV from 1200 hr^{-1} to 7200 hr^{-1} over the 2.5 % Co-VPO catalyst, the conversion of *n*-butane decreased with subsequent increase in selectivity to MA.

The highest specific yields of MA were obtained with ~ 3 % specific conversion for the 1.25 % and 2.5 % Co-VPO catalysts (2.1 and 1.9 % m^{-2} respectively). They were obtained at reaction temperatures of 400^oC and 275^oC respectively. The highest specific yield for the unpromoted catalyst was 0.9 % m^{-2} at a specific conversion of 1.1 % m^{-2} (at an operating temperature of 350^oC) and the specific yield of the 5.0 % Co-VPO catalyst was 1.8 % m^{-2} at a specific conversion of 2 % m^{-2} (operating temperature of 400^oC). At a specific conversion of 1 %, the 2.5 % and 5.0 % Co-VPO catalysts gave a 1 % specific yield. The 2.5 % Co-VPO catalyst, however, gave higher specific yields at lower operating temperatures compared to the other catalysts.

Over a 48 h period, the conversions and selectivities over the promoted and unpromoted VPO catalysts at constant temperature were stable within 2 %.

The Co-VPO catalyst (co-precipitation) investigated in this thesis were benchmarked in the Appendix (p. 271) against other Co-VPO catalysts that were either employed industrially or were investigated by academic research groups. The catalysts were compared with regard to the method of synthesis and performance in terms of conversions and selectivities. The comparison

is complicated by the differences in synthetic routes and different catalytic conditions reported in the literature.

4.3.1.2 Co-VPO catalyst synthesized via the precipitation/deposition method for n-butane oxidation

The optimal promoter loading was 2.5 % via a co-precipitation method, giving the best performing catalyst. A catalyst with similar % cobalt loading was synthesized via a precipitation/deposition method.

Table 4.14 Selectivity to MA over a 2.5 % Co-VPO synthesized via a precipitation/deposition method

Reaction T(^{o}C)	% X	% Selectivity	
		MA	CO_x
300	9	11	89
350	12	0	100
400	12	0	100

A 2.5 % Co-VPO catalyst (precipitation/deposition) was investigated under similar conditions as those for the 2.5 % Co-VPO catalyst (co-precipitation). The impregnation method of adding the cobalt promoter gave a catalyst that performed poorly compared to an incorporation method. There was 11 % selectivity to MA at a conversion of 9 % and operating temperature of 300^{o}C (Table 4.14).

There was total oxidation of *n*-butane at temperatures higher than 300^{o}C over the 2.5 % Co-VPO catalyst (precipitation/deposition) (Table 4.14). At temperatures higher than 300^{o}C there was, however, MA from the Co-VPO catalysts (co-precipitation) (Fig. 4.62).

The 2.5 % Co-VPO catalyst (precipitation/deposition), although showing the presence of the $VOHPO_4 \cdot 0.5H_2O$ phase which was a precursor to the active catalytic $(VO)_2P_2O_7$ phase, did not perform as well as the 2.5 % Co-VPO catalyst (co-precipitation). A $VOPO_4 \cdot 2H_2O$ phase was also present in the former catalyst. There was 100 % selectivity to carbon oxides over a 350-400^{o}C temperature range.

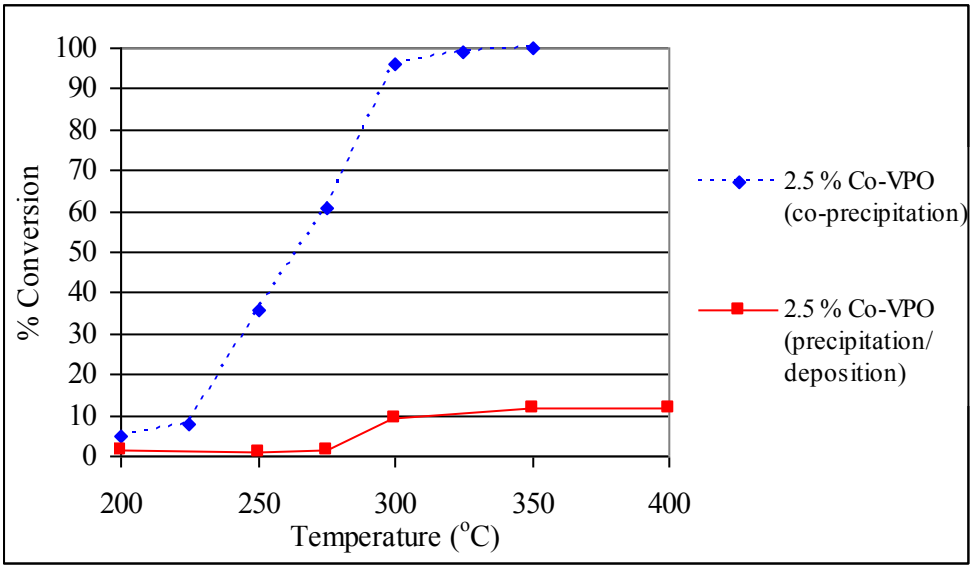

Fig. 4.64 Conversion of n-butane vs. temperature over 2.5 % Co-VPO catalysts synthesised via the co-precipitation and precipitation/deposition methods

Incorporating the promoter into the catalyst gave a more active catalyst than when the promoter was impregnated (Fig. 4.64).

4.3.1.3 Rh-VPO catalyst synthesized via the co-precipitation method for n-butane oxidation

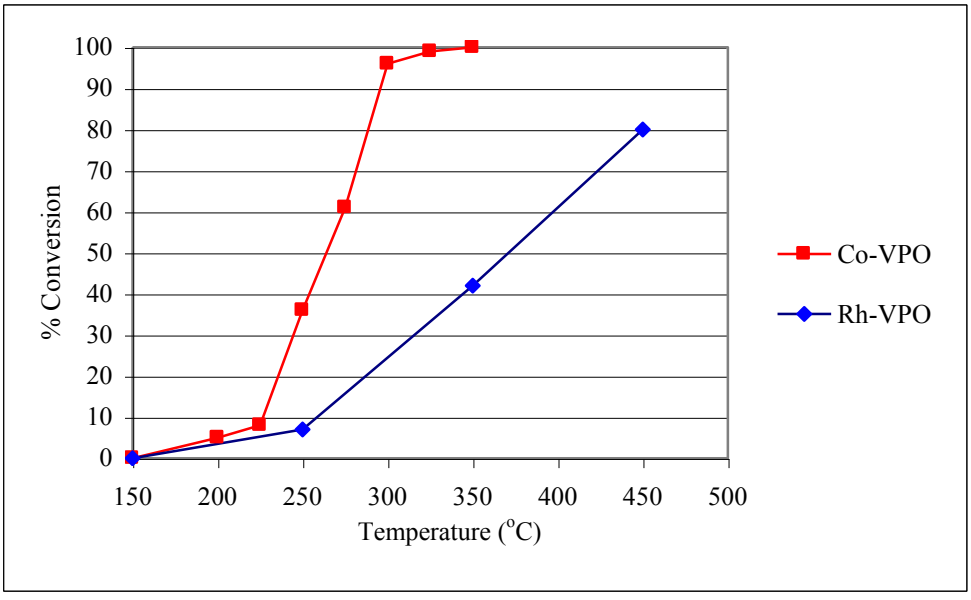

Fig. 4.65 Conversion of n-butane over a 2.5 % Rh-VPO and 2.5 % Co-VPO catalyst (co-precipitation) vs. temperature

The Co-VPO catalyst (co-precipitation) gave higher selectivity to MA and lower selectivities to carbon oxides compared to the Rh-VPO catalyst (co-precipitation) (Fig. 4.66).

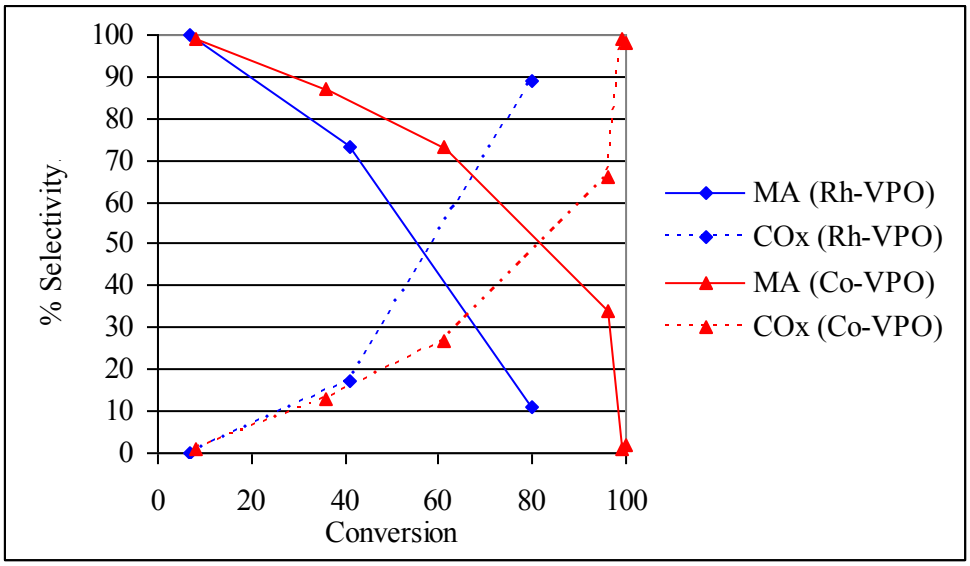

Fig. 4.66 Selectivities to MA and CO_x vs. conversion over a 2.5 % Rh-VPO (co-precipitation) and a 2.5 % Co-VPO catalyst (co-precipitation)

4.3.1.4 VPO-A and VPO-B catalysts synthesized via the co-precipitation method for n-butane oxidation

The co-precipitation method of incorporating gold into the VPO catalyst was unsuccessful. Inductively coupled plasma-mass spectrometry (ICP-MS) (Table 4.2) and energy dispersive X-ray (EDX) analysis (Table 4.3) confirmed the absence of gold in the synthesized catalysts (VPO-A and VPO-B). X-ray diffraction (XRD) analysis of VPO-A confirmed the presence of the $VOHPO_4 \cdot 0.5H_2O$ precursor phase. This was thus an unpromoted VPO catalyst.

The XRD patterns of VPO-A and a conventional unpromoted catalyst showed that VPO-A was more crystalline, even after calcination, where the VPO catalysts usually do not show any distinct phases or crystallinity.

The conversions and selectivities obtained from this catalyst were compared to the conventional unpromoted VPO catalyst (Fig. 4.67, 4.68).

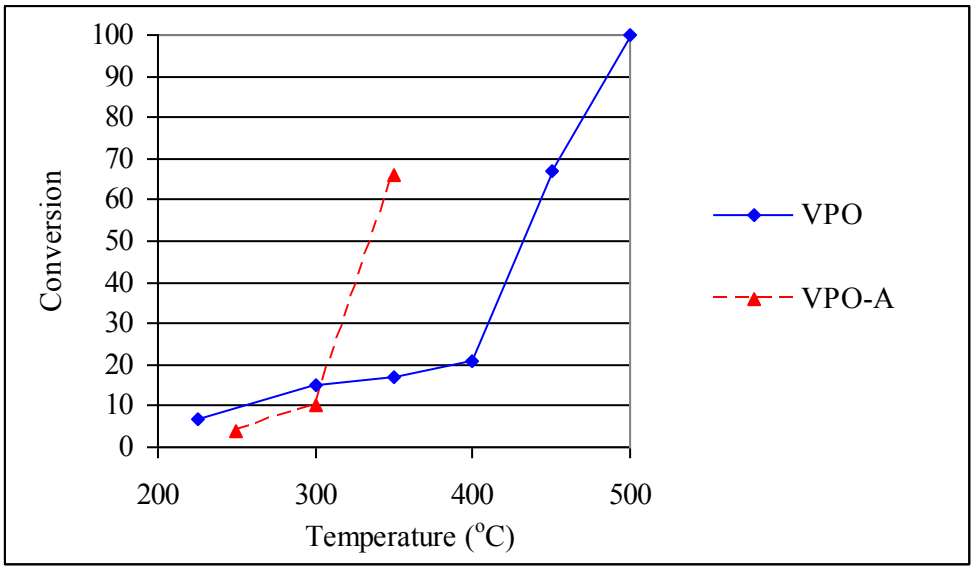

Fig. 4.67 Conversion of n-butane over VPO-A and an unpromoted VPO catalyst vs. operating temperature

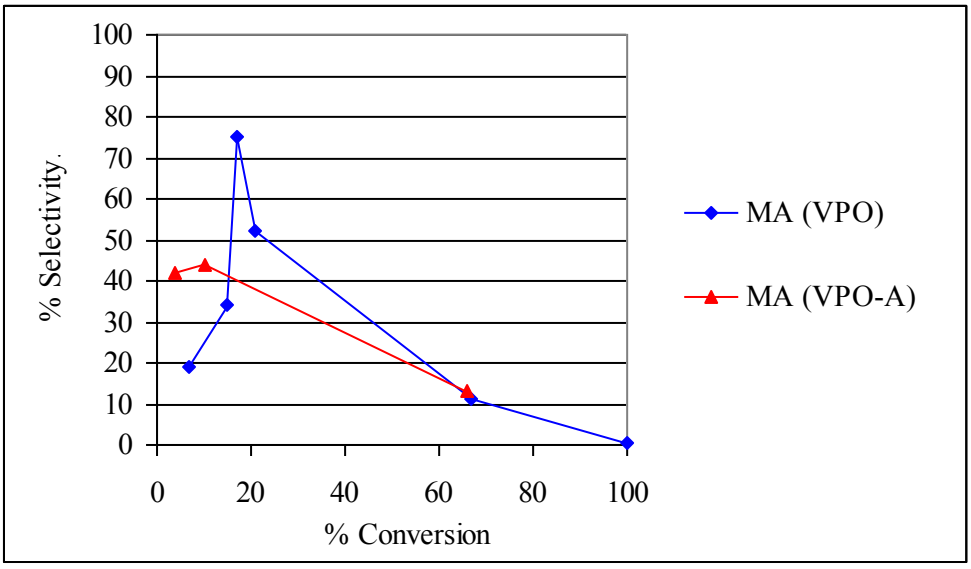

Fig. 4.68 Selectivity to MA vs. conversion over VPO-A and an unpromoted VPO catalyst

VPO-A was more active than the conventional unpromoted VPO catalyst at temperatures higher than 300°C (conversions higher than 20 %) (Fig. 4.68). The conventional unpromoted VPO catalyst gave higher selectivities to MA over a 300-400°C temperature range (conversions between 20 and 65 %).

The highest selectivity to MA was 75 % for the conventional unpromoted VPO catalyst at a conversion of ~ 20 %. The selectivity to MA obtained over VPO-A was 40 % at a similar conversion.

At low conversions (below 20 %), VPO-A gave higher selectivities to MA than the conventional unpromoted VPO catalyst.

4.3.1.5 Au-VPO catalyst synthesized via the precipitation/deposition method for n-butane oxidation

Gold was successfully impregnated onto the VPO, however, this catalyst did not give MA, but rather dehydrogenated *n*-butane(Table 4.15).

The dehydrogenation products included 1-butene, 2-butene and butadiene. Below 425^{o}C, there was total oxidation. There was a decrease in conversion from 93 % at 425^{o}C to 58 % at 450^{o}C. This was attributed to possible deactivation of the catalyst.

Table 4.15 Selectivity to butenes from the conversion of n-butane over a 2.50 % Au-VPO catalyst synthesized via the precipitation/deposition method

Reaction T(^{o}C)	% X	% Selectivity	
		Butenes	CO_x
250	4	0	100
300	13	0	100
350	83	0	100
400	94	0	100
425	93	10	90
450	58	5	95

The 2.5 % Au-VPO catalyst (precipitation/deposition) gave higher selectivities to carbon oxides than an unpromoted catalyst, specifically the selectivities to carbon dioxide obtained over the 2.5 % Au-VPO catalyst (precipitation/deposition) were higher compared to those obtained over the unpromoted catalyst (Fig. 4.69).

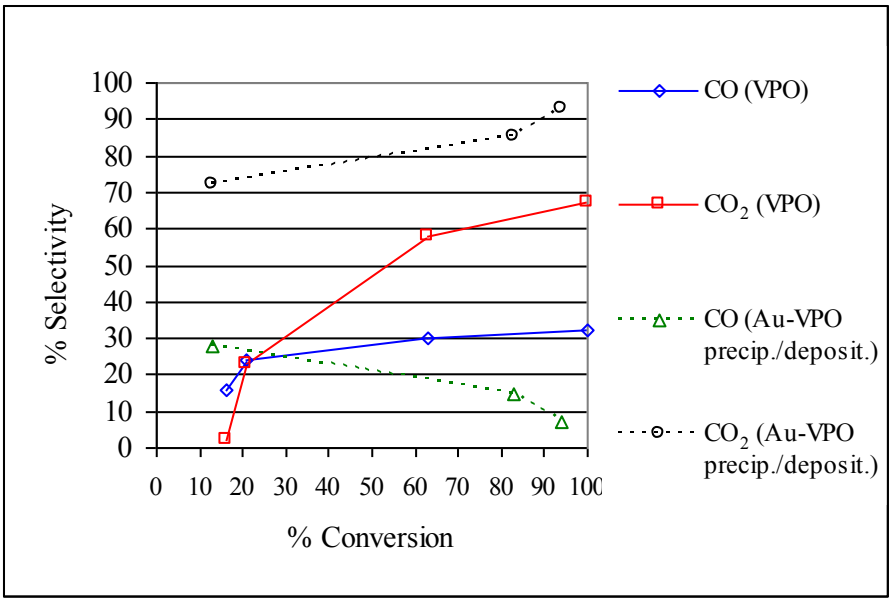

Fig. 4.69 Selectivities to carbon monoxide and carbon dioxide over unpromoted VPO and Au-VPO (precipitation/deposition) catalysts

Selectivities to carbon monoxide and carbon dioxide over the unpromoted VPO catalyst increased with increasing temperature. However, the selectivity to carbon dioxide increased with a concurrent decrease in selectivity to carbon monoxide when the operating temperature of the Au-VPO catalyst (precipitation/deposition) was increased (Fig. 4.69).

Gold has been widely reported as a catalyst for the oxidation of CO to CO_2 (Bondzie, V.A. *et al.* (2000), Choudary, T.V. *et al.* (2002), Haruta, M. (1997), Hutchings, G.J. *et al.* (2003), Wolf, A. *et al.* (2002)) and the catalysis here appears to be dominated by the gold species impregnated on the surface of the catalyst.

4.3.1.6 Selectivity profiles of co-precipitation synthesized VPO catalysts for n-butane oxidation

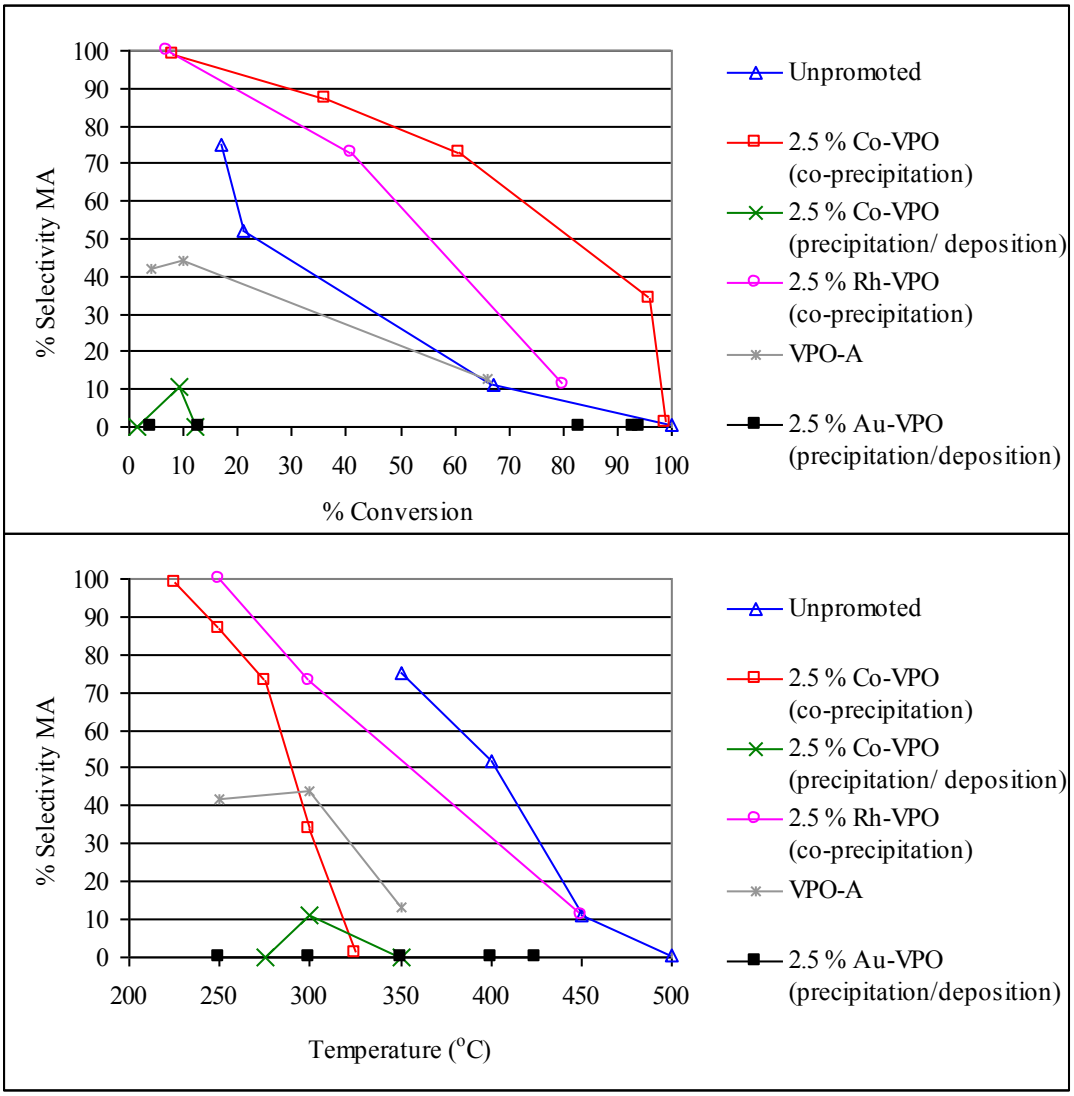

Fig. 4.70 Comparison of selectivity to MA over different VPO catalysts vs. conversion of n-butane and operating temperature

The 2.5 % Co-VPO catalyst (co-precipitation) was the best performing catalyst from all the VPO catalysts investigated in the oxidation of *n*-butane under the same catalytic conditions and theoretical promoter loading. It gave the highest selectivities to MA vs. conversion over a temperature range of 250 to 500°C (Fig. 4.70).

4.3.1.7 VMgO and Co-VMgO (co-precipitation) catalysts for n-butane oxidation

The Co-VMgO catalyst was more active than the unpromoted VMgO catalyst at lower operating temperatures (Fig. 4.71). A 10 % conversion was obtained at ~ 360°C for the Co-VMgO catalyst and at ~ 490°C for the VMgO catalyst.

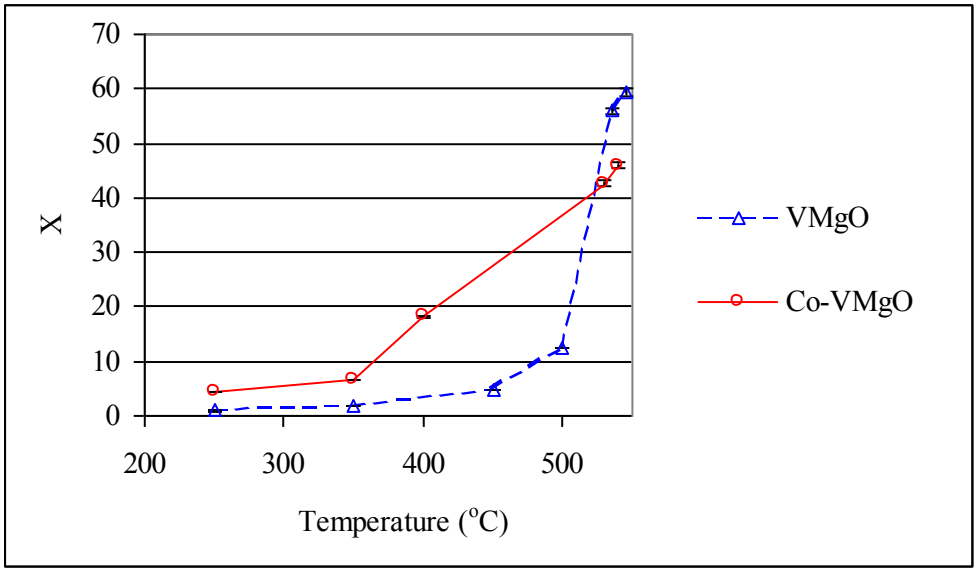

Fig. 4.71 Conversion of n-butane over VMgO and Co-VMgO catalysts (co-precipitation)

The Co-VMgO catalyst was less active than the VMgO catalyst above 500°C.

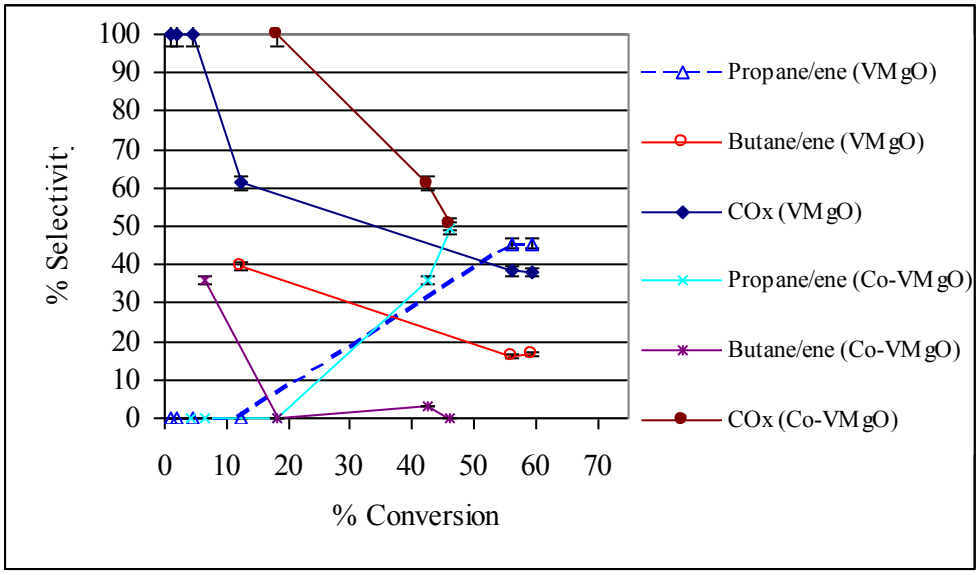

Fig. 4.72 Selectivity vs. conversion for the oxidation of n-butane over VMgO and 2.50 % Co-VMgO catalysts (co-precipitation)

The normally yellow/white catalysts turned black after testing. This was attributed to coke formation on the catalyst, which was confirmed by EDX analysis. The conversions and selectivities were constant over a reaction time of 36 h at constant temperature, even in the presence of this coke formation.

The incorporation of cobalt into VMgO gave lower selectivities to cracking products and butenes and higher selectivities to carbon oxides than an unpromoted catalyst.

4.3.2 Oxidation of n-hexane over VMgO, Co-VMgO (co-precipitation), VPO and Co-VPO (co-precipitation)

The incorporation of a promoter into a VPO catalyst gave a superior performing catalyst than impregnating the promoter for the selective oxidation of *n*-butane. Thus incorporating cobalt into the VPO and VMgO catalysts was further investigated in the oxidation of *n*-hexane and *n*-octane. The effect of voids, catalyst dilution and reactor material (glass and stainless steel) on conversion and selectivity was investigated.

4.3.2.1 Unpromoted VMgO and Co-VMgO catalyst synthesized via the co-precipitation method

The oxidation of *n*-hexane in a carborundum-packed reactor (Fig. 4.73) gave benzene, indicating that it was a thermal product, however, the selectivity to benzene was higher in a conventionally packed reactor (setup 3 in foldout section of the Appendix (p. 292)) containing the promoted and unpromoted VMgO catalysts compared to the carborundum-packed reactor. The largest selectivities obtained to a non-oxygenated product over the VMgO and Co-VMgO catalysts were to benzene.

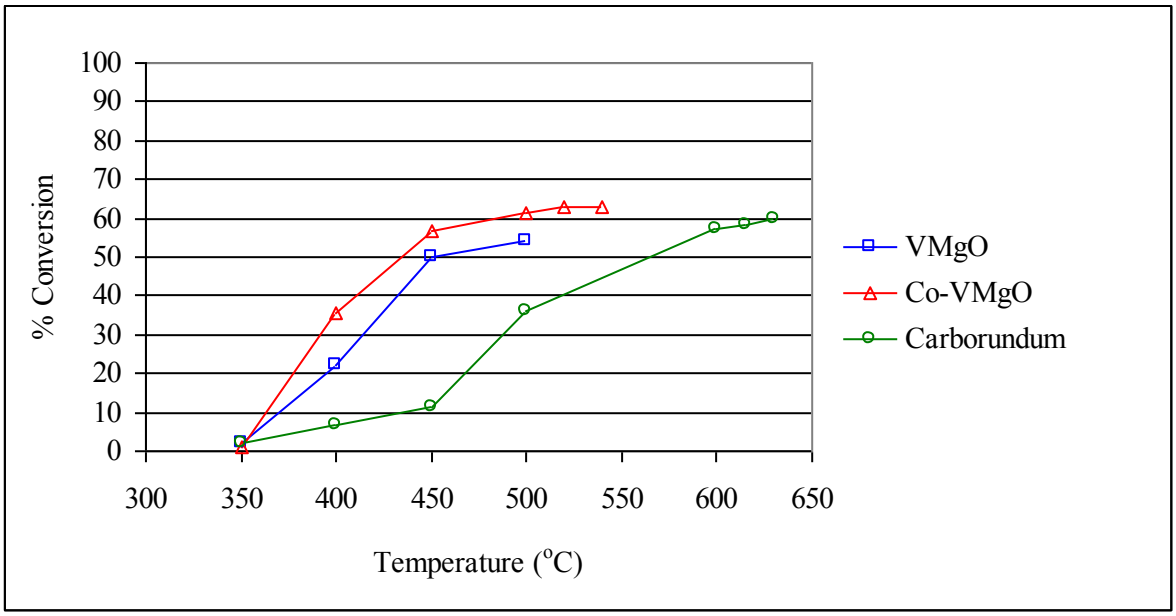

Fig. 4.73 Conversion of n-hexane over VMgO, Co-VMgO and a steel reactor fully packed with carborundum (GHSV = 3000 hr^{-1})

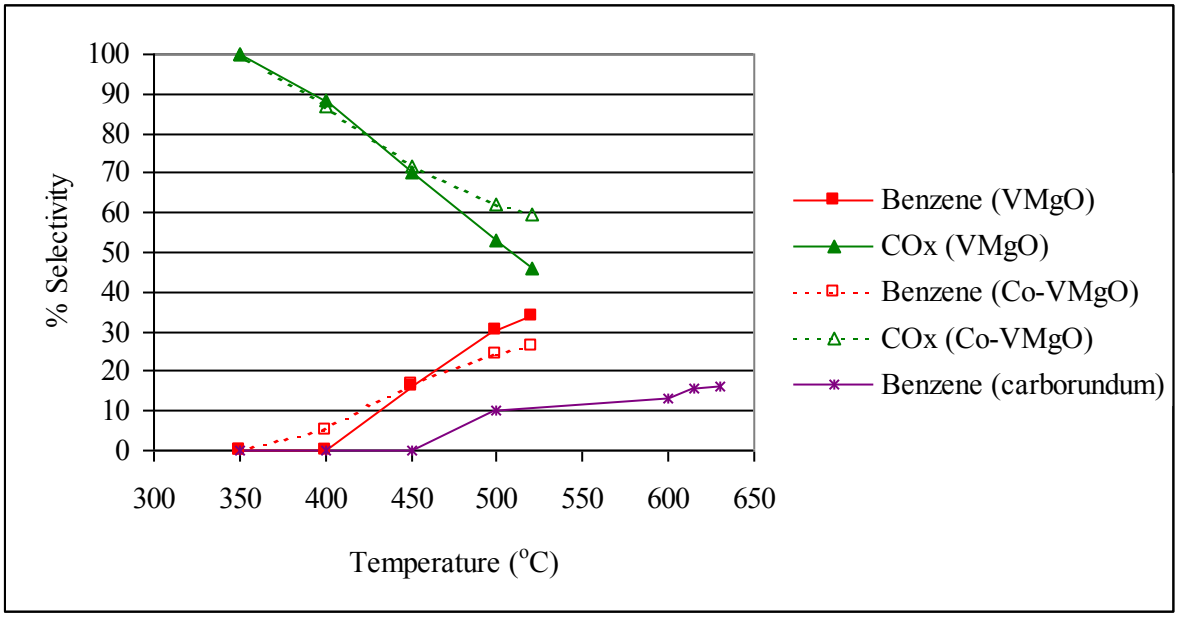

Fig. 4.74 Selectivities to benzene and carbon oxides over VMgO, Co-VMgO at a GHSV of 3000 hr^{-1} and in a stainless steel reactor fully packed with carborundum

The selectivity to benzene increased with a concurrent decrease in selectivity to carbon oxides as the operating temperature was increased for the VMgO and Co-VMgO catalysts at a GHSV of 3000 hr^{-1} in a stainless steel reactor (Fig. 4.74). The Co-VMgO catalyst was more

active than the VMgO catalyst. Above 450°C, the selectivity to benzene was higher and the selectivity to carbon oxides was lower over the unpromoted VMgO catalyst compared to the Co-VMgO catalyst.

Table 4.16 Selectivities to minor products from n-hexane conversion over a VMgO catalyst in a stainless steel reactor at a GHSV of 3000 hr^{-1}

Reaction T(°C)	% X	% Selectivity				
		Propane/Propene	Butane/Butenes	1-Hexene	2-Hexene (cis)	2-Hexene (trans)
400	22	0	0	0	7	4
450	50	0	2	3	5	3
500	54	0	4	4	5	4
520	48	0	6	5	6	4

Table 4.17 Selectivities to minor products from n-hexane conversion over a Co-VMgO catalyst in a steel reactor at a GHSV of 3000 hr^{-1}

Reaction T(°C)	% X	% Selectivity				
		Propane/Propene	Butane/Butenes	1-Hexene	2-Hexene (cis)	2-Hexene (trans)
400	36	0	0	0	5	3
450	57	0	2	3	4	3
500	62	3	1	3	4	3
520	63	3	1	3	4	3

The other products obtained over an unpromoted catalyst were butane, isomers of butene, 1-hexene and 2-hexene isomers (Table 4.16). The same products together with propane and propene were obtained over the promoted catalyst (Table 4.17). The selectivities to these products (excluding propane and propene) were similar for both catalysts.

The Co-VMgO catalyst was more active than the unpromoted catalyst. In both steel and glass-packed reactors, the conversion vs. temperature curves for *n*-hexane oxidation flattened at ~ 60 % for a Co-VMgO catalyst (co-precipitation) and just over 50 % for a VMgO catalyst (Fig. 4.75).

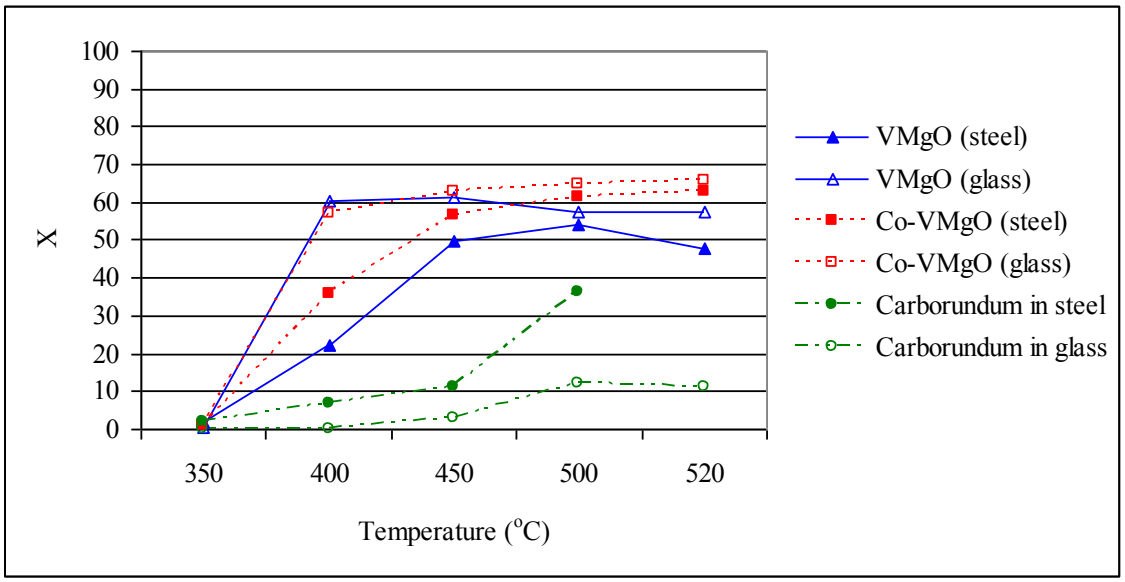

Fig. 4.75 % Conversions (X) of n-hexane obtained over neat carborundum, promoted and unpromoted VMgO catalysts in glass and steel reactors

The conversion vs. temperature curve flattened at ~ 30 % for *n*-octane oxidation over the unpromoted and promoted VMgO catalysts in a stainless steel reactor. This was attributed to oxygen depletion due to the high O_2:hydrocarbon ratio required for carbon oxide formation reactions (Table 4.24). There are more secondary carbons available in *n*-octane than *n*-hexane, thus the conversion vs. temperature curve flattened at a lower value of 30 %, compared to *n*-hexane oxidation, because of the availability of more carbon centres to form carbon oxides from a C_8 chain compared to a C_6 alkane, which gave a faster rate of oxygen depletion. The remaining oxygen in the feedstream formed water from oxidative dehydrogenation or combustion reactions. No other oxygenated products in significant quantities were obtained.

The VMgO catalyst generally gave higher selectivities to benzene and lower selectivities to carbon oxides than the Co-VMgO catalyst (Fig. 4.76). The same trends were observed in the stainless steel reactors.

The conversions of *n*-hexane in a glass reactor were generally higher than in a steel reactor for both promoted and unpromoted catalysts over a 250-520°C temperature range (Fig. 4.75). The conversions in a fully carborundum-packed steel reactor, operated under similar conditions employed for a catalytic system were, however, higher than conversions in a fully

carborundum-packed glass reactor. The conversion of *n*-hexane was 38 % in the fully carborundum-packed steel reactor and 12 % in the fully carborundum-packed glass reactor at 500°C. There was 8 % conversion in the steel reactor and zero conversion in the glass reactor at 400°C. The glass reactor was thus effective in limiting homogeneous reactions in the reactor. Both VMgO and Co-VMgO catalysts (co-precipitation) were inactive at 350°C. The flattened selectivities to benzene and carbon oxides were attributed to oxygen starvation in the reactor (Fig. 4.76).

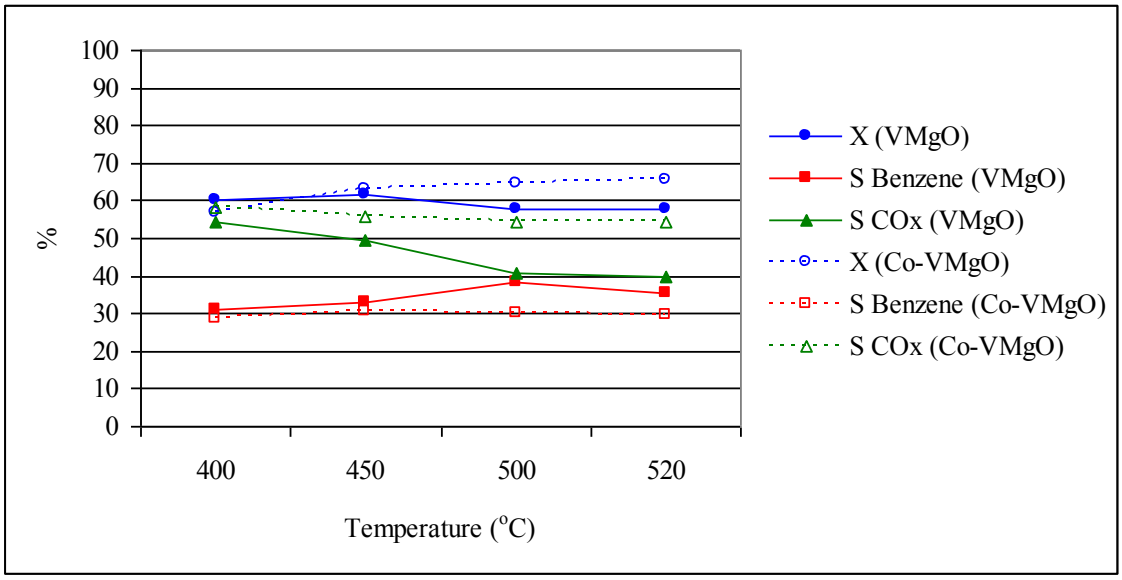

Fig. 4.76 Selectivities (S) to benzene and carbon oxides and conversions (X) of n-hexane over promoted and unpromoted VMgO catalysts in a glass reactor at a GHSV of 3000 hr^{-1}

Table 4.18 Selectivities to minor products from n-hexane conversion over a VMgO catalyst in a glass reactor

Reaction T(°C)	% X	% Selectivity				
		Propane/Propene	Butane/Butene	1-Hexene	2-Hexene (cis)	2-Hexene (trans)
400	60	0	4	3	4	3
450	62	6	1	3	4	3
500	58	6	2	4	5	4
520	58	6	6	4	5	4

The selectivities to 1-hexene, 2-hexene (cis) and 2-hexene (trans) in glass reactors are shown in Tables 4.18-4.19.

Table 4.19 Selectivities to minor products from n-hexane conversion over a Co-VMgO catalyst in a glass reactor

Reaction T(°C)	% X	% Selectivity				
		Propane/Propene	Butane/Butene	1-Hexene	2-Hexene (cis)	2-Hexene (trans)
400	57	3	1	3	3	3
450	63	4	1	3	3	2
500	65	5	1	3	3	3
520	66	5	2	3	3	3

The selectivity to C_{3-4} cracked products was higher in a glass reactor than in a stainless steel reactor under catalytic conditions (at similar conversions) (Fig. 4.77) in the 350 to 550°C temperature range. In both the steel and glass reactors, the cracking was inherent of catalytic behaviour and not a homogeneous reaction since there were no C_{3-4} cracked products over this temperature range under non-catalytic conditions in carborundum-packed reactors. The conversions obtained over the temperature range plotted in Fig. 4.77 were between 22 and 63 % in the glass reactors and between 57 and 66 % in the steel reactors. Selectivities to isomers of hexene were generally higher in the steel reactors than in the glass reactors under catalytic conditions (Fig. 4.77), however, selectivities to isomers of hexene were generally higher in the glass reactors compared to the steel reactors under non-catalytic conditions at similar conversions. The selectivities to C_{3-4} cracked products and isomers of hexene were generally higher over the unpromoted VMgO catalyst than the Co-VMgO catalyst in both steel and glass reactors.

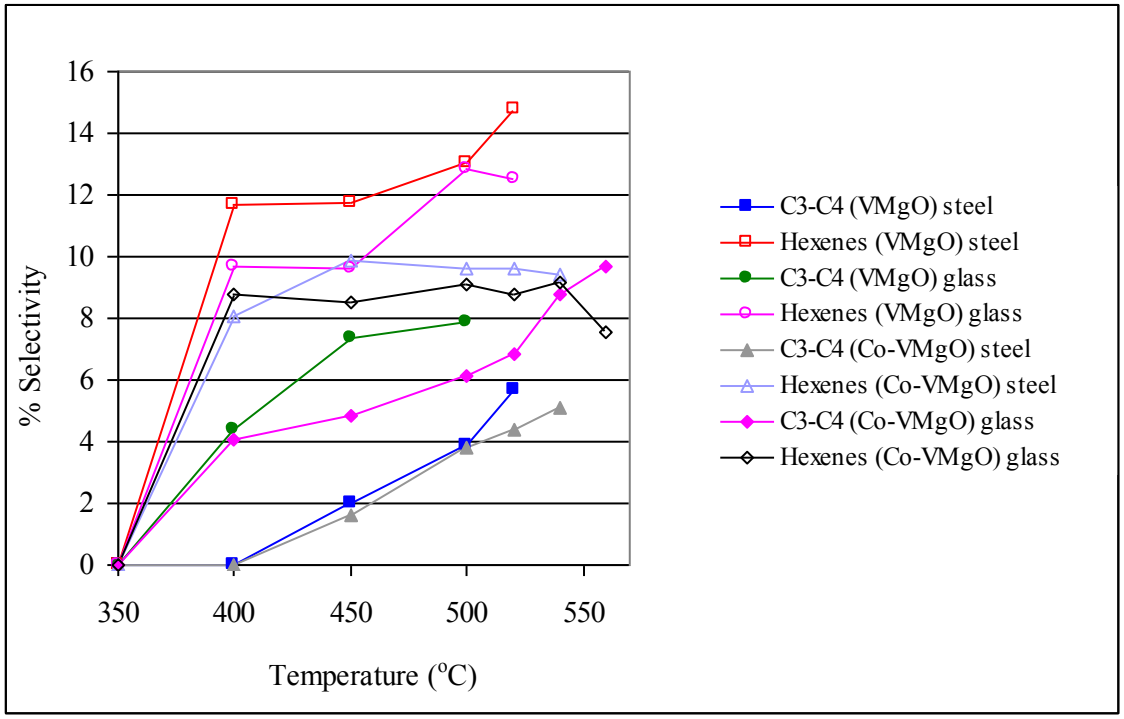

Fig. 4.77 Selectivities to C_{3-4} cracked products and isomers of hexene from n-hexane oxidation over catalysts packed in glass and steel reactors

The selectivity to benzene was compared at 10 % conversion under catalytic and non-catalytic conditions using stainless steel and glass reactors (Table 4.20). A conversion of 10 % was obtained at 500°C and below for all reactor systems in Table 4.20, where there was minimal decomposition of benzene to carbon oxides (Section 4.3.2.4).

Table 4.20 Selectivity to benzene under catalytic and non-catalytic conditions in glass and steel reactors at 10 % conversion

Reactor packing	Temperature	Benzene selectivity
Carborundum (steel)	450	0
Carborundum (glass)	500	10
VMgO (steel)	370	0
VMgO (glass)	355	5
Co-VMgO (steel)	370	2
Co-VMgO (glass)	355	5

There was higher selectivity to benzene in the glass reactors than in the steel reactors under catalytic and non-catalytic conditions at a conversion of 10 %.

4.3.2.2 The effect of voids and dilution on n-hexane oxidation over a VMgO catalyst

This investigation illustrated some of the problems associated with alkane activation with respect to the location of voids and the catalyst in the reactor. The effect of differently packed reactors and dilution factors on the product profile was investigated at a GSHV of 3000 hr^{-1} in stainless steel reactors. All percentages of conversions and selectivities are ± 1 %.

The products observed were C_{3-4} cracked products, isomers of hexene, benzene and carbon oxides. The product profile from *n*-hexane oxidation in an empty reactor and over a catalyst was the same, however, the effect the VMgO catalyst had on the conversion and product selectivity profile when diluted and combined with voids in the reactor was investigated (Fig. 4.78). A further illustration of the setups appear in the foldout section of the Appendix (p. 292).

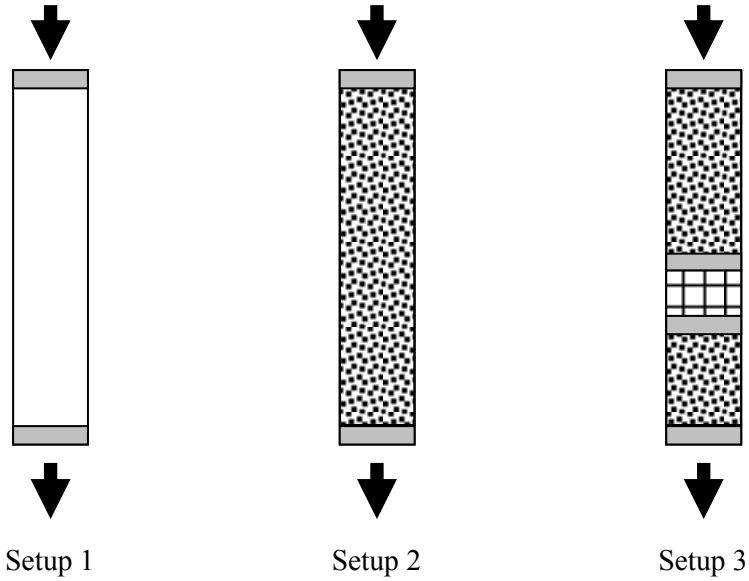

Fig. 4.78 The location of neat and diluted catalysts and voids in the reactor. The arrows indicate the direction of flow

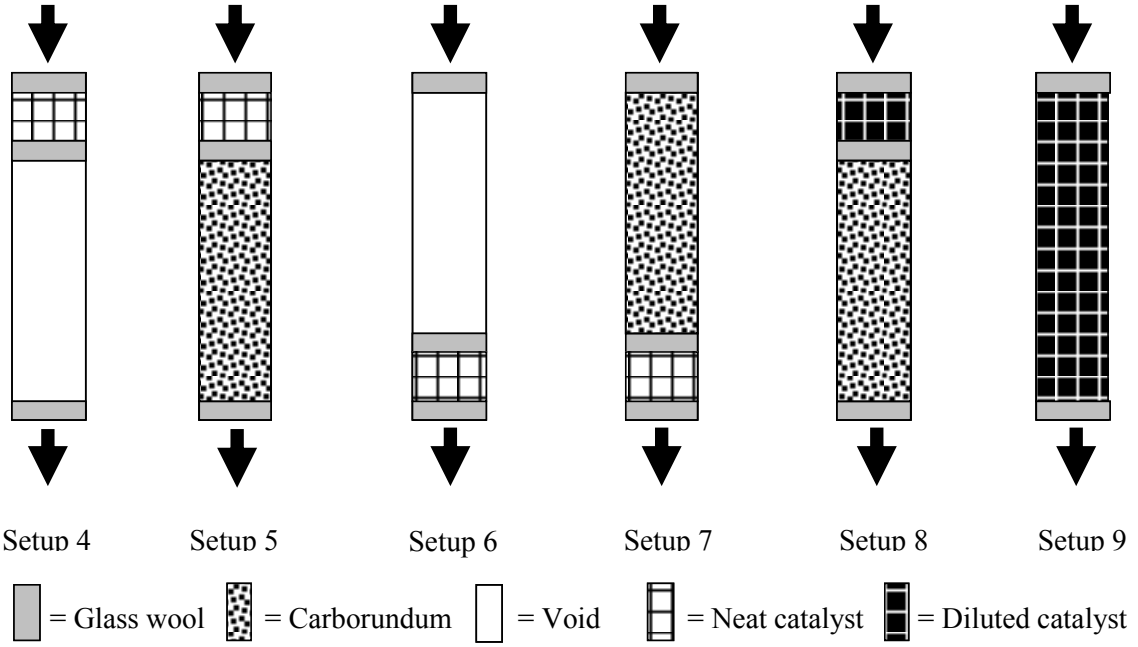

Fig. 4.78 (continued) The location of neat and diluted catalysts and voids in the reactor. The arrows indicate the direction of flow

The conversions from an empty reactor (Setup 1) and a reactor fully packed with carborundum (setup 2) were compared to determine the contribution made by large and small voids to the conversion. There was only significant conversion of *n*-hexane above 400°C in a fully carborundum-packed reactor (setup 2) (Fig. 4.78). A conventionally packed reactor, which included the catalyst is illustrated in setup 3. The conversion in this setup was lower than some other setups (1, 4 and 6) containing larger voids.

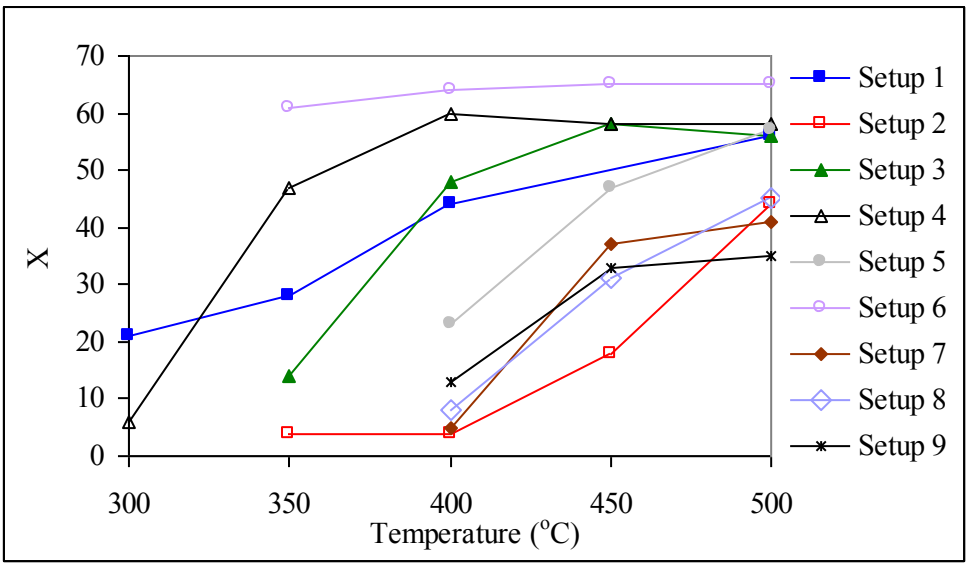

Fig. 4.79 Conversion (X) of n-hexane over the different setups over a 300-500°C temperature range

Voids following a catalyst bed (Setup 4) gave oxygen starvation at lower temperatures compared to the conventionally packed system (Setup 3) due to deep oxidation and/or combustion. This was seen from the flattening of the conversion vs. temperature curve at a lower temperature for setup 4 (400°C) than setup 3 (450°C).

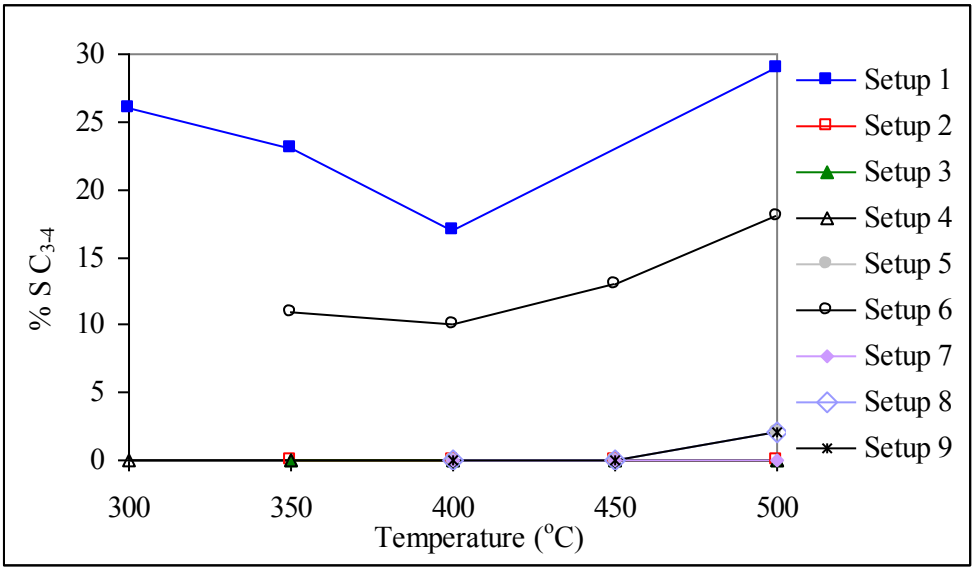

Fig. 4.80 Selectivity (% S) to C_{3-4} cracked products for the different setups over a 300-500°C temperature range

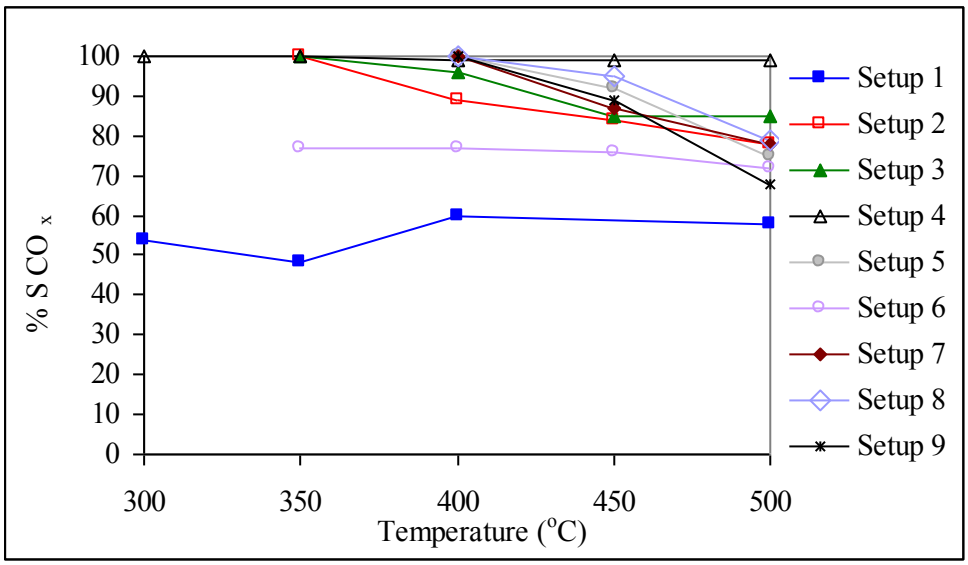

Fig. 4.81 Selectivity (% S) to CO_x for the different setups over a 300-500°C temperature range

Voids following a catalyst bed gave solely the production of carbon oxides, however voids preceding a catalyst bed gave cracked products and carbon oxides with higher conversions compared to an empty reactor (Figs. 4.80 and 4.81). There was a higher selectivity to carbon oxides obtained in a carborundum-packed reactor (84 %) (setup 2) than in an empty reactor (54 %) (setup 1) at a conversion of 20 %. A CO_2:CO molar ratio of 1 was obtained at this conversion in an empty reactor (setup 1) and 27 in a carborundum-packed reactor (setup 2).

The catalyst's contribution to the conversion of *n*-hexane was investigated by filling the voids with carborundum. There was poor selectivity to benzene under purely catalytic conditions (i.e. at temperatures of 400^{o}C and lower). The highest yield of benzene (11%) and the highest selectivity to benzene (19%) was obtained from both a catalytic and non-catalytic contribution to its formation at 500^{o}C (setup 5). The yield was higher than in a conventionally packed reactor (setup 3), which confirmed that a larger volume of carborundum packing post catalyst gave higher selectivities to benzene. There was little or no cracking in reactors containing carborundum. The only C_2 product was acetaldehyde in trace amounts (< 1 % selectivity) in setups 1 and 6.

Setup 6 gave the highest conversions (~ 60 %), however, there was mainly cracking and combustion. This was attributed to a combined catalytic and non-catalytic contribution. The highest selectivities to $C_{3\text{-}4}$ cracked products were obtained in setup 1, with setup 6 giving the next highest selectivities, however, when a void was located after the catalyst bed (setup 4), there was no cracking, but only combustion. Thus all products from the catalyst were converted to carbon oxides in the void post-catalyst. The production of carbon oxides was from a combination of catalytic and non-catalytic reactions.

Setup 1, which had the largest void volume and absence of a catalyst gave the lowest selectivities to carbon oxides (Fig. 4.81).

At 400^{o}C, where conversion was due essentially to the activity of the catalyst and not any gas phase reactions, the highest conversion (47 %) was obtained in the conventionally packed reactor (setup 3). The conversion in setup 7, where the catalyst was packed at the exit of

the reactor, was negligible and similar to that obtained in the fully carborundum-packed reactor. The conversion in setup 5, where the catalyst was packed at the entrance of the reactor was 21 %. This lower conversion than in setup 3 is attributed to the absence of a carborundum pre-heat zone preceding the catalyst. In setup 7, there was a pre-heat zone, however, there was no carborundum packing post catalyst. The feed was pre-heated but there was little conversion because the pre-heated catalytically activated feed did not pass through a carborundum packed region for subsequent conversion. A pre-heat zone and carborundum packing post-catalyst was thus necessary for a reaction. Products from the carborundum-packed region preceding the catalyst and from the catalyst were further converted in the intergranular space of the carborundum packed post-catalyst.

At 500^{o}C, where gas phase reactions were significant, the highest selectivity to benzene was obtained in setup 5 (i.e. 19 % selectivity and yield of 11 %), where the catalyst was packed at the entrance of the reactor followed by carborundum. This yield surpassed the 2 % yield obtained from an empty reactor, where cracked products dominated and the 7 % yield obtained from a fully carborundum-packed reactor (setup 2) at the same temperature.

Selectivity to benzene increased with increasing temperature in the carborundum-packed reactors (setups 2, 3, 5 and 7) with a concurrent decrease in selectivity to carbon oxides, which suggested that a mechanism to benzene formation was favoured over carbon oxide formation with increasing temperatures. A summary of the results obtained from the experiments conducted in carborundum-packed setups 2, 3, 5 and 7 appear in Table 4.22. The selectivities to benzene flattened with increasing conversions (Fig. 4.82) in setup 2 and increased sharply in setups 3 and 5.

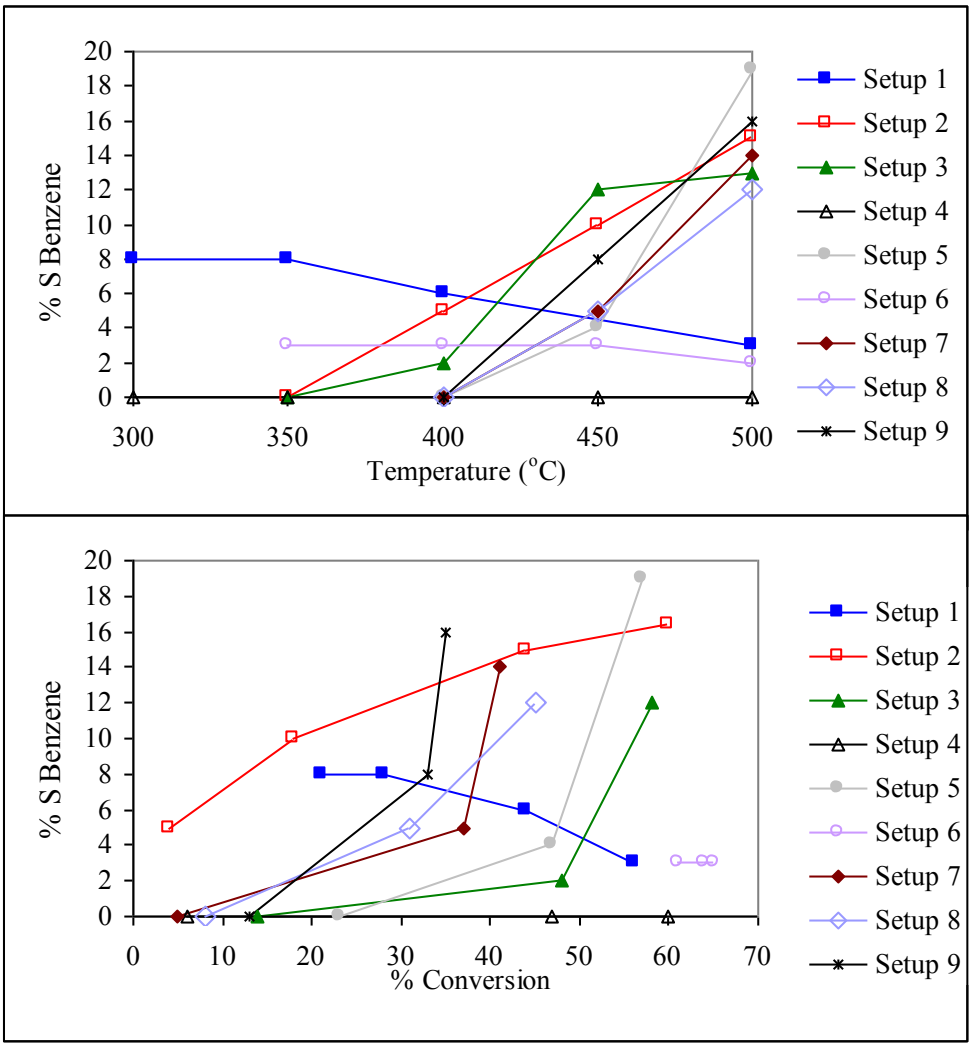

Fig. 4.82 Selectivity (% S) to benzene for the different setups vs. temperature (top) and vs. conversion (bottom)

Although the void in setup 1 gave the highest selectivities to isomers of hexene, which are intermediates to benzene (Fig. 4.83), cracking of the feed to C_3 and C_4 products was favoured with increasing temperature in the voids of setups 1 and 6, whilst there was 100 % selectivity to carbon oxides in setup 4.

The catalyst was diluted with carborundum (1:1 by volume) and packed at the entrance of the reactor (setup 8). Further dilution was achieved by diluting the catalyst with all the carborundum used to pack the reactor (setup 9). At 450°C a similar conversion of 32 % was obtained for setups 8 and 9 with a lower selectivity to carbon oxides in setup 9, compared to

setup 8, giving higher selectivities to benzene and isomers of hexene in setup 9. The conversion over an undiluted catalyst (setup 5) under similar reaction conditions (similar temperature) to setup 8 was higher with a similar selectivity to benzene. A higher selectivity to benzene was obtained in setup 9 and from the partially diluted catalyst in setup 8, than in setup 5 at a conversion of 32 %. Increasing the dilution of the catalyst improved the selectivity to benzene under similar operating conditions and conversions.

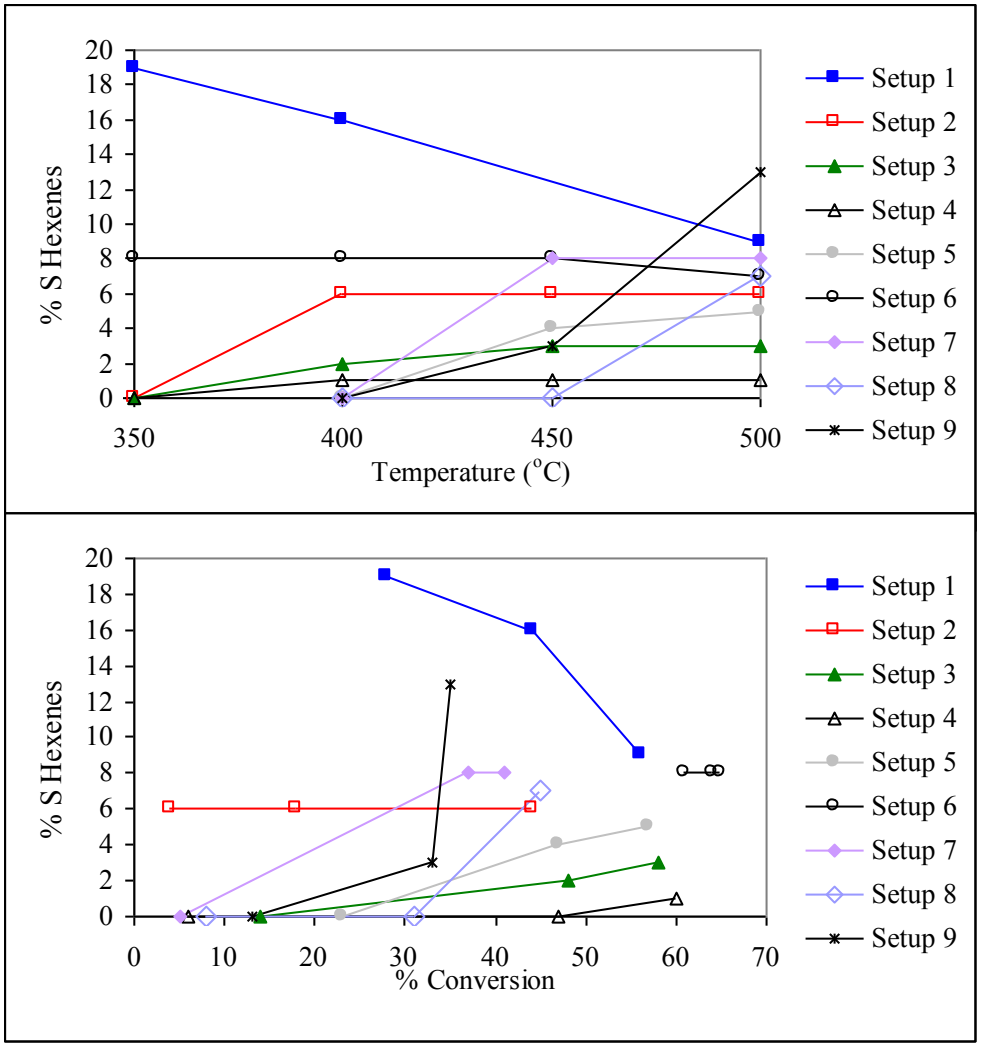

Fig. 4.83 Selectivity (% S) to isomers of hexene for the different setups vs. temperature and conversion

Table 4.21 Conversions and selectivities obtained from void reactor experiments over a 300°C to 500°C temperature range. The values are constant over the temperature range unless otherwise indicated

Setup	X	% S C_{3-4}	% S CO_x	% S Benzene	% S isomers of hexene
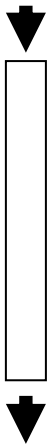 Setup 1	Increase from 20 to 55 % over the temperature range	Highest obtained from all void reactor setups	~ 60	Highest obtained from all void reactor setups	Maximum at 18 %. Highest selectivities obtained from all void reactor setups
 Setup 4	< 60 %	0	~ 99	0	~ 1 %
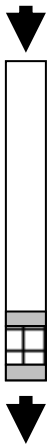 Setup 6	> 60 %	Second highest from all void reactor setups	~ 75	Second highest from all void reactor setups	~ 8 %

Table 4.22 Conversions and selectivities from carborundum-packed reactor experiments over a 300°C to 500°C temperature range. The values are constant over the temperature range unless otherwise indicated

Setup	X	% S C_{3-4}	% S CO_x	% S Benzene	% S isomers of hexene
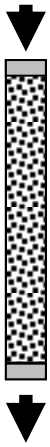 Setup 2	Conversion above 400°C	0	Decreases with Temp. but > 80 %	Increases with Temp.	~ 6 %
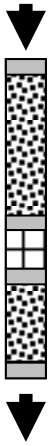 Setup 3	~ 58 %	0	Decreases with Temp. but > 80 %	Increases with Temp.	~ 3 %
 Setup 5	Increases to ~ 58 % at 500°C	0	Decreases with Temp. but > 80 %	Increases with Temp.	~ 5 %

Table 4.22 (continued)

Setup	X	% S C_{3-4}	% S CO_x	% S Benzene	% S isomers of hexene
 Setup 7	~ 38 %	0	Decreases with Temp. but > 80 %	Increases with Temp.	~ 8 %

4.3.2.3 Oxidation of reaction intermediates to benzene

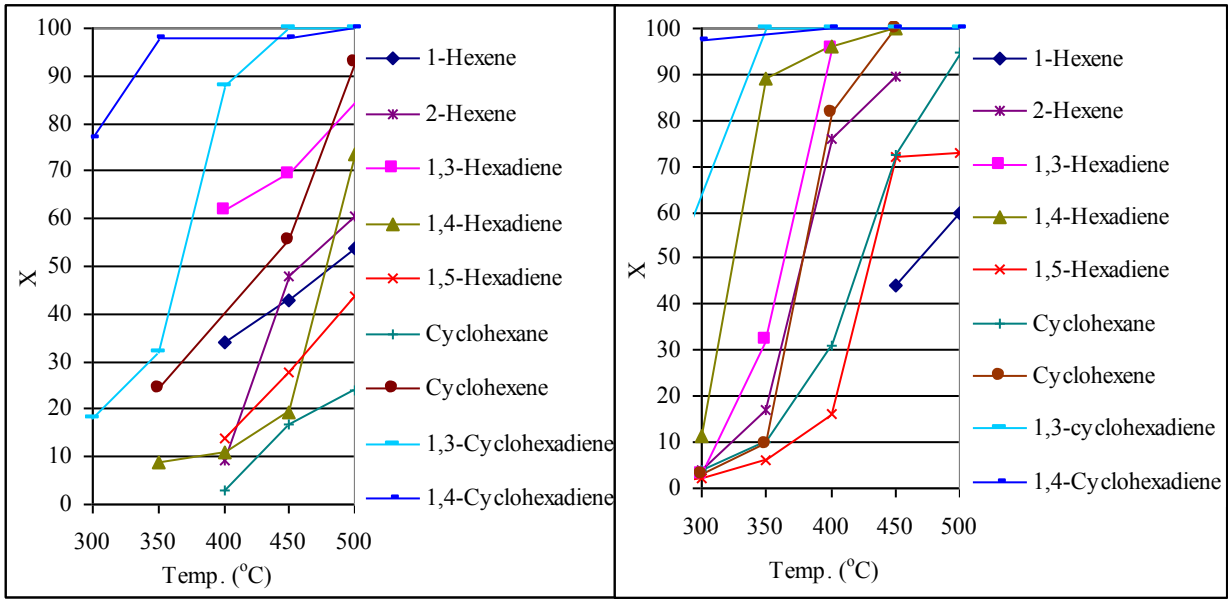

Fig. 4.84 Conversion (X in percentage) of proposed intermediates vs. temperature under non-catalytic (left hand side) and catalytic conditions (right hand side) for the formation of benzene from the oxidation of n-hexane

The non-catalytic and catalytic oxidation of cyclohexane, cyclohexene and several isomers of hexene, hexadiene and cyclohexadienes were investigated to identify the key intermediates to benzene formation from *n*-hexane oxidation. Mixtures of 1-hexene, 2-hexene, 1,3-hexadiene, 1,4-hexadiene, 1,5-hexadiene, cyclohexane, cyclohexene, 1,3-cyclohexadiene and 1,4-cyclohexadiene in air were oxidised in a fully carborundum-packed reactor (non-catalytic conditions) and a conventionally-packed reactor (setup 3) containing a VMgO catalyst.

A catalyst volume of 1 ml and a 50 ml min^{-1} flowrate were maintained for all testing. The conversions under catalytic conditions were generally higher than those under non-catalytic conditions at the same operating temperature (Fig. 4.84).

The same product profile obtained from the non-catalytic and catalytic oxidation of cyclohexane, which included cyclohexene, benzene and carbon oxides, was obtained by Michalakos, P. M. *et al*. (1993) from the oxidation of cyclohexane over a VMgO catalyst. The authors reported a 54 % selectivity to benzene with a 21 % conversion of cyclohexane at an operating temperature of 484^{o}C, a GHSV of ~ 3600 hr^{-1} and a hydrocarbon:O_2 molar ratio of 1:2 over a VMgO catalyst. A selectivity of 11 % benzene was obtained at a conversion of 21 % with a 1:3 molar ratio of hydrocarbon:O_2 in work carried out in this thesis. Panizza, M. *et al.* (2003) obtained the same product profile from the oxidation of cyclohexane over V_2O_5/SiO_2 and V_2O_5-Nb_2O_5/SiO_2 catalysts. No literature was found on the gas-phase oxidation of the alkenes used in this investigation over VMgO catalysts.

Benzene production was accompanied by the production of cyclohexene and isomers of cyclohexadiene from the oxidation of cyclohexane and linear alkenes in the carborundum-packed reactors. The highest selectivities to benzene were obtained from the oxidation of cyclic dienes under catalytic and non-catalytic conditions, which gave only benzene and carbon oxides (Figs. 4.85-4.86).

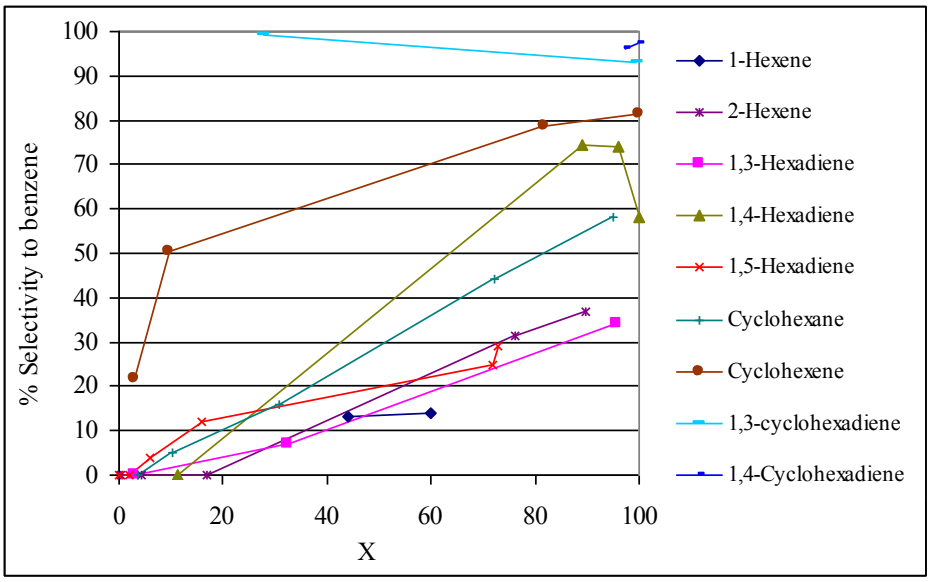

Fig. 4.85 Selectivity to benzene vs. conversion from the catalytic oxidation of the proposed intermediates

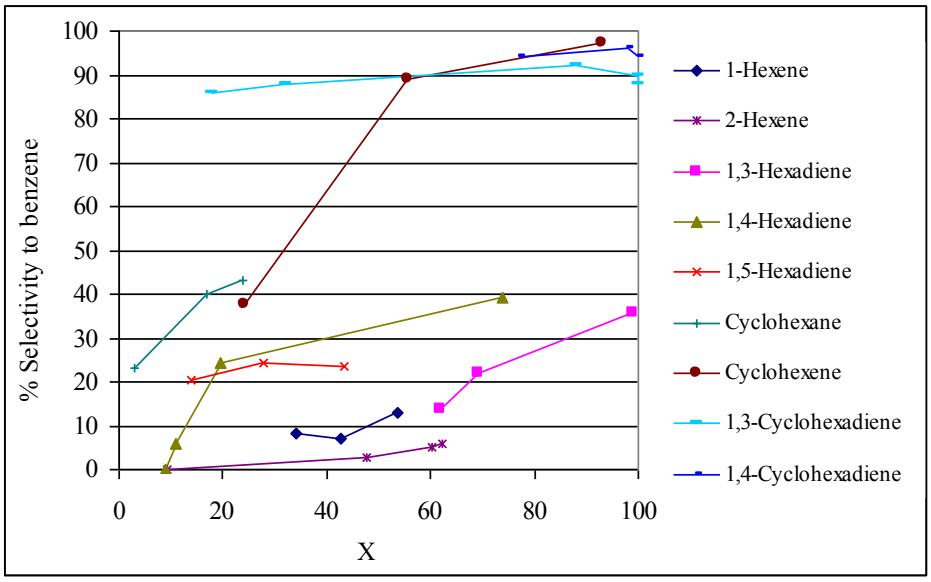

Fig. 4.86 Selectivity to benzene vs. conversion from the non-catalytic oxidation of the proposed intermediates

1-Hexene was not observed in the oxidation of *n*-hexane in the carborundum-packed reactors. It may have formed in small quantities and rapidly cyclised to give benzene.

The increasing selectivity to benzene with decreasing selectivity to carbon oxides suggested that there were competitive mechanisms to the formation of benzene from the oxidation of *n*-hexane.

4.3.2.4 Product stability investigation

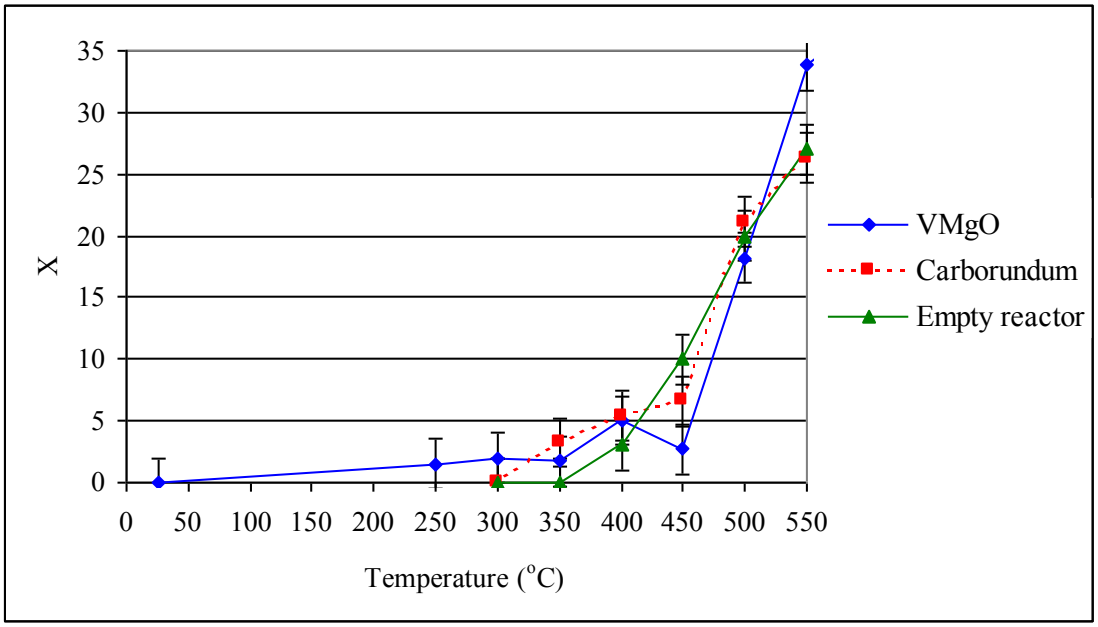

Fig. 4.87 Conversion (X in percentage) of benzene in air over a conventionally-packed VMgO catalyst, and in a carborundum-packed and empty reactor under similar operating

Benzene in air was passed through a conventionally packed reactor containing a VMgO catalyst, a fully carborundum-packed and an empty reactor at elevated temperatures to determine its thermodynamic stability (Fig. 4.87). Benzene decomposed significantly to carbon oxides at temperatures higher than 450°C. Since the conversion vs. temperature curves for the conventionally-packed reactor, fully carborundum-packed and empty reactors were similar, it was established that there was no decomposition of benzene over the catalyst, but decomposition occurred non-catalytically in the intergranular spaces of the carborundum. When benzene was co-fed with nitrogen (i.e. in the absence of air), there was no conversion up to a temperature of 600°C, as expected.

4.3.2.5 Unpromoted VPO and Co-VPO catalysts synthesized via the co-precipitation method for the oxidation of n-hexane

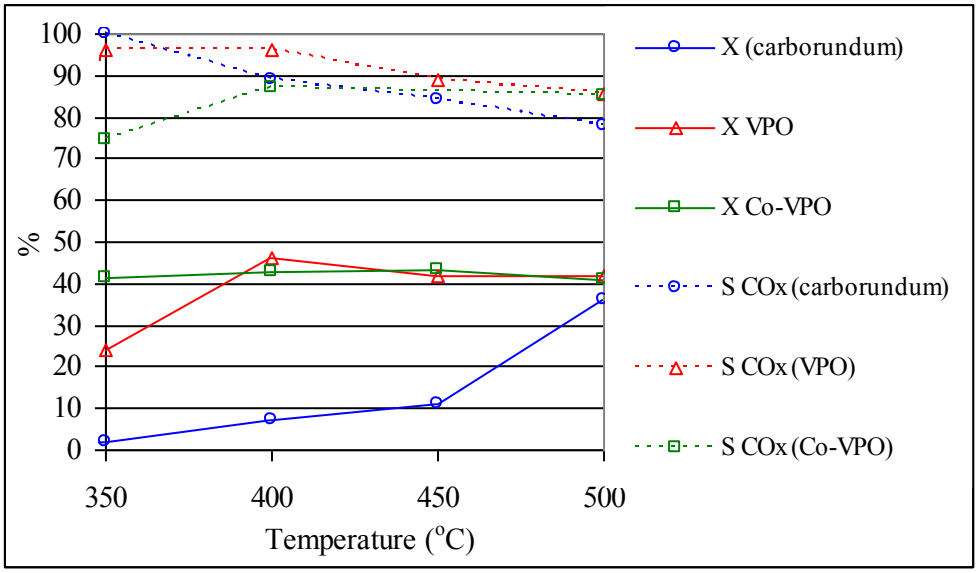

Fig. 4.88 Conversion (X) of n-hexane and selectivity (S) to carbon oxides over carborundum, VPO and 2.50 % Co-VPO catalysts

The conversions of *n*-hexane on VPO and Co-VPO catalysts were similar and the conversions of *n*-hexane in the carborundum-packed reactor were lower when compared at the same flowrate of 50 ml min^{-1} (Fig. 4.88). All conversions and selectivities were ± 1 %. Gas phase reactions that took place above 350°C in the carborundum-packed reactor gave C_{3-4} products, isomers of hexene, benzene and carbon oxides. The selectivity to benzene was lower over the VPO catalyst (less than 10 % selectivity) than in the carborundum-packed reactor (Fig. 4.89). The isomers of hexene that formed over the VPO catalyst could be converted to benzene or oxidised to carbon oxides. Trace amounts of MA (< 1 % selectivity) were produced from *n*-hexane conversion over the VPO catalysts.

The Co-VPO catalyst was more active than the VPO catalyst. The dominant products were carbon oxides. There was more cracking to C_{3-4} products over the VPO catalysts compared to the blank reactor (Fig. 4.89).

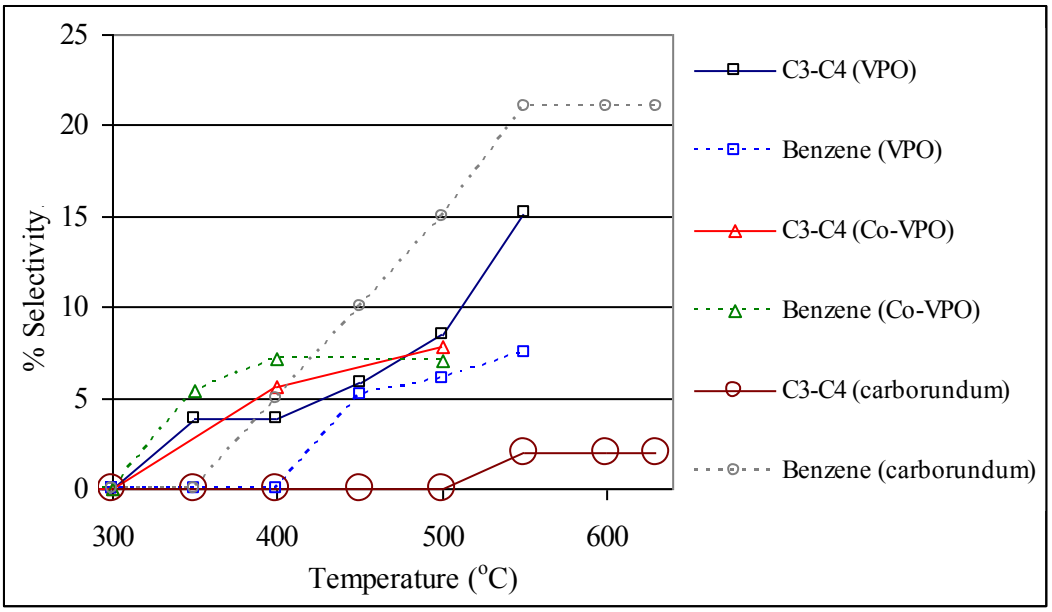

Fig. 4.89 Selectivity (S) to C_{3-4} products and benzene vs. temperature over carborundum, VPO and a 2.50 % Co-VPO catalyst (co-precipitation)

The conversion was less than 2 % at 350°C in a fully carborundum-packed reactor, indicating that there was negligible conversion due to homogeneous reactions (Fig. 4.88). At this temperature, the conversions over the VPO and Co-VPO catalysts were ~ 20 % and ~ 40, respectively (Fig. 4.88). The selectivity to benzene was 5 % over the Co-VPO catalyst (co-precipitation), whilst no benzene was produced over the VPO catalyst and in the fully carborundum-packed reactor (Fig. 4.89). At a similar conversion (40 %), the selectivity to benzene in a carborundum-packed reactor (15 %) was higher than in a catalytic system (7 %) (for VPO and Co-VPO). Selectivities to benzene were generally higher over the Co-VPO catalyst (co-precipitation) than the unpromoted catalyst at similar conversions. C_{3-4} cracked products were obtained over the catalysts (~ 4 % selectivity), but not in the fully carborundum-packed reactor at 400°C (Fig. 4.89). The promoted and unpromoted VPO catalysts catalyzed total oxidation with higher than 70 % selectivity at 400°C.

4.3.2.6 The effect of a void on n-hexane oxidation over a VPO catalyst

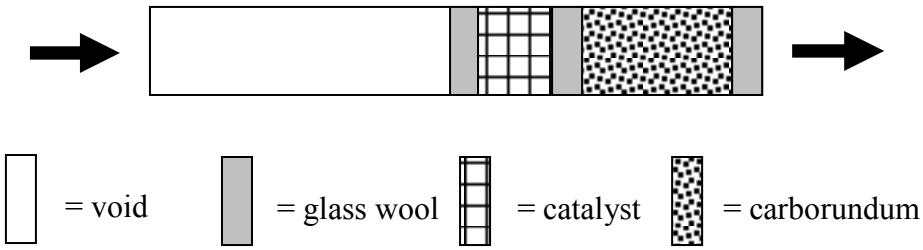

Fig. 4.90 A 2.50 % Co-VPO catalyst preceded by a void

The 2.5 % Co-VPO (co-precipitation) catalyst was tested at a GHSV of 3000 hr^{-1} in combination with a large void preceding the catalyst (Fig. 4.90). The low surface area to volume ratio preceding the catalyst is known to promote cracking of the alkane. It was expected that *n*-hexane would crack to give *n*-butane (amongst other products), which can subsequently be converted to MA over a 2.5 % Co-VPO catalyst (co-precipitation).

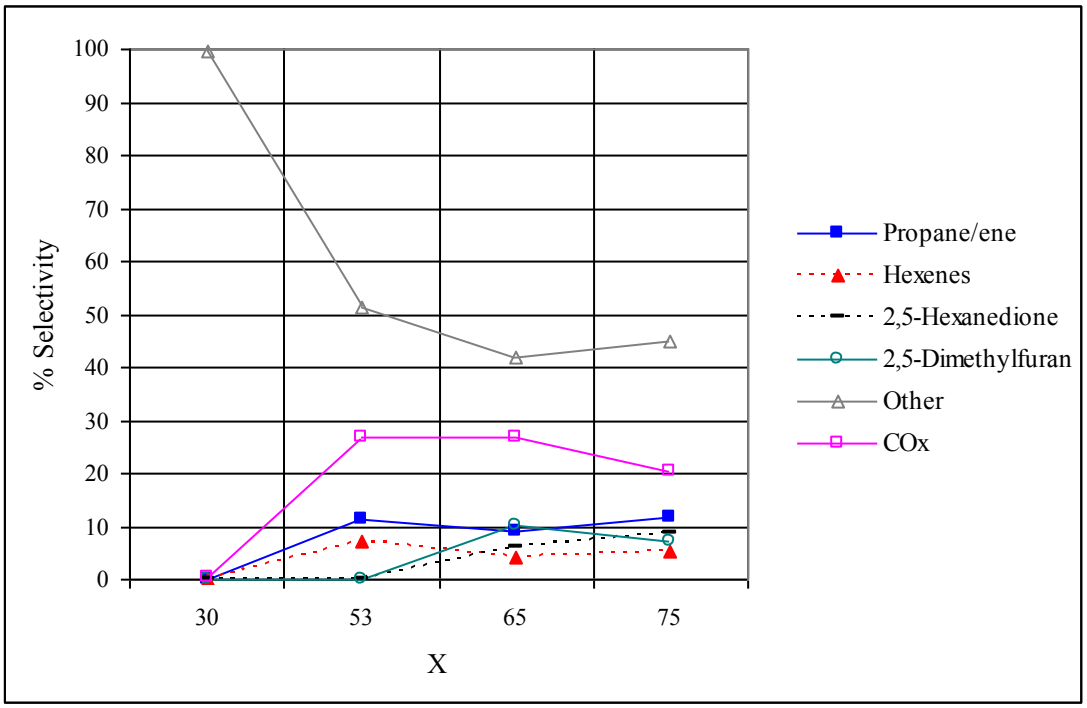

Fig. 4.91 Product selectivity profile vs. conversion for a 2.50 % Co-VPO catalyst (co-precipitation) preceded by a void

The highest selectivities obtained for particular oxygenated products apart from carbon oxides were to 2,5-dimethylfuran and 2,5-hexanedione. The selectivities to 2,5-dimethylfuran and 2,5-hexanedione were ~ 9 % at a conversion of 75 % (Fig. 4.91). Some of the non-oxygenated products obtained are illustrated in Fig. 4.92 (identified by gas chromatography-mass spectrometry (GC-MS)).

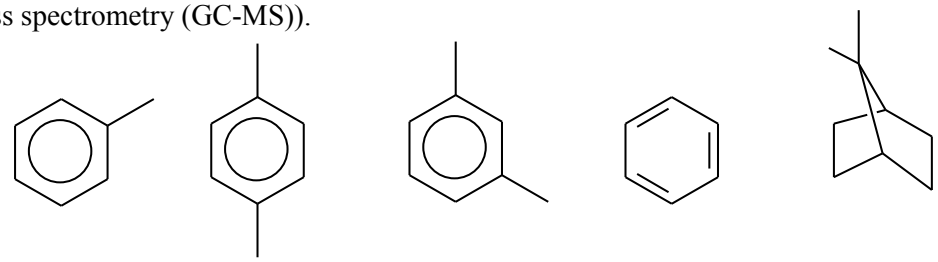

Fig. 4.92 Non-oxygenated products obtained from n-hexane conversion over a 2.50 % Co-VPO catalyst (co-precipitation) in a partially packed reactor

Some of the oxygenated products obtained are illustrated in Fig. 4.93 (identified by gas chromatography-mass spectrometry (GC-MS)).

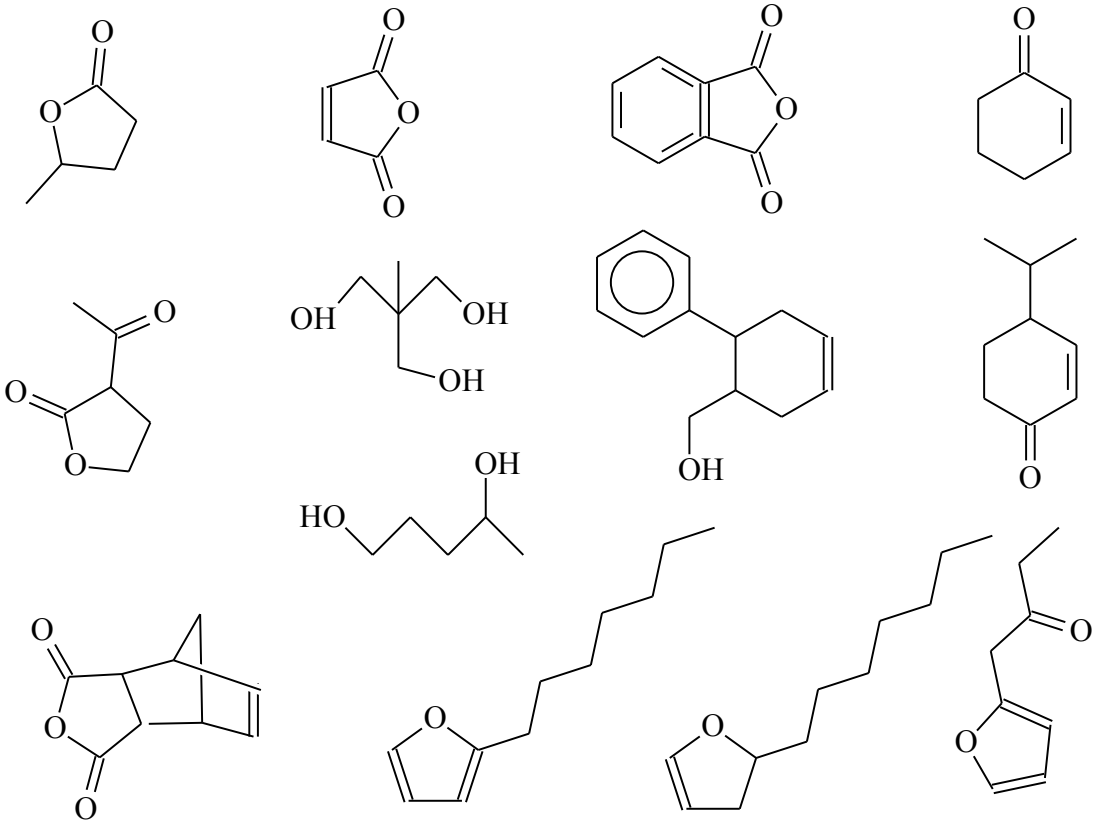

Fig. 4.93 Oxygenated products obtained from the conversion of n-hexane over a 2.50 % Co-VPO catalyst (co-precipitation) in a partially packed reactor

The degree of branching and oxygen insertion suggested complex chemistry. The product profile from *n*-hexane oxidation over a Co-VPO catalyst preceded by a void in the reactor was different to that obtained from a VMgO catalyst preceded by a void (setup 6). The bulk of the product selectivity profile from the Co-VPO catalyst preceded by a void consisted of aromatics and oxygenated aromatics, whilst the VMgO catalyst preceded by a void gave benzene as the only aromatic product with a selectivity of ~ 3 % within a 300-500^{o}C operating temperature range.

4.3.3 Oxidation of n-octane over VMgO, Co-VMgO, VPO and Co-VPO

4.3.3.1 Unpromoted VMgO and Co-VMgO catalysts synthesized via the co-precipitation method

The conversions of *n*-octane over the VMgO catalyst were between 20 and 30 % at different GHSVs (viz. 1990, 3307 and 4641 hr^{-1}) between 400 and 500^{o}C (Fig. 4.94). Cobalt improved the activity of the catalyst, giving higher conversions at similar GHSVs.

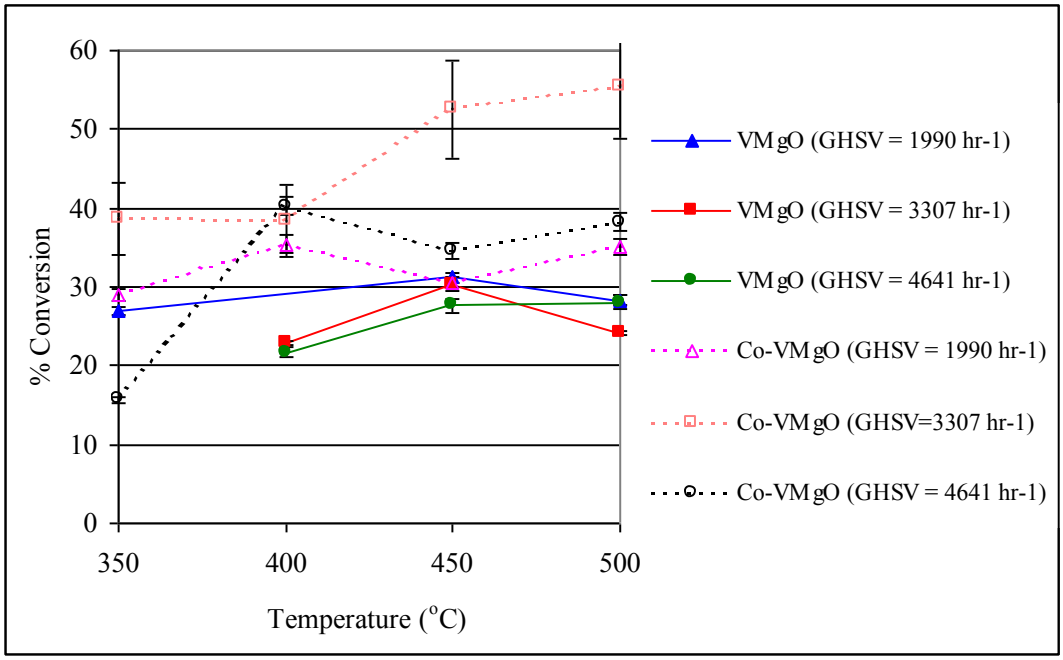

Fig. 4.94 Conversion of n-octane over VMgO and Co-VMgO (co-precipitation) catalysts at varying GHSVs

Figs. 4.95, 4.97-4.100 show the product selectivity profiles obtained from the VMgO and Co-VMgO catalysts at GHSVs of 1990, 3307 and 4641 hr^{-1} with their respective operating temperatures and conversions (indicated in brackets). The selectivity to carbon dioxide was generally higher than carbon monoxide for both promoted and unpromoted catalysts at all GHSVs.

The conversions were erratic with increasing temperature (Fig. 4.94), in that there was not a steady increase in conversion with increasing temperature.

The light yellow catalyst granules turned black during the reaction, which suggested coking of the catalysts which was confirmed by EDX analyses.

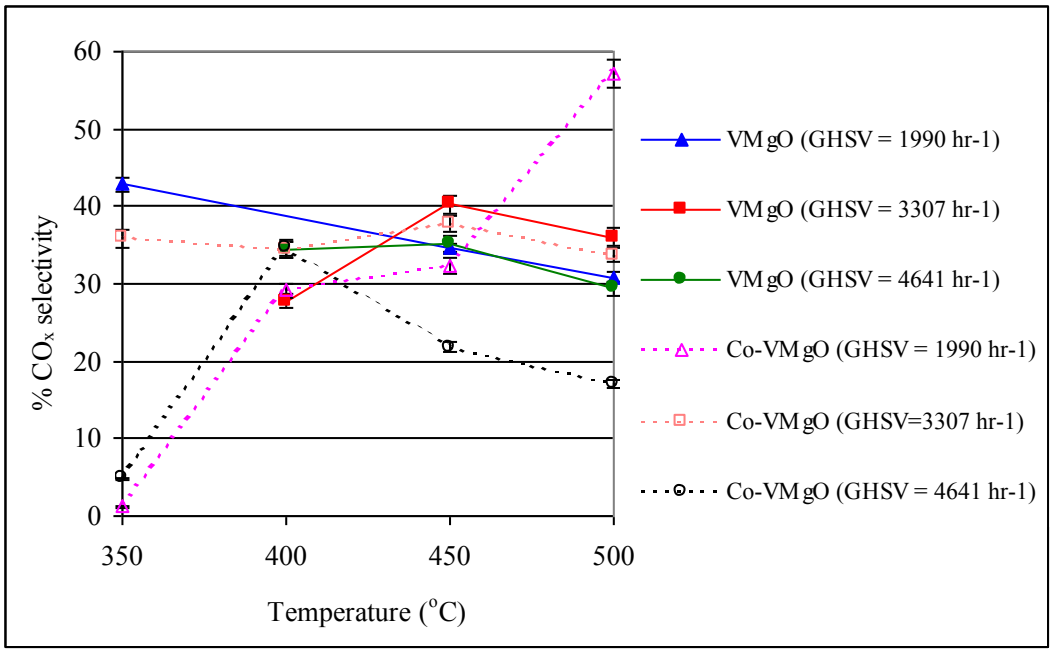

Fig. 4.95 Selectivity to CO_x over VMgO and Co-VMgO catalysts (co-precipitation) at varying GHSVs

The carbon oxide selectivity over VMgO and Co-VMgO catalysts generally increased with increasing temperature and stabilized between 30 and 40 % at operating temperatures higher than 400°C (Fig. 4.95).

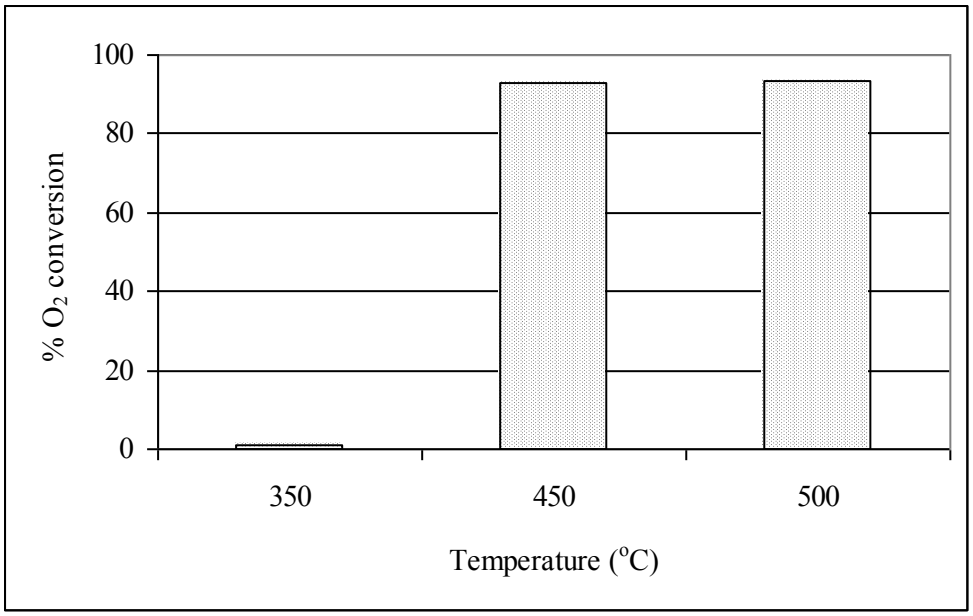

Fig. 4.96 Oxygen conversion for n-octane oxidized over a Co-VMgO catalyst (co-precipitation) at a GHSV of 4641 hr^{-1}

An elemental oxygen balance for the oxidation of *n*-octane to oxygenates confirmed that the conversion of oxygen approached 100 % at temperatures higher than 400°C (Fig. 4.96). This oxygen starvation in the reactor was responsible for the plateau in selectivities and conversions.

The reactions giving carbon oxides were oxygen demanding and were considered to see if oxygen was a limiting reactant. The molar O_2:hydrocarbon ratios were above stoichiometric (Tables 4.23-4.24) for C_4 oxidation and there was a deficiency of O_2 for C_6 and C_8 alkane oxidation to carbon oxides.

Table 4.23 Mole percentages of alkane feeds in air with their respective molar ratios of O_2:hydrocarbon (HC)

	n-Butane	*n*-Hexane	*n*-Octane
% Feed/air	1.0	7.8	7.3
% Air	99.0	92.2	92.7
% O_2	20.8	19.4	19.5
% N_2	78.2	72.8	73.2
Molar O_2:HC	19.8	2.4	2.5

Table 4.24 Most demanding reactions for oxygen in C_4, C_6 and C_8 oxidation with their respective O_2:hydrocarbon (HC) molar ratios required and supplied

Oxygen demanding equations	Molar ratio O_2:HC required	Molar ratio O_2:HC supplied
n -Butane conversion		
$CH_3(CH_2)_2CH_3 + {}^9/_2 O_2 \longrightarrow 4\,CO + 5\,H_2O$	4.5	19.8
$CH_3(CH_2)_2CH_3 + {}^{13}/_2 O_2 \longrightarrow 4\,CO_2 + 5\,H_2O$	6.5	19.8
$CH_3(CH_2)_2CH_3 + {}^1/_2 O_2 \longrightarrow C_4H_8 + H_2O$	0.5	19.8
n -Hexane conversion		
$CH_3(CH_2)_4CH_3 + 2\,O_2 \longrightarrow C_6H_6 + 4\,H_2O$	2	2.4
$CH_3(CH_2)_4CH_3 + {}^{13}/_2 O_2 \longrightarrow 6\,CO + 7\,H_2O$	6.5	2.4
$CH_3(CH_2)_4CH_3 + {}^{19}/_2 O_2 \longrightarrow 6\,CO_2 + 7\,H_2O$	9.5	2.4
n -Octane conversion		
$CH_3(CH_2)_6CH_3 + {}^{17}/_2 O_2 \longrightarrow 8\,CO + 9\,H_2O$	8.5	2.5
$CH_3(CH_2)_6CH_3 + {}^{25}/_2 O_2 \longrightarrow 8\,CO_2 + 9\,H_2O$	12.5	2.5

The selectivities to $C_{3\text{-}4}$ cracked products over VMgO and Co-VMgO catalysts at different gas hourly space velocities (GHSV) generally stabilised at ~ 3 % between 450 and 500°C (Fig. 4.97).

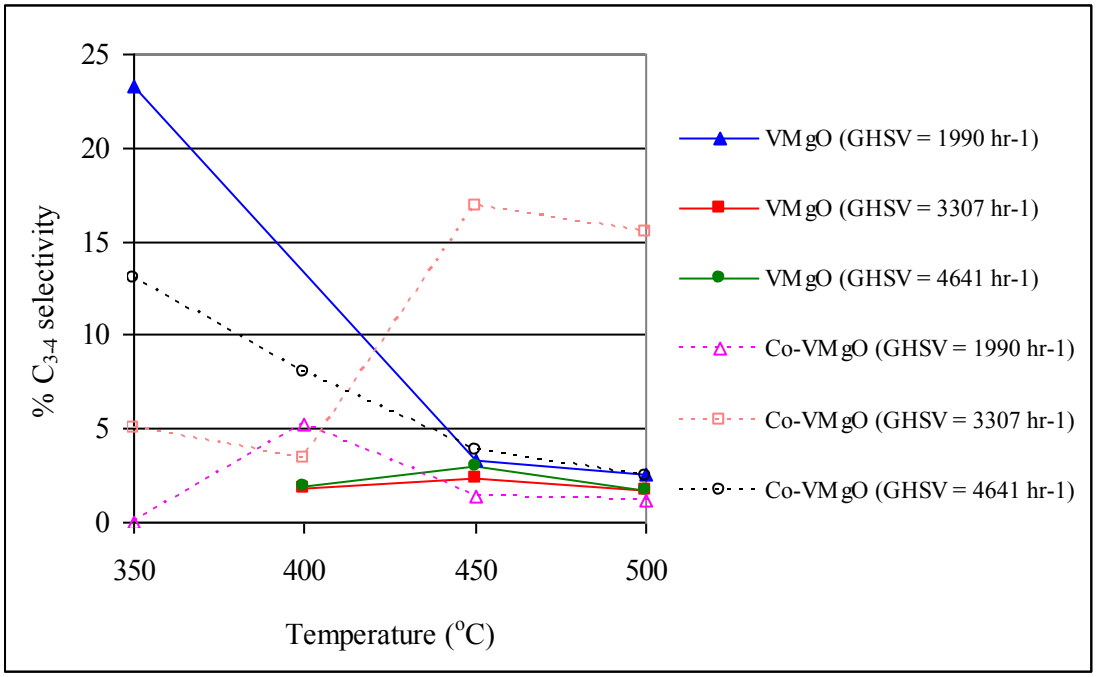

Fig. 4.97 Selectivity to $C_{3\text{-}4}$ cracked products over VMgO and Co-VMgO catalysts (co-precipitation) at varying GHSVs

The selectivities to aromatic compounds, which included benzene, toluene, ethylbenzene and isomers of xylene, generally stabilised between 15 and 20 % (Fig. 4.98).

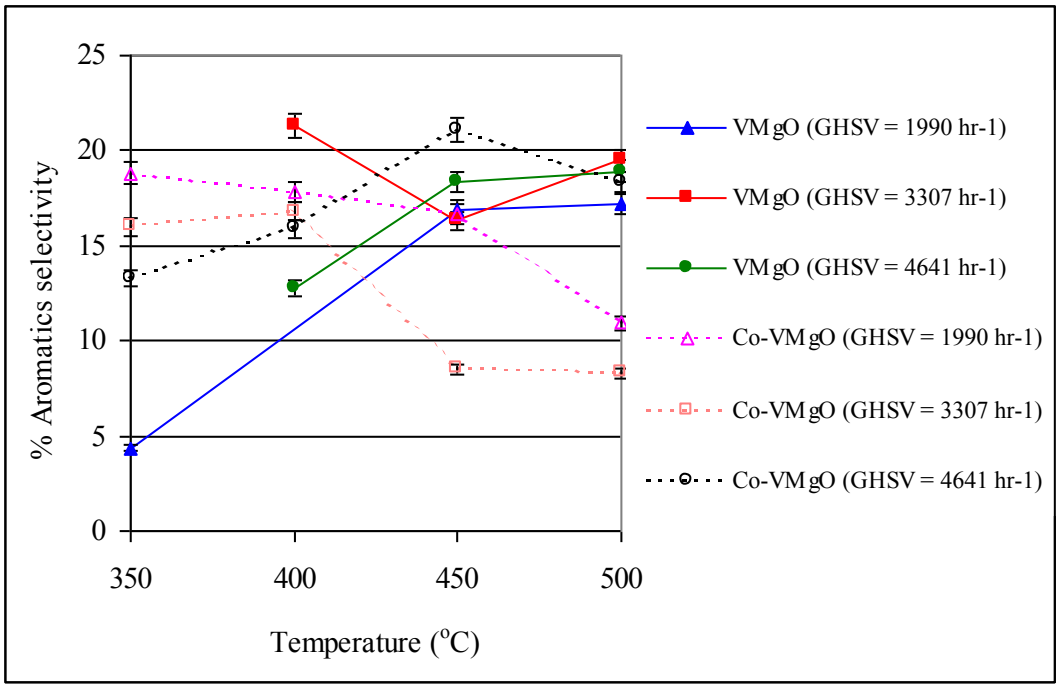

Fig. 4.98 Selectivity to aromatic products over VMgO and Co-VMgO catalysts (co-precipitation) at varying GHSVs

The selectivity to styrene was generally higher over the Co-VMgO catalyst (Fig. 4.99). Since no styrene and ethylbenzene were observed in any blank reactor run, these were catalytic products. The selectivities to styrene increased for both the unpromoted and promoted VMgO catalysts with increasing temperature at a GHSV of 4641 hr^{-1}. This was unusual for a typical selectivity vs. temperature curve, but the alkene precursors to styrene were produced homogeneously and catalytically, which contributed to this trend.

The average selectivities to alkenes, which included 1,3-octadiene, 3,5-octadiene and 1-ethylcyclohexene, were generally between 8 and 12 % over a temperature range of 350-500°C (Fig. 4.100).

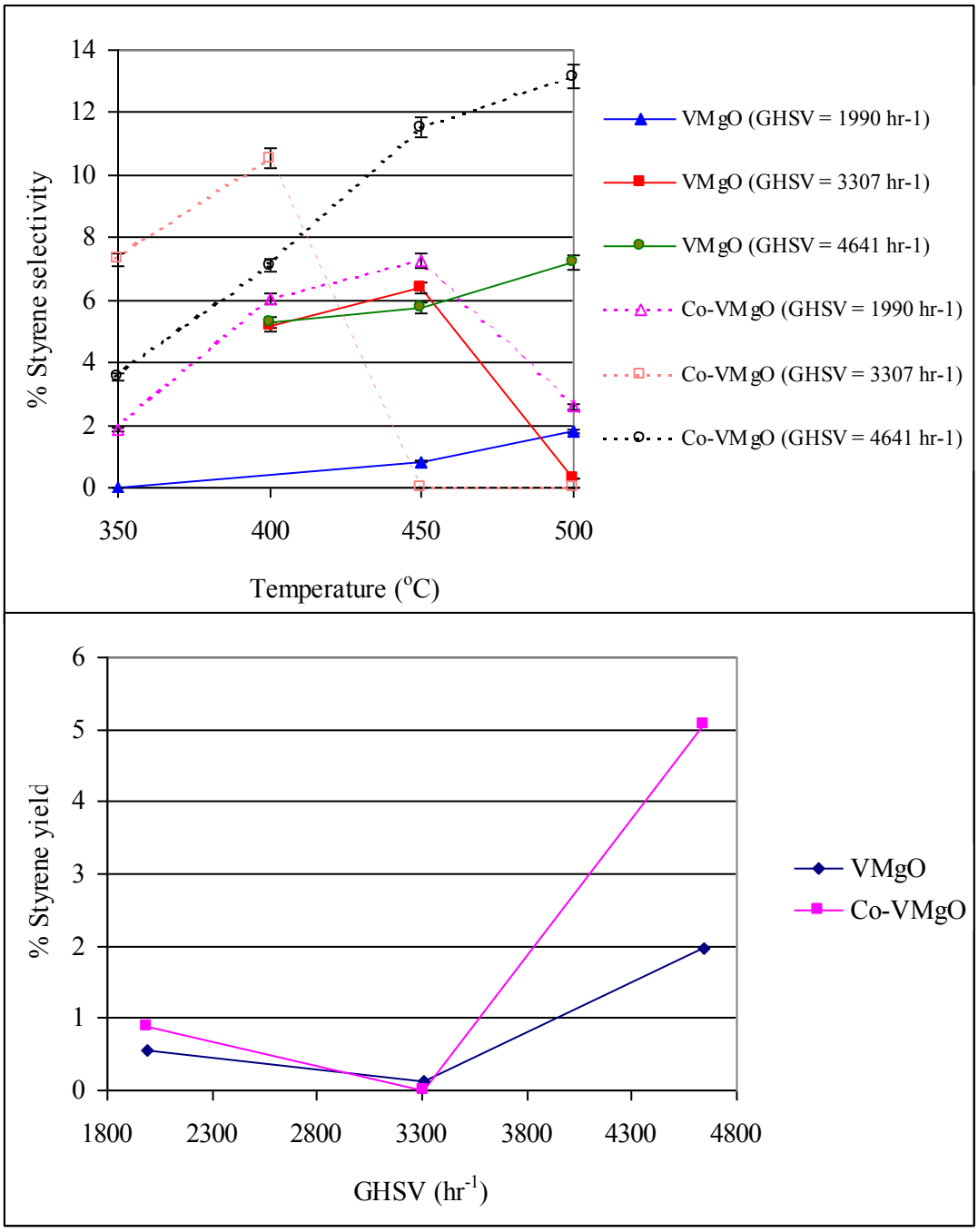

Fig. 4.99 (Top) Selectivity to styrene over VMgO and Co-VMgO catalysts (co-precipitation) at varying GHSVs, (Bottom) Yield to styrene at 500°C and varying GHSV

The other products included acetaldehyde, acetone, isomers of hexane and hexene, isomers of heptane and heptene and isomers of xylene.

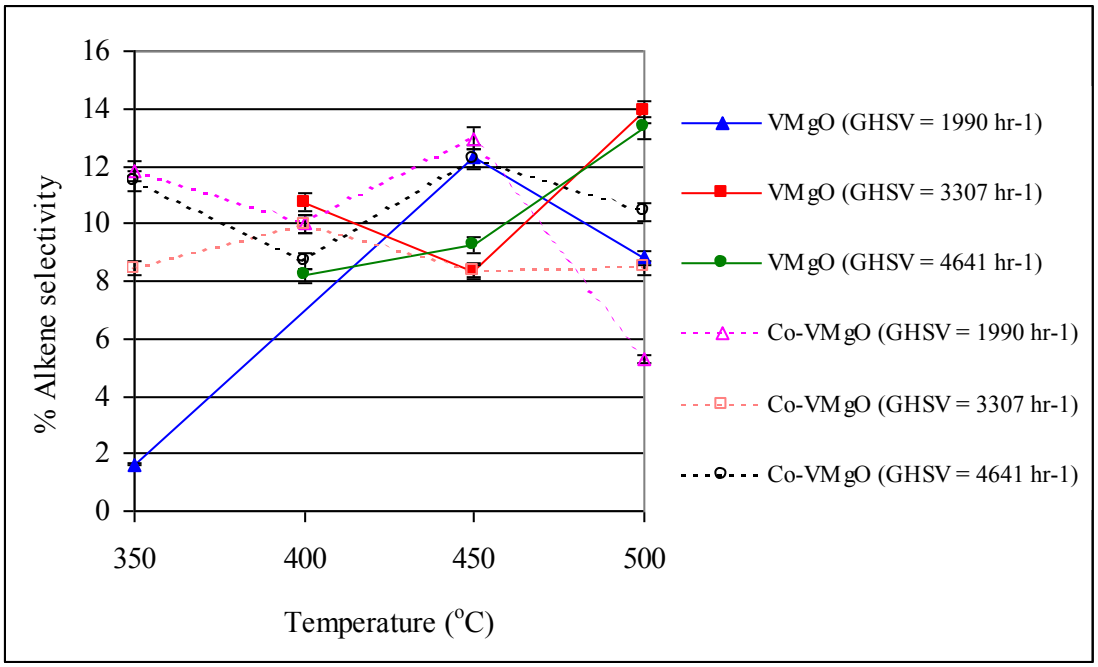

Fig. 4.100 Selectivity to alkenes over VMgO and Co-VMgO (co-precipitation) catalysts at varying GHSVs

The selectivities to individual products appear in Figs. 4.101-4.106.

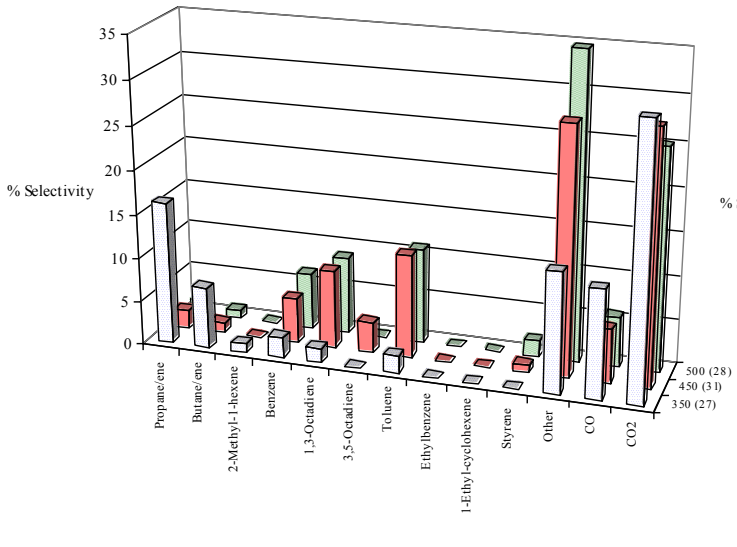

Fig. 4.101 Product selectivity profile over a VMgO catalyst at GHSV = 1990 hr^{-1} (conversion X within brackets)

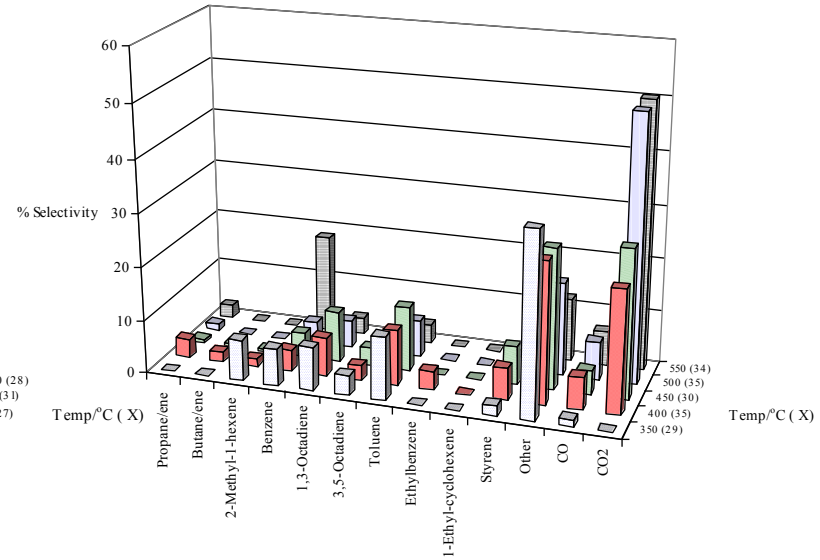

Fig. 4.102 Product selectivity profile over a Co-VMgO catalyst at GHSV = 1990 hr^{-1} (conversion X within brackets)

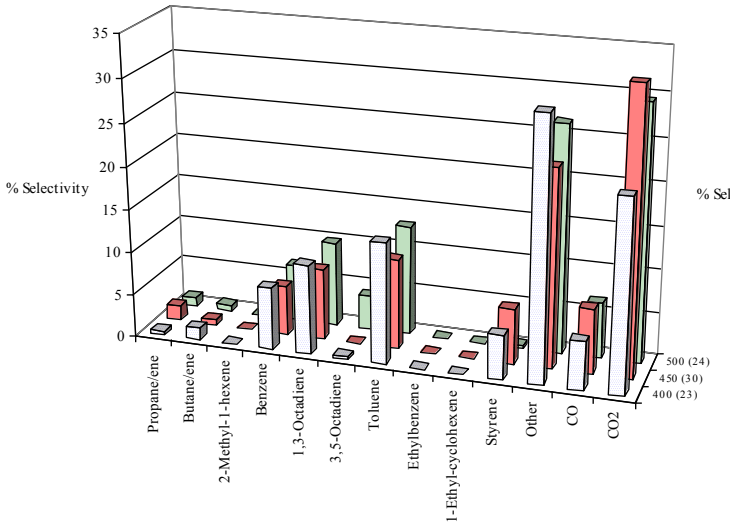

Fig. 4.103 Product selectivity profile over a VMgO catalyst at GHSV = 3307 hr^{-1} (conversion X within brackets)

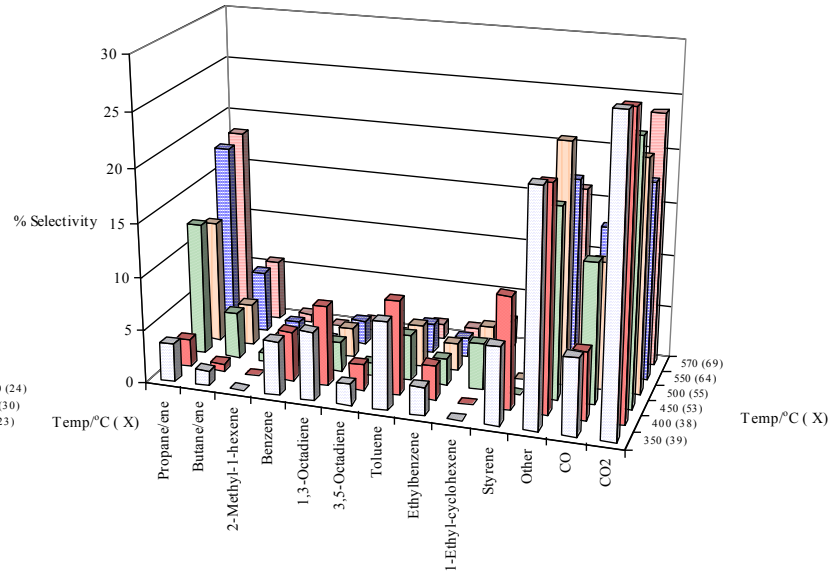

Fig. 4.104 Product selectivity profile over a Co-VMgO catalyst at GHSV = 3307 hr^{-1} (conversion X within brackets)

The highest yield to styrene (5 %) was obtained over the Co-VMgO catalyst at a GHSV of 4641 hr^{-1}, a conversion of 38 % and an operating temperature of 500°C (Fig. 4.99). The unpromoted VMgO catalyst gave a 2 % yield of styrene at the same GHSV and operating temperature (Fig. 4.99).

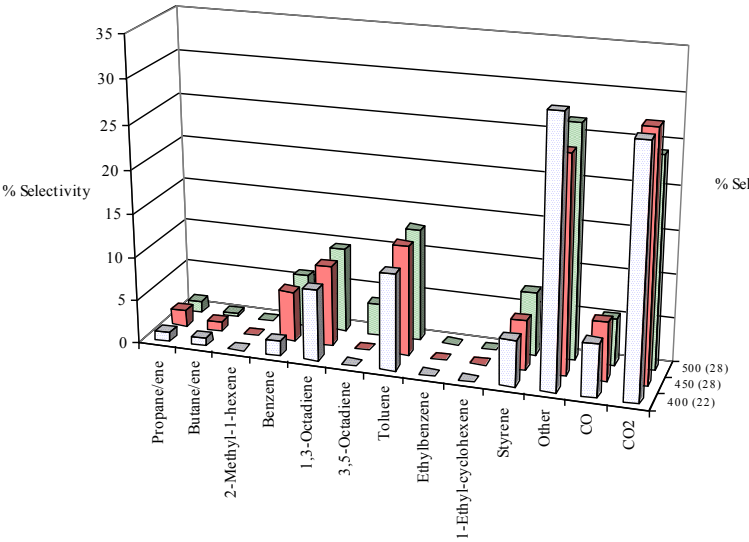

Fig. 4.105 Product selectivity profile over a VMgO catalyst at GHSV = 4641 hr^{-1} (X within brackets)

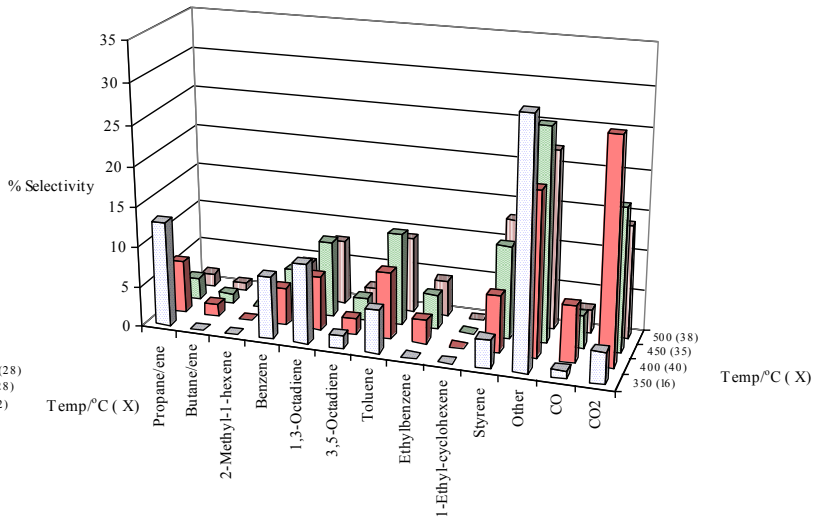

Fig. 4.106 Product selectivity profile over a Co-VMgO catalyst at GHSV = 4641 hr^{-1} (X within brackets)

4.3.3.2 Co-VPO catalyst synthesized via the co-precipitation method

At 350°C, where there were no homogeneous reactions, the highest selectivity (7 %) to styrene from *n*-octane oxidation was obtained over a 2.5 % Co-VMgO catalyst (co-precipitation) operated at a GHSV of 3307 hr^{-1}. A selectivity of 2 % was obtained at a GHSV of 1990 hr^{-1} and 4 % selectivity was obtained at a GSHV of 4641 hr^{-1} at the same operating temperature. A similar promoter loading of 2.5 % was incorporated into a VPO catalyst for the oxidation of *n*-octane at a GHSV of 3307 hr^{-1}. The non-oxygenated products were found in the organic layer in the catchpot, whilst the oxygenated products were trapped in the aqueous layer in the catchpot, which was found to have a pH of 1.

The cobalt promoter in the VMgO catalyst enhanced the selectivity to styrene from the oxidation of *n*-octane at 400°C and a GHSV of 3307 hr^{-1}. The cobalt promoted VPO catalyst, however, did not give any valuable product in high selectivity from the oxidation of *n*-octane under similar operating conditions (Fig. 4.107).

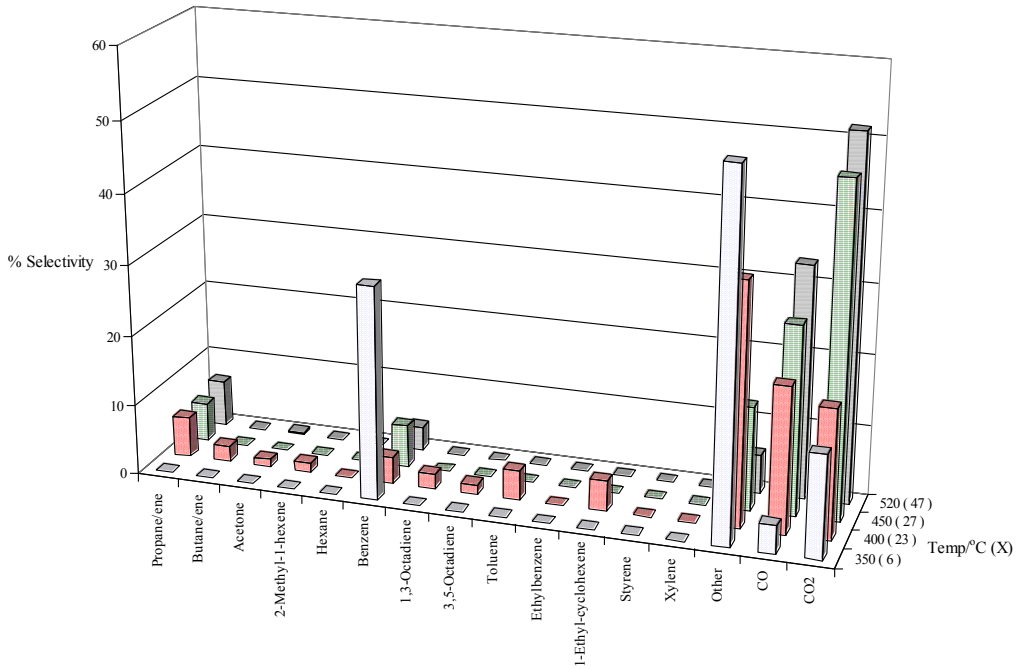

Fig. 4.107 Product selectivity profile over a Co-VPO catalyst (co-precipitation) at GHSV of 3307 hr^{-1} (X within brackets)

There was 30-80 % selectivity to carbon oxides between 400 and 500^{o}C. The largest portion of the product distribution, apart from carbon oxides, came from the aqueous layer in the catchpot and included cyclic oxygenates. Trace quantities of MA (selectivities of less than 1 %) at temperatures higher than 400^{o}C were obtained. It is likely that cracking of *n*-octane gave *n*-butane, which was oxidised over the VPO catalyst to maleic anhydride.

In contrast, the aqueous layer collected from the catchpot from the oxidation of *n*-octane over the VMgO and Co-VMgO catalysts (co-precipitation) did not contain any oxygenated products.

Carbon oxides dominated the product selectivity profile of Co-VPO. The other products trapped in the organic layer in the catchpot included acetaldehyde and isomers of heptane. Some of the other products trapped in the aqueous layer of the catchpot included acetaldehyde, furfural, maleic anhydride, 2-cyclopentene-1,4-dione, 2-H-pyran-2-one, 4-H-pyran-4-one, dihydro-3-methyl-2,5-furandione, benzaldehyde, benzoic acid, 3-methyl-2-cyclo-hexene-1-one, phthalic anhydride and benzofuran which were identified by GC-MS.

4.4 Summary of blank and catalytic reactions

A summary of the highest yields obtained (excluding carbon oxides) in the presence and exclusion of a catalyst over a temperature range of 250-500^{o}C appears in Table 4.25. A summary of selectivities to carbon oxides obtained from reactions in the presence and exclusion of catalyst appears in Table 4.26.

Table 4.25 Summary of products with highest yields apart from carbon oxides

Operating conditions

Conventionally-packed reactor

GHSV 3000 hr^{-1} (or 50 ml min^{-1} for blank reactor investigations)

Temperature range 200-500^{o}C

n-Butane oxidation	Main product	% Conversion	% Selectivity	% Yield	Temp. (^{o}C)
Carborundum-packed reactor	Isomers of butene	3	88	3	350
Unpromoted VPO	Maleic anhydride	17	75	13	350
1.25 % Co-VPO (co-precipitation)	Maleic anhydride	54	68	37	400
2.50 % Co-VPO (co-precipitation)	Maleic anhydride	61	73	45	275
5.00 % Co-VPO (co-precipitation)	Maleic anhydride	26	93	24	400
2.50 % Co-VPO (precipitation/deposition)	Maleic anhydride	9	11	1	300
2.50 % Rh-VPO (co-precipitation)	Maleic anhydride	42	85	36	350
VPO-A	Maleic anhydride	66	13	9	350
2.50 % Au-VPO (precipitation/deposition)	Isomers of butene	93	10	9	425
Unpromoted VMgO	Isomers of butene	12	40	5	500
2.50 % Co-VMgO (co-precipitation)	Propane/ene	35	25	9	500
	Isomers of butene	7	36	3	350
n-Hexane oxidation					
Carborundum-packed reactor	Benzene	36	10	4	500
Empty reactor	Propane/ene	56	22	12	500
Unpromoted VMgO	Benzene	54	30	16	500
2.50 % Co-VMgO (co-precipitation)	Benzene	62	24	15	500
Unpromoted VPO	Benzene	41	6	2	500
2.50 % Co-VPO (co-precipitation)	Benzene	41	7	3	500
n-Octane oxidation					
Carborundum-packed reactor	Benzene	1	100	1	350
Empty reactor	Propane/ene	49	34	17	400
Unpromoted VMgO	Toluene	30	11	3	450
	Styrene	30	7	2	450
2.50 % Co-VMgO (co-precipitation)	Styrene	38	11	4	400
2.50 % Co-VPO (co-precipitation)	Benzene	27	5	1	450

Table 4.26 Selectivities to carbon oxides from catalytic and non-catalytic investigations

Feed	Catalyst or reactor setup	Flowrate (ml min^{-1})	GHSV (hr^{-1})	Temperature range (^oC)	Selectivity to CO_x
Non-catalytic reactions					
n-Butane	Carborundum in glass	50		500-520	~ 80
n-Hexane	Carborundum in steel	50		400-500	> 80
n-Hexane	Carborundum in glass	50		500-520	> 40
n-Hexane	Empty steel	50		400-500	~ 60
n-Octane	Carborundum in steel	60		450-500	~ 95
n-Octane	Empty steel	60		400-500	~ 50
Catalytic reactions					
n-Butane	VPO		3000	400-500	48-100
n-Butane	2.5 % Co-VPO (co-precipitation)		3000	300-350	66-98
n-Butane	2.5 % Co-VPO (precipitation/deposition)		3000	350-400	100
n-Butane	2.5 % Rh-VPO (co-precipitation)		3000	450	89
n-Butane	VPO-A		3000	250-350	> 58
n-Butane	2.5 % Au-VPO (precipitation/deposition)		3000	300-400	100
n-Butane	VMgO		3000	535	37
n-Butane	2.5 % Co-VMgO (co-precipitation)		3000	530	61
n-Hexane	VPO		3000	350-550	> 70
n-Hexane	Co-VPO (co-precipitation)		3000	350-550	> 70
n-Hexane	VMgO (in steel)		3000	350-520	> 40
n-Hexane	Co-VMgO (co-precipitation) (in steel)		3000	350-520	> 60
n-Hexane	VMgO (in glass)		3000	400-520	> 40
n-Hexane	Co-VMgO (co-precipitation) (in glass)		3000	400-520	> 50
n-Octane	VMgO		3307	400-500	22-32
n-Octane	Co-VMgO (co-precipitation)		3307	350-570	30-40
n-Octane	Co-VPO (co-precipitation)		3307	400-520	39-84

References

Albonetti, S., Cavani, F., Trifirò, F., Venturoli, P., Calestani, G., Granados, M.L., Fierro, J.L.G., J. Catal., **160**, 54 (1996)

Bondzie, V.A., Parker, S.C., Campbell, C.T., Catal. Lett., **63**, 143 (1999)

Bordes, E., Courtine, P., J. Catal., **57**, 236 (1979)

Bordes, E., Catal. Today, **1**, 499-526 (1987)

Brutovsky, M., Gerej, S., Vasilco, F., Gerejova, J., Collection Czechoslovak Chem. Commun., **47**, 1290-1300 (1982)

Burrows, A., Kiely, C.J., Perregaard, J., Højlund-Nielsen, P.E., Vorbech, G., Calvino, J.J., López-Cartes, C., Catal. Lett., **57**, 121 (1999)

Busca, G., Cavani, F., Centi, G., Trifirò, F., J. Catal., **99**, 400-414 (1986)

Chaar, M.A., Patel, D., Kung, M.C., Kung, H.H., J. Catal., **105**, 489 (1987)

Chang, W.S., Chen, Y.Z., Yang, B.L., Appl. Catal. A: General, **124**, 221 (1995)

Choudary, T.V., Goodman, D.W., Top. Catal., **21**, 25 (2002)

Coulston, G.W., Simon, R.B., Kung, H., Birkeland, K., Bethke, G.K., Harlow, R., Herron, N., Lee, P.L., Science, **275**, 191 (1997)

Govender, N., Masters Thesis, University of Natal, Durban, South Africa, p 81 (2002)

Govender, N., Friedrich, H.B., Janse van Vuuren, M., Catal. Today, **97**, 315 (2004)

Haruta, M., J. Catal., **36**, 153 (1997)Horowitz, H.S., Blackstone, C.M., Sleight, A.W., Teufer, G., Appl. Catal., **38**, 193 (1988)

Hutchings, G.J., Appl. Catal., **72,** 1-32 (1991)

Hutchings, G.J., Scurrel, M.S., Cattech, **7**, 94 (2003) Kung, M.C., Kung, H.H., J. Catal., **134**, 668 (1992)

Kung, H.H., Michalakos, P., Owens, L., Kung, M., Anderson, P., Owen, O., Jahan, I., J. Amer. Chem. Soc., 389 (1993)

Kung, H.H., Kung, H.C., Appl. Catal., **157**, 106 (1997)

Lemonidou, A.A., Stambouli, A.E., Appl. Catal. A: General, **171**, 325 (1998)

Lopez-Nieto, J.M., Sole, J., Concepcion, P., Herguido, J., Menendez, M., Santamaria, J., J. Catal., **185**, 324 (1999)

Michalakos, P.M., Kung, M.C., Jahan, I., Kung, H.H., J. Catal., **140**, 226 (1993)

Mondain-Monval, P., Quanquin, B., Ann. Chim., **15**, 309 (1931)

Nakamura, M., Kawai, K., Fujiwara, Y., J. Catal., **34**, 345 (1974)

Olah, G.A., Halpern, Y., Stein, J., Mo, Y.K., J. Amer. Chem. Soc., **95**, 4960 (1973)

Olah, G.A., Molnar, A., Hydrocarbon Chemistry, Wiley, New York (1995)

Panizza, M., Resini, C., Busca, G., Lopez., E. F., Escribano, V.S., Catal. Letters, **89**, 199 (2003)

Pantazidis, A., Burrows, A., Kiely, C.J., Mirodatos, C., J. Catal., **177**, 325 (1998)

Perry, R.H., Green, D.W., Perry's Chemical Engineers' Handbook, The McGraw Hill Companies, Section 26, p 54 (1999)

Plate, A.F., Tarasova, G.A., J. Gen. Chem. U.S.S.R., **20**, 1193 (1950)

Ramis, G., Cristiani, C., Forzatti, P., Busca, G., J. Catal., **124**, 574 (1990)

Said, A.A., Abd El-Wahab, M.M.M., Thermochimica Acta, **249**, 318 (1995)

Sajip, S., Bartley, J.K., Burrows, A., Rhodes, C., Volta, J.C., Kiely, C.J., Hutchings, G.J., Phys. Chem. Chem. Phys., **3**, 2143 (2001)

Salama, T., Ohnishi, R., Shido, T., Ichikawa, M., J. Catal., **162**, 169 (1996)

Sheldon, R.A., Kochi, J.K., Metal-Catalysed Oxidations of Organic Compounds, Academic Press, New York (1981)

Shtern, V.A., The Gas Phase Oxidation of Hydrocarbons, Pergamon Press, London, p 79 (1964)

Sookraj, S.H., Engelbrecht, D., Confidential Report Number 290/97, Sastech R&D Applied Catalysis Research, p 24 (1997)

Sookraj, S.H., Engelbrecht, D., Catal. Today, **49**, 161 (1999)

Wolf, A., Schüth, F., Appl. Catal. A: General, **226**, 1 (2002)

Zazhigalov, V.A., Konovalova, N.D., Zaytzev, Yu. P., Belousov, V.M., Stoch, J., Krupa, R., Haber, J., Ukr. Khim. Zhurn., **53**, 1145 (1987)

Zazhigalov, V.A., Haber, J., Stoch, J., Pyatnitzkaya, A.I., Komashko, G.A., Belousov, V.M., Appl. Catal. A: General, **96**, 135 (1993)

Zazhigalov, V.A., Haber, J., Stoch, J., Bacherikova, I.V., Komashko, G.A., Pyatnitskaya, A.I., Appl. Catal. A: General, **134**, 225 (1996)

CHAPTER 5

DISCUSSION

The selective oxidation of medium chain linear alkanes (C_4-C_8) remains a major challenge for scientists. The secondary substituted carbons of linear alkanes are more reactive than the terminal carbons, which give poor activation of a specific carbon, thus giving a complicated product profile (Willock, D.J. (2005)). The oxidation of an alkane usually involves free radical processes at temperatures higher than 400^{o}C under gas phase conditions (Cavani, F. *et al.* (1999), Hutchings, G.J. *et al.* (1988), Sheldon, R.A. *et al.* (1981)). The discussion focuses on how catalytic and non-catalytic reactions (reactions in the absence of a catalyst) can be combined to obtain a selective product. The catalysts under investigation were VPO and VMgO. The selectivity of the catalyst was tested with the addition of promoters (cobalt, rhodium and gold) by different methods (either impregnation or incorporation). The method of promoter addition and the type of promoter gave different phases in the catalysts. The phases were identified and associated with either selective or non-selective oxidation.

The size and location of voids in a reactor and the material of construction of the reactor were used to obtain a desired product distribution under combined catalytic and non-catalytic conditions.

Selectivity to desired products was not only related to the reactor configuration and the type of catalyst but also to reaction conditions including alkane:oxidant ratio, residence time and dilution of the catalyst.

5.1 Catalytic vs. non-catalytic reactions

The product profile obtained from a purely catalytic system using VPO and VMgO is discussed in Section 5.1.1. The type of reactor configuration (which could be used to enhance non-catalytic reactions) and its effect on product distribution are discussed in the following four

sections (Section 5.1.2-5.1.5) with respect to the reactor's material of construction, the catalyst, inert packing material, residence time and dilution of the catalyst.

Little attention is given to reactions in the absence of a catalyst in the literature. This is a major concern with alkane oxidation since alkanes can react homogeneously (autoxidation) at low temperatures (~350^{o}C). These free radical reactions made a significant contribution to results obtained at low conversions. The influence of the reactor material, the particle size of inert packing material and the catalyst, the distribution and size of voids in the reactor, the residence time of the substrate in the reactor and the operating reaction temperature were some of the factors considered, with and without the presence of a catalyst, on the product profile.

The benefit of these non-catalytic reactions to selectivity was investigated by comparing product selectivity profiles from different reactor configurations for the oxidation of *n*-hexane (setups 1-9 on p 292 of the foldout section in the Appendix).

5.1.1 Product profiles from purely catalytic reactions over VPO and VMgO

The contribution made by a purely catalytic system before combining it with a non-catalytic one was ascertained. The product profiles from C_4, C_6 and C_8 oxidation over VPO and VMgO catalysts were compared under purely catalytic operating conditions. The products from a purely catalytic process were obtained from operating a reactor at a temperature where there was zero conversion in a blank reactor (which was a carborundum packed reactor at 350^{o}C). The conversions obtained for the catalytic system were usually below 10 % at this temperature. An incorporated cobalt promoter in the VPO catalyst gave higher selectivities than the use of a rhodium promoter in the oxidation of *n*-butane to MA, whilst the impregnation method of promoter addition generally gave carbon oxides under purely catalytic operating conditions. The incorporated promoter generally gave a more active catalyst for the oxidation of medium chainlength alkanes. The product profile obtained from the oxidation of medium chainlength alkanes under catalytic conditions was the same for promoted (incorporated promoter) and unpromoted VPO and VMgO catalysts.

Co-VMgO and VMgO gave carbon oxides and alkenes from the oxidation of both C_4 and C_6 alkanes under catalytic conditions (Sections 4.3.1.7 and 4.3.2.1). The oxidation of a C_8 alkane over these catalysts gave a mixture of aromatic products including toluene, benzene, isomers of xylene, cracked products, ethylbenzene and styrene (Section 4.3.3.1).

The oxidation of a C_6 alkane over promoted and unpromoted VPO gave benzene, cracked products and carbon oxides. The oxidation of a C_8 alkane over the VPO catalysts tested gave cyclic oxygenates (including furfural, maleic anhydride, 2-cyclopentene-1,4-dione, 2-H-pyran-2-one, 4-H-pyran-4-one, dihydro-3-methyl-2,5-furandione, benzaldehyde, benzoic acid, 3-methyl-2-cyclo-hexene-1-one, phthalic anhydride and benzofuran), benzene and carbon oxides.

When the catalytic and non-catalytic reactions were combined by increasing the temperature, the carbon oxide selectivities approached 100 % from C_6 and C_8 alkane oxidation over a VPO catalyst, however, the selectivities to alkenes, benzene and styrene increased and the selectivities to carbon oxides decreased with increasing temperatures over VMgO. VMgO was thus the less oxidizing catalyst.

The oxidation of *n*-hexane in single-gauze Pt/Rh reactors at very short contact times (in the region of μs) showed that although these reactions proceed via free radical mechanisms, the product profile was different, with predominantly cyclic oxygenates and no benzene obtained (O'Connor, R.P. *et al.* (2000)). The partial oxidation of *n*-hexane over a Pt-coated alumina foam monolith catalyst gave mainly cracked products and C_6 olefins and not benzene via homogeneous gas-phase reactions downstream of the catalyst (Dietz III, A.G. *et al.* (1996)). Benzene was obtained from free radical reactions in work carried out in this thesis. This emphasises how the different reactor, catalyst and catalytic conditions for free radical reactions employed in the literature and in work carried out in this thesis affect the production of benzene.

5.1.2 Residence time-selectivity relationships

Residence time is an important factor for controlling selectivity and cannot be ignored or discounted from the oxidation reactions of linear alkanes.

There was a trend of increasing selectivity to MA with increasing flowrate at a constant conversion. This increasing selectivity with increasing GHSVs at a constant conversion was attributed to shorter residence times and hence limited over-oxidation of MA to carbon oxides. This result confirmed the results obtained by Mallada, R. *et al.* (2000), where four small fixed beds of VPO catalysts separated by quartz wool were packed along the length of a 10 mm internal diameter reactor from entrance to the exit. The author reported decreasing selectivity to MA from *n*-butane oxidation as one progressed from the bed closest to the entrance of the reactor to the one at the exit, which indicated oxidation of MA with increasing residence time in the reactor. The residence time was an important factor to control conversion and over-oxidation. Short residence times gave low conversions and low selectivities to carbon oxides.

The oxidation of *n*-hexane over a VMgO catalyst gave benzene, isomers of hexene, carbon oxides and C_{3-4} products from cracking. Longer residence times and larger amounts of catalyst changed the product profile. Centi, G. *et al.* (1988a) reported on the oxidation of *n*-hexane over a VPO catalyst giving maleic anhydride, phthalic anhydride, benzoic acid, cracked products and carbon oxides. The authors reported 23 % selectivity to maleic anhydride at a conversion of 50 %. Benzoic acid, MA and phthalic anhydride were not obtained at selectivities higher than 1 % from *n*-hexane oxidation over a VPO catalyst in work carried out in this thesis. The difference in the product selectivity profile obtained in this thesis compared to that in the the literature was attributed to smaller amounts of catalyst (6 g of VPO catalyst used in the literature which is 12 times the amount used in this thesis) and higher flowrates (flowrate of 12 ml min^{-1} which was approximately 0.25 times that employed in this thesis) and different fuel:air ratios (hydrocarbon:oxygen molar ratio of 1.2 compared to 0.4 used in this thesis). The increased residence time enhanced the cracking reactions and hence gave larger selectivities to butane and subsequent oxidation to MA.

Further increasing the residence time was reported by Mikovsky, R.J. *et al.* (1971) to give selectivity to benzene of 90 % and conversions of *n*-hexane of higher than 80 % over tellurium loaded NaX and KX zeolites. Although the authors used a non-oxidative dehydrocyclisation process giving C_{1-5} cracked products and coke as other products with a contact time approximately 80 times larger than that employed in this thesis (i.e. 9 s in the literature compared to 0.12 s in work carried out in this thesis), longer residence times seem promising for cyclisation reactions and oxygen insertion reactions using VPO catalysts.

There was a decrease in carbon oxide selectivity with increasing GSHV in the oxidation of *n*-octane at 500^{o}C over VMgO and Co-VMgO catalysts (Fig. 4.94). Cavani, F. *et al.* (1999) attributed this decrease in selectivity to carbon oxides in free radical reactions to high mass transfer rates which favoured radical termination via interactions with the catalyst or carborundum surface rather than non-selective homogeneous decomposition reactions to carbon oxides. Increasing the surface area:void volume ratio with carborundum and catalyst in the reactor was found to decrease selectivity to cracking from free radical reactions in work carried out in this thesis (Tables 4.21-4.22). The high flow rates increased the mass transfer of radicals formed in the gas phase towards the catalytic surface, reactor wall surface and surface of the inert packing material, which acted as a radical scavenger.

The residence time played a key role in the yield to styrene (a purely catalytic product) from *n*-octane oxidation over a VMgO catalyst where decreasing residence times gave increasing yields to styrene (Fig. 4.99).

Benzene, which formed in the presence and absence of a catalyst, was oxidised to carbon oxides. This occurred in the voids and not the catalyst surface of a VMgO catalyst (Section 4.3.2.4). The residence time of the product thus needed to be high in the catalyst bed and low in the voids of the reactor to limit non-catalytic oxidation of benzene to carbon oxides. Decreasing the volume of voids post catalyst and packing the catalyst towards the exit of the reactor limited over-oxidation. The benefits of having a carborundum-packing post-catalyst under combined catalytic and non-catalytic conditions in the oxidation of *n*-hexane to benzene,

however, outweighed the disadvantages of benzene decomposition in the voids. This is discussed further in Section 5.1.3, where the highest yields to benzene were obtained in a system containing a catalyst packed at the entrance of the reactor and carborundum packed post-catalyst.

5.1.3 Void reactions and selectivity

In fixed-bed continuous flow reactors, the voids in the reactor allowed a gaseous or liquid mixture containing the substrate and oxidant to pass and thus permit the reaction between the substrate and the catalyst. The size of these voids was important in determining the selectivity to desired products. In the absence of a catalyst, autoxidation occurred in these voids at elevated temperatures (usually higher than 300^{o}C), giving mostly carbon oxides and cracked products. These reactions only occurred in the presence of an oxidant, making it an oxidation process. The product selectivity profiles and the conversion of *n*-hexane in voids, on neat catalysts and diluted catalysts were compared (Section 4.3.2.2).

The product profiles from *n*-hexane oxidation under catalytic and non-catalytic conditions were the same (including C_{3-4} cracked products, isomers of hexene, benzene and carbon oxides), however, the combination of catalysts and voids on the conversion and product selectivity profile was investigated.

Homogeneous oxidation of *n*-hexane, in the presence of molecular oxygen, gave isomers of hexene which easily cyclised to give benzene. The product selectivity profile was, however, complicated by cracked products. At similar conversions of different alkene intermediates, the selectivities to benzene were higher under catalytic conditions than under non-catalytic conditions (Section 4.3.2.2). The combination of a number of alkene products (intermediates) from homogeneous and heterogeneous reactions to give a single product (benzene) is an attractive feature of this type of system.

Free radical reactions were quenched at temperatures lower than 300^{o}C by carborundum packed into the reactor, which was seen by noting conversion in an empty reactor, but not in a

carborundum-packed reactor (Section 4.3.2.2). This packing increased the surface area to void volume ratio. This increased surface area limited conversion. Free radical reactions, however, became spontaneous at elevated temperatures (higher than 400^{o}C), even in the presence of carborundum. Although carborundum particles used as inert packing in the reactor can limit free radical reactions, the particle size of the packing was important. The larger the voids, the higher the conversion attributed to homogeneous reactions. The increased surface area to void volume ratio obtained by packing carborundum into an empty reactor provided a more oxidising homogeneous environment for carbon dioxide production by giving a higher carbon dioxide:carbon monoxide selectivity ratio compared to an empty reactor at similar conversions.

A trend of decreasing selectivity to benzene with increasing temperature in an empty reactor, with a concurrent increase in selectivity to C_{3-4} products and carbon oxides, suggested that cracking and total oxidation of *n*-hexane was favoured by large voids. A carborundum-packed reactor, however, showed a trend of increasing selectivity to benzene with increasing temperature, suggesting that carborundum limited over-oxidation and cracking of *n*-hexane. This higher selectivity to benzene in a packed reactor compared to an empty reactor was obtained at the same conversion (Fig. 4.82).

By increasing the size of the carborundum particles from 300 μm to 1000 μm in a reactor fully packed with carborundum, and hence increasing the void size of the inter-granular space, higher conversions were obtained under similar operating conditions, giving more cracking of *n*-hexane to C_{3-4} alkanes. The conversion increased with a decreasing ratio of surface area to void volume. An inert packing material of fine particle size reduced the void volume to surface area ratio, which was effective in limiting homogeneous reactions. On the other hand, very fine particles were avoided because they contributed to back-pressure and disturbed the steady state conditions of the reaction. For a 10 mm internal diameter reactor, which was adequate to limit radial thermal gradients and maintain a plug flow, a particle size of 300-600 μm was required.

The catalyst activated the substrate, which reacted homogeneously in the voids between inert packing in the reactor. This catalyst-initiated homogeneous reaction can be limited by packing the catalyst closer to the exit of the reactor, but work was directed into determining if the combination of catalytic and non-catalytic reactions could be combined in a reactor to improve the selectivity to a desired product. This was investigated by obtaining data from packing a reactor in different ways, i.e. changing the location of the catalyst and voids (Section 4.3.2.2). It was established that free radical reactions were promoted by voids in the reactor giving alkenes. The desired reaction was the conversion of alkenes to benzene.

It was established that the size of the voids played an important role in selectivity. The location of the voids relative to the catalyst was another important factor that determined both the product profile and selectivity in the oxidation of *n*-hexane. The different reactor setups used to establish the relationship between product selectivity profiles and void locations are illustrated on p. 292 of the foldout section in the Appendix.

The reactions in the reactor at 400^{o}C were attributed mainly to the catalyst and not homogeneous reactions. The oxidation of *n*-hexane over a VMgO catalyst packed at the exit of the reactor (setup 7) at this temperature gave lower conversion and poorer selectivity to benzene than a conventionally packed reactor (setup 3). When the catalyst was packed at the entrance to the reactor (setup 5), the selectivity to benzene was still lower than in a conventionally packed reactor. The selectivity to benzene was enhanced by packing carborundum before and after the catalyst. The mechanism of *n*-hexane oxidation to give hexenes, which cyclised to give benzene (Section 4.3.2.3), thus involved free radical generation in the voids of the reactor. The highest yield to benzene was obtained in setup 5 (Fig. 4.82), where there was a combination of catalytic and non-catalytic contribution to its formation. The substrate was thus activated by the catalyst and subsequently reacted in the voids. The selectivity vs. conversion plots indicated a sharp increase in the selectivity to benzene when there was a catalytic and homogeneous reaction contribution, whilst there was a decrease in selectivity to benzene and hexene with increasing temperatures when it was produced exclusively by homogeneous reactions (setup 1), which was

partly attributed to secondary oxidation of benzene and hexene to carbon oxides in a void. Projected data indicated that the VMgO catalyst would improve the selectivity to benzene in combination with homogeneous reactions at temperatures higher than 500^{o}C, though combustion of benzene would be a factor at these temperatures (Section 4.3.2.4).

There is a lot of controversy in the literature over mechanisms for free radical reactions because of the complexity in identifying the intermediates. Some of the proposed mechanisms in the literature are discussed in Chapter 1.

The production of benzene was always accompanied by hexene in catalytic and non-catalytic reactions with VPO and VMgO catalysts. Thus, a relationship between hexene and benzene as products was investigated (Section 4.3.2.3). The selectivity to hexene did not decrease with increasing selectivity to benzene (with increasing temperature, which would give an indication of the direct oxidation of hexene to benzene), however, because hexene was formed both catalytically and non-catalytically. A mechanism for the oxidation of *n*-hexane to benzene over VMgO dominated at temperatures higher than 300^{o}C when small voids were present between carborundum particles (300-600 μm) in the reactor. Benzene was oxidised to carbon oxides in larger voids at temperatures higher than 250^{o}C (Fig. 4.87). In a reactor fully packed with carborundum and catalyst particles between 300-600 μm in diameter, increasing benzene selectivity was associated with decreasing selectivities to carbon oxides. It was proposed that benzene and CO_x formed via competitive mechanisms and carborundum quenched the CO_x formation pathway.

A mechanism for the oxidation of *n*-hexane giving benzene was proposed based on the catalytic and non-catalytic oxidation of the proposed intermediates (Section 4.3.2.3) and is shown in Fig. 5.1.

The proposed intermediates included 1-hexene, 2-hexene, 1,3-hexadiene, 1,4-hexadiene, 1,5-hexadiene, cyclohexane, cyclohexene, 1,3-cyclohexadiene and 1,4-cyclohexadiene.

Carbon oxides were produced in every step of the proposed mechanism, with the least selectivities to carbon oxides from the oxidation of the cyclohexadienes and cyclohexene.

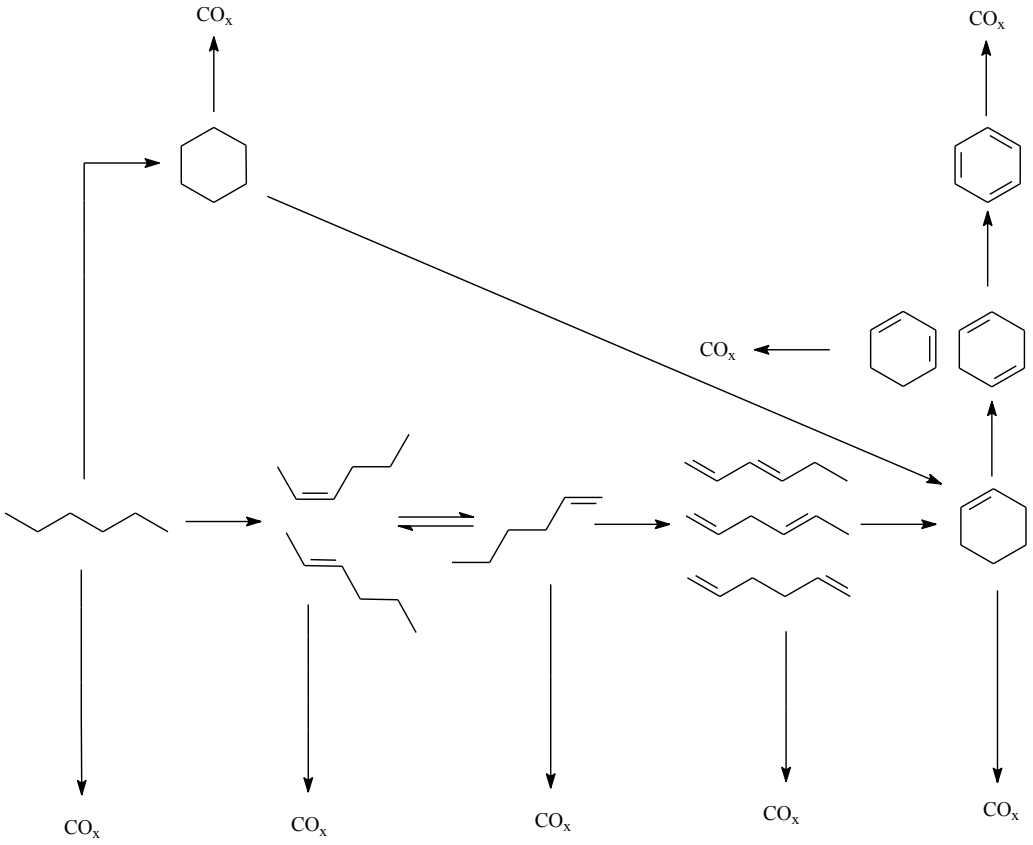

Fig. 5.1 Proposed mechanism for the oxidation of n-hexane to benzene under catalytic and non-catalytic conditions

1-hexene was only seen in the presence of a VMgO catalyst and not from any non-catalytic reactions. Hoog, H. *et al.* (1939) established that an equilibrium existed between 1- and 2-hexene in the reactor and that 1-hexene cyclised more rapidly than 2-hexene. The higher selectivity to benzene from 1-hexene than 2-hexene oxidation was confirmed. It can thus be hypothesised that *n*-hexane was converted to cis and trans isomers of 2-hexene, which were subsequently converted to 1-hexene. 1-Hexene was further dehydrogenated to give 1,3-, 1,4- and 1,5-hexadiene, which cyclised to give cyclohexene, which was further dehydrogenated to give 1,3- and 1,4-cyclohexadiene. There were higher conversions of cyclohexenes than linear alkenes to benzene at similar operating temperatures.

Since cyclohexane was observed in the product profile of *n*-hexane oxidation, an alternative parallel route to benzene formation may exist, where the alkene cyclised to give cyclohexane, which was subsequently dehydrogenated to give benzene.

Since the products obtained from the catalytic and non-catalytic oxidation of *n*-hexane were identical, it was believed that the same (free radical) mechanism probably applied. Since conversions were substantially higher for reactions in the presence of VMgO than without, it could be concluded that VMgO was a catalyst for these reactions.

The effect of voids on the oxidation of *n*-hexane over VPO and VMgO catalysts were compared by the introduction of a void (unpacked region) preceding the VPO catalyst in the reactor (Section 4.3.2.6). Homogeneous reactions in this unpacked region of the reactor gave butane and butanes from the cracking of *n*-hexane, which was subsequently oxidised over the VPO catalyst to give MA. There was poor selectivity to MA (less than 1 %) but this showed that there was a combination of catalytic and non-catalytic reactions giving a catalytic product. The void also oxidised *n*-hexane to carbon oxides. This reactor setup gave oxygen insertion and Diels Alder type reactions forming large bicyclic oxygenated molecules.

One of the selective products from this VPO system included 2,5-dimethylfuran. 2,5-dimethylfuran did not form in a conventionally packed reactor, nor in a fully carborundum-packed or empty reactor, thus suggesting that the alkane was activated in the void preceding the catalyst and oxidised over the VPO catalyst. The mechanism to its formation may be likened to the oxidation of *n*-butane over a VPO catalyst to give maleic anhydride. Fig. 5.2 illustrates the similarities in the mechanism in forming cyclic oxygenates over a VPO catalyst.

n-Butane underwent alkane hydrogen abstraction on the VPO catalyst (step 1, equation 5.1), followed by allylic hydrogen abstraction (step 2), then 1,4-dienic oxygen insertion (step 3), followed by allylic oxygen insertion (step 4). It was proposed that *n*-hexane also underwent alkane and allylic hydrogen abstraction followed by 1,4-dienic oxygen insertion (steps 1-3, equation 5.2). The two extra terminal carbons remain on the furan ring as methyl groups giving 2,5-dimethylfuran.

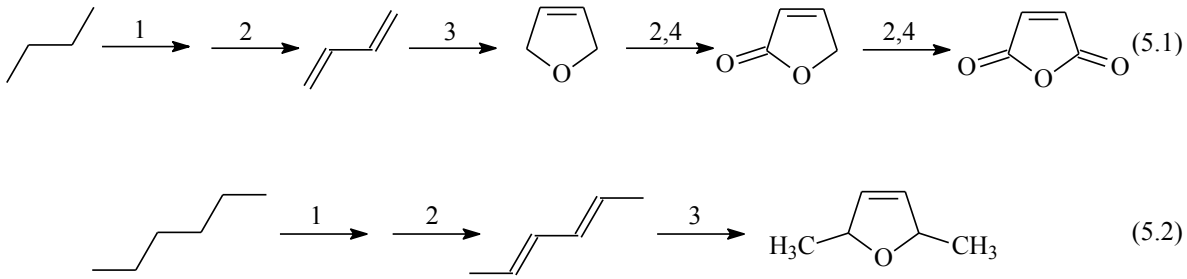

Fig. 5.2 H-abstraction and subsequent cyclisation of n-butane and n-hexane over a VPO catalyst

The combination of catalytic and non-catalytic reactions to give a selective product worked well for the poorly oxidising VMgO catalyst. The more oxidising catalyst, VPO, gave a large number of oxygenated products and poor selectivity.

The VMgO catalyst gave cyclisation of alkenes without oxygen insertion (Sections 4.3.2.1 and 4.3.3.1) (as opposed to oxygen insertion with a VPO catalyst (Sections 4.3.2.5 and 4.3.3.2)) and the selectivities to alkenes and benzene were generally higher over a VMgO catalyst than a VPO catalyst at similar conversions and operating conditions, suggesting that the pyrovanadate phase (identified as the active phase according to Coulston, G.W. *et al.* (1997) and Albonetti, S. *et al.* (1996)) in the VPO catalyst was more oxidising than the orthovanadate phase (identified as the active phase) in the VMgO catalyst.

Another reaction that gave an improved selectivity to a desired product by combining catalytic and non-catalytic reactions was the oxidation of *n*-octane to styrene. The selectivity to styrene from *n*-octane oxidation over a VMgO catalyst increased with increasing temperature (300-500^{o}C). This did not correlate with a conventional selectivity vs. temperature curve, where there is a decrease in selectivity to non-CO_x products with increasing temperature. The selectivity to alkenes increased with increasing temperature and these cyclised over the catalyst to give styrene. The oxidation of *n*-octane to styrene was thus proposed to involve homogeneous reactions. The oxidative dehydrogenation of *n*-octane to alkenes, which subsequently cyclised to styrene, was purely catalytic at 350^{o}C, where there was negligible homogeneous contribution to the reaction. Styrene was only produced catalytically.

5.1.4 Catalyst diluton and selectivity

Increasing the dilution of the VMgO catalyst increased the selectivities to benzene and isomers of hexene (which were obtained catalytically and non-catalytically from the oxidation of *n*-hexane) at similar conversions (Section 4.3.2.2). Dilution of the catalyst thus limited overoxidation in a process that was both catalytic and non-catalytic. Benzene was oxidised in the voids of carborundum (and not under catalytic conditions) to give carbon oxides (Section 4.3.2.4). The selectivities to carbon oxides were lower at similar conversions in a reactor containing diluted catalyst (setup 9) compared to undiluted (setup 3) and less diluted catalysts (setup 8). This suggested that dilution of a catalyst limited over-oxidation of *n*-hexane.

5.1.5 Effect of reactor material on the catalysis

Oxidation reactions were initiated in glass and stainless steel reactors. These reactions were catalysed by the Co, Mn, Fe and Cu ions present in the stainless steel, where these metals are known to be active in a redox cycle (Sheldon, R.A. *et al.* (1981)). Molecular oxygen was activated by silica (which usually activated molecular oxygen to give an O_2^- species), which was responsible for free radical reactions in the glass reactor (Cavani, F. *et al.* (1999)). The reactor material thus influenced the conversion of the alkane in the absence of a catalyst, thus giving a catalytic and non-catalytic contribution to the conversion of an alkane at temperatures higher than 400^{o}C for medium chainlength alkanes.

Secondary products are reported in the literature as not being an issue at low conversions (typically lower than 10 %), however, there were non-catalytic reactions, even at conversions lower than 10 % in work carried out in this thesis, giving secondary products (such as the oxidation of *n*-hexane to isomers of hexene, which gave benzene as a secondary product).

The oxidation of *n*-hexane over a VMgO catalyst was investigated under the same catalytic conditions in a steel and glass reactor (Section 4.3.2.1). The selectivities to benzene were higher in a glass reactor than in a steel reactor at similar conversions. Higher selectivities to carbon oxides were obtained in a steel reactor compared to a glass reactor at temperatures

higher than 300°C and at similar conversions. Carbon oxide production was the most oxygen demanding reaction, with each secondary carbon in the alkane able to undergo oxidation to give either CO or CO_2. The lower selectivities to carbon oxides in the carborundum-packed glass reactor compared to the carborundum-packed steel reactor meant that there was more available oxygen for alkene production via a catalytic process. The alkenes cyclised to give benzene and thus the selectivity to benzene in a glass reactor was generally higher, both in the presence and absence of a catalyst. Since benzene was formed from competitive mechanisms of hexene oxidation to either carbon oxides or benzene (Section 4.3.2.3), this indicated that the glass reactor (from combined catalytic and non-catalytic processes) enhanced the mechanism giving benzene. A glass reactor was more suitable than a steel reactor in limiting combustion in the selective oxidation of alkanes.

Higher conversions were obtained in a steel reactor than in a glass reactor at similar operating temperatures when fully packed with carborundum, however, the conversion in a glass reactor was higher with the introduction of a catalyst. The yields to carbon oxides were generally higher in a steel reactor than in a glass reactor under catalytic conditions, which may be responsible for the low conversions because each secondary substituted carbon can react to give carbon oxides.

Above a critical temperature (~250°C and in the presence of oxygen) in a reactor, aromatics are the most stable of all hydrocarbons (Rossini, F.D. (1947)). Thus with any free radical process, such as the oxidation of *n*-hexane in a reactor in the absence of catalyst, benzene readily formed.

Wagner, A.F. *et al.* (1990) proposed that the addition of O_2 to an alkyl radical formed via an initiation step produces an excited alkylperoxy species which, at high temperature, is quickly decomposed to the alkene and $HO_2^{\bullet}$ via an intermediate alkylhydroperoxy species (* denotes intermediate species in equations 5.3, 5.4 and 5.5):

$$C_nH^{\bullet}_{2n+1} + O_2 \rightleftharpoons C_nH_{2n+1}O^{\bullet}_2{}^{*} \quad (5.3)$$

$$C_nH_{2n+1}O^{\bullet}_2{}^{*} \rightleftharpoons C_nH_{2n}O_2H^{\bullet}{}^{*} \quad (5.4)$$

$$C_nH_{2n}O_2H^{\bullet}{}^{*} \longrightarrow C_nH_{2n} + HO^{\bullet}_2 \quad (5.5)$$

The oxidative dehydrogenation of C_6 and C_8 alkanes over the VPO and VMgO catalysts gave alkenes which cyclised to benzene. There was subsequently a steep increase in the conversion of benzene to carbon oxides in a carborundum-packed reactor at temperatures higher than 450°C (Section 4.3.2.4). Norrish, R.G.W. *et al.* (1956) proposed that benzene oxidation occurred via the subsequent hydroxylation of the ring to a dihydroxy-derivative, after which on further oxidation the ring is ruptured. The decomposition products are rapidly degraded to CO and CO_2 (Fig. 5.3).

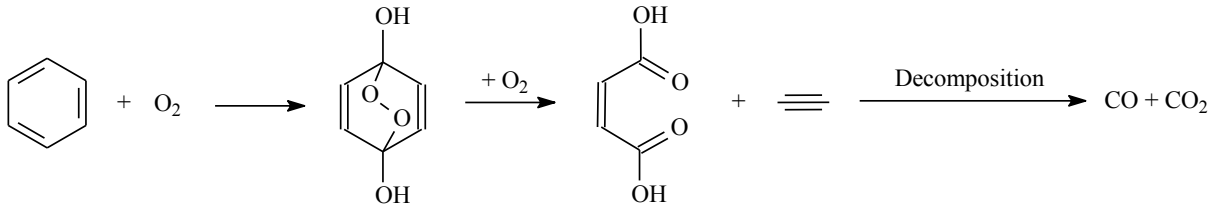

Fig. 5.3 Reaction scheme for the oxidation of benzene and subsequent decomposition to carbon oxides (adapted from Shtern, V.A. (1964))

The selectivity to carbon monoxide from *n*-octane oxidation was generally higher in an empty reactor than in a carborundum-packed reactor at similar flowrates and operating temperatures in work carried out in this thesis. The same was observed for *n*-hexane oxidation in an empty reactor and carborundum-packed reactor. Pope, J.C. *et al.* (1929) hypothesised that the first stable products of hydrocarbon oxidation are the aldehydes with one less carbon atom as in the initial hydrocarbon (equation 5.6). The authors proposed that further oxidation of this aldehyde results in the subsequent formation of shorter chain length aldehydes.

This hypothesis can be represented in the following way:

$$C_8H_{18} + O_2 \longrightarrow C_7H_{15}CHO + H_2O \quad (5.6)$$

$$C_7H_{15}CHO + O_2 \longrightarrow C_6H_{13}CHO + H_2O + CO \quad (5.7)$$

$$C_7H_{15}CHO + 1.5O_2 \longrightarrow C_6H_{13}CHO + H_2O + CO_2 \quad (5.8)$$

Pope, J.C. *et al.* (1929) proposed two reactions for aldehyde degradation. The first reaction producing carbon monoxide (equation 5.7) and the second reaction producing carbon dioxide (equation 5.8). They reported the same result with oxidation of the secondary substituted carbons of the alkane chain as opposed to the terminal carbons in the above reaction scheme. Shtern, V.Y. (1964) reported that the selectivity to carbon monoxide is favoured over carbon dioxide from the free radical degradation of alkanes.

Acetaldehyde was a product from the possible aldehyde degradation reactions to give carbon oxides from C_6 and C_8 alkane oxidation in carborundum-packed and empty stainless steel reactors.

5.2 Catalyst structure-activity relationships

The VPO and VMgO catalysts were extensively investigated in the oxidative dehydrogenation of *n*-butane in the literature. There is little literature on the oxidation of longer chain linear hydrocarbons over these catalysts (Sections 1.3.1.4 and 1.3.1.5). An investigation into the heterogeneous oxidation of C_6 and C_8 linear alkanes over these catalysts was carried out to observe trends in the product profiles from a highly oxidising and weakly oxidising catalyst.

The VPO catalyst was more oxidising than VMgO, giving MA from *n*-butane oxidation, whilst the oxidation of the same substrate with VMgO under similar reaction conditions gave alkenes. Only trace amounts of MA were obtained over VPO and lower selectivities to alkenes were obtained over VMgO from the oxidation of C_6 and C_8. The higher selectivities to cracking over VPO compared to VMgO indicated that VPO is a more acidic catalyst. Cracked C_6 gave a C_4 alkane, which was converted to MA over the VPO catalyst. The VPO and VMgO catalysts selectively activated C_4 and shorter linear hydrocarbons but there was

poor selectivity in the activation of longer hydrocarbons. The XRD patterns of used VPO catalysts from the oxidation of *n*-butane, *n*-hexane and *n*-octane appeared similar, indicating the presence of the same $(VO)_2P_2O_7$ phase, however, the product profiles were different as expected. The hydrocarbon could be adsorbed onto the mixed metal oxide catalyst surface at many points along its length. The active site distribution is an important factor in the selective oxidation of medium chainlength alkanes. Due to increased number of secondary substituted carbons in longer alkanes, there were multiple sites that could be activated, which gave poor selectivity (discussed in Section 5.3).

Over a lifetime of the catalyst, from precursor stage to calcination and finally testing in a reactor, the physical and chemical attributes of the catalyst changed. The morphology of the catalyst changed from the precursor stage through to catalyst conditioning and during a reaction (Sections 4.1.1 and 4.1.3). The phase present in the catalyst precursor was related to performance of the catalyst. It was essential that the precursor phases were the dominant $VOHPO_4{\cdot}0.5H_2O$ (vanadyl hydrogen phosphate) phase for the VPO catalyst and the $Mg_3(VO_4)_2$ (magnesium orthovanadate) phase for the VMgO catalyst, which were considered ideal phases to ensure high selectivity catalysts. The intermediate phases varied with different promoters and different methods of their addition to the catalyst, however, the selective VPO catalysts had a dominant vanadyl pyrophosphate phase and the selective VMgO catalysts had a dominant orthovanadate phase in the used catalysts. Although most intermediate phases were converted to these final phases after a reaction, the presence of these ideal precursor phases prior to a reaction was important in the performance of the catalyst.

Different promoters gave different intermediate phases after calcination of the precursor. These different phases were correlated to the reactivity of the catalyst. The types of phases that gave selective oxidation and the types that gave over-oxidation were identified. This is discussed in detail in Section 5.2.1.

The most selective VPO catalysts for the oxidation of *n*-butane to MA were obtained when a $VOHPO_4 \cdot 0.5H_2O$ precursor phase lost crystallinity when calcined and gave the $(VO)_2P_2O_7$ phase after reaction (Section 4.1.1).

XRD patterns of these catalysts showed that the vanadyl pyrophosphate was the dominant phase in the used VPO catalyst. The $Mg_3(VO_4)_2$ (orthovanadate) phase was dominant in the precursor, calcined and used VMgO catalysts. The used VMgO catalysts, however, showed the presence of minor meta- and pyro-vanadate phases in work carried out for this thesis. The dominant pyrovanadate phase in the VPO catalyst oxidised C_6 and C_8 alkanes mainly to carbon oxides. A substrate adsorbed on the surface of the VPO catalyst had access to more oxygen (supplied by the P_2O_7 units) than a substrate adsorbed on the surface of a VMgO catalyst (where oxygen is predominantly supplied by VO_4 units) (Graselli, R. *et al.* (1980)). In a simplistic approach to understanding the structure-activity relationship, these phases were seen as influencing the oxidising nature of the catalyst. The formation of these minor phases did not inhibit the activity of the VMgO catalyst with time on-stream, however, they contributed to non-selective reactions in the VMgO catalyst. This was confirmed by time on stream experiments, which showed an increase in carbon oxide selectivity at constant temperature.

VMgO is well reported as a selective catalyst for the oxidation of *n*-butane to isomers of butene. At ~ 540^{o}C there was a yield of 10 % to butenes with a 34 wt. % VMgO catalyst in work carried out in this thesis. Chaar, M.A. *et al.* (1987) reported a yield of 20 % to butenes with a 20 wt. % VMgO catalyst at this temperature under similar reaction conditions (Appendix, p. 273). A higher wt. % of V_2O_5 on MgO gave lower selectivities to butenes and higher selectivities to carbon oxides. The catalyst with the higher wt. % of V_2O_5 used in work carried out in this thesis contained the orthovanadate phase, which was partially converted to a metavanadate phase during reaction. This was not observed for the lower wt. % of V_2O_5 on MgO reported in the literature. The metavanadate phase has been reported in the literature to be more oxidising in nature and may be responsible for the higher selectivities to carbon oxides (Kung, H.H. *et al.* (1997)).

VMgO investigated in work carried out in this thesis is compared to VMgO investigated in the literature with respect to conversions of *n*-butane and selectivities to isomers of butene (Appendix, p. 273). At a similar conversion of 42 %, a selectivity of 25 % to isomers of butene was obtained over the VMgO catalyst (Fig.4.72), whilst 52 % was obtained in the literature over a similar VMgO catalyst (~ 34 wt. % V_2O_5/MgO). The conditions for testing these catalysts were different. The feed concentration employed in work carried out in this thesis was 1 % *n*-butane in air, which is a 1:21 volumetric ratio of alkane:O_2. The hydrocarbon concentrations employed in the literature were usually a 1:2 volumetric ratio of alkane:O_2. The fuel lean conditions employed in work carried out in this thesis resulted in larger selectivities to carbon oxides compared to selectivities reported in the literature, and consequently lower selectivities to isomers of butene. The hydrocarbon to oxygen ratio is important for selectivities to carbon oxides.

The FT-IR spectra of the VMgO catalyst (34 wt. % V_2O_5 from ICP-MS analysis) and the Co-VMgO catalyst (34 wt. % V_2O_5 from ICP-MS analysis) had sharper IR bands compared to FT-IR spectra of catalysts with lower V_2O_5 loadings in the literature (Chaar, M.A. *et al.* (1987)). Chaar, M.A. *et al.* (1987) reported that it was usual for the number of absorption bands in the FT-IR spectra to increase with increasing V_2O_5 content from ~ 19 wt. % upwards. This suggested increasing crystallinity with increasing vanadia loadings. The amorphous nature of the catalyst was preferred for improved yield to the alkene.

FT-IR spectra of the VPO catalysts showed a V=O stretching band at 975 cm^{-1} which was absent in the VMgO catalysts. The active catalytic site that inserts an oxygen into the substrate typically contained a V=O species (Busca, G. *et al.* (1986)).

The morphology of the VPO catalyst was important for activity and selectivity to MA from *n*-butane oxidation. The VPO catalysts showed signs of disintegration after time on stream, however, the plate-like shape of the crystallites did not change. The scanning electron microscope (SEM) images of the unpromoted VPO catalyst showed a plate-like morphology. The SEM image of the used catalyst showed disintegration of these plates and smaller plates

(Section 4.1.3.1). This may be attributed to redox conditions in the reactor, with the continuous removal and replenishment of lattice oxygen on the surface of the catalyst (Govender, N. *et al.* (2004)). The stability of the *n*-butane to MA reaction over VPO was not affected by this change in crystallite size over time (Section 4.3.1.2).

Catalysts containing the ideal phases in the precursor, calcined and used catalysts for maximum selectivity, needed to be considered together with morphological features in identifying a selective catalyst.

The average vanadium oxidation state (AV) may be used to predict the selectivity of a VPO catalyst. Although this was not an *in-situ* technique of identifying the oxidation state of a metal in the catalyst, it gave an indication of how selective the catalyst may be. The VPO catalysts with an AV closer to +4 were more selective to MA in the oxidation of *n*-butane (Sections 4.3.1.1-4.3.1.7). The phases present in the catalyst determined the AV of the catalyst during a reaction. If, according to a Mars and van Krevelen mechanism, vanadium switches between a +4 and +5 oxidation state during the redox cycle, V^{4+} on the surface of the catalyst can then activate molecular oxygen, and the surface layer can be oxidised to a certain extent to V^{5+}, which provides the capacity to oxidise adsorbed hydrocarbons (Centi, G. *et al.* (1995)). The VPO catalysts synthesised via the precipitation/deposition method had AV values closer to +5 than the VPO catalysts synthesised via the co-precipitation method, thus the former method of incorporation gave a catalyst with a higher capacity for deep oxidation. This was confirmed by higher selectivities to CO_2 (Section 4.3.1.2). Impregnation of VPO with a cobalt promoter gave a catalyst that contained mixed phases of $VOHPO_4 \cdot 0.5H_2O$ and $VOPO_4 \cdot 2H_2O$ (with V in a more oxidised state) thus giving a more oxidised catalyst (Section 4.1.1.3).

The VMgO catalysts had higher AV values (closer to +5) than the VPO catalysts, but the VMgO catalyst did not have the highly oxidising vanadyl species on its surface (confirmed by IR analysis in Sections 4.1.2.1 and 4.1.2.9) and was thus less involved in oxygen insertion reactions with hydrocarbons than the VPO catalyst. The VMgO catalyst thus gave alkenes,

rather than oxygenates, as well as lower selectivities to carbon oxides (Sections 4.3.1.7, 4.3.2.1 and 4.3.3.1).

The highly oxidising and acidic characteristics of VPO made this catalyst poor for selective partial oxidation of hydrocarbons longer than a C_4, where cracking was a problem. The longer chainlength hydrocarbons cracked over the VPO catalyst giving C_4 hydrocarbons (40 % conversion of *n*-hexane gave 8 % selectivity to $C_{3\text{-}4}$ cracked products over promoted and unpromoted VPO (Fig. 4.89)), which were subsequently oxidised over the VPO catalyst to MA (with overall selectivities of less than 1 %). The cracked products thus reacted further, adding to the complexity of the product profile.

The over-oxidation of the C_6 and C_8 alkanes was benchmarked against an industrial VPO catalyst from BP Amoco. The performance of the Co-VPO catalyst (co-precipitation) investigated in the oxidation of *n*-octane was compared to the commercial VPO catalyst, which was tested under similar operating conditions (comparative graphs of conversions and selectivities appear on p. 271 in the Appendix). The product profiles over both the Co-VPO and commercial VPO catalysts were the same. At 400^{o}C, the conversion from the commercial catalyst was higher (~ 39 %) than that obtained from the Co-VPO catalyst (~ 25 %). At 350^{o}C, where the same conversion of 6 % was obtained over the commercial and Co-VPO catalysts, the selectivity to benzene was higher over the commercial catalyst (48 %) than the Co-VPO catalyst (30 %). The Co-VPO catalyst gave a higher selectivity to carbon oxides compared to the commercial catalyst at this temperature (19 % and 3 %, respectively), however, at 400^{o}C, the selectivity to carbon oxides was higher over the commercial catalyst (67 % compared to 39 % over the Co-VPO catalyst). This comparison of the Co-VPO catalyst to an industrial catalyst highlights its ability to limit over-oxidation at this temperature (10 % yield CO_x from Co-VPO compared to 26 % yield from the commercial catalyst).

5.2.1 The influence of promoters and their incorporation methods on the structure and activity of the catalyst

The incorporation of promoters modified the structural properties and phase composition of the catalyst. The type of precursor phases was related to the type of promoter added to the catalyst and its location (either incorporated into the structure of the catalyst via a co-precipitation technique or impregnated onto the surface via a precipitation/deposition technique). The types of products were correlated to specific phases. A promoter was used to improve the activity and selectivity of catalysts at low operating temperatures, where free radical gas phase reactions did not occur and secondary oxidation products were not obtained.

Cobalt was the best promoter of the VPO catalyst with respect to activity and selectivity in the oxidation of *n*-butane to MA and *n*-hexane to benzene, when incorporated via the co-precipitation technique, of the three promoters investigated (viz. cobalt, rhodium and gold).

The co-precipitation method of promoter incorporation was generally superior to the precipitation/deposition method in improving the activity and selectivity of the VPO catalyst. An understanding of the poor performance of the catalysts synthesised via the precipitation/deposition method was attempted by relating the structural and compositional attributes of the catalyst to its activity.

The incorporation and impregnation techniques of promoter addition gave VPO catalysts with different morphologies (Sections 4.1.1.2, 4.1.1.3). The co-precipitation method of promoter addition generally gave a plate-like/rosette morphology, whilst impregnation completely destroyed this morphology giving a non-uniform structure (disintegrated platelets) and poorer selectivity to MA from *n*-butane oxidation (SEM data in Sections 4.1.3.3, 4.1.3.5 and selectivity data in Section 4.1.3.6). The non-uniform (disintegrated platelet) structure was obtained when the catalyst precursor consisted of mixed phases (seen in SEM images of Co, Rh and Au promoters impregnated onto VPO (Figs. 4.39, 4.42 and 4.46, respectively)). Besides the method of promoter addition, the type of promoter changed the morphology of the catalyst. A selective VPO catalyst usually had a platelet morphology and the type of promoter affected the

arrangement of these platelets. Opened rosettes or spaced out platelets (obtained with an incorporated cobalt promoter) were more active and selective to MA at similar conversions than tightly packed platelets (obtained with an incorporated rhodium promoter) (Sections 4.3.1.2-4.3.1.4).

These catalysts, with their different morphologies, contained the $(VO)_2P_2O_7$ phase after use. Although these catalysts contained the same phase after use, their performances could be related to the different morphologies seen from SEM images (Section 4.1.3). The higher activities and selectivities of a Co-VPO catalyst compared to a Rh-VPO catalyst (both catalysts having the promoter incorporated) (Figs. 4.65-4.66) was not merely a surface area effect because both catalysts had a similar surface area of ~22 m^2/g.

The impregnation method of adding a cobalt promoter gave a multiple phased VPO catalyst precursor, which was confirmed by XRD analysis (Section 4.1.1.3). Calcination of this precursor gave a crystalline material. It was found that, for different promoters and different methods of promoter addition, a poorly crystalline calcined VPO catalyst precursor gave enhanced selectivities to MA compared to a crystalline material.

A precipitation/deposition method usually gave a more oxidised vanadium species (than from incorporation) in the VPO catalyst seen from average vanadium oxidation states (Section 4.1.7). The average oxidation state was related to the phases present in the catalyst. A dominant crystalline V_4O_9 phase in the calcined impregnated catalyst gave decreased selectivity to MA and increased selectivities to carbon oxides (Section 4.1.1.6). The phases in the calcined catalysts were converted to the dominant $(VO)_2P_2O_7$ phase during a reaction. The V_4O_9 phase was poorly converted to $(VO)_2P_2O_7$ during a reaction. Although the $(VO)_2P_2O_7$ phase was the catalytically active phase (Ebner, J.R. *et al.* (1993)), the source of this phase was important in determining the selectivity of the catalyst. The VPO catalyst precursor with a dominant V_4O_9 phase present generally enhanced over-oxidation compared to when a dominant

$VOHPO_4 \cdot 0.5H_2O$ phase was present. Another precursor phase to give $(VO)_2P_2O_7$, which was identified in the poorly selective catalysts for MA, was $VOPO_4 \cdot 2H_2O$.

The pH of the reaction mixture (catalyst precursor synthesis) was related to the phases that were present in the catalyst. The liquid phase of the reaction mixture for a co-precipitation method of incorporating a promoter was acidic (~ pH 1). The catalyst precursor phase that formed was $VOHPO_4 \cdot 0.5H_2O$. The precipitation/deposition method of incorporating the cobalt promoter into the VPO catalyst involved changing the pH to ~ 8 that gave a $VOPO_4 \cdot 2H_2O$ phase. The VPO catalyst was thus pH sensitive and disintegrated in a basic medium. Catalysts with the dominant $VOPO_4 \cdot 2H_2O$ precursor phase had a lower surface area compared to those containing a dominant $VOHPO_4 \cdot 0.5H_2O$ precursor phase (Section 4.1.6).

The improved activity of the cobalt incorporated VPO catalysts compared to the unpromoted catalyst may be explained by the proximity of vanadyl species on the surface of the catalyst. The (020) plane reflection intensity appeared lower and the peaks broader in the XRD patterns of the Co-VPO catalysts (co-precipitation) than in the XRD pattern of the unpromoted VPO catalyst (Sections 4.1.1.2, 4.1.1.3). Busca, G. *et al.* (1986) reported that the (020) plane possesses Brønsted acid sites and active lattice oxygen (V=O species), which are the two strong functions necessary for the selective oxidation of *n*-butane to MA. The authors also reported that a decrease in intensity of the (020) plane reflection was attributed to disorder in the plane caused by *trans* to *cis* rearrangement of the V=O units about the (020) plane of the idealized $(VO)_2P_2O_7$ structure. The *trans* conformation of the $(VO)_2P_2O_7$ structure is illustrated in Fig. 5.4.

When transformed to the *cis* isomer, both oxygens on V=O lie above the plane. Busca, G. *et al.* (1986) reported that this arrangement leads to the formation of a highly reactive pair of vanadium ions, which are able to activate the alkane with a coordinative attack.

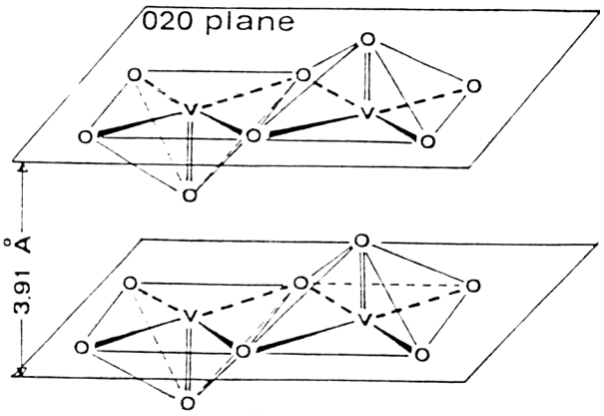

Fig. 5.4 The (020) plane on the surface of the VPO catalyst showing the trans conformation of the $(VO)_2P_2O_7$ structure (Busca, G. et al. (1986))

There was a larger amount of promoter added to a VPO catalyst when it was impregnated onto the surface of the catalyst than when incorporated into its structure. The promoter was coordinated with the catalyst when introduced via the precipitation/deposition method but not when incorporated via the co-precipitation method. Evidence of this was a shift of the V=O band (from a reference position on an unpromoted catalyst) in the IR spectrum of the VPO catalyst promoted via the precipitation/deposition, but no V=O bond shift was observed for the co-precipitation method (Sections 4.1.2.1-4.1.2.3). This coordination was detrimental to the performance of the catalyst by enhancing the selectivities to carbon oxides. This suggested that the promoter enhanced the selectivity and activity of the VPO and VMgO catalyst to non-CO_x products when in a non-coordinative state.

There was an optimum promoter loading in a catalyst to get a maximum selectivity to a desired product (Section 4.3.1.1). The promoter loading affected the crystallinity and surface area of the catalyst and there was an optimum promoter loading to give a maximum catalyst surface area (Section 4.1.6). Beyond a certain amount of promoter the crystallinity of the catalyst decreased. The optimum amount of cobalt promoter incorporated into VPO for the highest selectivity in the oxidation of *n*-butane to MA was ~ 2.3 molar % of Co/V (Section 4.3.1.1). Although it was difficult to identify any promoter metal phases via XRD techniques

because of the low concentration of metal, there was, however, a change in the morphology. The promoter increased the surface area of the catalyst by giving smaller sized platelets on the surface of the VPO catalyst (Section 4.1.3.2).

The cobalt incorporated VPO catalysts gave higher yields to MA than those reported in the literature at lower than conventional operating temperatures (350-450^{o}C) (Appendix, p. 269). It was confirmed that the improved activity and selectivity of this Co-VPO catalyst was not merely a surface area effect, by examining specific conversions and specific selectivities of unpromoted and promoted catalysts (Section 4.3.1.1).

Rhodium, although in the same group as cobalt, did not give similar performance when incorporated into the VPO catalyst. The incorporation of rhodium was expected to share the same kind of chemistry as cobalt and thus give a similar promoted catalyst in terms of morphology and P:V ratios, however, this was not the case. The rhodium promoted catalyst, under similar reaction conditions, gave lower selectivities to MA and higher selectivities to carbon oxides (Section 4.3.1.3).

The co-precipitation method of introducing rhodium into the catalyst gave a $VOHPO_4{\cdot}0.5H_2O$ phase. The $VOHPO_4{\cdot}0.5H_2O$ phase remained crystalline even when the catalyst was calcined, when usually VPO catalysts gave multiple phases or poor crystallinity when calcined (Sections 4.1.1.2, 4.1.1.4). Rhodium thus had the ability to stabilise the $VOHPO_4{\cdot}0.5H_2O$ phase at elevated temperatures (~ 550^{o}C), as seen from XRD data. When this material was tested in a reactor with an *n*-butane in air mixture, it was converted to the $(VO)_2P_2O_7$ phase with time on stream, improving the selectivity to MA compared to an unpromoted catalyst. This catalyst, however, did not perform as well as a Co-VPO (co-precipitation) catalyst, which did not retain the crystallinity of the $VOHPO_4{\cdot}0.5H_2O$ phase after calcination. Hence, although the co-precipitation methods of incorporating rhodium and cobalt into the catalyst gave the ideal $VOHPO_4{\cdot}0.5H_2O$ precursor phase, the rhodium promoted catalyst was less selective to MA. This suggested that a loss of crystallinity and/or development of multiple phases from the precursor phase during calcination, gave a more selective VPO

catalyst and this appeared to be the key difference between the two catalysts (Sections 4.1.1.2 and 4.1.1.4). This superior performance of 2.5 % Co-VPO (co-precipitation) was not merely a surface area effect since both catalysts had a similar surface area of ~22 m^2/g.

Rhodium metal is known to oxidatively dehydrogenate an alkane to give alkenes (Krummenacher, J.J. *et al.* (2004), Schmidt, L.D. *et al.* (2003)). Alkenes are intermediates to MA production over a VPO catalyst and their formation is the rate-determining step before cyclisation and oxygen insertion reactions (Zazhigalov, V.A. *et al.* (1993)). Rhodium as a promoter did not, however, improve the selectivity to MA by giving alkenes. Its poor performance was attributed to the poor conversion of the precursor phase to give the catalytically active $(VO)_2P_2O_7$ phase.

A common feature of the VPO catalysts that gave good activity and selectivity was a P:V ratio of ~1. This ratio indicated that the $(VO)_2P_2O_7$ phase was the dominant phase, and was confirmed from XRD patterns of used catalysts. The molar P:V ratio obtained for the Co-VPO catalyst (precipitation/deposition) via ICP-AES and EDX analyses was approximately half that of the unpromoted and Co-VPO catalysts (co-precipitation). This indicated that there was a loss of phosphorous from the catalysts when the promoter was impregnated. The decomposition of the $VOHPO_4 \cdot 0.5H_2O$ phase with the impregnation technique was confirmed by the decrease in P:V ratio and higher promoter/vanadium ratios than theoretical values, moreover, the impregnation technique gave a catalyst deficient in vanadium compared to an unpromoted catalyst (Section 4.1.4). The P:V ratio was related to the phase composition of the catalyst, which influenced the redox properties of the catalyst. The phases present in the used catalysts included $VOPO_4$ and $(VO)_2P_2O_7$ which had theoretical P:V ratios of 1. A P:V ratio above or below 1 suggested segregation of the phosphate and vanadate phases in the catalyst.

According to Zazhigalov, V.A. *et al.* (1993), a molar Co:V % in the region of 20 and higher causes segregation of cobalt from the catalyst framework on the surface and gives rise to lower selectivities by catalysing total oxidation reactions. Both EDX and ICP-AES analyses of the 2.5 % (theoretical molar %) Co-VPO catalyst (precipitation/deposition) indicated an actual

molar % of Co:V higher than 13, which may have resulted in segregation of the cobalt on the catalyst surface. EDX, which is a point analysis, indicated regions with a Co:V ratio close to 0 thus suggesting segregation. This can, although not exclusively, explain the 100 % selectivity to carbon oxides obtained using an impregnation method.

For incorporated promoted catalysts, the P:V ratios were lower in Rh-VPO compared to Co-VPO and lower than 1. Rh-VPO gave lower yields to MA than Co-VPO under similar reaction conditions (Figs. 4.65-4.66). The corollary to this is that higher selectivities to carbon oxides were obtained from a VPO catalyst having a P:V ratio lower than 1.

Gold was selected as a promoter since gold has become a topical metal in catalysis, but there was little literature on gold promotion of a catalyst for the activation of alkanes (Hazin, P.N. *et al.* U.S. Patent (2005), Shul'pin, G.B. *et al.* (2005)). Not all promoters may be incorporated into the VPO catalyst. The Au species needed to be easily reduced before being incorporated via a co-precipitation method. This technique failed in the preparation of a Au-VPO catalyst. Although energy dispersive X-ray (EDX) and inductively coupled plasma-atomic emission spectroscopy (ICP-AES) and inductively coupled plasma-mass spectrometry (ICP-MS) analyses indicated the absence of gold in the co-precipitation catalysts (VPO-A and VPO-B), the addition of gold to the synthesis mixture modified the morphology of the catalyst.

The gold species may have been too large to be incorporated into the catalyst, however, these species hindered the formation of a single $VOHPO_4 \cdot 0.5H_2O$ catalyst precursor phase. The catalyst so obtained gave higher selectivities than a conventional unpromoted catalyst at similar conversions. Thus metal species present during the catalyst preparation may modify the catalyst's structure, giving better activity and selectivity, yet not be incorporated.

The V_4O_9 phase was present in the calcined VPO-A and VPO-B catalysts. This phase usually formed with the use of a weakly reducing solvent in the reduction step of the synthesis of the VPO catalyst according to Miyake, T. *et al.* (1995). The V_4O_9 phase formed from the $VOHPO_4 \cdot 0.5H_2O$ phase gave a rosette morphology, which was seen in the SEM image of VPO-A. Although the $VOHPO_4 \cdot 0.5H_2O$ phase was converted to the intermediate V_4O_9 phase to give

the catalytically active $(VO)_2P_2O_7$ phase, the morphology was different from the ideal open platelets of an unpromoted VPO catalyst which gave selective oxidation of *n*-butane to MA.

A novel gold impregnated VPO catalyst met the structural and phase composition requirements for a good performing VPO catalyst for the selective oxidation of *n*-butane to MA. It possessed the ideal $VOHPO_4 \cdot 0.5H_2O$ precursor phase, the platelet morphology and an average vanadium oxidation state between 4 and 5, however, it gave carbon oxides as the prime products. The decrease of carbon monoxide and increase in carbon dioxide production with increasing temperatures, suggested that the Au species present in the catalyst was responsible for overoxidation. Cationic and metallic gold in other catalysts are known to be efficient for the oxidation of CO to CO_2 (Bond, G.C. *et al.* (2000), Hutchings, G.J. *et al.* (2003)). At 400^oC, this gold impregnated catalyst gave a 100 % yield to CO_2 from the oxidation of *n*-butane.

FT-IR spectroscopy indicated that there was coordination between the Au species and the VPO catalyst. VPO can supply oxygen to the Au species, which successively oxidises the substrate. Once the Au is reduced in this way, the VPO catalyst has an abundance of activated oxygen to reoxidise the Au.

Gold phases could not be identified in the XRD patterns. The reason for this may be attributed to the small amounts present in the catalyst and poor sensitivity of the technique. Wolf, A. *et al.* (2002) reported that when a gold catalyst is synthesised via the precipitation/deposition method at a pH of 8, the gold particles become highly dispersed on the surface of the catalyst with particle sizes of between 2 and 5 nm and it would be difficult to detect such small particles via XRD.

The FT-IR pattern of this catalyst showed a band at 1400 cm^{-1} (attributed to the presence of a PO_3^- group), which was unique to catalysts prepared by the precipitation/deposition method (Section 4.1.2). The impregnation of gold onto the catalyst, however, gave interesting data on the phase composition of the catalyst. The distinct PO_3^- group identified via FT-IR and the V_4O_9 phase from XRD analysis suggested that there was segregation of phosphates and vanadates in the Au-VPO (precipitation/deposition) catalyst.

These segregated phases were present in catalysts which gave almost 100 % selectivity to carbon oxides.

The following mechanism, which was proposed by Bond, G.C. *et al.* (2000) for the oxidation of CO on gold particle surfaces, has been modified in this thesis to explain the high selectivity to carbon dioxide from *n*-butane oxidation over a VPO catalyst:

$$Au^0 + CO \longrightarrow Au^0 \ldots CO \qquad (5.1)$$

A carbon monoxide molecule from oxidation of an alkane is initially chemisorbed on the surface of a gold atom (equation 5.1).

An OH^- ion migrates from the support (which is the VPO catalyst in work carried out in this thesis) to a Au^{3+} ion creating an anion vacancy on the support (equation 5.2).

$$Au^{3+} + OH^- \longrightarrow Au^{2+} \ldots OH \qquad (5.2)$$

A carboxylate group forms (equation 5.3) from the combination of products from equations 5.1 and 5.2:

$$Au^0 \ldots CO + Au^{2+} \ldots OH \longrightarrow Au^{2+} \ldots COOH + Au^0 \qquad (5.3)$$

An oxygen molecule then occupies the anion vacancy (represented by Δ^- in equation 5.4) on the support (the VPO catalyst):

$$O_2 + \Delta^- \longrightarrow O_2^- \ldots \Delta^- \qquad (5.4)$$

The O_2^- occupying the anion vacancy (equation 5.4) in the support then oxidises the carboxylate group by abstracting a hydrogen atom, forming carbon dioxide and a hydroperoxide ion HO_2^- (equation 5.5):

$$Au^{2+} \ldots COOH + O_2^- \ldots \Delta^- \longrightarrow Au^{2+} + CO_2 + HO_2^- \ldots \Delta \qquad (5.5)$$

The hydroperoxide ion then oxidises a further carboxylate species forming another CO_2 molecule and restoring two hydroxyl ions to the VPO support surface:

$$Au^{2+} \ldots COOH + HO_2^- \ldots \Delta \longrightarrow Au^{2+} + CO_2 + 2\ OH^- + \Delta \qquad (5.6)$$

$$Au^{2+} + \Delta \longrightarrow Au^{3+} + \Delta^- \qquad (5.7)$$

The nett reaction is thus:

$$2\ CO + O_2 \longrightarrow 2\ CO_2 \qquad (5.8)$$

There were many factors that made impregnation of a promoter a poor method for improving the performance of a VPO catalyst compared to incorporation:

(i) The surface area of the catalyst was smaller with impregnation. These catalysts were usually less porous and less crystalline than co-precipitated catalysts seen from SEM and XRD data.

(ii) A platelet morphology was ideal for good selectivity to MA. The precipitation/deposition method did not give this morphology.

(iii) An ideal P:V ratio of ~1 (to confirm the presence of the active $(VO)_2P_2O_7$ catalytic phase) was not obtained, which was attributed to segregated P and V phases.

(iv) A high degree of overoxidation was generally noted from these catalysts using different promoters (The oxidation of *n*-butane gave 100 % selectivity to carbon oxides over a 250 to 500^{o}C temperature range), which was accompanied by degeneration of the $VOHPO_4{\cdot}0.5H_2O$ precursor phase giving separate vanadate and phosphate phases.

The incorporation of cobalt into VPO (2.5 theretical Co:V molar %) gave the best performing catalyst from all promoted catalysts tested for the oxidation of *n*-butane to MA. The highest yield obtained in work carried out in this thesis (45 %) was obtained at 275^{o}C, which was a cooler operating temperature than those reported in the literature (p. 269, Appendix).

The incorporation of the cobalt promoter in the VMgO catalyst did not enhance the surface area of the catalyst significantly, as it did with VPO, however, the promoter enhanced the activity of the catalyst. This increased activity was associated with higher selectivities to carbon oxides.

The sponge-like appearance of the Co-VMgO catalyst seen from SEM analysis contrasted to that of the corrugated surface of the unpromoted catalyst. This clearly showed a difference in morphology between the two catalysts, where XRD analysis did not.

The Co-VMgO catalysts gave more cracking than an unpromoted catalyst at similar conversions and temperatures higher than 500^{o}C from the oxidation of *n*-butane, suggesting that cobalt increased the bronsted acidity of the VMgO catalyst. The VPO catalyst was acidic by nature and the addition of a cobalt promoter did not significantly enhance the acidity to give higher selectivities to cracking.

The cobalt promoted and unpromoted VMgO catalysts had the same magnesium orthovanadate phases present and similar V:Mg molar ratios. The promoted catalyst gave increased selectivity to isomers of alkenes, which was beneficial for selective formation of cyclic products such as benzene from the oxidation of *n*-hexane, and styrene from the oxidation of *n*-octane.

It is proposed that oxidative dehydrogenation of a C_8 alkane gave C_8 alkenes, which subsequently cyclised to give ethylbenzene, which underwent further dehydrogenation over a VMgO catalyst giving styrene. This higher acidity of the promoted VMgO catalyst may contribute to longer retention of alkenes on the surface of the catalyst and hence cyclisation to give ethylbenzene and styrene. This was confirmed by higher yields of styrene obtained over the cobalt promoted catalyst.

5.3 Relationship between hydrocarbon chainlength and feed composition on selectivity

The VPO and VMgO catalysts gave good selectivity to MA and butenes, respectively, from C_4 oxidation, however, carbon oxides dominated the product profile from the oxidation of longer chainlength alkanes under the same reaction conditions (with selectivities higher than 30 %, Fig. 4.26).

Free radical reactions in the absence of catalysts were more significant with longer chainlength hydrocarbons at temperatures higher than 350^{o}C. The product profile also became

more complex (there were more products from C_6 and C_8 hydrocarbons compared to C_4). These many products from C_6 and C_8 oxidation can react with each other or the surface of the reactor or packing material (as with the homogeneous cyclisation of alkenes) at temperatures higher than 350^{o}C adding to the complexity of the product profile (Section 4.2.2).

Isomers of butene from the oxidation of *n*-butane did not cyclise easily due to the strained conformation of a C_4 ring, whilst the isomers of hexene and octene from *n*-hexane and *n*-octane oxidation, respectively, cyclised giving aromatic and cyclic products.

C_8 molecules underwent cyclisation and oxygen insertion in an empty reactor. Cyclisation without oxygen insertion was observed for C_6 molecules under similar operating conditions. The selectivity to these oxygenated products did not decrease with increasing temperature, thus indicating some complex free radical chemistry.

Longer chain length alkanes were also reactive at more sites on the chain due to the increasing number of reactive secondary substituted carbons that can react homogeneously. The relative rates of alkane oxidation should ideally follow the order *n*-butane < *n*-hexane < *n*-octane (Willock, D.J. (2005)). This order parallels the number of secondary substituted carbons present in the molecule that are more reactive than the terminal primary substituted carbons. The longer the alkane, the more secondary carbons were present for reaction and higher conversions were thus expected from *n*-octane. Carbon oxide formation is very demanding on oxygen and if there is a high selectivity to carbon oxides, there are more carbons in *n*-octane than shorter chain hydrocarbons. Thus the conversion for *n*-octane was lower for the similar molar ratio of alkane:O_2 (Table 4.24). Although carbon oxides are the dominant products from hydrocarbon oxidation, this does not exclude primary and secondary generated products becoming oxygen demanding and further limiting the conversion, resulting in a plateau in conversion with increasing temperature.

Conversion of *n*-hexane and *n*-octane was obtained at temperatures higher than 300^{o}C in carborundum-packed stainless steel reactors (in the absence of a catalyst). Besides temperature, another contributing factor to gas phase reactions was the reactant mixture

compositions relative to the flammability range. Feedstocks with compositions that were close to or fell within the flammability range were more likely to react homogeneously (Appendix, p. 255). This was observed from increased alkane conversion in a blank reactor for feed compositions close the flammability range under similar reaction conditions. The selectivity to carbon oxides increased as the feed composition approached the flammability region.

The feed composition affected selectivity. The selectivity to alkenes increased with increasing alkane:air ratios, however, the conversions decreased. Since C_6 and C_8 alkenes were intermediates to benzene and styrene, this ratio affected their selectivities, with higher alkane:air ratios giving higher selectivities to benzene and styrene.

Alkane:air ratios were related to over-oxidation products. At a similar operating temperature of 540^{o}C, 34 wt. % of V_2O_5 on MgO as the catalyst gave a yield of 10 % to isomers of butene, whilst the yield reported in the literature was 22 % (p. 273 in the Appendix). This was attributed to the oxygen richer environment employed in work carried out in this thesis (hydrocarbon:oxygen = 1:21) compared to the literature (hydrocarbon:oxygen = 1:2) which gave lower selectivities to carbon oxides and higher selectivities to isomers of butene.

The selectivity to C_2 and C_3 cracked products were more significant from C_6 and C_8 alkane oxidation than from a C_4 substrate under non-catalytic conditions. The activation energy to form C_2 and C_3 from a C_4 substrate is just less than twice of that to form a linear C_4 free radical species. So the C_4 molecule is more likely to give C_4 products. C_{3-4} cracked products and alkene isomers formed in the presence and absence of a catalyst from C_6 and C_8 oxidation. According to Gibbs free energy calculations, the formation of C_3 products is spontaneous from the oxidation of C_6 alkanes at temperatures around 400^{o}C (Section 1.3.1.6).

References

Albonetti, S., Cavani, F., Trifirò, F., Venturoli, P., Calestani, G., Granados, M.L., Fierro, J.L.G., J. Catal., **160**, 54 (1996)

Bond, G.C., Heterogeneous Catalysis: Principles and Applications, 2nd edition, Oxford University Press, p 9 (1987)

Busca, G., Cavani, F., Centi, G., Trifirò, F., J. Catal., **99**, 400 (1986)

Busca, G., Lorenzelli, V., Oliveri, G., Ramis, G., New Developments in Selective Oxidation II, p 253 (1994)

Cavani, F., Trifirò, F., Catal. Today, **51**, 565 (1999)

Centi, G., Trifirò, F., Catal. Today, **3**, 155 (1988)

Centi, G., Cavani, F., Trifirò, F., Selective Oxidation by Heterogeneous Catalysis, Kluwer Academic/ Plenum Publishers, p 26 (2001) Chang, W.S., Chen, Y.Z., Yang, B.L., Appl. Catal. A: General, **124**, 221 (1995)

Coulston, G.W., Simon, R.B., Kung, H., Birkeland, K., Bethke, G.K., Harlow, R., Herron, N., Lee, P.L., Science, **275**, 191 (1997)

Dietz III, A.G., Carlsson, A.F., Schmidt, L.D., J. Catal., 176, **459** (1996)

Ebner, J.R., Thompson, M.R., Catal. Today, **16**, 51 (1993)

Gao, X., Ruiz, P., Xin, Q., Guo, X., Delmon, B., J. Catal., **148**, 56 (1994)

Govender, N., A Comparative Study of VPO Catalysts in the Oxidation of Butane to Maleic Anhydride, Masters Thesis, University of Kwazulu-Natal, Howard College, Durban, p 27 (2002)

Govender, N., Friedrich, H.B., Janse van Vuuren, M., Catal. Today, **97**, 315 (2004)

Graselli, R., Burrington, J., J. Adv. Catal., **30**, 133 (1980)

Hazin, P.N., Galloway, F.M., Ledford, J.S., Nuyen, A.H., U.S. Patent application 20050137422 (2005)

Hoog, H., Herheus, J., Zuiderweg, F.J., Trans. Faraday Soc., **35**, 993 (1939)

Hutchings, G.J., Scurrell, M.S., Woodhouse, J.R., J. Chem. Soc., Chem. Commun., 254 (1988)

Hutchings, G.J., Scurrel, M.S., Cattech, **7**, 94 (2003)

Krummenacher, J.J., Schmidt, L.D., J. Catal., **222**, 429 (2004) Mallada, R., Sajip, S., Kiely, C.J., Menéndez, M., Santamaría, J., J. Catal., **196**, 3 (2000)

Kung, H.H., Kung, H.C., Appl. Catal., **157**, 106 (1997)

Mikovsky, R.J., Silvestri, A.J., Dempsey, E., Olson, D.H., J. Catal., **22**, 374 (1971)

Miyake, T., Doi, T., Appl. Catal. A: General, **131**, 43 (1995)

Norrish, R.G.W., Taylor, G.W., Proc. Roy. Soc., **A 234**, 160 (1956)

O'Connor, R.P., Schmidt, L.D., Chem. Eng. Sci., **55** 5693 (2000)

Pope, J.C., Dykstra, F.J., Graham, E., J. Amer. Chem. Soc., **51**, 2203 (1929)

Rossini, F.D., Selected Values of Properties of Hydrocarbons, U.S. Govt., Printing Office (1947)

Schmidt, L.D., Klein, E.J., Leclerc, C.A., Krummenacher, J.J., West, K.N., Chem. Eng. Sci., **58**, 1037 (2003)

Sheldon, R.A., Kochi, J.K., Metal-Catalysed Oxidations of Organic Compounds, Academic Press, New York (1981)

Shtern, V.A., The Gas Phase Oxidation of Hydrocarbons, Pergamon Press, London, p 79 (1964)

Shul'pin, G.B., Shilov, A.E., Süss-Fink, G., Tet. Lett., **42**, 7253 (2001)

Willock, D.J., Annu. Rep. Prog. Chem., Sect. B, **101**, 344 (2005)

Wolf, A., Schüth, F., Appl. Catal. A: General, **226**, 1 (2002)

Zazhigalov, V.A., Haber, J., Stoch, J., Pyatnitzkaya, A.I., Komashko, G.A., Belousov, V.M., Appl. Catal. A: General, **96**, 135 (1993)

CHAPTER 6

CONCLUSION

The oxidation of medium chainlength linear alkanes could proceed catalytically and non-catalytically (refering to reactions in the absence of a catalyst) in a continuous flow, fixed-bed micro-reactor at temperatures higher than 300^{o}C. Alkenes, which were products of both catalytic and non-catalytic oxidation processes, were intermediates in the oxidation of *n*-butane to MA, *n*-hexane to benzene and *n*-octane to styrene. The products from non-catalytic reactions could be combined with a catalytic process to give improved selectivities to these desired products.

The reaction conditions and the reactor configuration may be optimised for maximum selectivity to intermediates (obtained from combined catalytic and non-catalytic reactions) of a desired product. Non-catalytic reactions are related to the surface area and voids in a reactor and the reactor material. There was an optimum surface area:void volume ratio in the blank reactor to give the highest selectivities to alkenes from the oxidation of medium chainlength alkanes. Increasing the surface area:void volume ratio post catalyst also contributed to an improved selectivity. The carborundum particles limited cracking and carbon oxide production at temperatures lower than 400^{o}C, however, at temperatures higher than 400^{o}C, homogeneous reactions became significant. The homogeneous reactions gave mainly carbon oxides and cracked products as the surface area:void volume ratio decreased.

The location of these voids was important for selectivity to desired products. The optimal reactor setup to harness a catalytic and non-catalytic contribution to achieve the highest yields of benzene from *n*-hexane oxidation was to pack a catalyst (VMgO) at the entrance of the reactor and fill the remaining post-catalyst space in the reactor with carborundum. Catalyst dilution in combination with homogeneous reactions in the reactor also improved the selectivity to benzene. Thus, increasing the dilution of the VMgO catalyst with carborundum gave

decreasing selectivities to over-oxidation products with concurrent increasing selectivities to benzene from *n*-hexane oxidation when compared at similar operating temperatures.

One of the major challenges in the oxidation of medium chainlength alkanes was to limit the production of carbon oxides. It was found that in a free radical process, the generation of carbon oxides could be limited by maintaining the carbon to oxygen ratio larger than stoichiometric. The type of reactor material was also important in limiting the production of carbon oxides. Non-catalytic reactions occurred in both glass and steel reactors, usually at temperatures higher than 400^{o}C, however, alkenes were produced at lower temperatures and in higher selectivities in a glass than in a steel reactor. Secondary oxidation of alkenes and benzene gave carbon oxides. The selectivity to carbon oxides was limited in the glass reactor. The residence time of the substrate and the products could be used to control overoxidation. There was an optimum flowrate for the highest selectivity to alkenes and lowest selectivity to carbon oxides.

Selectivity in free radical homogeneous reactions, although generally considered to be uncontrollable in the literature, were shown to be controlled by residence time.

The type of promoter and its method of introduction into a catalyst determined the phases present in the VPO catalyst. These phases could be associated with selective or non-selective reactions. The active phase in the VPO catalyst was $(VO)_2P_2O_7$. Although this phase was always present in a used catalyst with the different methods and promoters employed, the precursor phases that were converted to give this phase were important in determining the selectivity of the catalyst. $VOHPO_4{\cdot}0.5H_2O$, $VOPO_4{\cdot}2H_2O$ and V_4O_9 were identified as precursor phases to this active phase, however, the most selective catalyst was obtained when the precursor contained a dominant $VOHPO_4{\cdot}0.5H_2O$ phase. Moreover, the poor conversion of $VOPO_4{\cdot}2H_2O$ and V_4O_9 phases to $(VO)_2P_2O_7$ gave poor selectivity.

Besides finding the suitable promoter and method of addition to enhance the selectivity of a VPO catalyst, the amount of promoter was important. The amount of promoter could

increase the surface area of the catalyst, however, beyond an optimum promoter loading there was a decrease in surface area.

The morphology of the catalyst was another determining factor for a selective catalyst. The addition of a promoter was a means of changing the morphology of the catalyst. The oxidation of *n*-butane to MA was used as a model reaction for the oxidation of medium chainlength alkanes (longer than C_4). The incorporation of cobalt into the VPO catalyst gave the ideal $VOHPO_4 \cdot 0.5H_2O$ precursor phase and ideal platelet morphology for the best selectivity in the oxidation of *n*-butane to MA.

There were a few other features of a selective VPO catalyst for the oxidation of *n*-butane to MA besides the phase composition and morphological features that were identified. The average vanadium oxidation states (AV) of the VPO catalyst could be used as an indicator of its over-oxidation capability. Catalysts having AV values around 5 gave higher selectivities to carbon oxides compared to catalysts with AV values lower than 5 and closer to 4. Another feature of a selective VPO catalyst was having a P:V ratio around 1.

The incorporation method of promoter addition to the VPO catalyst was superior to impregnation, which was attributed to morphology, precursor phase composition, P:V ratio and AV. Not having these ideal features gave a catalyst active in the oxidation of an alkane to carbon oxides over a 200-500^oC temperature range (as in the case of gold impregnated onto VPO).

Cobalt incorporated VPO catalysts performed poorly in the selective oxidation of C_6 and C_8 alkanes, with major selectivity to carbon oxides, cracked products and a number of cyclic and linear oxygenates. The cracking of *n*-octane gave butane, which was oxidised to MA over the VPO catalyst but in very low selectivity. The method of cracking a long chain hydrocarbon to give MA via butane was not viable, since the product distribution was complex and dominated by carbon oxides.

The less oxidising VMgO catalyst with an orthovanadate active phase ($Mg_3(VO_4)_2$) gave higher selectivities to alkenes/cyclic products from the oxidation of C_4, C_6 and C_8 alkanes.

The VMgO catalyst was selective in the oxidation of linear alkanes to alkenes and could thus be successfully combined with homogeneous reactions (also giving alkenes) to give a selective secondary product. Thus, isomers of hexene cyclise to give benzene and isomers of octene cyclise to give styrene. The selectivities to these cyclic products increased with increasing temperature because the intermediates to their formation were produced via free radical reactions, which became significant with increasing temperature. The cobalt promoter enhanced the oxidation of the linear alkane to alkenes, which enhanced the selectivity to these cyclic products. The oxidation of benzene was not catalytic and thus its selectivity was limited by the free radical reactions in the voids of the reactor.

The VMgO catalyst was more suited than VPO to C_6 and C_8 oxidation. The catalyst was more selective by giving less over-oxidation.

The product profile was related to the length of the hydrocarbon chain, with longer hydrocarbons giving more cracked products, which may in turn be oxidised, thus giving a complex product distribution. The number of secondary substituted carbons is higher for longer hydrocarbons thus contributing to the increased complexity of the product distribution.

The oxidation reaction of *n*-butane to MA over a VPO catalyst is selective, but the oxidation of longer alkanes over this catalyst gave poor selectivity to any one product. The location of active sites on the surface of the VPO catalyst may be ideal for activation and subsequent oxidation of *n*-butane via a concerted mechanism to MA and not ideally located for longer alkanes such as *n*-hexane and *n*-octane. These were probably too close together thus enabling multiple activation of carbon centres of the adsorbed substrate giving a wide product distribution, chiefly carbon oxides. The multiply activated substrate reacts homogeneously to give many products.

Cyclisation reactions usually find application in the petroleum industry. The aromatic compounds formed from the cyclisation and dehydrogenation of *n*-hexane and *n*-octane in work carried out in this thesis had higher octane ratings than the linear alkane substrates. The selective products from *n*-butane oxidation (MA), *n*-hexane oxidation (benzene, 2,5-

hexanedione and 2,5-dimethylfuran) and *n*-octane oxidation (ethylbenzene and styrene) added value to the alkane substrate. These products were generated from alkenes that were more reactive than the alkane substrate. Selectivities to alkenes from alkane oxidation were improved by a combination of catalytic and non-catalytic processes. A catalyst that is selective to alkenes, such as VMgO that can be combined with a non-catalytic process (which can be optimized for alkene generation by means of the type of reactor material, surface area:void volume ratio in the reactor, location of catalyst in the reactor, substrate to oxidant ratio and residence time) showed promise in improving the selectivity to a desired secondary product.

APPENDIX

XRD data

Instrument: Philips PW1130

Experimental conditions

X-Ray source	:	Cobalt	Used wavelength	:	K-Alpha
Voltage	:	40 kV	K-Alpha1 wavelength	:	1.78897
Amperage	:	25 mA	K-Alpha2 wavelength	:	1.79285
Divergence slit	:	1 °	K-Alpha wavelength	:	1.78897
Receiver slit	:	0.15 °	Step size	:	0.05 °2θ
Scan from	:	5 °2θ	Count between steps	:	2 seconds
Scan to	:	100 or 105 °2θ			

Unpromoted VPO (precursor)		2.5 % Co-VPO (co-precipitation) (precursor)		2.5 % Co-VPO (precipitation/deposition) (precursor)		2.5 % Co-VPO (co-precipitation) (used)	
2θ	Relative Intensity	2θ	Relative Intensity	2θ	Relative Intensity	2θ	Relative Intensity
13.41	1.17	13.82	1.36	7.53	14.52	13.63	18.99
17.51	11.72	15.80	3.39	11.58	12.47	14.69	2.31
18.31	14.16	16.24	7.31	15.01	51.80	16.41	8.35
21.47	5.39	17.51	10.59	28.66	3.08	17.99	2.90
22.78	12.88	18.11	12.13	30.14	17.83	21.49	11.81
25.09	1.60	21.47	5.16	34.07	33.22	26.69	40.63
28.26	13.81	22.79	9.97	44.89	23.08	33.20	100.00
31.62	22.65	25.85	4.93	52.28	100.00	34.96	51.51
33.51	11.27	28.08	9.97	53.73	4.28	36.34	2.94
35.45	100.00	28.90	10.56	58.93	11.77	39.44	14.09
37.40	10.80	30.72	5.78	77.24	22.89	43.06	12.54
39.19	5.93	31.45	18.44	80.51	3.48	44.92	5.04
40.13	6.63	32.76	14.44			49.18	17.34
43.69	11.17	33.40	10.55			50.73	24.33
44.90	2.66	33.80	6.39			52.29	12.98
47.34	5.26	35.44	100.00			55.13	2.72
49.69	1.85	36.73	8.77			58.23	9.54
51.64	4.08	37.55	24.01			66.41	5.79
52.33	5.95	40.09	6.06			68.15	4.42
54.46	2.71	42.20	2.34			69.21	14.30
56.05	6.91	43.73	13.48			74.10	3.86
57.57	13.43	44.85	2.24			74.70	6.27
		47.16	4.21			75.62	6.45
		50.38	3.91				
		51.43	2.04				
		52.35	6.13				
		53.05	1.78				
		54.40	2.93				
		56.23	7.47				
		57.55	13.89				

2.5 % Rh-VPO (co-precipitation) (precursor)		2.5 % Rh-VPO (precipitation/deposition) (precursor)		2.5 % Au-VPO (precipitation/deposition) (precursor)		VMgO precursor	
2θ	Relative Intensity	2θ	Relative Intensity	2θ	Relative Intensity	2θ	Relative Intensity
18.16	41.35	8.28	9.05	14.22	0.88	8.06	12.09
21.32	5.69	14.39	65.75	17.66	16.71	13.29	1.33
22.88	28.08	30.11	10.44	18.10	22.43	21.53	2.99
23.88	10.10	44.99	26.35	21.57	5.57	24.58	25.07
25.23	4.43	50.19	25.31	22.99	15.54	26.85	1.52
28.26	20.87	52.43	100.00	25.59	2.27	33.25	0.96
31.57	44.41	63.05	10.83	28.27	14.97	38.66	2.75
32.40	9.76	77.11	67.68	31.73	23.06	42.34	1.35
33.62	17.54			32.67	2.59	43.13	7.34
34.02	19.61			33.56	13.39	44.72	7.49
35.55	100.00			35.58	100.00	50.25	100.00
37.41	17.14			37.41	9.30	52.20	17.68
39.35	15.21			39.30	5.38	59.97	2.28
40.11	10.62			40.13	6.65	61.20	0.39
41.03	4.23			43.83	21.30	69.76	18.05
42.82	2.88			44.79	77.59	73.79	41.53
43.75	9.59			46.69	7.01	73.98	34.22
44.94	9.56			47.47	7.82	77.12	3.33
47.28	12.20			49.78	3.25	77.57	13.45
49.74	5.93			51.90	24.34	83.45	1.75
50.86	5.43			52.41	37.40		
52.31	32.40			54.57	4.99		
54.44	2.94			56.24	9.60		
56.17	13.86			57.77	18.33		
57.71	16.16			59.79	2.08		
57.91	17.84			69.98	4.87		
60.89	7.30			64.10	1.25		
62.89	2.32			65.54	4.11		
64.00	3.37			66.47	6.79		
65.73	6.55			68.02	3.04		
66.44	8.09			70.96	2.48		
67.31	5.92			72.24	2.37		
70.88	4.68			75.14	9.46		
				76.80	15.07		

VMgO (calcined)		2.5 % Co-VMgO (precursor)		2.5 % Co-VMgO (calcined)		2.5 % Co-VMgO (used)	
2θ	Relative Intensity	2θ	Relative Intensity	2θ	Relative Intensity	2θ	Relative Intensity
4.35	0.45	6.60	0.59	3.13	4.15	3.16	1.87
20.93	0.43	9.93	2.69	6.81	0.26	18.06	2.11
34.47	0.78	13.32	1.22	10.37	0.70	21.90	1.21
40.86	7.76	21.60	4.00	40.97	7.74	22.95	5.35
43.09	10.99	27.31	0.80	43.12	7.88	24.89	0.51
44.29	1.44	39.54	4.58	44.11	1.40	30.85	2.37
44.82	2.16	43.15	11.26	44.89	2.38	31.62	18.49
50.26	100.00	44.52	10.75	50.21	100.00	34.63	17.13
52.36	4.51	48.05	1.67	52.30	12.80	36.52	10.70
63.33	0.44	50.21	100.00	73.83	43.24	37.62	1.32
73.78	45.74	52.23	20.99	77.20	1.18	39.04	1.75
77.29	0.81	52.33	19.67			41.06	32.58
		59.80	2.18			42.05	16.89
		69.41	6.86			42.64	6.99
		70.01	9.79			43.18	11.08
		73.73	38.74			44.67	3.23
		77.18	1.20			49.35	2.60
		81.13	0.60			50.27	100.00
		89.51	5.55			50.94	16.78
						51.16	13.39
						52.32	6.51
						56.09	1.23
						57.55	0.59
						59.83	3.13
						61.58	1.63
						62.90	4.06
						64.34	1.07
						66.03	2.69
						67.24	2.78
						68.74	6.69
						69.53	2.36
						72.33	5.72
						73.87	47.36
						74.06	33.21
						74.93	23.71
						77.42	3.76
						81.41	0.48
						83.76	1.15
						87.35	2.57
						89.60	6.15
						89.86	3.95

VPO-A		VPO-B		$VOHPO_4 \cdot 0.5H_2O$ (literature) Bordes, E., Catal. Today, **1**, 511 (1987)		$VO(H_2PO_4)_2$ (literature) Bordes, E., Catal. Today, **1**, 511 (1987)	
2θ	Relative Intensity	2θ	Relative Intensity	2θ	Relative Intensity	2θ	Relative Intensity
18.18	26.25	17.59	9.22	17.44	3	16.1	m
21.50	3.34	18.40	8.60	18.00	100	25.8	s
22.93	24.23	21.54	5.58	21.37	2	28.8	s
25.34	3.18	23.03	7.48	22.76	40	30.6	m
28.22	18.97	28.26	9.02	25.20	5	32.6	s
31.59	32.58	31.66	13.73	27.76	23	34.8	m
33.51	13.30	33.57	7.91	31.39	32	36.6	s
35.53	100.00	35.50	100.00	33.26	18	42.0	m
37.41	13.84	37.61	6.62	35.00	35	44.1	w
39.42	9.85	40.20	4.94	37.20	10	45.3	vw
40.16	7.54	43.78	11.02	39.09	27	47.4	vw
40.95	2.44	44.67	68.09	39.88	7	50.2	m
42.90	2.07	47.35	3.85	40.69	5	52.7	w
43.76	10.53	49.62	2.50	42.60	6	53.0	w
47.33	5.90	52.09	25.01	43.53	4	54.2	vw
49.92	2.18	52.46	10.87	46.17	6	54.5	vw
52.06	16.53	54.52	2.61	47.04	5	55.8	w
52.35	14.07	56.18	5.44	47.50	2	56.9	vw
53.25	0.61	57.69	12.07	49.40	5	59.8	w
				51.46	4	60.8	w
				51.73	6	63.6	w
				54.01	1	63.9	m
				55.86	7	68.4	w
				56.84	3		
				57.51	9		
				57.85	8		
				59.27	2		

XRD band intensities are identified by s = strong, m = medium, w = weak and vw = very weak. The VPO catalyst precursors contained the $VOHPO_4 \cdot 0.5H_2O$ and $VO(H_2PO_4)_2$ phases which were assigned based on the literature (Bordes, E., Catal. Today, **1**, 511 (1987)).

FT-IR wavenumber assignments for the VPO catalyst [a,b,c]

Wavenumber/cm^{-1}	Vibration	Anion
1265, 1250, 1220	ν_{as}O-PO^-	cyclic $P_4O_{12}^{4-}$
1190, 1155, 1130	ν_sO-PO^-	cyclic $P_4O_{12}^{4-}$
	$\nu_{as}PO_3$	$P_2O_7^{4-}$
1080-1060	ν_sPO_3	$P_2O_7^{4-}$
1010	νV=O	
990, 945, 925	ν_{as}POP	$P_2O_7^{4-}$
		cyclic $P_4O_{12}^{4-}$
1340, 1285	ν_{as}O-PO^-	PO_3^-
825	ν_{as}POP	PO_3^-
745	ν_sPOP	$P_2O_7^{4-}$
795, 745, 680	ν_{as}O-PO^-	cyclic $P_4O_{12}^{4-}$
< 700	Deformation vibrations	

[a] Bordes, E., Courtine, P., J. Catal., **57**, 244 (1979)

[b] Brutovsky, M., Gerej, S., Vasilco, F., Gerejová, J., Collection Czechoslovak Chem. Commun., **47**, 1298 (1980)

[c] Busca, G., Cavani, F., Centi, G., Trifirò, F., J, Catal., **99**, 403 (1986)

TEM images of promoted VPO and VMgO catalysts and TEM-EDX data

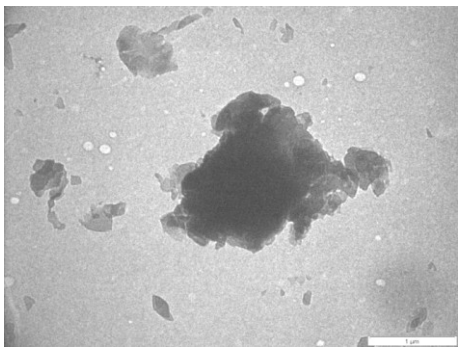

TEM of a 2.5 % Co-VPO catalyst (co-precipitation) – thick section

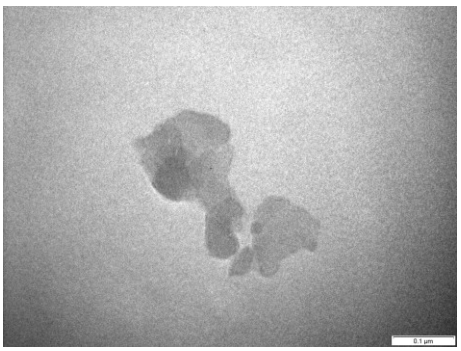

TEM of a 2.5 % Co-VPO catalyst (co-precipitation) – thin section

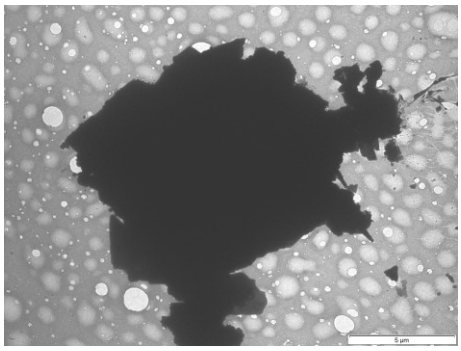

TEM of a 2.5 % Co-VPO catalyst (precipitation/deposition) – thick section

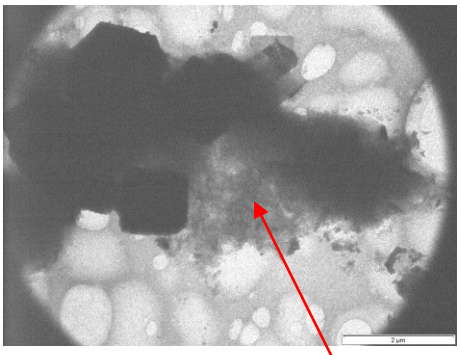

TEM of a 2.5 % Co-VPO catalyst (precipitation/deposition) – thin section

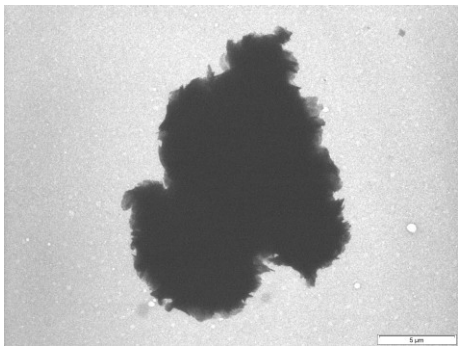

TEM of a 2.5 % Rh-VPO catalyst (co-precipitation) – thick section

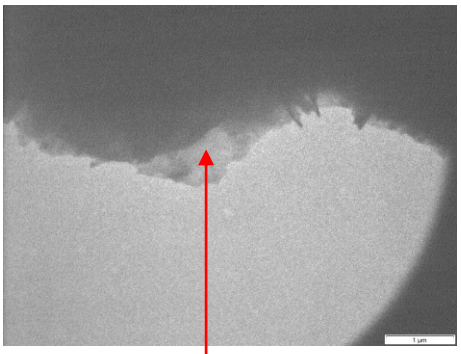

TEM of a 2.5 % Rh-VPO catalyst (co-precipitation) – thin section

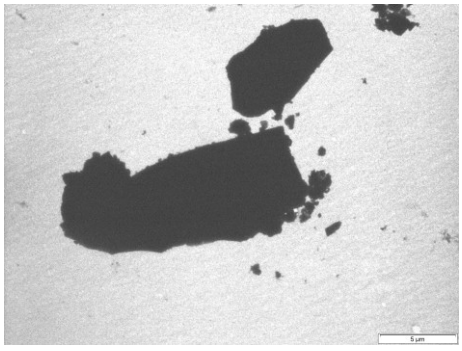

TEM of a 2.5 % Rh-VPO catalyst (precipitation/deposition) – thick section

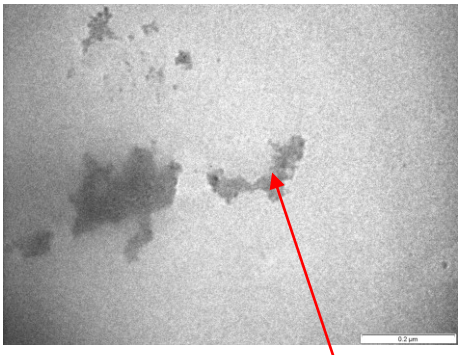

TEM of a 2.5 % Rh-VPO catalyst (precipitation/deposition) – thin section

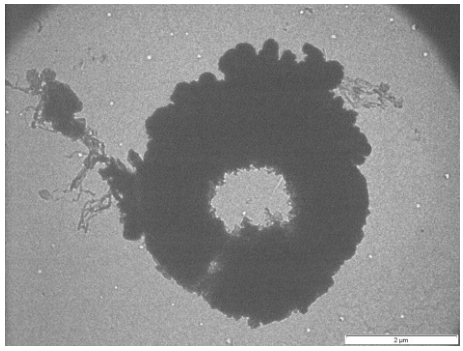

TEM of a 2.5 % Au-VPO catalyst (precipitation/deposition) – thick section

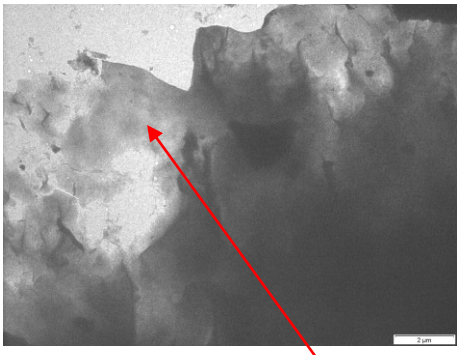

TEM of a 2.5 % Au-VPO catalyst (precipitation/deposition) – thin section

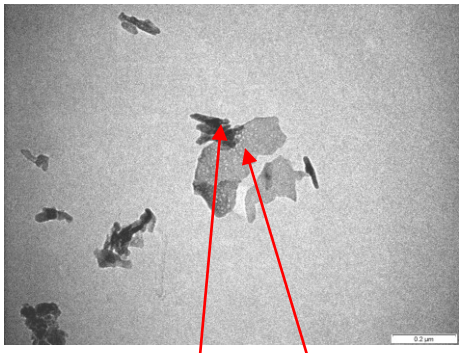

TEM of a 2.5 % Co-VMgO catalyst (co-precipitation) – thick and thin sections

Molar percentages of promoter:vanadium determined from transition electron microscopy-energy dispersive X-ray (TEM-EDX) analyses. The TEM images of the thin and thick sections referred to in the table appear above

Promoter loading (%)	Promoter	Catalyst	Promoter inclusion method	Promoter:vanadium %	
				Thin Section	Thick Section
2.5	Co	VPO	Co-precipitation	8	6
2.5	Co	VPO	Precipitation/deposition	22	4
2.5	Rh	VPO	Co-precipitation	5	4
2.5	Rh	VPO	Precipitation/deposition	12	7
2.5	Au	VPO	Precipitation/deposition	7	40
2.5	Au	VPO	Precipitation/deposition	1	24
2.5	Co	VMgO	Co-precipitation	7	3

GC column specifications

Specifications for columns used in the Varian 3700 isothermal GC (TCD)

Pre-column
Stainless steel

Support……Chromosorb WHPSP

Dimensions……..Length : 1 m

OD : 1/8”

ID : 2.2 mm

Mesh range……..80/100

Liquid phases……...OV-225 weight % 10

Temperature range……...20-275^{o}C

Analytical Column

Stainless steel

Support……Carboxen^{TM} 1000

Dimensions……..Length : 2.5 m

OD : 1/8”

ID : 2.2 mm

Mesh range……...60/80

Maximum temperature…….225^{o}C

Specifications for column used in the Perkin Elmer XL autosystem (FID)

Chrompak capillary column

Coating…….CP-Sil 24CB

Dimensions……..Length : 30 m

ID : 0.32 mm

OD : 0.45 mm

Maximum allowable Temperature……...225^{o}C

Specifications for column used in the HP 6890 GC-MS (SASOL)

Capillary column

Model Number…….HP 19091S – 001

HP-PONA Methyl Siloxane

Max. temp……....325°C

Nominal length…….....50.0 m

Nominal diameter…….....200.00 µm

Nominal film thickness……....0.50 µm

Mode…….....constant flow

Initial flow……...0.5 mL/min

Nominal initial pressure……..1.445 Bar

Average velocity…….……16 cm/sec

Outlet……..…….MS detector

Outlet pressure……..……...ambient

Specifications for column used in the Perkin Elmer XL Autosystem GC-MS (University of KwaZulu-Natal, Chemical Engineering Department)

Capillary column

ELITE 5 ms

Max. temp…….…...325°C

Nominal length……....30.0 m

Nominal diameter……....250.00 µm

Nominal film thickness……....0.25 µm

GC parameters

GC parameters for n-butane oxidation (TCD)

Isothermal Varian 3700 GC

Detector temperature……...…130^{o}C

Column temperature……....22^{o}C

Injector temperature……150^{o}C

TCD filament temperature……..…150^{o}C

Output……..…Negative

Range……...0.5 mV

Carrier gas: He (instrument grade), Supplier: Afrox

Perkin Elmer XL Autosystem GC (FID)

Detector temperature……...230^{o}C

Injector A…….....220^{o}C

Carrier A……..9.0 psig

Split flow ……50.2

Column temperature program for the Perkin Elmer XL Autosystem

Initial……70^{o}C Held : 1 minute

Setpoint ……...……200^{o}C Held : 2 minutes

Rate……..7^{o}C/minute

Carrier gas: Nitrogen (instrument grade), supplier: Afrox

Flame gases for FID: Hydrogen and air (instrument grade), supplier: Afrox

GC parameters for n-hexane and n-octane oxidation

Isothermal Varian 3700 GC

Detector temperature……...…130^{o}C

Column temperature……....22^{o}C

Injector temperature……....150^{o}C

TCD filament temperature……...…150^{o}C

Output……..…Negative

Range……...0.5 mV

Carrier gas: He (instrument grade), Supplier: Afrox

Perkin Elmer XL Autosystem GC

Detector temperature……...250^{o}C

Injector A…….220^{o}C

Carrier pressure program for Perkin Elmer XL Autosystem

Initial……2.0 psig Held : 8.00 minutes

Setpoint……5.0 psig Held : 999 minutes

Rate…….....1.0 psig/minute

Split flow ……50.2

Column temperature program for Perkin Elmer XL Autosystem

Initial…….……...……40^{o}C Held : 8 minutes

Setpoint ……...…210^{o}C Held : 2 minutes

Rate……..7^{o}C/minute

Carrier gas: Nitrogen (instrument grade), supplier: Afrox

Flame gases for FID: Hydrogen and air (instrument grade), supplier: Afrox

Control parameters on Perkin Elmer XL Autosystem GC for online sampling

Initial valve settings:

Valve 1: Split ON

Valve 2: Split OFF

Valve 3: GSV OFF

Valve 4: NONE

Valve 5: NONE

Valve 6: NONE

Timed Events:

Valve 2……set to OFF at 0.00 min

Valve 3 ……...set to OFF at 0.01 min

Valve 2……set to ON at 0.02 min

Valve 2……set to OFF at 0.08 min

Valve 3……set to ON at 0.60 min

Valve 3……set to OFF at 0.68 min

GC-MS parameters for HP 6890 (Sasol Technology Pty Ltd)

Detector……...…260^{o}C

Injector…..……....……250^{o}C

Carrier pressure……....…0.547 Bar Held : 999 minutes

Split flow ……..…49.9 ml min^{-1}

Column temperature program

Initial…….……...….55^{o}C Held : 2 minutes

Setpoint ……...….200^{o}C Held : 5 minutes

Rate……..10^{o}C/minute

GC-MS parameters for Perkin Elmer XL Autosystem GC-MS (University of KwaZulu-Natal, Chemical Engineering Department)

Detector……...…200^{o}C

Injector…..……....…280^{o}C

Carrier flowrate……...…1.00 ml min^{-1} Held : 999 minutes

Split flow ……....…50.0 ml min^{-1}

Column temperature program

Initial…….……...…40^{o}C Held : 8 minutes

Setpoint ……...…200^{o}C Held : 2 minutes

Rate……..7^{o}C/minute

Table of volumetric flowrates of feeds, catalyst volumes and gas hourly space velocities employed for catalyst investigations

Feed	Volume of catalyst (mL)	Flowrate of alkane in air mixture (mL min^{-1})	Flowrate of air (mL min^{-1})	Flowrate of alkane (HPLC pump) (mL min^{-1})	GHSV (hr^{-1})
n-Butane	1	50			3000
n-Hexane	1	25			1500
	1	50			3000
	1	100			6000
n-Octane	2		62	0.03	1990
	2		103	0.05	3307
	2		144	0.07	4641

Table of % (v/v) of feeds in air employed in the mechanistic investigation into the conversion of *n*-hexane to benzene

Compound	% (v/v) Compound in air
1-Hexene	8.5
cis-2-Hexene	6.9
trans-2-Hexene	7.2
1,3-Hexadiene	5.7
1,4-Hexadiene	5.4
1,5-Hexadiene	9.8
Cyclohexane	5.0
Cyclohexene	4.0
1,3-Cyclohexadiene	4.5
1,4-Cyclohexadiene	2.9

Table of lower flammability limits (lfl) and upper flammability limits (ufl) at atmospheric pressure and different temperatures for n-butane, n-hexane and n-octane in air

Feed	P (atm)	Temp. (°C)	lfl (%v/v)	ufl (%v/v)	% Feed in air used (v/v)
n-butane	1	25	1.8	8.4	1.0
	1	250	1.7	9.1	1.0
	1	300	1.5	9.8	1.0
	1	350	1.4	10.6	1.0
	1	400	1.3	11.4	1.0
	1	450	1.2	12.3	1.0
	1	500	1.1	13.3	1.0
	1	550	1.0	14.4	1.0
n-hexane	1	25	1.7	7.7	7.8
	1	300	1.6	8.3	7.8
	1	350	1.4	9.0	7.8
	1	400	1.3	9.7	7.8
	1	450	1.2	10.5	7.8
	1	500	1.1	11.3	7.8
	1	550	1.0	12.2	7.8
n-octane	1	25	1.0	6.5	7.3
	1	300	0.9	7.0	7.3
	1	350	0.8	7.6	7.3
	1	400	0.8	8.2	7.3
	1	450	0.7	8.8	7.3
	1	500	0.7	9.6	7.3
	1	550	0.6	10.3	7.3

Perry, R.H., Green, D.W., Perry's Chemical Engineers' Handbook, The McGraw Hill Companies, Section 26, p 54 (1999)

Typical GC traces and carbon mol balance calculations

GC traces from n-butane oxidation

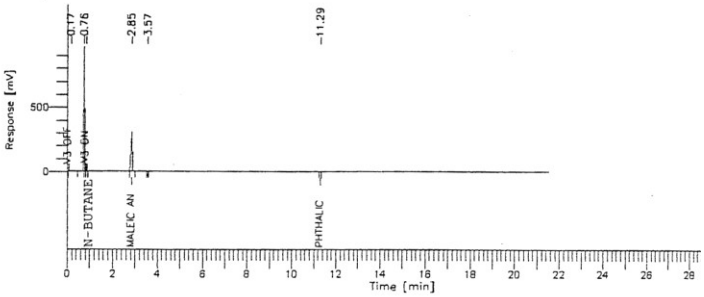

Report

Peak #	Time [min]	Component Name	Area [µV·s]	Area [%]	BL	Area/Height [s]	Amount of NBA ng\L
1	0.172		6260.92	0.30	BB	16.32	0.0063
2	0.755	**n-Butane**	961244.27	46.51	BB	0.93	0.9612
3	0.844	**Acetic acid**	30019.77	1.45	BB	0.95	0.0300
4	2.852	**Maleic anhydride**	1066140.68	51.58	BB	3.01	0.0001
5	3.570		1792.64	0.09	BB	2.50	0.0018
6	11.288	**Phthalic anhydride**	1337.20	0.06	BB	3.05	0.0001
			2066795.49	100.00			

GC trace from Perkin Elmer autosystem (FID) GC

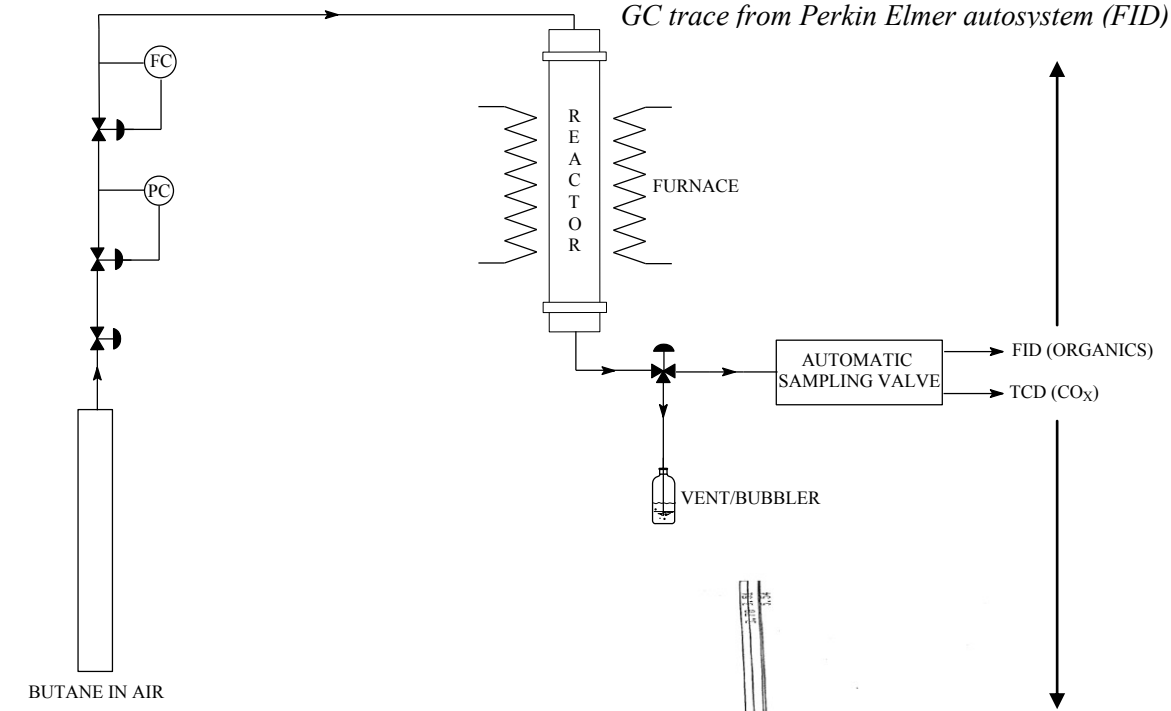

Reactor setup for n-butane feed

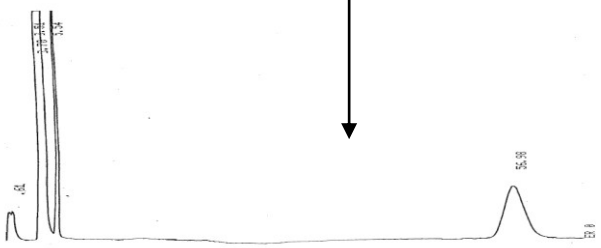

FILE 1.	METHOD 0.	RUN 7	INDEX 7	
PEAK#	AREA%	RT	AREA	BC
1	0.009	0.61	224	01
2	14.74	3.51	378856	02 OXYGEN
3	81.706	3.7	2100064	03 NITROGEN
4	1.352	5.54	34748	01 CARBON MONOXIDE
5	2.193	56.98	56368	01 CARBON DIOXIDE
TOTAL	100.		2570260	

GC trace from Varian 3700 (TCD) GC

n-Butane was fed into the reactor from a premix cylinder containing ~1 % *n*-butane in air (the actual % of *n*-butane in air was certified by the supplier). The feed was maintained at atmospheric pressure (which was monitored by a pressure gauge) and a certain flowrate (which was monitored by a rotameter). The products from the conversion of *n*-butane over the different catalysts (viz. maleic anhydride, isomers of butene, carbon oxides), including the *n*-butane feed, were calibrated on the gas chromatograph (GC) using standards. All products and unreacted feed from the reactor filled a 500 μL sample loop before being flushed to the GCs (one equipped with an FID (for the determination of organic components) and the other with a TCD (for the determination of carbon oxides)) (discussed in Section 4.3.1, Chapter 4). All the components in the outlet stream from the reactor were quantified on a carbon mol basis using calibration curves. The amounts of components were also based on the 500 μL sample loop that was maintained at 160^{o}C. The amount in moles of *n*-butane fed into the reactor was determined using the gas law equation where the volume was 500 uL. The total mols of feed into the reactor must equate to the total mols of unreacted feed and products out of the reactor based on carbon, which is illustrated in the equation below.

Carbon mol balance calculation for *n*-butane oxidation to maleic anhydride over a VPO catalyst:

$$n\text{-Butane feed} + O_2 \rightarrow \text{MA} + CO + CO_2 + \text{unreacted } n\text{-butane}$$

$$\text{i.e. 4 carbons} + 0 \text{ carbons} \rightarrow 4 \text{ carbons} + 1 \text{ carbon} + 1 \text{ carbon} + 4 \text{ carbons}$$

$$\% \text{ carbon mol balance} = \frac{n(\text{products}) \text{ X } 100}{n(\text{feed})} \qquad (n = \text{number of moles})$$

$$= \frac{[4 \text{ X } n\text{MA} + 1 \text{ X } n\text{CO} + 1 \text{ X } n\text{CO}_2 + 4 \text{ X } n(\text{unreacted } n\text{-butane})] \text{ X } 100}{4 \text{ X } n(n\text{-butane feed})}$$

GC traces from n-hexane oxidation

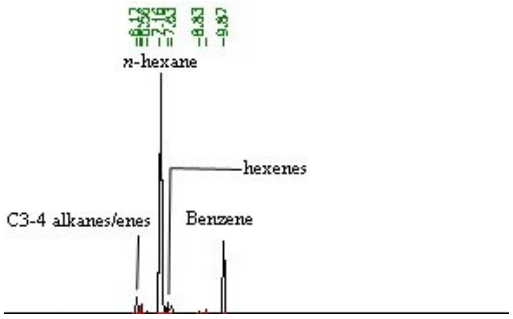

GC trace from Perkin Elmer autosystem (FID) GC (VMgO and VPO catalysts)

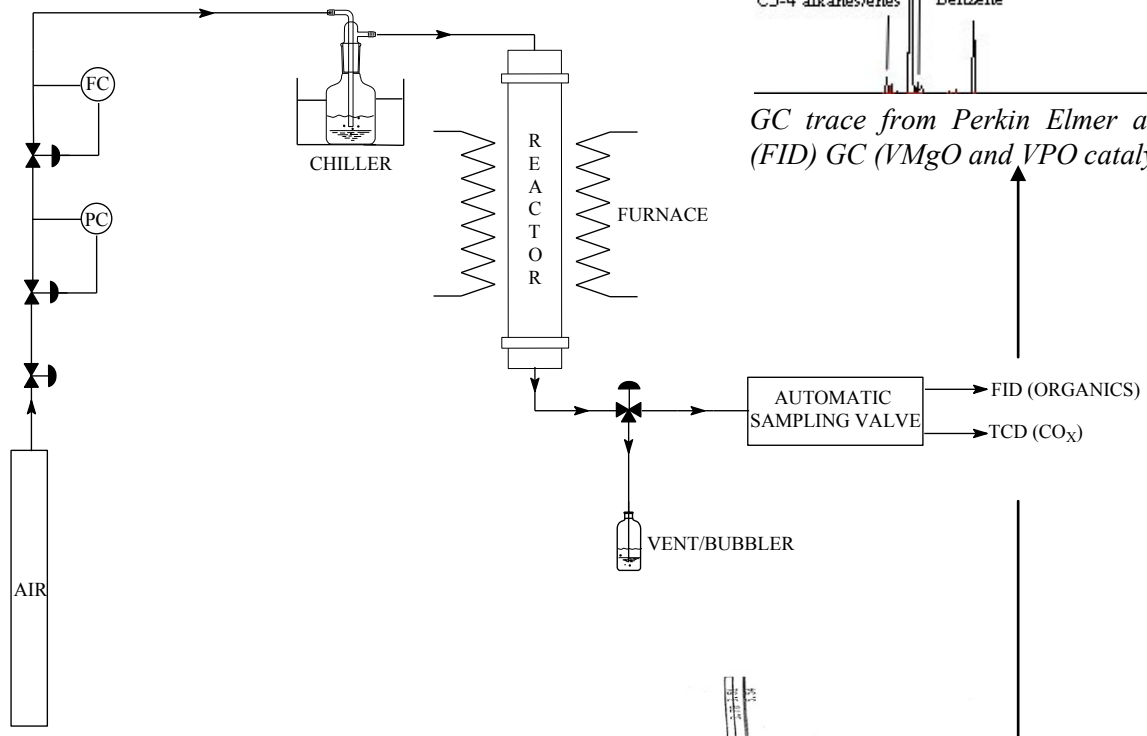

Reactor setup for n-hexane feed

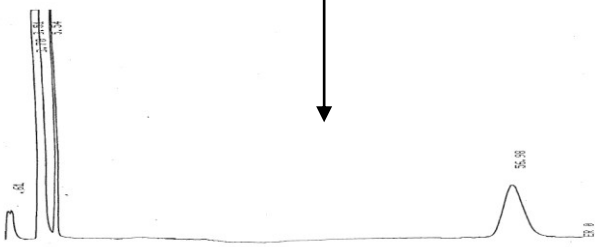

FILE 1. METHOD 0. RUN 7 INDEX 7

PEAK#	AREA%	RT	AREA	BC	
1	0.009	0.61	224	01	
2	14.74	3.51	378856	02	OXYGEN
3	81.706	3.7	2100064	03	NITROGEN
4	1.352	5.54	34748	01	CARBON MONOXIDE
5	2.193	56.98	56368	01	CARBON DIOXIDE
TOTAL	100.		2570260		

GC trace from Varian 3700 (TCD) GC

Air was bubbled into *n*-hexane maintained 5^{o}C in a bubbler, thus maintaining a vapour pressure of 0.079 bar and thus giving a 7.8 % (v/v) percentage of *n*-hexane in air mixture (discussed in Section 4.1.2, Chapter 4). The rest of the reactor system was the same as that of the *n*-butane system and hence the mass balances were calculated in a similar manner.

GC traces from n-octane oxidation

GC traces from the Perkin Elmer autosystem (FID) GC

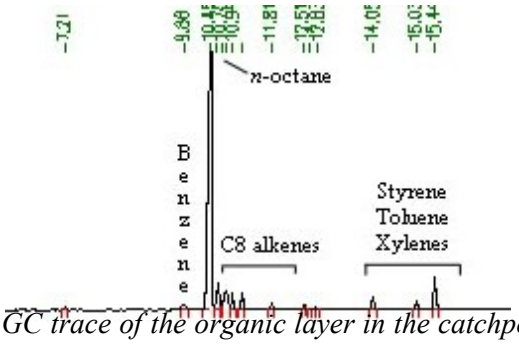

GC trace of the organic layer in the catchpot (VMgO and VPO catalyst, excludes styrene for the VPO catalyst)

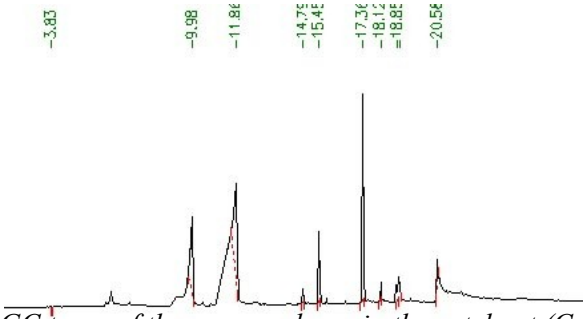

GC trace of the aqueous layer in the catchpot (Co-VPO catalyst (co-precipitation))

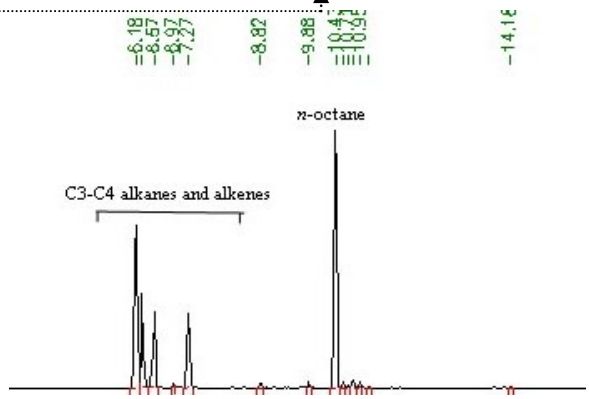

GC trace from the Perkin Elmer autosystem (FID) GC. Online sample showing slight stripping of n-octane from the catchpot

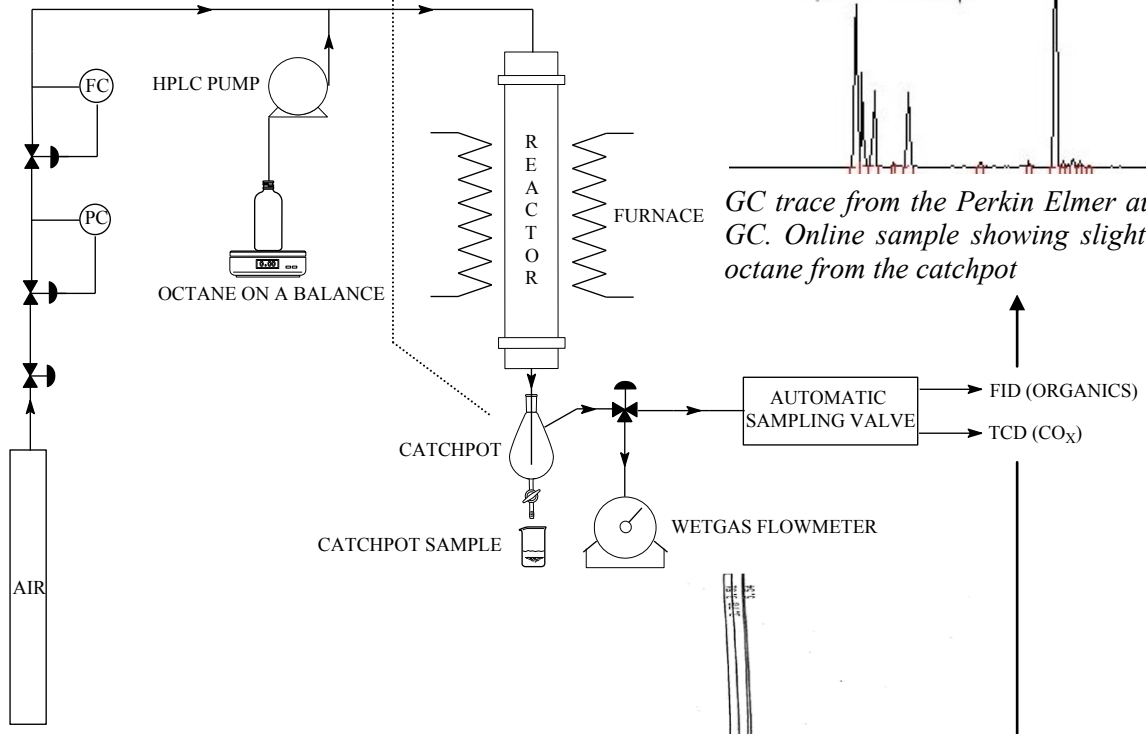

Reactor setup for n-octane feed

FILE 1. METHOD 0. RUN 7 INDEX 7

PEAK#	AREA%	RT	AREA	BC	
1	0.009	0.61	224	01	
2	14.74	3.51	378856	02	OXYGEN
3	81.706	3.7	2100064	03	NITROGEN
4	1.352	5.54	34748	01	CARBON MONOXIDE
5	2.193	56.98	56368	01	CARBON DIOXIDE
TOTAL	100.		2570260		

GC trace from the Varian 3700 (TCD) GC

n-Octane was introduced into the reactor via an HPLC pump. Air was fed into the system from a gas cylinder. The fuel to air ratio was maintained by controlling the flowrates of air and *n*-octane into the reactor. This is discussed in Section 4.1.3 of Chapter 4. The mass of *n*-octane fed into the system was recorded on a balance. The products from the reactor entered a catchpot which was cooled by wrapping copper tubing around the catchpot with water at 7^{o}C flowing through it. Organic and aqueous samples condensed in the catchpot. The water was produced from the oxidative dehydrogenation processes and combustion in the reactor. There was a negligible amount of products trapped in the aqueous layer. The organic layer, however, was composed of mainly unreacted octane, and contained the aromatics, alkenes and cracked liquid products from the reaction. The catchpot was periodically emptied and the masses of the organic and aqueous layers recorded. A sample of each layer was injected into the GC. There were many products and thus calibration of each component was time consuming so a method of using response factors was employed. The percentage areas obtained from the GC were a representation of the mass percent of the components in the organic sample.

Calculation of a response factor:

Three components A, B and C were made up in a volumetric flask with the following masses:

Respective masses of the components added to the volumetric flask

	Component A	Component B	Component C
Mass Component (g)	2	3	5

The mass percentages of the components were calculated:

Mass percentages of components in the volumetric flask (theoretical)

	Component A	Component B	Component C
Mass %	20	30	50

The mass percentages in the volumetric flask should be in theory proportional to the peak area percentages obtained from the GC, however, the mass percentages obtained from the GC vary due to unsaturated and oxygenated compounds. Alkanes have percentages close to the theoretical value, however, olefins have higher and oxygenates lower values.

Percentage areas of components obtained from the GC

	Component A	Component B	Component C
Peak area %	22	20	58

The response factor is calculated as follows:

$$\text{Response factor} = \frac{\text{actual mass percentage}}{\text{theoretical peak area percentage from GC}}$$

Calculated response factors

	Component A	Component B	Component C
Response factor	1.10	0.67	1.16

The peak area percentage of each component was multiplied by its respective response factor, which was either calculated as above or obtained from the literature. Once the peak area percentages were multiplied by their respective response factors, they were normalized to 100 %. Some components were not identified and were assigned an estimated molar mass and response factor and grouped. The normalized peak area percentages (corresponding to mass percentages) were multiplied by the mass of the organic layer obtained from the catchpot. The masses of the respective compounds in the catchpot were thus obtained. These masses were converted to mols of carbon by initially converting these masses to mols and subsequently

multiplying them by the number of carbons in the compound as performed in the example for *n*-butane to maleic anhydride oxidation.

The gaseous products exited the catchpot and entered a wetgas flowmeter. The wetgas flowmeter measured the total volume of gaseous products leaving the reactor. Carbon monoxide and carbon dioxide from an online 500 μL sample loop containing a gaseous sample from the reactor were quantified by a thermal conductivity detector (TCD). The total mols of carbon oxides were determined by scaling the amount in 500 μL up to the total gaseous volume recorded by the wetgas flowmeter.

The catchpot sample and wetgas volume were collected over the same time; hence the carbon mol balance is given by:

$$n_{\text{feed (balance)}} = n_{\text{catchpot (organic and aqueous phases)}} + n_{\text{organic gaseous products}} + n_{\text{CO (wetgas)}} + n_{\text{CO2 (wetgas)}}$$

Sample calculation of carbon mol balance for the reactor setup for n-octane oxidation

ONLINE ANALYSIS								Component →	Propane/ene	Butane/ene	Ethanal	Hexane/ene	Acetone	Benzene	Octane	1,3-Octadiene	3,5-Octadiene	Toluene			Styrene			
File	Date	CO	CO_2	CH_4	% CO	% CO_2	% CH_4	Retention Time →	6.182	6.302	6.576	7.17	7.281	9.92	10.442	10.619	10.729	10.84	10.96	11.148	15.458	Other	Total	PA octane
b133001d	17/08/2004 20:45	68823	345046	0	2.932	14.699	0	Peak area % from GC trace	14.2	5.9	4.94		3.87	4.37	47.34	2.68		2.70	1.36	1.25	1.57	9.82	90.18	192892
Calibration gradients		1.51E+11	1.89E+11			Response Factors			1.00	1.00	0.35	1.00	0.49	1.12	0.97	1.00	1.00	1.07	1.00	1.00	1.00	1.00		
Mol CO_x in 500uL sample		4.55E-07	1.83E-06			Peak area % X Response Factor			14.2	5.90	1.7	0.00	1.9	4.89	46	2.68	0	2.89	1.36	1.25	1.57	9.82	94.11	
						Normlisation to 1																		
						Peak area % X Response Factor / Total peak are			0.151	0.0627	0.018	0.000	0.020	0.0520	0.49	0.0285	0.000	0.0307	0.0145	0.0133	0.0167	0.104	1.00	
						Mass of other components in sample loop based on octane calibration						m from calibration curve →			1.0850E+10										
									5.50E-06	2.28E-06	6.7E-07	0.00E+00	7.3E-07	1.89E-06	1.8E-05	1.04E-06	0.00E+00	1.12E-06	5.27E-07	4.84E-07	6.08E-07	3.80E-06		
						Carbon number			3	4	2	6	2	6	8	8	8	7	8	8	8	8		
						Mm			44.0962	58.123	44.053	86.1766	58.0798	78.1134	114.2302	110.1986	110.1986	92.1402	100	100	104.151	100		
						Carbon mols of components			3.74E-07	1.57E-07	3.04E-08	0.00E+00	2.53E-08	1.46E-07	1.25E-06	7.53E-08	0.00E+00	8.50E-08	4.21E-08	3.87E-08	4.67E-08	3.04E-07		
			WETGAS																					
			File	Date	Initial Wetgas Volume	Final Wetgas Volume	Total Volume																Total mol (excluding CO_x)	
			r133001d	17/08/2004 08:25	15357.41	15476.31	118.9	Mol of components in Total v →	0.0889	0.0374	0.00723	0.000	0.00601	0.0346	0.296	0.0179	0.000	0.0202	0.0100	0.00921	0.0111	0.0723	0.611	

Total mol carbon oxides						Mol CO_x in 500uL sample loop		Mol CO_x in total volume		
File	Date	Initial Wetgas Volume	Final Wetgas Volume	Total Volume		CO	CO_2	CO	CO_2	Total COx
r133001d	17/08/2004 08:25	15357.41	15476.31	118.9		4.55E-07	1.83E-06	0.11	0.43	0.54

Sample calculation of carbon mol balance for the reactor setup for n-octane oxidation (continued)

OFFLINE ANALYSIS							Benzene	Octane	1,3-Octadiene	3,5-Octadiene	Toluene			Ethylbenzene		Styrene			
File	Date	Inlet Mass of Octane	Total Catchpot mass	Organic	Aqueous	Retention Time →	9.871	10.473	10.604	10.708	10.81	10.945	11.134	14.059	15.038	15.446	Other	Total	PA octane
r133001d	17/08/2004 08:25	39.38	36.3035	20.7192	15.5843	Peak area % from GC trace →	1.41	74.81	3.46	1.10									
		Response Factor					1.12	0.97	0.00	1.00	1.07	1.00	1.00	1.03	1.00	1.00	1.00	Total	
		Peak area % X Response Factor					1.58	73	0	1.10									
		Normlisation to 1																	
		Peak area % X Response Factor / Total peak area %					0.017	0.77	0.00	0.012									
		Mass % of component X Total organic mass from catchpot																Total	
							0.35	16	0	0.24									
		Carbon number					6	8	8	8	7	8	8	8	8	8	8		
		Mm					78.1134	114.23	110.1986	110.1986	92.1402	100	100	106.167	100	106.167	100	Total mol (catchpot) organic	
		Carbon mols of components					0.027	1.1	0.00	0.017									

CARBON MASS BALANCE						
Carbon number	8					
Mm	114.2302	Offline	Online			
Inlet Mass of Octane	Total mol in of Octane	Total mol (catchpot) organic	Total mol CO_x	Total mol (excluding CO_x)	Total mol out	Carbon mol balance/ %
39.38	2.758	1.49	0.543	0.611	2.64	95.8

Gas chromatography-mass spectrometry (GC-MS) trace of the aqueous layer from the catchpot from n-octane oxidation over a Co-VPO catalyst (co-precipitation)

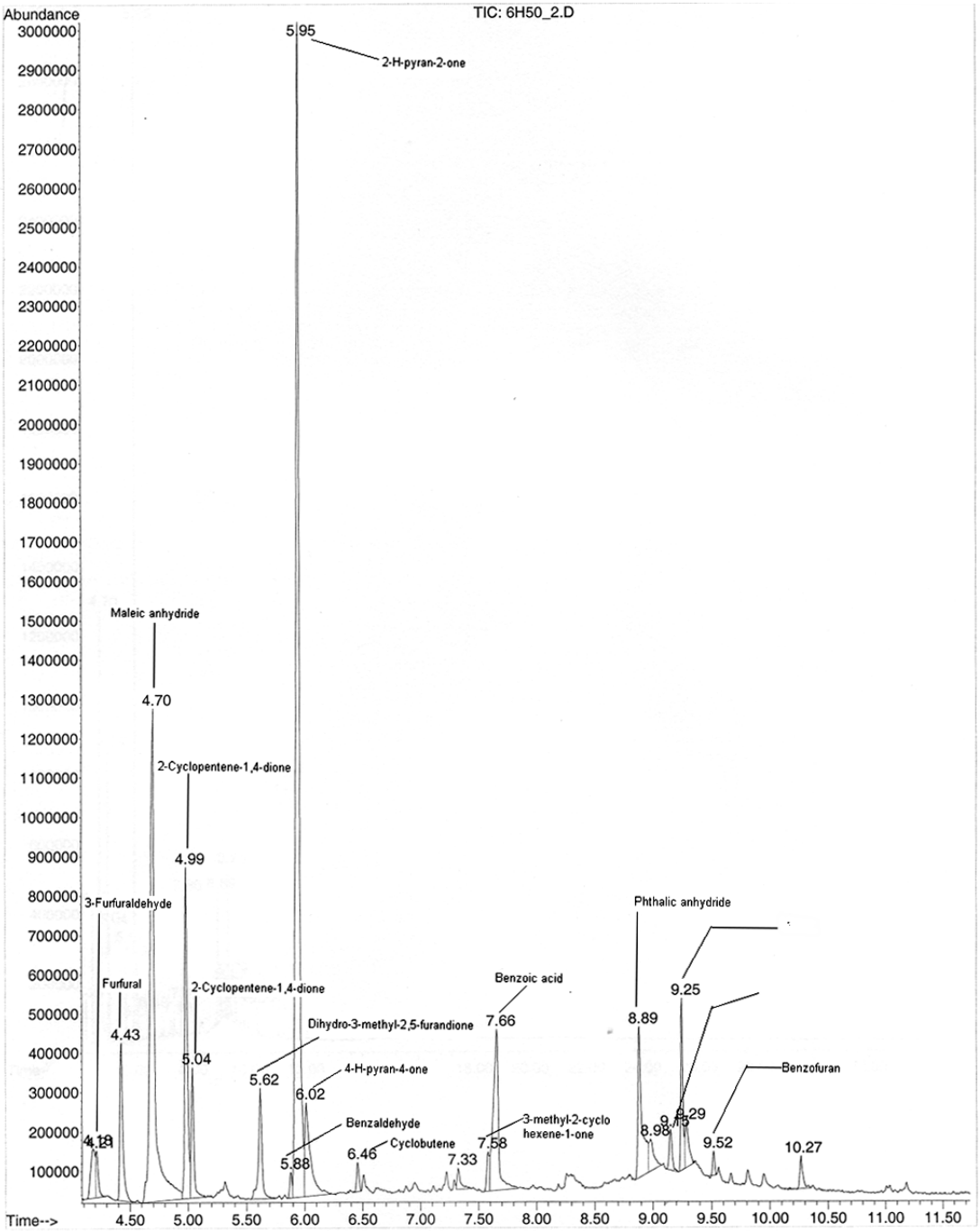

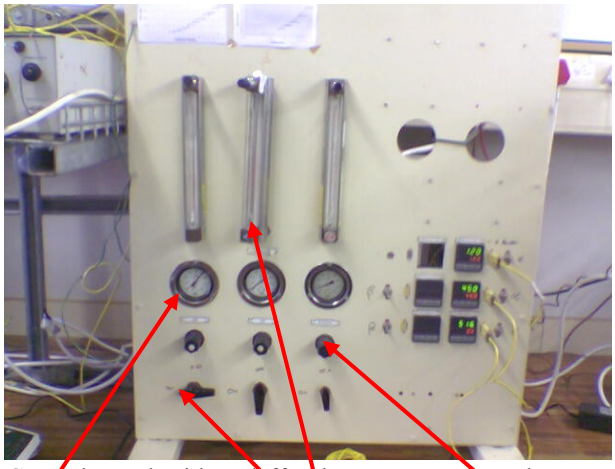

Control panel with on/off valves, pressure regulators, pressure gauges and rotometers regulating gas pressures and flowrates of feeds to the reactors. Digital displays of the temperature controllers also shown.

Chiller used to cool the *n*-hexane to 5°C, thus maintaining a vapour pressure of 0.079 bar to give a 7.8 % (v/v) of *n*-hexane in air mixture when air is bubbled through it.

High performance liquid chromatography (HPLC) pump used to feed liquid *n*-octane into an air stream preceding the reactor.

n-Octane placed on a balance. The HPLC pump draws the alkane from the bottle.

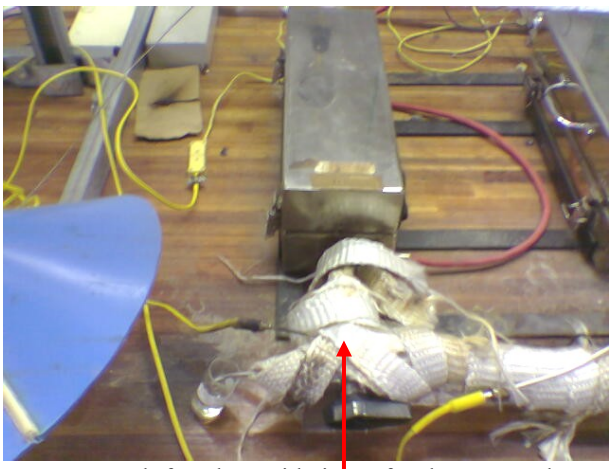

Reactor used for the oxidation of *n*-butane and *n*-hexane. The product stream lines were heated and insulated.

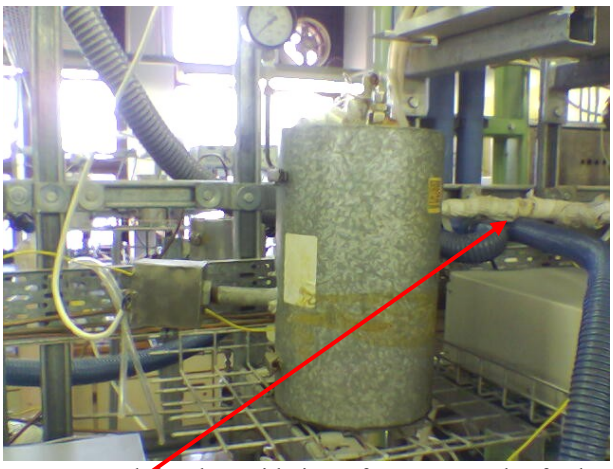

Reactor used for the oxidation of *n*-octane. The feed stream lines were heated and insulated.

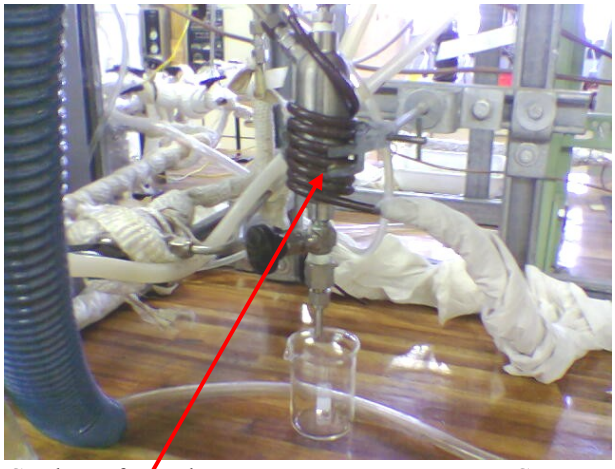

Catchpot from the *n*-octane reactor system. Copper cooling coils with water circulating at 5°C keeps the catchpot cool to condense products from the reactor.

Wetgas flowmeter used to record the total volume of gas collected per unit time.

Integrator linked to the Varian gas chromatograph (GC) used to quantify CO and CO_2.

6-port and 10-port Valco rotary valves containing two 500 µL sample loops which sample to the Perkin Elmer autosystem (equipped with an FID) and Varian GC (equipped with a TCD).

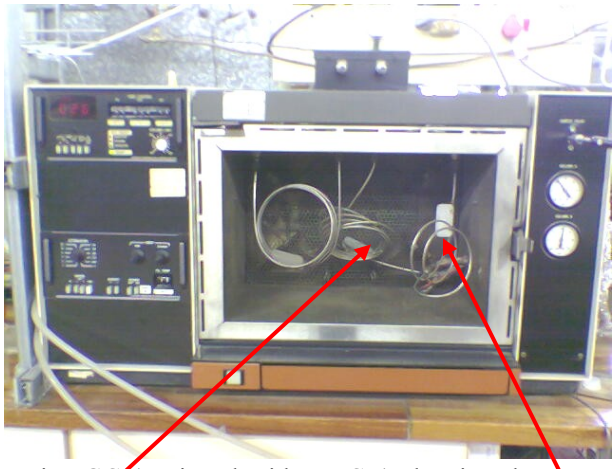

Varian GC (equipped with a TCD) showing the pre-column on the right hand side and the analytical column in the middle. Used for carbon oxide separation and quantification.

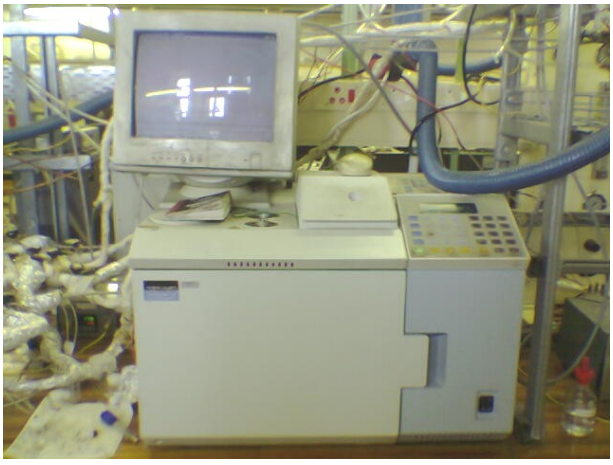

Perkin Elmer GC used to quantify the hydrocarbon products.

Description of vanadium-phosphorous-oxide catalyst phases

Structural characteristics of phases present in the vanadium-phosphorous oxide catalyst

Phase	*Structural characteristics*
β-$VOPO_4$	*Iso*-structural with *β*-$VOSO_4$ with vanadium in the +5 oxidation state. Features corner sharing distorted VO_6 octahedra.[1]
α_I-$VOPO_4$	*Iso*-structural with α-$VOSO_4$ with vanadium in the +5 oxidation state. Features corner sharing distorted VO_6 octahedra.[1]
α_{II}-$VOPO_4$	Similar structure to *α*-$VOPO_4$ with elongation along the a-axis due to trapped water.[1]
$(VO)_2P_2O_7$	Vanadium in the +4 oxidation state. Features edge-sharing VO_6 octahedra.[1]
β*-phase	Features vanadium in the +4 oxidation state. Transforms into *β*-$VOPO_4$ at 500°C and above.[1]
B'-phase	Reported to be oxidized equivalent to the *β*-phase. Also postulated to feature vanadium in the +4 oxidation state.[1]
γ-$VOPO_4$, δ-$VOPO_4$	Polymorphic. Pairs of edge sharing octahedra with trans vanadyl oxygens alternatively unshared and shared with phosphate tetrahedra.[2]

[1] Hodnett, B.K., Catal. Rev. Sci. Eng., **27**, 390 (1985)
[2] Centi, G., Trifiró, F., Chem. Rev., **88**, 57 (1988)

Operating conditions, synthesis methods and results for cobalt promoted VPO catalysts for the oxidation of n-butane to maleic anhydride in this thesis and in the literature (highest reported yields)

Company	Reducing solvent/s	Synthetic route	*n*-Butane feedgas composition	Operating Temp. (°C)	Gas hourly space velocity (hr^{-1})	Molar surface P:V ratio	BET surface area ($m^2 g^{-1}$)	Molar % Co:V (bulk)	Co salt/introduction	% Conversion	% Yield	% Selectivity	Ref.
Academic	Isobutanol/ benzyl alcohol	Organic	1 % in air	275	2878	1.1	23	2.3	$Co(acac)_3$/ co-precipitation	61	45	73	1
Chevron	Isobutanol	Organic	1.50 % in air	380	-	-	-	-	-	-	57	-	2
US Patent	Aqueous HCl	Aqueous	1.50 % in air	420	6840	-	-	6.5	$CoCl_3$/ impregnation	95	59	62	3
Instituto de Investigaciones en Catalisis	Isobutanol/ benzyl alcohol	Organic	1.50 % in air	392	2500	2.6	-	7	Co acetate/ co-precipitation	74	29	39	4
Instituto de Investigaciones en Catalisis	Isobutanol/ benzyl alcohol	Organic	1.50 % in air	392	2500	3.6	-	13	Co acetate/ co-precipitation	50	28	56	4
Instituto de Investigaciones en Catalisis	Isobutanol/ benzyl alcohol	Organic	1.50 % in air	392	2500	3.7	42	13	Co acetate/ impregnation	85	30	35	4
Instituto de Investigaciones en Catalisis	Isobutanol/ benzyl alcohol	Organic	1.50 % in air	392	2500	3.8	42	19	Co acetate/ impregnation	80	30	37	4
Safarik University Kosice	Aqueous HCl	Aqueous	1 % in air	407	2520	1.2	-	20	-	32	16	50	5
Union Carbide (UCB)	Aqueous HCl	Aqueous	1.50 % in air	450	1893	1.14	-	19	-	-	55	-	6
Union Carbide (UCB)	Aqueous HCl	Aqueous	1.50 % in air	480	1893	1.14	-	10	-	-	45	-	6
Union Carbide (UCB)	Aqueous HCl	Aqueous	1.50 % in air	453	1893	1.1	-	25	-	-	43	-	6
Union Carbide (UCB)	Aqueous HCl	Aqueous	1.50 % in air	431	1439	1.14	-	19	-	-	46	-	6
Union Carbide (UCB)	Isobutanol	Organic	1.50 % in air	387	1028	1.14	20	20	-	90	59	66	6
Union Carbide (UCB)	Methanol	Organic	1.50 % in air	405	1028	1.14	-	20	-	-	60	-	6
Standard Oil Co. Ohio	Hexachlorobutadiene	Organic	1.1 % in air	437	1890	1.2	-	20	-	89	50	56	7
Institut de Recherched sur la Catalyse	Isobutanol	Organic	$C_4H_{10}/O_2/He$ = 1.5/18.5/80	430	1000	-	9.1	1	$Co(acac)_3$/ co-precipitation	60	48	80	8
Institut de Recherched sur la Catalyse	Isobutanol	Organic	1.50 % in air	430	2000	2.1	-	12.6	$Co(acac)_3$/ co-precipitation	51	12	23	9
Academic	Isobutanol	Organic	$C_4H_{10}/O_2/He$ = 1.6/18/80	400	1000	1.1	16	1	$Co(acac)_3$/ co-precipitation	25	18	71	10
Academic	Isobutanol	Organic	$C_4H_{10}/O_2/He$ = 1.6/18/81	400	1000	1.1	16	5	$Co(acac)_3$/ co-precipitation	25	16	62	10

References for preceding Table of operating conditions, synthesis methods and results for cobalt promoted VPO catalysts for the oxidation of n-butane to maleic anhydride

1. Govender, N., Friedrich, H.B., Janse van Vuuren, M., Catal. Today, **97**, 321 (2004)
2. Schneider, R.A., U.S. Patent 4,043,943 (1977), assigned to Chevron Research Co.
3. U.S. Patent 4,209,423 (1980)
4. Cornaglia, L.M., Carrar, C.R., Petunchi, J.O., Lombardo, E.A., Appl. Catal. A: General, **183**, 177-187 (1999)
5. Brutovsky, M., Gerej, S., Coll. Czech. Chem. Commun., **47**, 406 (1983)
6. Lemal, R., Vekemans, J., U.S. Patent 3,987,063 (1976) assigned to UCB
7. Lemanski, M.F., Bremer, N.J., Milberger, E.C., U.S. Patent, 4,293,498 (1981), assigned to Standard Oil Co. Ohio
8. Sananés-Schulz, M.T., Tuel, A., Hutchings, G.J., Volta, J.C., J. Catal., **166**, 388-392 (1997)
9. Ben Abdelouahab, F., Olier, R., Ziyad, M., Volta, J.C., J. Catal., **157**, 687-697 (1995)
10. Sajip, S., Bartley, J.K., Burrows, A., Sananés-Schulz, M.T., Tuel, A., Volta, J.C., Kiely, C.J., Hutchings, G.J., New J. Catal., **25**, 125-130 (2001)

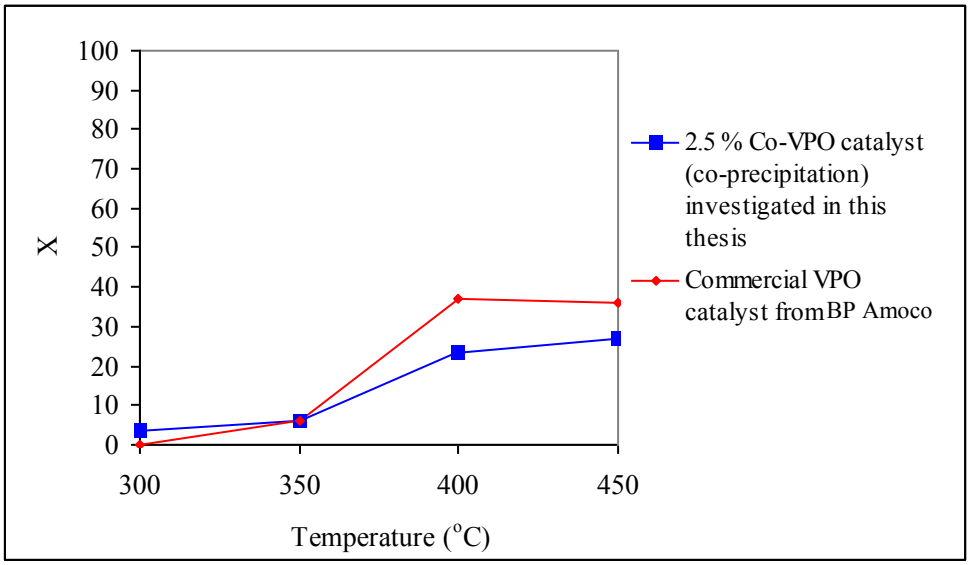

Conversion vs. temperature curves for the oxidation of n-octane on a Co-VPO catalyst (co-precipitation) investigated in this thesis and a commercial VPO catalyst synthesized by BP Amoco

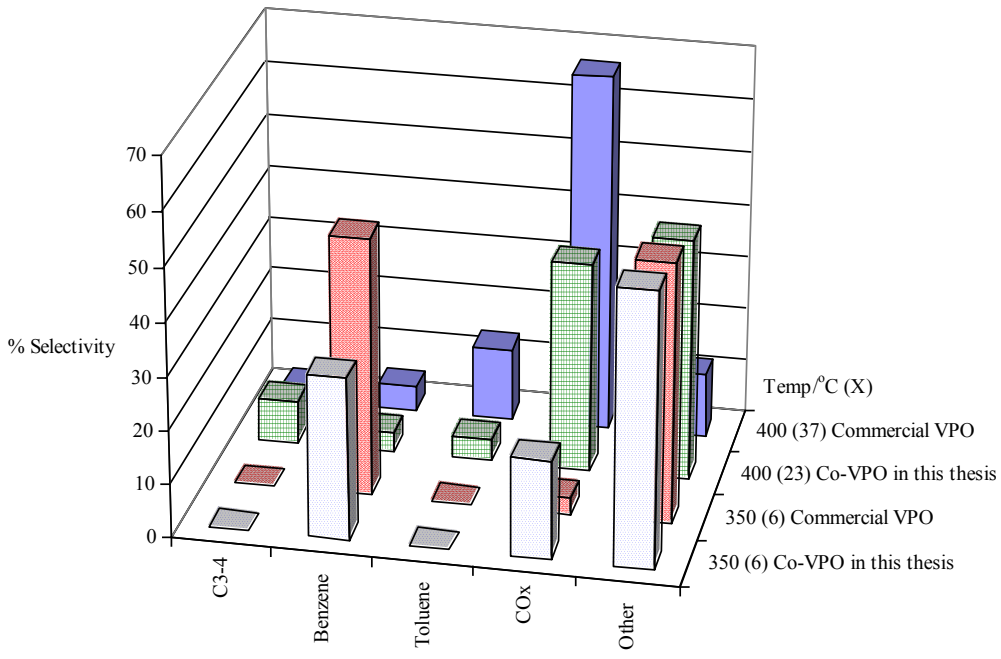

A comparison of the selectivity to some major products obtained from the oxidation of n-octane on a Co-VPO catalyst (co-precipitation) investigated in this thesis and a commercial VPO catalyst synthesized by BP Amoco. The catalysts were compared at 350°C and 400°C with the conversions obtained at these temperatures shown within brackets

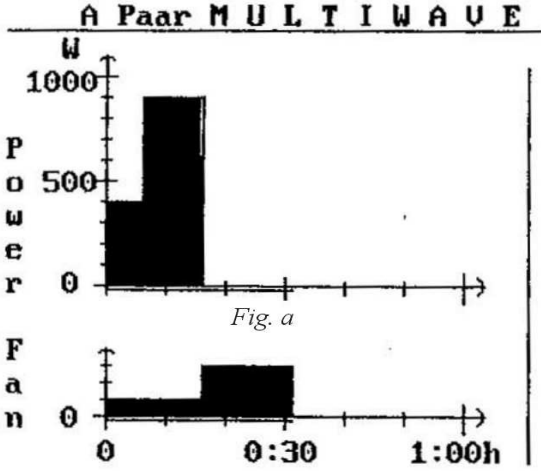

Fig. a

Fig. b

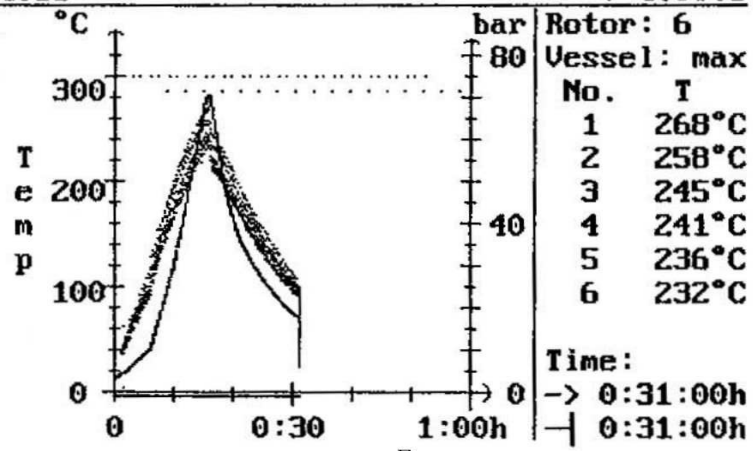

Fig. c

Fig. a is a graph of the power supplied to the microwave vs time. Fig. b is a graph of the power supplied to the fan in the microwave vs time. Six samples were digested at a time in separate vessels. The temperature in each vessel is shown in Fig. c which is a graph of temperature in each vessel vs time. The digestion time was 31 minutes.

Power W	Time mm:ss
400	6:00
900	10:00
0	15:00
0	0:00
0	0:00
0	0:00
0	0:00
0	0:00

Table 1

Ves	Weight max /g	Reag 1 /ml HCl	Reag 2 /ml HNO_3	Reag 3 /ml	Remark
1	0.100	3.50	1.50		
2	0.100	3.50	1.50		
3	0.100	3.50	1.50		
4	0.100	3.50	1.50		
5	0.100	3.50	1.50		
6	0.100	3.50	1.50		

Table 2

Table 1 shows the power supplied to the microwave over the digestion period. Table 2 shows the amounts of reagents the were added to the samples in the Anton Paar microwave digestion vessels containing the catalyst samples.

Comparison of results obtained from the literature to results obtained from work carried out in this thesis for n-butane oxidation over a VMgO catalyst

Feed	Catalyst	wt % V_2O_5/MgO	Temp. (°C)	X	% S Butenes	Cyclohexene	Benzene	Reference
1 % *n*-Butane in air	orthovanadate VMgO	34	500	12	40			This thesis
1 % *n*-Butane in air	orthovanadate VMgO	34	545	59	17			This thesis
n-Butane	orthovanadate VMgO	40	540	9	66			Kung, H.H., Kung, M.C., Appl. Catal., A: General, **157**, 117 (1997)
n-Butane	orthovanadate VMgO	20	500	10	59			Blasco, T.,López Nieto, J.M., Appl. Catal., A: General, **157**, 134 (1997)
n-Butane	orthovanadate VMgO	20	540	40	50			Blasco, T.,López Nieto, J.M., Appl. Catal., A: General, **157**, 134 (1997)
n-Butane	orthovanadate VMgO	5		59	22			Vidal-Michel, R., Hohn, K.L., J. Catal., **221**, 133 (2004)
n-Butane	orthovanadate VMgO	15		53	25			Vidal-Michel, R., Hohn, K.L., J. Catal., **221**, 133 (2004)
n-Butane	orthovanadate VMgO	25		62	26			Vidal-Michel, R., Hohn, K.L., J. Catal., **221**, 133 (2004)
4 % *n*-Butane, 8 % O_2 in He	0.3 g VMgO dil.with 2 X SiO_2	3	540	36	13			Chaar, M., Patel, D., Kung, M.C., Kung, H.H., J. Catal., **105**, 489 (1987)
4 % *n*-Butane, 8 % O_2 in He	0.3 g VMgO dil.with 2 X SiO_2	8	540	51	32			Chaar, M., Patel, D., Kung, M.C., Kung, H.H., J. Catal., **105**, 489 (1987)
4 % *n*-Butane, 8 % O_2 in He	0.3 g VMgO dil.with 2 X SiO_2	19	540	59	49			Chaar, M., Patel, D., Kung, M.C., Kung, H.H., J. Catal., **105**, 489 (1987)
4 % *n*-Butane, 8 % O_2 in He	0.1 g VMgO dil.with 2 X SiO_2	19	540	34	56			Chaar, M., Patel, D., Kung, M.C., Kung, H.H., J. Catal., **105**, 489 (1987)
4 % *n*-Butane, 8 % O_2 in He	0.1 g VMgO dil.with 2 X SiO_2	25	540	56	50			Chaar, M., Patel, D., Kung, M.C., Kung, H.H., J. Catal., **105**, 489 (1987)
4 % *n*-Butane, 8 % O_2 in He	0.1 g VMgO dil.with 2 X SiO_2	35	540	42	52			Chaar, M., Patel, D., Kung, M.C., Kung, H.H., J. Catal., **105**, 489 (1987)
4 % *n*-Butane, 8 % O_2 in He	0.1 g VMgO dil.with 2 X SiO_2	54	540	31	54			Chaar, M., Patel, D., Kung, M.C., Kung, H.H., J. Catal., **105**, 489 (1987)
n-Butane	orthovanadate VMgO	24	500	12	73			Bhattacharya, D., Bej, S.K., Rao, M.S., Appl. Catal. A: General, 87, 38 (1992)
n-Butane	orthovanadate VMgO	40		27	61			Kung, M.C., Kung, H.H., J. Catal., **134**, 668 (1992)
n-Butane	orthovanadate VMgO + 1 wt % K	40		20	53			Kung, M.C., Kung, H.H., J. Catal., **134**, 668 (1992)
n-Butane	orthovanadate VMgO	40	475	4	69			Michalakos, P.M., Kung, M.C., Jahan, I., Kung, H.H., J. Catal., **140**, 231 (1993)
n-Butane	orthovanadate VMgO	40	500	8	68			Michalakos, P.M., Kung, M.C., Jahan, I., Kung, H.H., J. Catal., **140**, 231 (1993)
Cyclohexane	orthovanadate VMgO	40	484	8		47	36	Michalakos, P.M., Kung, M.C., Jahan, I., Kung, H.H., J. Catal., **140**, 231 (1993)
Cyclohexane	orthovanadate VMgO	40	484	11		44	41	Michalakos, P.M., Kung, M.C., Jahan, I., Kung, H.H., J. Catal., **140**, 231 (1993)
Cyclohexane	orthovanadate VMgO	40	484	21		27	54	Michalakos, P.M., Kung, M.C., Jahan, I., Kung, H.H., J. Catal., **140**, 231 (1993)

Maleic anhydride safety data [3,4]

1. Product identification

Synonyms: cis-Butenedioic anhydride, 2,5-furandione, toxilic anhydride

Molecular weight: 98.06 g mol^{-1}

Chemical formula: $C_4H_2O_3$

2. Hazards identification

Corrosive substance. Causes burns to skin and eyes. May cause irritation and/or allergic reaction in the respiratory tract. Melted material causes thermal burns. May be harmful if swallowed.

Potential health effects

Inhalation:

Inhalation of the dust or vapor may cause irritation of the nose and throat. Coughing, sneezing and burning of the throat may be experienced. May cause allergic respiratory reactions.

Ingestion:

Corrosive. Toxic. Swallowing can cause sore throat, abdominal pain and vomiting. May cause burns to the digestive tract.

Skin contact:

Corrosive. May not cause immediate burning of the skin, but prolonged contact with moist skin may cause reddening and blistering or burns.

[3]Chemdat[R], The Merck Chemical Database, 2000
[4]http://www.jtbaker.com/msds/m0364.htm

Eye contact:

Corrosive. Dust or vapor causes burns or irritation of the eyes with swelling. Sensitivity to light and double vision may occur.

Chronic exposure:

Repeated inhalation may cause chronic bronchitis of the asthmatic type. Repeated skin contact may lead to dermatitis or sensitization.

3. First aid measures

Inhalation:

Move subject to fresh air. If not breathing, give artificial respiration. If breathing is difficult, give oxygen and call a physician.

Ingestion:

Induce vomiting immediately as directed by medical personnel. Never give anything by mouth to an unconscious person.

Skin contact:

In case of contact, immediately flush skin with plenty of soap and water for at least 15 minutes while removing contaminated clothing and shoes. Wash clothing before reuse. Call a physician immediately.

Eye contact:

Immediately flush eyes with plenty of water for at least 15 minutes, lifting lower and upper eyelids occasionally. Get medical attention immediately.

4. Fire fighting measures

Fire:

Flash point…….....102^{o}C

Auto-ignition temperature…….……..477^{o}C

Flammable limits in air (% (v/v): lower flammability limit = 1.4; upper flammability limit = 7.1

Explosion:

Above the flash point, vapor mixtures are explosive within the flammable limits noted above.

Fire extinguishing media:

Alcohol foam or carbon dioxide may be used to extinguish fires. DO NOT USE dry chemical, multipurpose dry chemical or loaded stream media because of explosion potential due to reactivity of basic compounds in these extinguishing media.

5. Physical and chemical properties

Appearance…….....White crystals

Odour……..……Sharp irritating acrid odour

Solubility……....16.3 g per 100ml water @ 25^{o}C, slowly hydrolyses

Specific gravity……..1.48

Boiling point……..….202^{o}C

Melting point…….…….53^{o}C

Vapor density (Air=1).....3.38

Vapour pressure (mm Hg)……..0.16 @ 20^{o}C

Description of instrumental techniques

1. Inductively coupled plasma-atomic emission spectroscopy (ICP-AES)

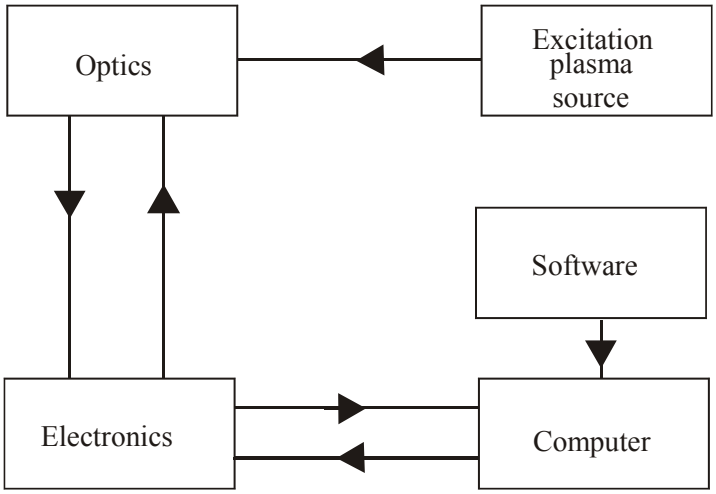

Fig. A1 Flow diagram of the standard configuration of an ICP-AES instrument

The inductively coupled plasma-atomic emission (ICP-AES) spectroscopic method of analysis is an essential tool in assaying elements as traces and in high concentrations. ICP-AES analysis involves introducing the elements to be analysed into an argon plasma induced by a high radio frequency (indicated by the "excitation plasma source" box in Fig. A1), where the temperature is in the order of 8000 K. The sample, in the form of an aerosol, is introduced into the plasma via a peristaltic pump and nebuliser (Fig. A2) where it is excited.

When the atoms of an element are excited, their electrons change orbitals by absorbing energy and emit light with a wavelength characteristic of each element when they return to their initial orbital. Each element can thus be characterized by its emission wavelength and they can be quantified by the intensity of light.

A plasma generator supplies the energy required to make the electrons change their atomic orbital. High frequency radiation is used to heat a stream of argon and to form plasma via an induction coil. The temperature varies between 5000 K and 10000 K (depending on the zone of the plasma). The sample added to the plasma is reduced to the state of individual atoms.

When the plasma excites these atoms, they re-emit the energy acquired in the form of electromagnetic radiation (light). This energy is composed of wavelengths characteristic of the elements present. The discrimination of these wavelengths is performed by an optical system called a monochromator represented by the optics box in Fig. A1. The beam of light is focused by a convergent lens onto the primary slit of the monochromator and then reaches a holographic diffraction grating. The grating separates the beam into the component lines of its different wavelengths corresponding to the elements in the analysed sample. In this system, the only moving component is the grating. Rotation about its axis sends all the wavelengths present onto the plane of the exit slit. A photomultiplier behind the exit slit receives this radiation and transforms it into electrical signals that are captured by the data processing system. Each angular position of the grating corresponds to a well-defined wavelength. Thus, each beam of light passing through the exit slit of the monochromator is characteristic of the element analysed.

The intensity of the light beam captured by the photomultiplier, represented by the electronics box in Fig. A1, is measured. It is proportional to the concentration of each element analysed by the data processing system represented by the computer and software boxes in Fig. A1. For a specific intensity, the computer system gives the concentration of the element analysed based on calibration curves.

1.1 The torch and ICP plasma generator

The sample is drawn into a capillary tube by means of a peristaltic pump (shown in Fig. A2) and is sent to the nebuliser, where a fog of fine droplets is formed. The fog is carried to the spray chamber before being transferred to the torch, where it is ionized.

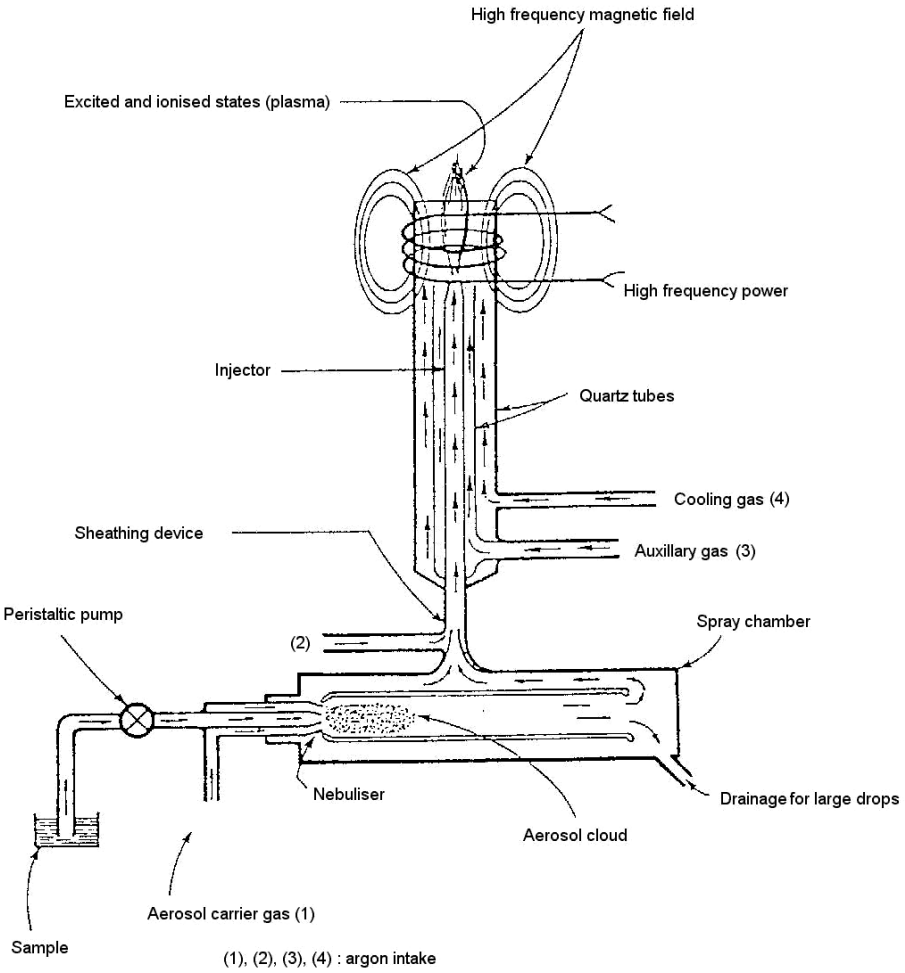

Fig. A2 Schematic view of the ICP source [5]

The ICP torch is formed from three concentric tubes, connected to the argon source of which two surrounds the central injector connected to the nebuliser via a sheathing system. The inlets (1) nebuliser and (2) coating gas are used for the formation, transport and injection of the aerosol into the plasma core, at the same time contributing to plasma generation.

There are two argon inlets to the torch itself: (3) for the auxillary gas in the case of organic samples and (4) for both cooling and supplying the plasma.

[5] Skoog, D.A., West, D.M., Holler, F.J., *Fundamentals of Analytical Chemistry*, 7th edition, Saunders College Publishing, p 632 Chapter 26 (1996)

2. Inductively coupled plasma-mass spectrometry (ICP-MS)

Another ICP instrument employed in this study was an inductively coupled plasma-mass spectrometer (ICP-MS) to determine the bulk elemental composition of the catalysts. The ICP-MS instrument employs a plasma (ICP) as the ionization source (as with ICP-AES) coupled with a mass spectrometer (MS) analyzer to detect the ions produced. It can simultaneously measure most elements in the periodic table and determine analyte concentration down to the sub nanogram-per-liter (ng/l) or parts-per trillion (ppt) level. It can perform qualitative and quantitative analyses, and since it employs a mass analyzer, it can also measure isotopic ratios.

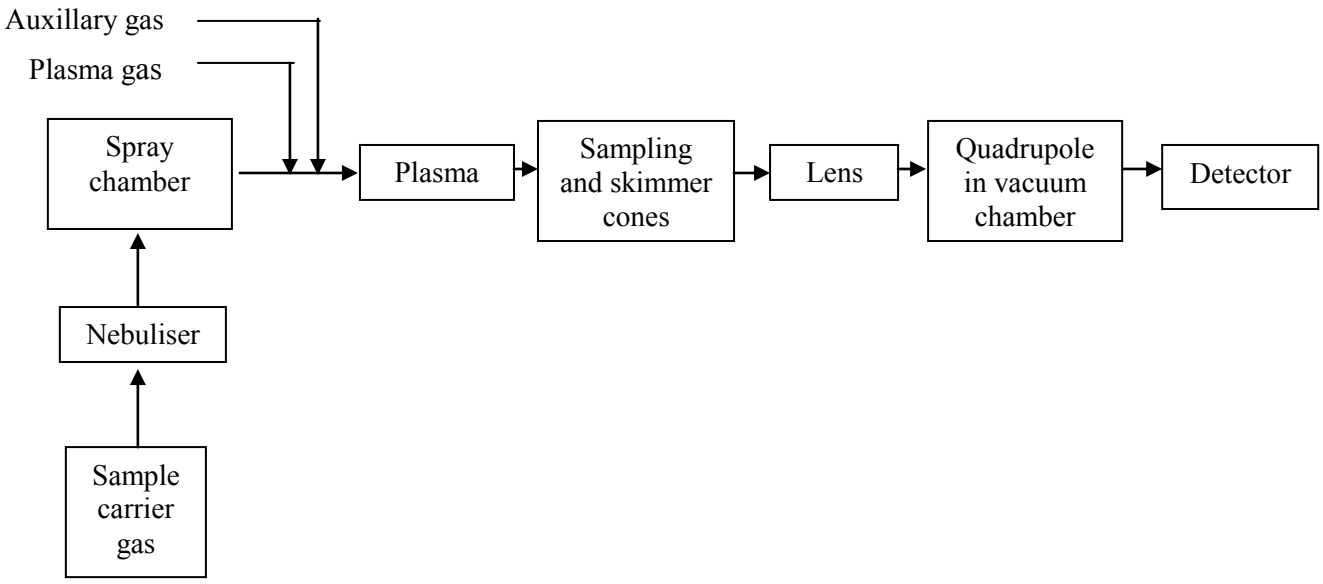

Fig. A3 ICP-MS setup (modified from http://www.agilent.com)

The ions produced in the plasma are extracted into the mass spectrometer (Fig. A3) which is maintained at high vacuum (typically 10-4 Pa) by differential pumping to permit the analyte ions to be extracted through a pair of orifices, known as the sampling and skimmer cones.

The analyte ions are then focused by a series of ion lenses into a quadrupole mass analyzer, which separates the ions based on their mass/charge ratio. The term quadrupole is used since the mass analyzer consists of four parallel stainless steel rods to which a combination of

radiofrequency and direct current voltages are applied. The combination of these voltages allows the analyzer to transmit only ions of a specific mass/charge ratio.

Finally, the mass of ions are measured using an electron multiplier, and are collected by a counter for each mass number. Each elemental isotope appears at a different mass (e.g. ^{27}Al would appear at 27 amu (atomic mass units)) with a peak intensity directly proportional to the initial concentration of that isotope in the sample solution.

3. Fourier Transform-infrared spectroscopy (FT-IR)

The vibrational and rotational energies of molecules can be studied by infrared spectroscopy. A common application of FT-IR spectroscopy is for "group frequency" analyses. With the exception of a few homo-nuclear molecules such as O_2, N_2 and Cl_2, all molecular species absorb infrared radiation. Certain functional groups in molecules show certain vibrations in which only the atoms in the group move. Since the rest of the molecule is mechanically uninvolved in the vibration, a group vibration will have a characteristic frequency that remains constant no matter what molecule the group is in. This group frequency can be used to reveal the presence or absence of the group in the molecule and this is frequently of tremendous help in characterizing the molecular structure. In FT-IR spectroscopy the micron (μ = 10^{-4} cm) may be used as the dimension for wavelength. Using this unit, the visible region is about 0.4-0.7 μ, the near infrared is about 0.7-2.5 μ, the fundamental infrared region is about 2.5-50 μ and the far infrared is about 50 μ to a fraction of a mm. The reason for a division at about 2.5 μ is that absorption caused by fundamental vibrational transitions fall on the long wavelength side of 2.5 μ. The reason for a division at about 50 μ is largely instrumental.[6]

[6] http://www.uksaf.org/tech/list.html

The properties that electromagnetic radiation and molecules have in common are energy and frequency. However, the frequency, ν, in hertz (Hz) in this part of the spectrum is an inconveniently large number so a number that is proportional to frequency is commonly used. This is called the wavenumber, ω (cm^{-1}), which denotes the number of waves in a 1 cm long wave train. This unit is related to the other units by:

$$\omega = \nu/c = 1/\lambda_{cm} = 10^4/\lambda_{\mu}$$

where λ_{cm} and λ_{μ} are the wavelengths expressed in cm and μ respectively. Grating instruments deliver spectra where the horizontal coordinate is linear with wavenumber. Results are reported in wavenumbers since these are proportional to molecular properties, frequency and energy. The vertical coordinate in an FT-IR spectrum is usually presented linearly with sample transmittance. Transmittance is defined as the radiant power of the radiation which is incident on the sample, divided into the radiant power transmitted by the sample.

In a typical infrared spectrometer, a source simultaneously emits all the infrared frequencies of interest. These radiation frequencies are about the same order of magnitude as the molecular vibrational frequencies. The molecule that matches the vibrational frequency of the source shall absorb some of the radiation. Most of the other frequencies are transmitted. This particular molecule has increased its vibrational energy through the radiation it has absorbed. In order for any infrared absorption to occur, the molecular vibration must cause a change in molecular dipole moment.

Fourier-transform instruments contain no dispersing element, and all wavelengths are detected and measured simultaneously. In order to separate wavelengths, it is necessary to modulate the source signal in such a way that it can subsequently be decoded by a Fourier transformation, a mathematical operation that requires a high-speed computer. The theory of Fourier-transform measurements appears in the literature.[7]

[7] Skoog, D.A., Leary, J.J., Principles of Instrumental Analysis, 4th edition, Philadelphia Saunders College Publishing, pp. 113- 120 and 266-270 (1992)

4. Gas chromatography

The word "chromatography", formed from the Greek word "chroma" meaning "color" and "graphein" meaning "to write", was coined by M. Tswett around 1900 to describe his process of separating mixtures of plant pigments. He washed the pigments down a column of adsorbent powder ($CaCO_3$). Such a separation of the components of a mixture for qualitative or quantitative analysis, or for isolation and recovery of the components is the desired end of any type of chromatography.[8]

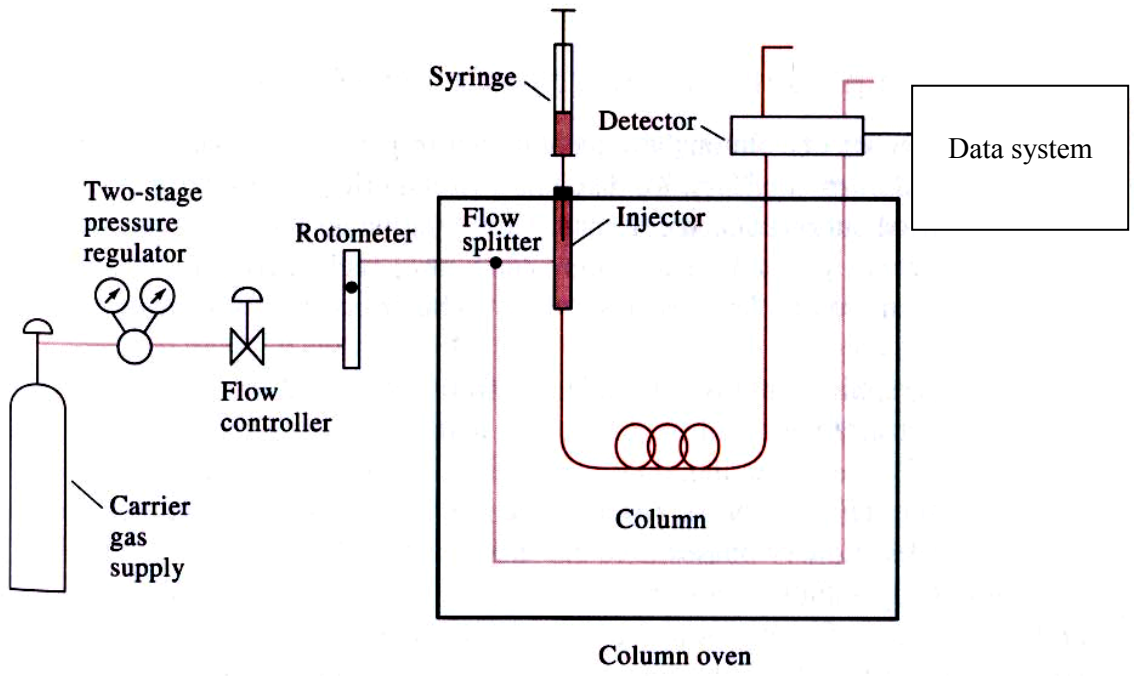

Fig. A4 Gas chromatograph

[8] Skoog, D.A, West, D.M., Holler, F.J., Fundamentals of Analytical Chemistry, 7th edition, Saunders College Publishing, p 665 (1991)

A schematic illustrating the components of a typical gas chromatograph appears in Fig. A4. A gas chromatograph consists of a flowing mobile phase or carrier gas (which must be chemically inert such as nitrogen and helium used in this study), a flow splitter (which is employed to deliver only a small fraction of the injected sample to the column head, with the remainder going to waste, so as not to flood the column), an injection port (equipped with a septum to allow a needle to enter for sample introduction and seals when the needle is removed (Fig. A5)), a separation column containing the stationary phase and a detector.

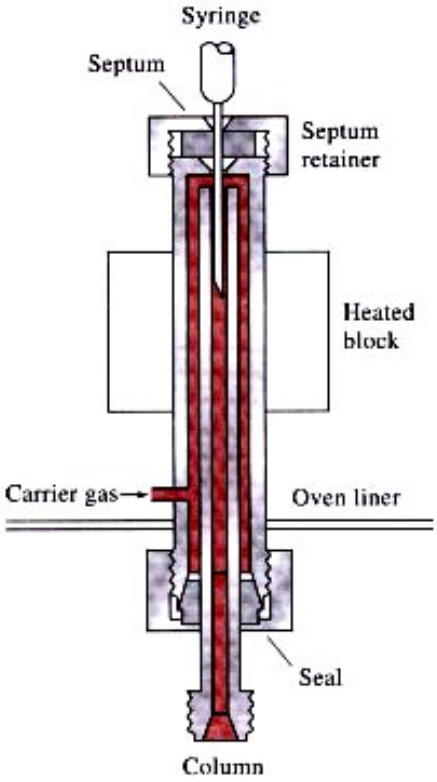

Fig. A5 A heated sample injection system

A flash vaporizer port (in the region of the heated block) is located at the head of the injector (Fig. A5). The liquid sample introduced into the port is vaporized in this region and thus the temperature of this zone is usually maintained 50^{o}C above the boiling point of the least volatile component in the sample.

The organic components are separated due to differences in their partitioning behaviour between the mobile phase and the stationary phase in the column. In gas chromatography, the mixture to be separated is vaporized and swept over a relatively large adsorbent surface inside a long narrow tube or column. A steady stream of inert carrier gas moves the vapours of the mixture along the column. The different components are moved along the column at different rates and, under proper circumstances, become separated.

Since the partitioning behaviour is dependant on temperature, the separation column is usually contained in a thermostatically controlled oven. Starting at a low oven temperature, where low boiling components elute, and increasing the temperature over time to favour elution of the high-boiling components accomplishes separation of components with a wide range of boiling points.[9]

Each component has a characteristic retention time in the column for a given set of instrumental conditions. These retention times serve as a means of qualitative analysis.

There are two types of GC columns, viz. packed and capillary columns. Packed columns are typically a glass or stainless steel coil that is filled with the stationary phase. Capillary columns on the other hand, are thin fused silica (purified silicate glass) capillaries (typically 10-100 m in length and 250 μm inner diameter that have the stationary phase coated on the inner surface. Capillary columns provide higher separation efficiency than packed columns but are easily overloaded by too much sample. The stationary phase can be polar, intermediate or non-polar in nature. The ideal stationary phase is judged by the types of components to be separated.

The sensitivity of detection for a given detector varies according to peak height which serves as a means of quantitative analysis.

[9] http://www.chem.vt.edu/chem.-ed/sep/gc/gc.html

Two detectors were employed in this study viz. a flame ionization detector (FID) and a thermal conductivity detector (TCD).

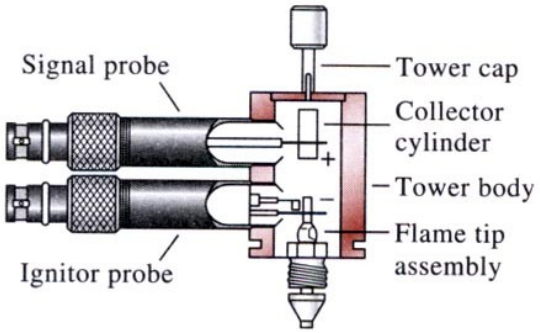

Fig. A6 Flame ionization detector

In a flame ionization detector, the effluent from the column is mixed with hydrogen and air and then ignited electrically. Most organic compounds, when pyrolysed at the temperature of a hydrogen and air flame, produce ions and electrons that can conduct electricity through the flame. A potential of a few hundred volts is applied across the burner tip and a collector electrode located above the flame. The resulting current (~ 10^{-12} A) is then directed into a high-impedance amplifier for measurement. The flame ionization detector responds to the number of carbon atoms entering the detector per unit time hence it is a mass-sensitive rather than concentration-sensitive device. As a consequence, this detector has the advantage that changes in flow rate of the mobile phase have little effect on detector response. The detector is insensitive to non-combustible gases such as H_2O, CO_2, SO_2 and NO_x. The sample is destroyed in this analytical technique.

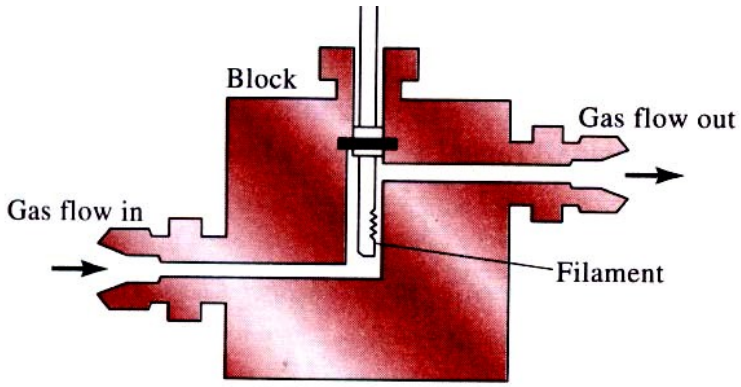

Fig. A7 Thermal conductivity detector

The operation of the thermal conductivity detector (Fig. A7) is based on changes in the thermal conductivity of the gas stream induced by the presence of analyte molecules. The sensing element is an electrically heated element whose temperature at constant electrical power depends on the thermal conductivity of the surrounding gas. The heated element may be platinum, gold, tungsten wire or a semiconducting thermistor. The resistance of the wire or thermistor is a measure of its temperature, which depends in part upon the rate at which the surrounding gas molecules conduct energy away from the detector element to the walls of the metal block in which it is housed.

The thermal conductivities of hydrogen or helium are roughly 6 to 10 times greater than those of most organic compounds. Thus, the presence of even small amounts of organic materials causes a relatively large decrease in the thermal conductivity of the column effluent; consequently, the detector undergoes a marked rise in temperature. The disadvantage of the thermal conductivity detector is that it has a relatively low sensitivity compared to other detectors employed.

5. X-ray diffraction (XRD)

In wavelength-dispersive spectrometers (Fig. A8), wavelengths are separated by Bragg diffraction from a single crystal. The X-ray source is usually of high intensity (approx. 3 kW) with a stabilized high-voltage supply. This is necessary because large losses of characteristic radiation occur due to the relatively low reflectivity of the dispersive crystals. The detector is mounted on a goniometer, which allows the detector to accept one wavelength at a time at the 2θ diffraction angle, and covers a broad range from a few degrees to 150 degrees. Either a proportional or scintillation counter detector is used, or both in tandem arrangement. The associated electronics include a DC power supply, linear amplifier and recorder.

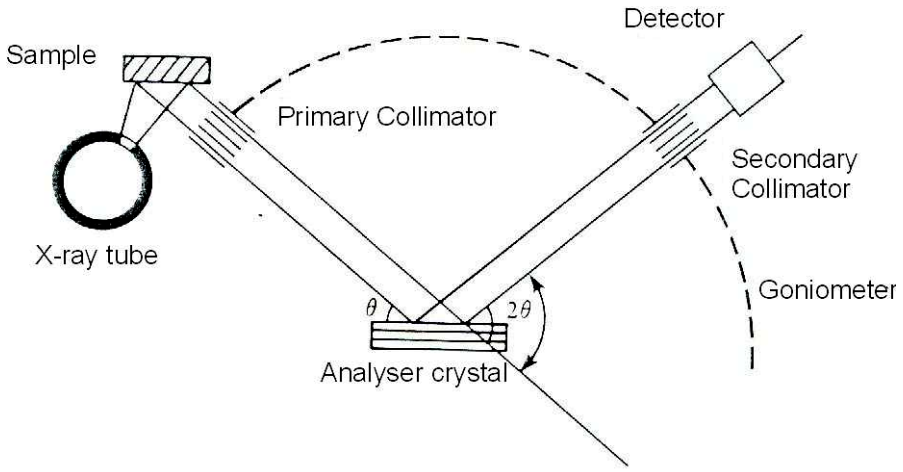

Fig. A8 A schematic representation of an XRD spectrometer

Bombarding a suitable target with electrons produces the X-rays. When the electrons hit the target, they "move" electrons around the orbitals, which results in a series of emission wavelengths as the atom returns to an unexcited state. The resulting electron excitation in the source produces a broad band of energies that are high energy X-rays. The sample is irradiated with the high energy X-rays to produce a secondary beam of fluorescent X-rays. These X-rays are passed through a collimator and directed to a single analyzer crystal that separates the

wavelengths. The wavelengths of the X-rays produced by the powdered sample and diffracted by the analyzer crystal obey the Bragg equation:

$$n\lambda = 2d\sin\theta$$

λ = wavelength of X-rays
d = spacings of atoms in the powdered sample
n = integer

The Bragg equation links the d-spacings on the powdered sample to the angle of turn of the analyzer crystal. The data obtained shows a series of lines of varying intensities at different 2θ values, obtained as the analyser crystal turns. A qualitative analysis of the sample is thus carried out.[10]

6. Scanning electron microscopy (SEM)[11]

In the scanning electron microscope (SEM), a very fine "probe" of electrons with energies up to 40 keV is focused at the surface of the specimen in the microscope and scanned across it in a pattern of parallel lines. A number of phenomena occur at the surface under electron impact: most important for scanning microscopy is the emission of secondary electrons with energies of a few tens eV and re-emission or reflection of the high-energy backscattered electrons from the primary beam. The intensity of emission of both secondary and backscattered electrons is very sensitive to the angle at which the electron beam strikes the surface, i.e. to topological features on the specimen. The emitted electron current is collected and amplified. Variations in the resulting signal strength as the electron probe scans across the specimen are used to vary the brightness of the trace of a cathode ray tube being scanned in synchronism with the probe. There is thus a direct positional correspondence between the electron beam scanning across the specimen and the fluorescent image on the cathode ray tube.

[10] Brady, J.E., Holum, J.R., *Chemistry: The Study of Matter and its Changes*, John Wiley and Sons Publishers, p 386 (1993)

[11] http://www2.arnes.si/~sgszmera1/sem/sem/html

The magnification produced by the scanning electron microscope is the ratio between the dimensions of the final image display and the field scanned on the specimen. Usually, the magnification range of the SEM instrument is between 10 and 200 000 X and the resolution is between 4 and 10 nm (40 – 100 angstroms).

7. Energy dispersive X-ray spectrometry (EDX)[12]

As the electron beam of the scanning electron microscope scans across the sample surface, it generates X-ray fluorescence from the atoms in its path. The energy of each X-ray photon is characteristic of the element that produced it.

A solid-state detector composed of Si and Li, is responsive to the energies of the characteristic X-rays. Instruments utilizing these detectors are called energy-dispersive X-ray spectrometers. The EDX microanalysis system collects the X-rays, sorts and plots them by energy and automatically identifies and labels the elements responsible for the peaks in this energy distribution.

Hence, an entire X-ray spectrum from several elements in a specimen can be stored at one time.

The EDX data are typically compared to either known or computer-generated standards to produce a full quantitative analysis showing the sample composition. The EDX instrument is also capable of giving maps of distributions of elements over areas of interest.

The detector must operate at liquid-nitrogen temperatures, and a reservoir attached to the detector must be filled periodically with liquid nitrogen. The pre-amplifier, pulse processor and pileup-rejection circuitry constitute a sophisticated electronic package to maintain the quantitative properties of the signals produced in the detector. These are necessary to ensure high performance with respect to energy resolution, data-acquisition times and signal-to-noise ratio (i.e. detection limit).

[12] http://www2.arnes.si/~sgszmera1/eds/eds.html

8. Gas chromatography-mass spectrometry (GC-MS)

The gas chromatography-mass spectrometer (GC-MS), as the name suggests, is composed of two parts viz. a gas chromatograph, which separates a chemical sample mixture into its pure chemicals and a mass spectrometer, which identifies the pure chemicals.

After the molecules in the sample are separated in the GC, they pass through a mass spectrometer. The molecules are blasted with electrons which cause them to fragment and turn into positively charged ions. The ions pass through an electromagnetic field that filters the ions based on mass. Only a certain range of masses is allowed to pass through the filter and enter a detector which counts the number of ions with a specific mass. This information is sent to a computer and a mass spectrum is created. Usually a mass spectrum will display a peak for the unfragmented molecule of the specimen. This is commonly the greatest mass detected, called the "parent mass." The parent mass reveals the mass of the molecule while the other peaks indicate the molecule's structure. A molecule has a characteristic mass spectrum which is based on its fragmentation pattern. It is thus identified by comparing the mass spectrum to known compounds, which is usually in a library in the software package. Quantitative analysis can be carried out by measuring the relative intensities of the mass spectra.[13]

[13] http://sites.netscape.net/dougfrm

Voids and catalyst dilution setups

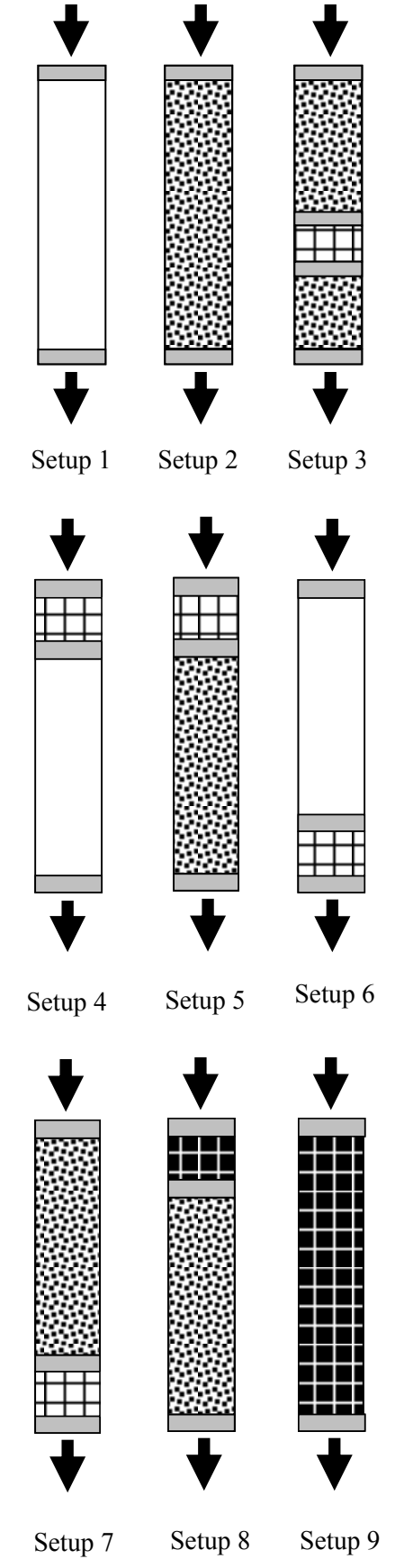

Description of catalysts tested

Catalyst	Description
VPO-1	Unpromoted VPO
VPO-2	1.25 % Co-VPO
VPO-3	2.50 % Co-VPO
VPO-4	5.00 % Co-VPO
2.5 % Co-VPO (precipitation/deposition)	Co impregnated onto a VPO catalyst
2.5 % Rh-VPO (co-precipitation)	Rh incorporated into a VPO catalyst
VPO-A	Failed attempt at incorporating 2.5 % Au into a VPO catalyst
VPO-B	Failed attempt at incorporating 5.0 % Au into a VPO catalyst
Au-VPO (precipitation/deposition)	2.5 Au impregnated onto a VPO catalyst
VMgO	Unpromoted VMgO catalyst
Co-VMgO	2.5 % Co incorporated into a VMgO catalyst